Defining the molecular signaling mechanism in epidermal stem cell regulation and cancer

By

Raghava Reddy Sunkara

(LIFE09201304013)

Tata Memorial Centre, Mumbai

A thesis submitted to the

Board of Studies in Life Sciences

In partial fulfillment of requirements

For the Degree of

DOCTOR OF PHILOSOPHY

Of

HOMI BHABHA NATIONAL INSTITUTE

July 2020

Homi Bhabha National Institute

Recommendations of the Viva Voce Committee

As members of the Viva Voce Committee, we certify that we have read the dissertation prepared by **Mr. Raghava Reddy Sunkara** entitled "**Defining the molecular signaling mechanism in epidermal stem cell regulation and cancer**" and recommend that it may be accepted as fulfilling the thesis requirement for the award of Degree of Doctor of Philosophy.

09/12/2020

Chairperson – Dr. Santosh Kumar — Date:

09/12/2020

Guide/Convener – Dr. Sanjeev Waghmare — Date:

December 1, 2020

External Examiner – Dr. Colin Jamora — Date:

9/12/2020

Member – Dr. Sanjay Gupta — Date:

09/12/2020

Member-- Dr. Ashok Varma — Date:

Final approval and acceptance of this thesis is contingent upon the candidate's submission of the final copies of the thesis to HBNI.

I hereby certify that I have read this thesis prepared under my direction and recommend that it may be accepted as fulfilling the thesis requirement.

9/12/2020

Date:
Place: Navi Mumbai

Dr. Sanjeev Waghmare
Guide

STATEMENT BY AUTHOR

This dissertation has been submitted in partial fulfillment of requirements for an advanced degree at Homi Bhabha National Institute (HBNI) and is deposited in the Library to be made available to borrowers under rules of the HBNI.

Brief quotations from this dissertation are allowable without special permission, provided that accurate acknowledgement of source is made. Requests for permission for extended quotation from or reproduction of this manuscript in whole or in part may be granted by the competent authority of HBNI when in his or her judgment the proposed use of the material is in the interests of scholarship. In all other instances, however, permission must be obtained from the author.

Mr. Raghava Reddy Sunkara

DECLARATION

I, hereby declare that the investigation presented in the thesis has been carried out by me. The work is original and has not been submitted earlier as a whole or in part for a degree / diploma at this or any other Institution / University.

Mr. Raghava Reddy Sunkara

List of Publications arising from the thesis

Journals:

1. "SFRP1 in Skin Tumor Initiation and Cancer Stem Cell Regulation with Potential Implications in Epithelial Cancers". **Sunkara RR**, Sarate RM, Setia P, Shah S, Gupta S, Chaturvedi P, Gera P, Waghmare SK. Stem Cell Reports. 2020 Feb 11; 14(2):271-284.
2. "Sfrp1 loss results in reduction of HFSCs which is restored by BMP/AKT/GSK3β-mediated signaling". **Sunkara RR**, Darshan Mehta, Waghmare SK. (Manuscript under preparation).

Conferences:

1. Poster presentation on the topic entitled "**Understanding the role of SFRP1 in hair follicle stem cell regulation**" at Gordon research Conference meeting and seminar entitled "Tissue Niches and Resident Stem Cells in Adult Epithelia" held from 18th Aug 2018 to 24th Aug 2018, New Hampshire, USA.

2. Poster presentation on the topic entitled "**Defining the role of SFRP1 in epidermal stem cell regulation and cancer"** at **"**International Congress of Cell Biology" held from January 27-31, 2018, Hyderabad, India.

3. Poster presentation on the topic entitled "**Role of SFRP1 in epidermal stem cell regulation and cancer"** at "A Conference of New Ideas in Cancer - Challenging Dogmas" held from February 26-28, 2016, Mumbai, India.

4. Poster presentation on the topic entitled "**Defining the role of SFRP1 in epidermal stem cell regulation**" at inStem-IFOM Conference on "Inflammation and Tissue Homeostasis" held from February 3-5, 2016, Instem, Bengaluru, India

Other Publications:

1. "Context-dependent effect of $sPLA_2$-IIA induced proliferation on murine hair follicle stem cells and human epithelial cancer". Chovatiya GL*, **Sunkara RR***, Roy S, Godbole SR, Waghmare SK. EBioMedicine. 2019 Oct; 48:364-376. (* equal first author)
2. "Secretory phospholipase A_2-IIA overexpressing mice exhibit cyclic alopecia mediated through aberrant hair shaft differentiation and impaired wound healing response". Chovatiya GL, Sarate RM, **Sunkara RR**, Gawas NP, Kala V, Waghmare SK. Sci Rep. 2017 Sep 14;7(1):11619.
3. "Understanding the binding affinities between $SFRP1^{CRD}$, $SFRP1^{Netrin}$, Wnt_{5B} and Frizzled Receptors 2, 3 and 7 using MD Simulations". **Raghava R. Sunkara***, Shruti Koulgi*, Vinod Jani, Uddhavesh Sonawane, Rajendra Joshi, Nikhil Gadewal and Sanjeev K Waghmare. (* equal first author) [Manuscript under revision]

Review Articles:

1. "Developmental signaling in maintenance and regulation of cancer stem cells". Sweta Dash, **Raghava R. Sunkara**, Sanjeev K Waghmare. Biomedical Research Journal, 2015, Volume: 2, Issue: 1, Page: 37-56

2. "EMT imparts cancer stemness and plasticity: new perspectives and therapeutic potential". Roy S, **Sunkara RR**, Parmar MY, Shaikh S, Waghmare SK. Front Biosci (Landmark Ed). 2021 Jan 1;26:238-265.

09/12/2020

Mr. Raghava Reddy Sunkara

I dedicate this thesis to my beloved family, friends and teachers for their endless support and encouragement

Acknowledgements

I would like to express my deepest gratitude to a number of people, without whose support and encouragement this thesis would have been a farfetched dream. Foremost, I would like to express my deepest gratitude to my research advisor, Dr. Sanjeev Waghmare for his guidance, encouragement, advice and constant support throughout my PhD tenure. I am grateful to him for giving me the opportunity and freedom to work and express myself. I have learnt to respect as well as enjoy my work at the same time. I have acquired excellent working practice, to have good ethical and moral values under his guidance.

I would like to specially thank Dr. Sudeep Gupta, Director, ACTREC and Dr. Prasanna Venkatraman, Dy. Director, CRI, ACTREC and Dr. HKV Narayan, Dy. Director, ACTREC for providing admirable infrastructure and a welcoming environment to work with. I am also thankful to Dr. Shubhada Chiplunkar (former Director, ACTREC) for providing excellent infrastructure, encouragement and endless support throughout the tenure.

I am immensely grateful to the members of my doctoral committee: Dr. Santosh Kumar (Chairperson), Dr. Sanjay Gupta and Dr. Ashok Varma for their constructive criticism and encouragement in the past six years which inspired me to widen my research perspectives. I extend my sincere thanks to Dr. Akihiko Shimono from RIKEN, Kobe, Japan for providing Sfrp1 knockout mice. I am extremely thankful to Dr. Sanjay Gupta and Sanket Shah (Gupta lab) for performing *in silico* analysis of the data from TCGA database.

I am eminently thankful to Dr. Arvind Ingle and Dr. Rahul Thorat and all the staff of Laboratory Animal Facility without whose support this work would not be possible. I specially thank Mr. Surendra for his ever-present support in maintaining the mouse strains. I would also like to thank members of the histology department Mr. Chavan, Mr. Sakpal and Mr. Dinesh for providing extensive help in the histology work. Further, I am extremely thankful to members flow cytometry facility (Ms. Shyamal Vetale and Mr. Ravindra Joshi) and imaging facility (Mrs. Vaishali Kailaje, Mrs. Tanuja Dighe and Mr. Jayraj Kasale). I am also thankful to the people in the Director's office (Mrs. Pritha Menon and Mrs. Lata Shelar), programme office (Mrs. Maya Dolas, Mrs. Sharvari Joshi), administration, accounts, dispatch, purchase, stores and photography department for their constant support throughout the tenure.

I would like to specially acknowledge ACTREC for providing me with the fellowship and Department of Biotechnology (DBT) and Tata Memorial Centre (TMC) for providing the funds for the research work. I am grateful to Homi Bhabha National Institute (HBNI) and Sam Mistry and Patel fellowship for providing the financial support to attend the international conference.

I am extremely grateful to all former and current members of Waghmare lab. I sincerely thank my seniors Dr. Rahul Sarate and Dr. Gopal Chovatiya for their constant support at work and healthy discussions during the last six years. I am also thankful to Sweta, Nilesh, Sayoni, Sushant, Harsh, Priyanka and Darshan for their support and making the lab environment so vibrant and lively. My special thanks to Bane Sir, Nirmala Ma'am and Ganesh Ji for making the things available whenever required and for their constant support in the smooth functioning of the laboratory. I would like to thank all the JRFs and trainees (Prachi, Saloni, Manan, Saima, Apoorva, Prasanna, Monali, Priyanka and Deepanjali) for their help and contribution in the smooth progress of the project.

I specially thank all of my batch mates, Ajay, Pravin, Shalini, Raghu, Rajashree, Ram chandra, Asmita, Shalaka, Rai Kamal, Rahul, Mythreye, dhanashree, Burhan, Anuja and Vasudha for all the unconditional support and love they have provided me in the past 6 years. I will cherish all the beautiful moments that I had with you guys. My warm wishes and love goes to my dearest friends Ajay, Pravin and Shalini for always being there for me and supporting me through all the ups and downs in the past 6 years. I specially thank Raghu for coping up with me as a roommate for the last 6 years with minimal complaints.

Of paramount importance, I extend my deepest gratitude and love to my mom, dad and brother for their unconditional love and support. They have always believed in me and have always been happy and proud of my accomplishments.

Thesis Summary:

Mammalian adult tissues contain resident stem cells (SCs), which play an important role in the maintenance of tissue homeostasis and regeneration following injury, throughout the life of an organism. SCs are uniquely endowed with the ability to both self-renew and differentiate, such that they can replenish the SCs pool while continuing to give rise to differentiated cells that are essential for tissue function. The process of self-renewal and differentiation are carefully controlled as unchecked proliferation of SCs can lead to the development of tumors. Various developmental signalling pathways such as Wnt, Notch and Hedgehog pathways have been reported to govern the cyclic activity and differentiation of stem cells. Deregulation within these signalling cascades disrupts normal tissue homeostasis that leads to cancer development. Further, within the tumors there exists a unique population that has similar characteristics of tissue stem cells, which are involved in tumor maintenance and heterogeneity. These cells are named as cancer stem cells (CSCs) that are responsible for therapy resistance and tumor relapse after treatment. Though deregulated developmental signalling pathways were reported in maintaining CSCs in multiple cancers; however, a complete understanding of CSCs regulation seems be a distant reality.

In the first Part of the study, we have tried to understand the role of Sfrp1 in HFSCs maintenance and regulation. Here we found that Sfrp1 loss affected the initial formation of HFSCs i.e. decreased HFSCs pool was observed in both the $Sfrp1^{+/-}$ and $Sfrp1^{-/-}$ mice as compared to WT mice. However, the increased proliferation in $Sfrp1^{-/-}$ mice HFSCs restored the HFSCs pool by PD49. This increase in the $Sfrp1^{-/-}$HFSCs proliferation could be due to decrease in Runx1 and P21 levels and increase in Cyclin-D1 levels. Further, Sfrp1 knockout mice showed delay in wound re-epithelialization suggesting that Sfrp1 loss affects the HFSCs function. Importantly, decrease in the HFSCs markers such as Lgr5 and Axin2 was observed in $Sfrp1^{-/-}$ HFSCs as there was a decrease in the Wnt/β-catenin signalling. This decrease in

the Wnt/β-catenin signalling could be due to the activated Bmp signalling, which in turn inactivates Akt signalling thereby activating Gsk-3β that phosphorylates and inactivates β-catenin. In conclusion, our work demonstrates a new hierarchical level of regulation embedded within HFSCs that inhibits aberrant activation of Wnt signalling in the absence of Sfrp1, by regulating Akt activity through the expression of Bmp signalling agonists (Bmpr1a) and antagonists (Noggin).

In the second part of the study, we explored the role of Sfrp1 in tumor aggressiveness and CSCs regulation. Previous report from our lab has shown that Sfrp1 loss results in increased sensitivity to chemical induced carcinogenesis. However, the functional properties and molecular mechanism remained unexplored. Here, we have shown that $Sfrp1^{-/-}$ mice tumors were primarily of mixed/mesenchymal phenotype as compared to epithelial phenotype of WT tumors. Importantly, the FACS sorted cells are indeed CSCs by performing the serial transplantation assay (The gold standard assay) and limiting dilution assays. Further, the tumor propagating cell (TPC) frequency was also enhanced in $Sfrp1^{-/-}$ CSCs. This enhanced tumorigenicity and aggressiveness could be due to the increased levels of growth factor receptors in $Sfrp1^{-/-}$ CSCs, such as Ghr, Pdgfra, and Tgfbr3, and their downstream signalling molecules Akt3, Erk and Stat2, which are associated with CSC maintenance, tumor aggressiveness and metastatic potential. The expression of Sox-2 (stemness marker), involved in regulating tumor initiation and CSC regulation, was upregulated in $Sfrp1^{-/-}$ CSCs. Further, we have shown an inverse correlation between Sfrp1 and Sox-2 in mice SCC. Importantly, this inverse correlation between Sfrp1 and Sox-2 was extrapolated to human skin cancer where a similar correlation was observed. In addition, restoration of Sfrp1 levels decreased the expression of Sox-2 in cutaneous skin SCC cell lines thereby establishing their inverse correlation in human skin cancer. As epidermis share certain similarities with oral and breast epithelia in tissue architecture and in tumor progression, we further expanded our studies to

OSCC and breast cancer. Our results (Real time PCR and IHC) have shown that Sfrp1 levels were lower and Sox-2 levels were higher within these cancers. Further, to validate the inverse relation of Sfrp1 and Sox-2 in large cohort of samples we have also performed *in silico* analysis of data from TCGA data base on skin cancer, HNSCC, breast cancer and pancreatic adenocarcinoma (PAAD) samples. The results showed an inverse relation of Sfrp1 and Sox-2 within these cancers even in large cohort of samples with in TCGA data base. Of paramount importance, within the TCGA data, we have found that loss of Sfrp1 results in overall poor survival in skin cancer, HNSCC, breast cancer and PAAD patients. In conclusion, this study provides compelling evidence that Sfrp1 plays pivotal role in skin tumor initiation and CSCs regulation. Importantly, Sfrp1 and Sox-2 expression showed an inverse correlation in mice skin SCC. The murine skin SCC data was further extrapolated and validated in human epithelial cancers such as skin cancer, HNSCC and breast cancer which also showed an inverse correlation of Sfrp1 and Sox-2. In particular, low levels of Sfrp1 showed overall poor survival in skin cancer, HNSCC, breast cancer and PAAD patients suggesting that Sfrp1 could be used as a prognostic marker within these cancers. This study accentuates the importance of using murine epithelial model systems for studying molecular signalling in human epithelial cancers. Overall, future studies are necessary to understand the precise molecular mechanism of Sfrp1 that is involved in CSC regulation with respect to tumor aggressiveness, proliferation and EMT regulation, which may further pave way in the development of treatment strategies in cancer.

Salient findings:

Objective 1:

1. Sfrp1 loss showed an initial decrease in the HFSCs pool in mice skin
2. Loss of Sfrp1 leads to increased HFSCs proliferation at PD23 (telogen-to-anagen transition) and decrease in label retaining cells (LRCs) in $Sfrp1^{-/-}$ mice skin as compared to WT mice at PD49 (2^{nd} telogen). However, no change in proliferation or decrease in LRCs was observed in $Sfrp1^{+/-}$ mice.
3. Decrease in the Runx1 and P21 protein levels while increase in the Cyclin–D1 levels are observed in the Sfrp1 knockout mice as compared to WT
4. Sfrp1 loss leads to delay in wound re-epithelialization as compared to WT
5. Decreased active β-catenin signalling was observed in Sfrp1 knockout mice as compared to WT
6. No redundancy from other SFRP family proteins was observed in the absence of Sfrp1 in mice skin
7. Sfrp1 loss showed a decrease in the expression of HFSCs markers genes such as Lgr5 and Axin2 (targets of Wnt/β-catenin signalling)
8. Increased Bmp signalling and inactivation of PI3K/AKT signalling might be responsible for increase in the active Gsk-3β levels in both the $Sfrp1^{+/-}$ and $Sfrp1^{-/-}$ mice as compared to WT mice skin
9. We propose a model that, in HFSCs the activated Bmp signalling inhibits the activity of the Akt signalling. This in turn increases the active Gsk-3β levels which inhibit the aberrant activation of (β-catenin) Wnt signalling in the absence of Sfrp1.

Objective 2:

1. Enhanced mesenchymal phenotype was observed in Sfrp1$^{-/-}$ SCC as compared to WT SCC
2. CSCs from the Sfrp1$^{-/-}$ induced skin tumors are more aggressive, and possess high tumorigenic potential as compared to WT tumors
3. The tumor propagating cell (TPC) frequency was higher in Sfrp1$^{-/-}$ CSCs as compared to WT CSCs with Sfrp1$^{-/-}$ CSCs as low as 5000 are capable of giving rise to tumors in NOD/SCID mice.
4. Sfrp1 loss results in increased growth factor receptors in Sfrp1$^{-/-}$ CSCs, such as Ghr, Pdgfra, and Tgfbr3, and their downstream signalling molecules such as Akt3, Erk and Stat2, which are associated with CSC maintenance, tumor aggressiveness and metastatic potential
5. Increase in K8 and VIM1(1/2) expression, important markers for tumor progression and epithelial to mesenchymal transition of SCC, in Sfrp1 knockout mice SCC
6. Sfrp1 loss showed an increased Sox-2 expression and EMT markers (Twist1, Twist2, Snai1, Zeb1 and Vimentin) expression within CSCs
7. Sfrp1 and Sox-2 showed inverse correlation in multiple human epithelial cancers and Sfrp1 loss is associated with overall poor survival of the patients.

Chapter1: Introduction

1.1 Stem cells and their potency:

Stem cells (SCs) are a group unspecialized cells, which are capable of dividing and renewing themselves for long periods of time and maintain themselves in an undifferentiated state. Secondly, SCs give rise to tissue or organ specific differentiated cells with specialized functions, in which they reside to maintain the normal homeostasis of the tissue. Broadly, the SCs are classified into two different groups: the embryonic SCs and the adult/somatic/tissue SCs. Embryonic SCs are found in the inner cell mass of blastocysts, whereas adult SCs reside in a specialized micro-environment in the adult tissues known as SCs "niche". Depending upon the potency the SCs are further classified as follows.

Totipotent stem cells:

Totipotent SCs have the highest differentiation potential that are capable of differentiating into cells of both embryonic (i.e. cells of all the three germ layers) and extra-embryonic structures (Placenta). Therefore, the totipotent cell has the potential to give rise to the whole organism. One of the best examples of a totipotent cell is the zygote, which is formed after fertilization of egg with sperm.

Pluripotent stem cells:

Pluripotent SCs are capable of differentiating into cells of all the three germ layers (ectoderm, mesoderm and endoderm) i.e. they are capable of giving rise to any cell type in an organism. However, they cannot form the extra-embryonic tissues that support the foetal development such as placenta. The pluripotent cells cannot develop into a foetal or adult organism because they lack the potential to organize into an embryo. Embryonic SCs are a good example for pluripotent SCs.

Multipotent stem cells:

The multipotent SCs have the potential to self-renew and differentiate into multiple specialised cell types present in a specific tissue or organ. Tissue SCs are mostly multipotent SCs, which can give rise to different cell types of the respective tissue in which they reside. Multipotent tissue SCs are involved in maintaining adult tissue homeostasis throughout the life of an organism by producing daughter progenitor cells, which further undergoes terminal differentiation. Further, multipotent SCs get activated upon tissue injury to repair or replenish the tissue. Examples: i) Hematopoietic stem cells (HSC) which can give rise to all the cells of both lymphoid and myeloid lineages. ii) hair follicle stem cells (HFSC) which can give rise to cells of hair follicle, sebaceous gland and interfollicular epidermis iii)) Intestinal stem cells (ISC) can give rise to enterocytes, goblet cells, enteroendocrine cells, tuft cells, and Paneth cells.

Oligopotent stem cells:

These SCs have limited plasticity and have the ability to differentiate into only a few types of cells. Oligopotent SCs are less potent as compared to multipotent or pluripotent SCs but more potent as compared to unipotent SCs. Example: lymphoid stem cells can generate T cells, B cells, and plasma cells but not red blood cell or platelets.

Unipotent stem cells:

Unipotent SCs can only differentiate into one cell type. However, they have the indefinite potential to self-renew them self which distinguishes them from the committed progenitors. These SCs are the least potent and most limited type of SCs. Example: Sebaceous gland stem cells and muscle stem cells.

1.2 Embryonic stem cells:

Embryonic stem cells (ESCs) are isolated from the inner cell mass (ICM) of the pre-implantation blastocyst, a hollow sphere of cells containing an outer layer of trophoblast cells (trophectoderm), which give rise to the placenta and the ICM. The ESCs have two distinctive properties: self-renewal and pluripotency [1, 2]. The human ESCs for the research purpose are primarily obtained from embryos that are developed by in vitro fertilization technique in the *in vitro* fertilization clinic. In human ESCs, the transcription factors Oct4, Sox-2 and Nanog collaborate to form regulatory circuitry consisting of specialized auto-regulatory and feed forward loops thereby contributing to their pluripotency and self-renewal [3]. Further, in case of murine ESCs the pluripotency is regulated by Oct3/4 and Nanog transcription factors whose expression is in turn regulated by Sox-2 [4, 5]. Importantly, ESCs cells can be directed towards the differentiation programme of a specific lineage, such as nerve cells, heart muscle cells and blood cells by manipulating their behaviour through alteration of the chemical composition as of the media i.e. by addition of growth factors such as Fgf, Vegf, Scf and Pdgf to the media that drive ESCs differentiation or by inserting the regulatory genes in the ES cells [6, 7]. Owing to their indefinite self-renewal ability and differentiation into mature cell types, ESCs have massive potential in regenerative medicine and tissue engineering.

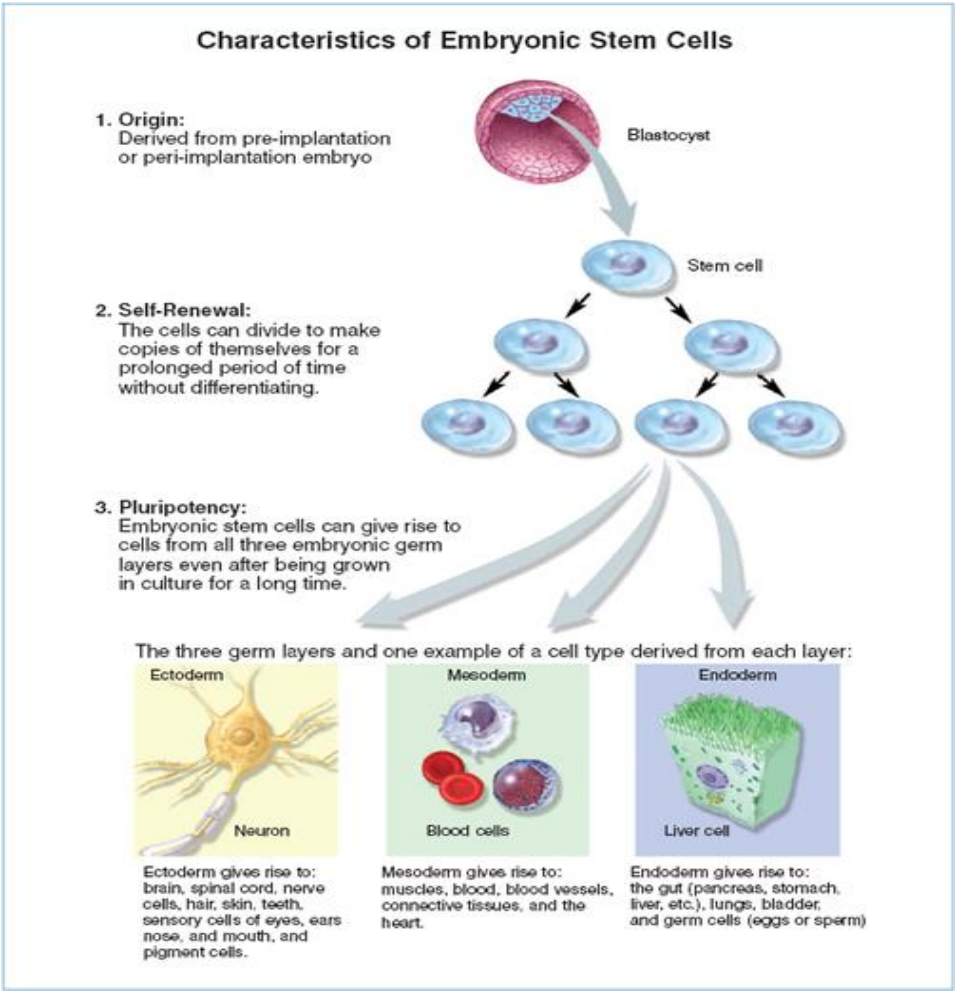

Figure 1.1: Characteristics of embryonic stem cells

(Adapted from Yu J. and Thomson J. 2014, Embryonic stem cells, NIH)

Pictorial representation of characteristics of embryonic stem cells; source of origin, self-renewal and differentiation into cells of all the three germ layers

1.3 Adult stem cells and niches:

The adult SCs are also called as tissue or somatic SCs. The adult SCs undergo self-renewal and are lineage restricted i.e. they can only differentiate into specialized cells of specific lineages. The adult SCs are either multipotent, oligopotent or unipotent. The primary roles of adult SCs in a living organism are to maintain the tissue homeostasis and repair the tissue upon injury of their respective tissues. Unlike ESCs, tissue SCs are relatively quiescent and

have limited plasticity. These adult SCs reside in a specialized micro-environment called as stem cell “niche”. Different types of adult SCs have their own specific niches, whereas, the location and nature of the niche varies from tissue to tissue. The SC niche is the specialized tissue compartment that hosts not only SCs but also every other components necessary for their proper function, including neighbouring cell populations, molecular signals and other extracellular components [8].Within the SC niche, the self-renewal of SCs, the transition of SCs between quiescent & activated states, rate of SC division and cell division axis (symmetrical or asymmetrical) are tightly regulated. This in turn, maintains tissue homeostasis and replenishes the tissue in case of injury, while loss in the regulation of SC divisions can lead to tumor generation [9, 10].

1.3.1 Epidermal stem cells niche:

Epidermis is a highly regenerative tissue of the body with an epidermal turnover time of 8-10 days in mice. The epidermis is maintained by the epidermal SCs present in the basal layer during normal tissue homeostasis. However, upon injury both epidermal SCs and hair follicle SCs (HFSCs) collectively contribute to wound re-epithelialization. The HFSCs are multipotent in nature, which can give rise to cells of all the epidermal lineages i.e. hair follicle (HF), sebaceous gland (SG) and the inter-follicular epidermis (IFE). The HFSCs express markers such as CD34, α6-integrin. In case of HFSCs, the bulge region of the follicle, which is located below the sebaceous gland in the permanent region of the follicle acts as the SCs niche. The HF cycles stereotypically between phases of growth (Anagen phase), regression (Catagen phase) and rest (Telogen phase), which is commonly referred to as “hair follicle cycle” [11, 12]. The HF cycle is fuelled by the HFSCs present in the bulge while maintaining a pool of SCs to perpetuate tissue regeneration. Due to continuous advancements in HF research, more and more cell types, including dermal Papilla (DP), adipose tissue, lymphatic vessels, nerves and immune cells, have been identified in

contributing to the HFSC niche [13-17]. The DP secretes Bmp4, the adipose tissue secretes Bmp2 and the keratin 6+ inner bulge layer secretes Bmp6 and Fgf18 during telogen, which inhibits HFSCs activation. However, during the telogen-to-anagen transition, the DP secretes Bmp inhibitors, Fgf7 and Fgf10, and the adipocyte progenitors secrete Pdgfα, which activates HFSC subsequently leading to HF cycle progression [18]. As multiple factors are involved in governing the HFSC in the niche, the combined overall outcome of various signalling molecules within the niche determines HFSC activation and proliferation during the hair regeneration. Importantly, pathological changes of the HFSC niche can lead to dysregulated hair growth or HFSC loss in diseased states such as androgenetic alopecia [19] and lichen planopilaris [20].

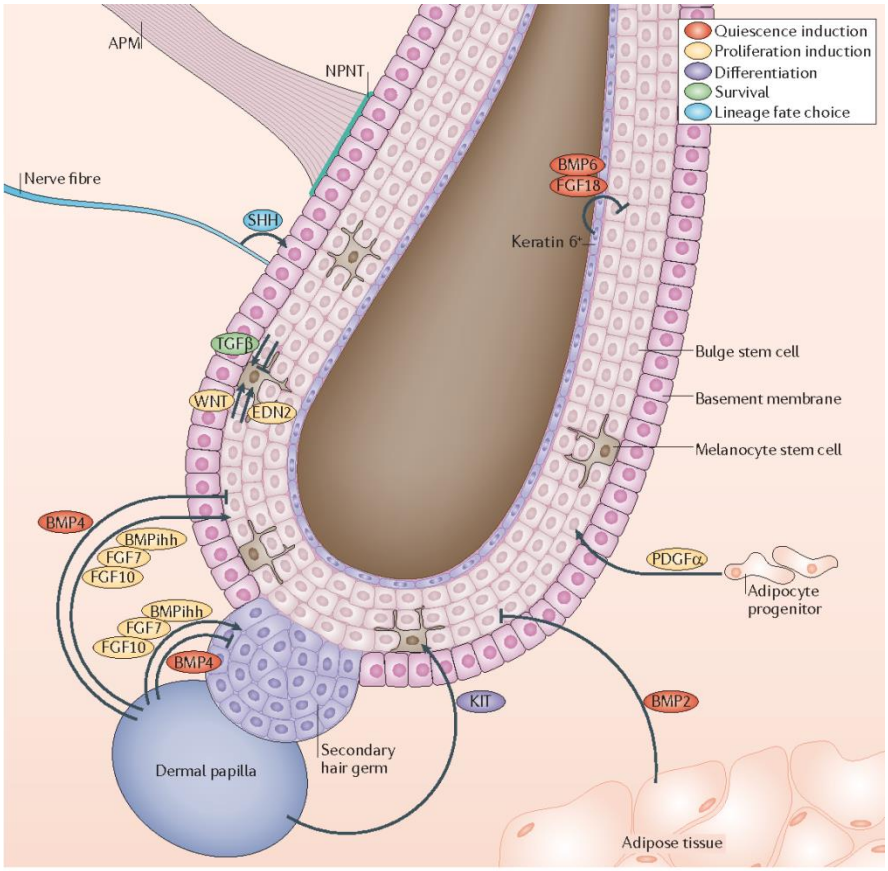

Figure 1.2: Microenvironment surrounding hair follicle stem cells

(Adapted from Solanas G, Benitah SA., 2013, Nat Rev Mol Cell Biol.)[18]

The diagram shows the interactions between hair follicle stem cells with neighbouring cell populations and the surrounding stroma. Signals emanating from dermal papilla, the keratin 6+ bulge layer or mature and progenitor adipocytes control the behaviour of bulge stem cells and consequently affect hair follicle cycling.

1.3.2 Hematopoietic stem cell niche:

The life span of red blood cells (RBC) in mice is around 30-60 days and 120 days in humans. The blood cells are replenished by a process known as haematopoiesis. This demand by the haematopoiesis is fuelled by the hematopoietic stem cells (HSCs). HSCs are of two types; the long-term quiescent HSC or "reserved HSCs" and the other actively cycling HSC or "primed HSC". The Primed HSCs are the workhorse that supports the daily normal homeostasis, whereas, reserved HSCs function as a "backup" to replenish lost active SCs in response to injury or pathological conditions [21-23]. It was earlier reported that the osteoblastic cell lining of the endosteum in trabecular bone acts as a HSCs niche. However, recent reports have shown that the vasculature of endosteum i.e. sinusoids with car cells and the arterioles that run along the endosteal area acts as a primary niche for HSCs. The reserved or dormant HSCs are found around the arterioles where factors such as CXCL12, CXCL4, TGF-β1 and SCF secreted by the perivascular, endothelial, megakaryocyte, Schwann and sympathetic neuronal cells promote their maintenance. Further, primed or active HSCs are located near sinusoidal niches which are likely diverse in their influence for self-renewal, proliferation and differentiation [24-26].

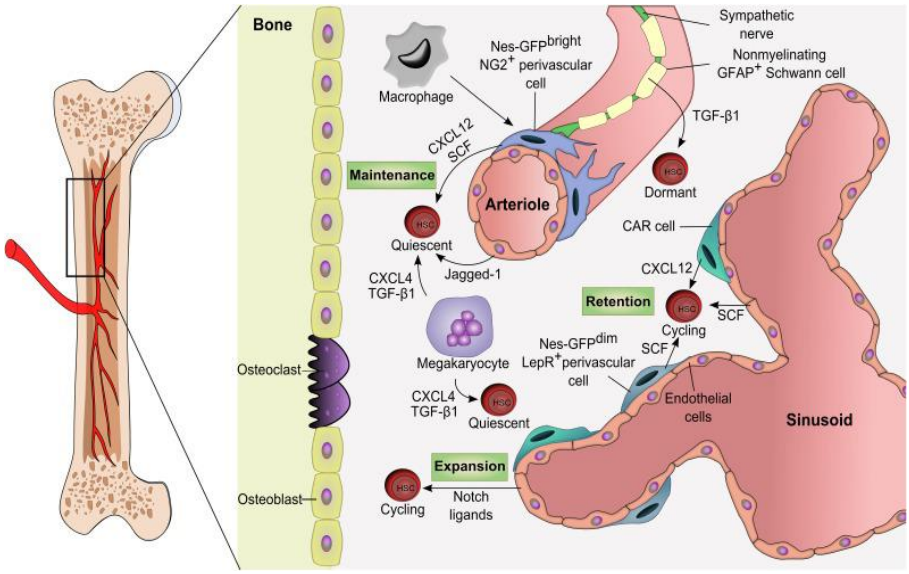

Figure 1.3: The HSC niche in adult bone marrow

(Adapted from Boulais P. and Frenette P. 2015, Blood) [26]

The diagram shows the HSC niche where the dormant HSCs are located near the arterioles and is regulated by C-X-C motif chemokine 12 (CXCL12), C-X-C motif chemokine 4 (CXCL4), stem cell factor SCF, and transforming growth factor- β1 (TGF-β)1secreted by different cells. The cycling HSCs are located near sinusoidal niches where CXCL12, SCF from perivascular cells regulate their retention where as notch ligands from endothelial cells promote expansion.

1.3.3 Intestinal stem cell niche:

The intestinal epithelium cells are one of the most actively cycling cells in our body. The turn over time for the entire intestinal epithelium is approximately 3-5 days [27]. The high cell turnover in the intestinal epithelium is fuelled by the Intestinal stem cells (ISCs), which reside at the base of the intestinal crypts [28]. Different studies have reported the presence of two types of ISCs. Lgr5 marks the actively cycling ISCs and the quiescent ISCs are marked by Bmi1, Hopx, mTERT and Lrig1 markers [29]. ISCs at the crypt base generate actively proliferating transit-amplifying cells, which rapidly move upward giving rise to cells of

absorptive lineage (enterocytes and goblet cells), and of the secretory lineage (enteroendocrine cells, tuft cells & Paneth cells). ISC niche comprises of both epithelial cells i.e. Paneth cells, and the stromal compartment, where mesenchymal cells secreted ligands and soluble factors regulate ISC behaviour [30, 31]. Depending upon their functional and phenotypic properties, the mesenchymal cells of the niche can be clearly demarcated such as α-SMA+ myofibroblasts and α-SMA- mesenchymal cells (CD34+ GP8+ mesenchymal cells and Foxl1+ mesenchymal cells) [32-34]. CD34+GP8+ mesenchymal cells produce the niche factors such as Wnt2b, Gremlin1, and R-spondin1 that promote the maintenance of $Lgr5^{+}$ ISCs [33]. Further, ablation of $Foxl1^{+}$ mesenchymal cells led to an abrupt cessation of proliferation of both ISCs and transit-amplifying progenitor-cells [34].

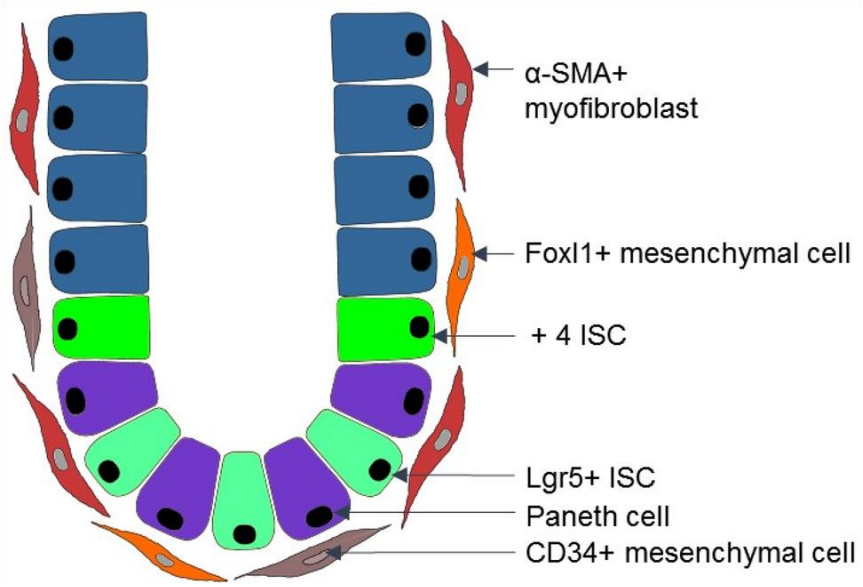

Figure 1.4: Intestinal stem cells niche

(Adapted from Pastuła A, et al. 2019, Arch Immunol Ther Exp (Warsz))[35]

The diagram represents the intestinal crypt where two different intestinal stem cell populations reside at its base. The actively cycling ISCs are marked by Lgr5 the and the quiescent ISCs are marked by Bmi1, Hopx, mTERT and Lrig1 markers. The intestinal stem cell niche comprises of Paneth cells and the mesenchymal cells such as α-SMA+

myofibroblasts and α-SMA- mesenchymal cells (CD34+ mesenchymal cells and Foxl1+ mesenchymal cells)

1.4 Cancer stem cells:

Cancer is a heterogeneous disease showing both inter-tumor and intra-tumor heterogeneity. The tumor heterogeneity is explained by two different models i.e. clonal evolution model and Cancer stem cell (CSCs) model. According to CSC model, within the tumors there exists a unique population, which has similar characteristics of tissue SCs, and are involved in tumor maintenance and heterogeneity. This unique cell population within tumor are called as CSCs, which exhibit indefinite self-renewal capacity. The CSCs are capable of generating all the differentiated cell types within the tumour and attributes to therapy (chemo/radio therapy) resistance and contribute to tumor relapse [36, 37].

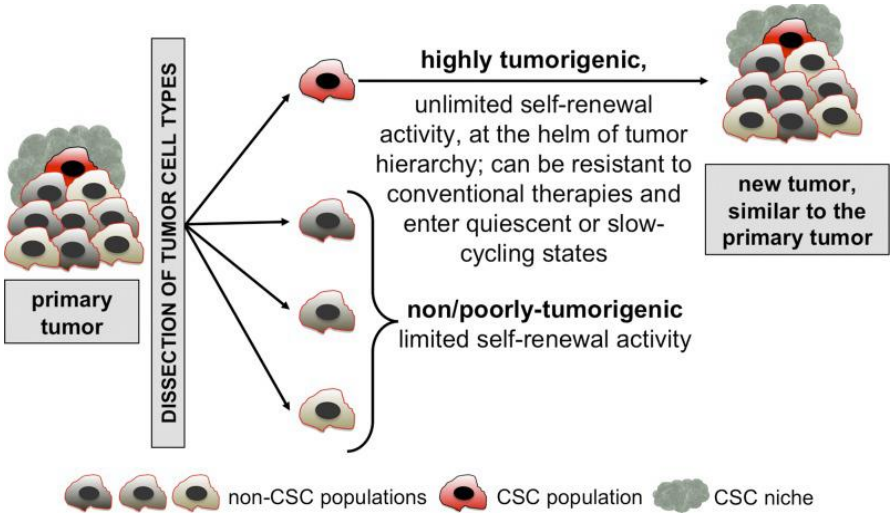

Figure 1.5: Tumor heterogeneity and Cancer stem cells

(Adapted from Baccelli I. and Trumpp A., 2012, J Cell Biol.)[38]

Lapidot and co-workers showed that a sub-group of cancer cells expressing $CD34^{+}/CD38^{-}$ markers from AML were capable of forming leukemia when transplanted into

NOD/SCID mice. Later, Dick and colleagues in 1997, have shown that leukemic cells that express $CD34^{+}CD38^{-}$/Lin- (HSC markers) undergo self-renewal, and are more efficient at propagating the leukaemia in immune-deficient mice. These cells are named as leukemic stem cells (LSCs) that were able to differentiate *in vivo* into leukemic blasts, indicating that there is a hierarchy in AML [39]. Further, in breast cancer (solid tumors), Al Hajj et al. in 2003, for the first time have shown that, there exists a subgroup of cells expressing $CD44^{+}CD24^{-/low}/Lin^{-}$ markers which acts as tumor initiating cells. These cells generated tumors at cell numbers as low as 100 cells when injected into immune-deficient mice. Further, they gave rise to both $CD44^{+}CD24^{-/low}/Lin^{-}$ cells as well as other differentiated cells within the tumors and are designated as breast CSCs (BCSCs) [40]. Subsequently, CSCs were discovered and prospectively isolated from different solid tumors, including brain cancers [41, 42], melanoma [43], colon [44], pancreatic [45], and head and neck cancers [46] etc. In addition, Zhang et al. in 2010, showed a sub-group of cells in oral squamous cell carcinoma (OSCC) that express CD133, possess CSC like properties such as higher clonogenicity, invasiveness, and increased *in vivo* tumorigenicity as compared to $CD133^{-}$ counterparts [47]. In case of skin squamous cell carcinoma (SCC) Liu et al. in 2015, have shown that Lgr5+ cells acts as CSCs like cells and administration of Ginsenoside Rh2 (GRh2) inhibited SCC growth, through reduction in the number of Lgr5+ CSCs [48].

However, this method of CSC isolation raised several questions as CSCs isolation from solid tumors requires preparation of single cell suspension of the tumors and their subsequent injection into immune compromised mice. This practice disturbs the niche surrounding the cancer cells which might change their natural behaviour. Therefore, it's uncertain whether the isolated CSCs have similar function within the undisturbed primary tumor. The first unambiguous evidence to support the existence of CSCs in solid tumors came from 3 independent research groups in brain, skin and intestinal tumors. They had used lineage

tracing technique in genetically engineered mouse models to show that CSCs emerge *de novo* and fuel the tumor growth [49-51]. CSCs are involved in therapy resistance and tumor relapse. Thus understanding the molecular mechanisms that drive these properties within CSCs may yield critical insights to develop targeted therapies against CSC.

Chapter 2: Review of Literature

2.1 Architecture of the Skin

Skin is the largest and most complex organ in the body and accounts for about 15% of the total adult body weight [52]. It plays a central role in protecting the organism from dehydration and environmental insults, as well as in regulating the body temperature. The thickness of the skin varies between 0.5mm to 4mm depending on the region of the body. Mammalian skin consists of three important layers; the epidermis, dermis and hypodermis (Figure 2.1). The epidermis is derived from ectoderm, which is the keratinised stratified squamous epithelium of the skin, mainly involved in protection against environmental insults and fluid loss. The epidermis rests on basement membrane that separates it from the dermis.

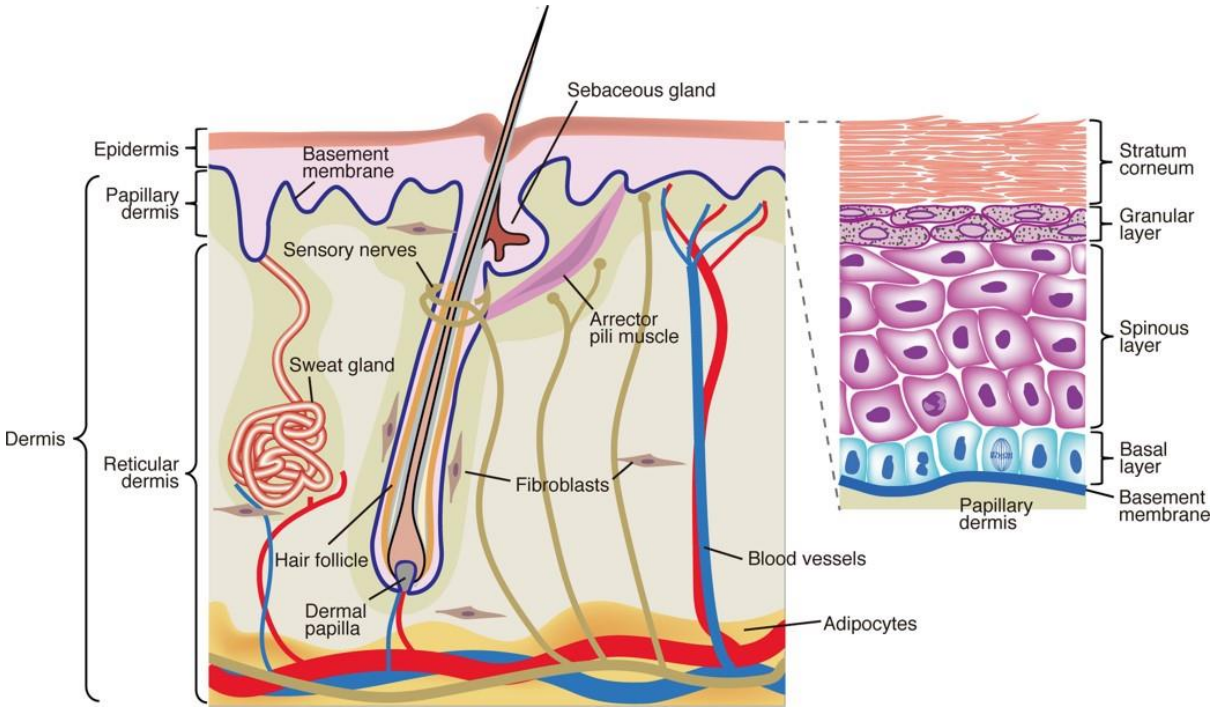

Figure 2.1: Architecture of mammalian skin

(Adapted from *Fujiwara* H. et al, 2018, *Dev Growth Differ.*) [53]

The dermis is derived from endoderm, which is mainly made up of connective tissue with an average thickness of about 1-2mm. The dermis is further subdivided into papillary layer and reticular layer that are separated by vascular plexus. The papillary layer is the cell rich layer

close to the epidermis, and mainly consists of fibroblasts and a fine network of collagen and elastin fibres. The reticular layer consists of thick bundles of collagen and elastin fibres that is present beneath the papillary layer. The dermis is highly traversed with nerves and blood capillaries, which is mainly involved in sensation and thermoregulation. The hypodermis (Subcutis) mainly consists of adipose tissue that anchors the skin to the underlying structures with the help of dense connective tissue strands that extend deep into hypodermis from the dermis [54-56].

2.2 The Epidermis

Epidermis is a stratified squamous epithelium that forms the outermost layer of the skin. During embryogenesis, the epidermis develops from the neuro-ectoderm layer of the embryo. Wnt and Bmp signalling play an important role during epidermal specification and differentiation of the ectodermal cells [57]. Three main cell populations that reside in the epidermis include keratinocytes, melanocytes, and Langerhans cells. Keratinocytes are the predominant cell type of epidermis, which are constantly generated in the basal layer that goes through maturation, differentiation and migration to the surface. The thickness of the epidermis varies from about 0.05–1 mm depending on body part.

2.2.1 The Epidermis development and stratification:

In vertebrates, the epidermis originates from embryonic surface ectoderm, which is a simple epithelium expressing cyto-keratins K8 and K18 [58]. The formation of epidermis is a sequential multistage process, which includes different steps such as epidermal specification and commitment, proliferation, stratification and terminal differentiation. In mice, the development of epidermis starts during the embryonic day E8.5, where the surface ectoderm develops into the epidermal basal layer by replacing the expression of K8 and K18 with keratin 5 (K5) and keratin 14 (K14), which is known as epidermal commitment [59]. The

basal layer then undergoes asymmetric cell division and forms an intermediate layer [59, 60]. The cells of intermediate layer undergo proliferation and maturation to form spinous layer expressing keratin 1 (K1) and keratin 10 (K10) [60]. Subsequently, the cells of spinous layer continue to undergo differentiation, maturation and migrate upwards to form involucrin and transglutamase positive granular layer. These cells further rearrange their cytoskeletal networks, become flattened and terminally differentiate to form the filaggrin and loricrin expressing cornified cell layer (Figure 2.2) [61-63]

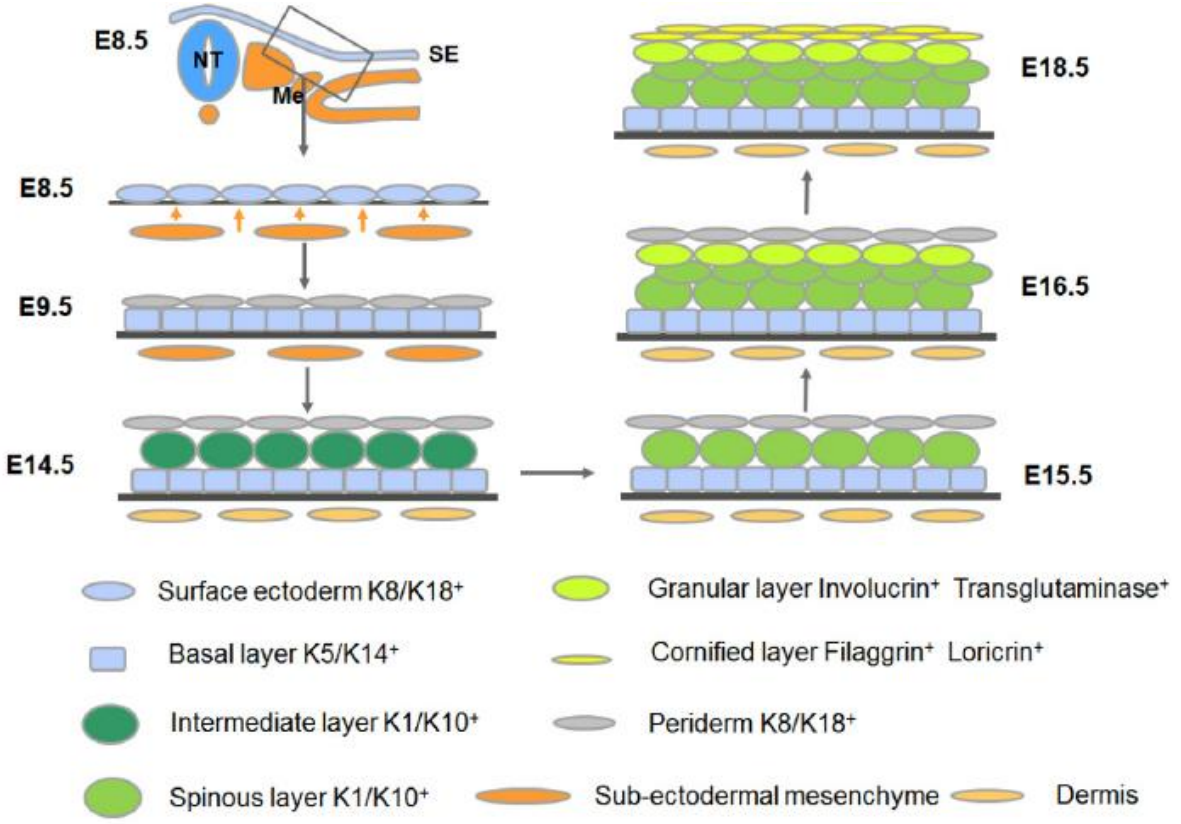

Figure 2.2: Epidermis development and stratification

(Adapted from Liu s. et al, 2013, Int J Mol Sci.)[64]

The sequential process of mouse epidermal development and stratification is represented. The surface ectoderm develops into basal layer of epidermis, which consequently gives rise to different layers of the epidermis. The different layers of epidermis are labelled in color and

their specific markers are represented. E-embryonic day, NT- nural tube, Me-mesoderm, SE-surface ectoderm (Sometime small letter while some capital)

2.3 Epidermal compartments of the skin:

The human and mouse skin epidermis contains various appendages such as hair follicles (HF), inter follicular epidermis (IFE), sebaceous glands (SG) and sweat glands. Importantly, the HF, IFE and SG are well studied with respect to their own resident stem cells (SCs) population that are involved in their regulation and to maintain tissue homeostasis [62, 65-67]. . The role of the individual compartment and different SCs pool in the regulation of the skin homeostasis is described below.

2.3.1 The interfollicular epidermis (IFE) and IFE stem cells:

The stratified squamous epithelial region of the epidermis located between the orifices of the periodically spaced HFs is called as interfollicular epidermis (IFE). The different layers of the IFE include the stratum basale (basal layer of epidermis attached to basement membrane), stratum spinosum, stratum granulosum, and stratum corneum (Figure 2.3) [68]. The estimated epidermal turnover time in mice is about 8-10 days [69]. The constant turnover of the IFE is maintained by the SCs that reside in the basal layer. The SCs present in the basal layer undergo asymmetric cell divisions giving rise to a committed suprabasal cell and a proliferative basal cell [70, 71]. During early epidermal development (E12.5), the basal layer cells within the single layered epidermis divide laterally within the plane of the epithelium (symmetrical) i.e. cell divisions are parallel to the basement membrane. However, on the onset of epidermal stratification, the number of parallel divisions decrease and consequently the number of basal cells undergoing perpendicular (asymmetrical) cell divisions increase giving rise to suprabasal layer cells [70].

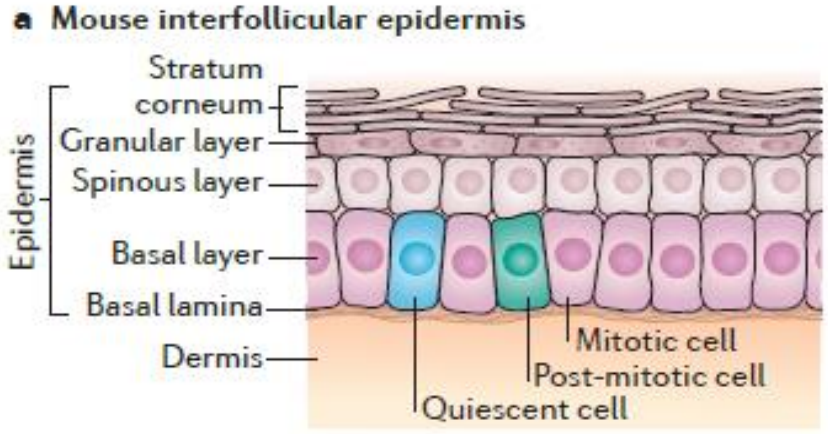

Figure 2.3: Different Layers of the mouse epidermis

(Adapted from Solanas G et al, 2013, Nat Rev Mol Cell Biol.)[18]

2.3.1.1 IFE stem cells:

It has been a long debated topic, as to whether there exists a single or two different stem cell populations in IFE that are involved in skin homeostasis. Two seemingly opposite theories have been proposed to explain IFE homeostasis. Based on morphological and proliferation studies, some studies have proposed that the IFE is organized into discrete 'epidermal proliferative units' (EPUs), comprising of slow-cycling SCs together with around 10 transit-amplifying cell progeny, which undergo terminal differentiation after a fixed number of cell divisions[69, 72]. The existence of EPUs was further supported by lineage tracing experiments. Mackenzie in 1997, had sub-epidermally injected retrovirus expressing LacZ into mice and showed the presence of discrete columns of blue cells from the basal cells to the most differentiated uppermost layer of cells demonstrating the existence of EPUs in the basal IFE [73]. Further, Clayton et al, in 2007, suggested that IFE is maintained by a single progenitor cell population based on the quantitative analysis of lineage tracing data in the IFE of Ah*cre*^{ERT}: R26EYFP$^{/EYFP}$ reporter mice[74]. These progenitor cells undergo both symmetric and asymmetric divisions randomly to ensure epidermal homeostasis [74, 75].

However, recent reports dismiss the notion of existence of one SC population in IFE. Studying the proliferation dynamics and analysis of clonal fate data in mouse tail skin using $K14^{CreER}$ (long term SCs) and Inv^{CreER} (short term SCs) systems, the existence of two distinct cell populations in IFE, i.e. a slow cycling SC and a more rapidly proliferating CP cell population was well demonstrated [76]. In this model the two cell populations were interdependent and the $K14^{CreER}$ SCs were the source of the Inv^{CreER+} progenitors. Further, a recent study by using H2BGFP pulse-chase experiment identified two different SCs populations within IFE. One subpopulation termed as LRCs (express Dlx1), which divide at a slower rate and retain the GFP label, whereas the other subpopulation that divide rapidly lose their GFP label, which are termed as non-LRCs (express Slc1a3). The LRCs comprises of ~35% and non-LRCs are ~65% of the total basal layer cells [77]. The detailed molecular profiling of these subpopulations demonstrated that the LRCs and non-LRCs are molecularly distinct and represent two separate SC populations**.** Importantly, these subpopulations are spatially segregated within the basal layer, which are involved in the homeostatic process as well as contribute to epidermal regeneration during injury [77]. Furthermore, the Lgr6+ stem cells were also reported to be involved in IFE homeostasis [78].

2.3.1.2 Signalling during epidermal stratification:

The mouse epidermis is one of the most rapidly regenerating tissues and turns over every 7–10 days [69]. The epidermis is constantly renewed in order to maintain its barrier function. Epidermal stratification requires a series of coordinated events, which regulate proliferation and differentiation of the basal keratinocytes. The transcription factor p63 plays a pivotal role in epidermal development during embryogenesis as well as its maintenance in adult animal [79]. Expression of p63 by the surface ectoderm is a crucial step in the epidermal fate specification [80] and epidermal stratification. The surface ectoderm of mice lacking p63 fails to adopt an epidermal fate, and therefore stratification and barrier formation are absent.

As a consequence, mice lacking p63 are born with a single layer of ectodermal cells covering their bodies and die shortly after birth due to dehydration [79, 80]. The TAp63α (p63 containing p53 like trans-activating domain) is expressed prior to K14 expression, and regulates the expression of transcription factor AP-2γ which in turn regulates the expression of K14 [79, 81]. Additionally, ΔNp63 is required for the maintenance of K14 expression in the basal layer [82]. Further, ΔNp63α plays a dual role in the basal keratinocytes, where it is required for the proliferation of basal keratinocytes and also plays an important role in their differentiation. ΔNp63α maintains the proliferation within the basal keratinocytes by inhibiting P21 and 14-3-3σ (genes induced during epidermal differentiation) [83, 84]. Additionally, ΔNp63α, in cooperation with Notch, induces K1 expression in the intermediate layer and results in formation of spinous layer. These spinous layer cells further undergo maturation and with draw from the cell cycle. Mice lacking ΔNp63α fail to express K1 and do not withdraw from cell cycle [85]. In continuation, the formation of spinous layer is also regulated by various transcription factors such as interferon regulatory factor 6 (IRF6), 14-3-3σ, I kappaB kinase alpha (IKKα), and (OVO like transcriptional repressor 1) Ovol1 [85-88]. Unlike embryonic epidermis, the proliferating basal cells directly differentiate into post mitotic spinous keratinocytes upon initiation of terminal differentiation. Notch signalling plays an important role in blocking the proliferation and initiating terminal differentiation. Inhibition of Notch 1 results in hyper-proliferation of basal layer [89] and over expression of RBP-J, a downstream mediator of signaling through both Notch1 and Notch2, resulted in a dramatic decrease in the expression of spinous markers and the development of an extremely thin spinous layer [90]. Conversely, overexpression of NICD under the control of a K14 promoter resulted in an expansion of the spinous layer [90].

Further, Ca^{2+} plays an important role in the terminal differentiation of epidermis. An increasing gradient of extracellular Ca^{2+} concentration is present from the basal to the cornified layers both in utero, and in mature epidermis [91]. During terminal differentiation, the PKC proteins (PKCα, PKCη) function specifically during the transition from spinous to granular cells by contributing to the downregulation of K1 and K10 expression [92, 93]. In addition, PKC activation induces expression of loricrin, filaggrin, and transglutaminase that are markers of granular keratinocytes. Furthermore, mice lacking the Ca^{2+}-sensing receptor display reduced loricrin and filaggrin expression, suggesting its role in the formation of the granular layer [94]. The final step in the epidermal stratification is the formation of epidermal barrier. The transcription factor kruppel like factor 4 (Klf4) is expressed in the upper spinous layer and granular layers that plays an important role in barrier formation [95]. Mice lacking Klf4 develop normal basal and spinous layers, but fail to form a proper barrier owing to the formation of immature cornified envelops [95]. In contrast, ectopic expression of Klf4 under K5 promoter in the basal layer resulted in accelerated formation of the epidermal barrier [96]. Additionally, grainyhead like epithelial transactivator (Grhl3/Get1), a transcription factor, is also involved in epidermal barrier formation. Though mice lacking Grhl3/Get1 express normal levels of loricrin, filagrin and involucrin; however, epidermal barrier defects were observed due to defects in lipid metabolism and cell adhesion [97].

2.3.2 The sebaceous gland:

Sebaceous gland (SG) is a holocrine gland and is a component of pilosebaceous unit. The SG development starts during the 5^{th} stage (bulbous peg stage) of HF morphogenesis from the Lrig1+ SCs [98]. The MTS24+ and Lgr6+ SCs of the isthmus and Lrig1+ SCs of the junctional zone (JZ) was reported to contribute to the maintenance of the SG [78, 99, 100]. The SG is connected to the JZ, which lies below the infundibulum and above the isthmus

region of the HF. The basal layer of the SG is continuous with the outer root sheath of the HF and mainly consists of proliferative cells.

The sebocytes undergo different stages of maturation at discrete zones within the SG. There are three different zones in the SG; the peripheral zone, maturation zone and necrotic zone (Figure 2.4). The peripheral zone consists of single layer of basal keratinocytes, which opens into maturation zone that consists of enlarged sebocytes containing lipid droplets [101]. As the maturation of the sebocytes continues they progressively accumulate lipids that are driven towards necrosis zone (degradation zone) at the centre of SG. In the necrosis zone, fully matured sebocytes with pyknotic nuclei, undergo lysis resulting in the secretion of sebum into hair canal through a excretory duct of SG [102].

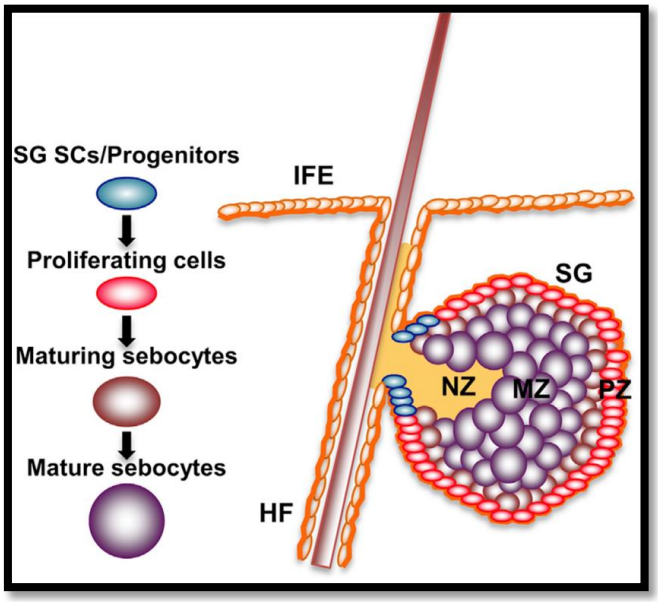

Figure 2.4: Different zones of the sebaceous gland

(Adapted from Yosefzon Y. et al. 2018, Mol Cell.) [103]

The sebaceous gland is an epidermal appendage located above the bulge region in the pilosebaceous unit. Different zones within the lobule of the SG are represented by different colour coding. SG: sebaceous gland, HF: Hair follicle, IFE: Inter follicular epidermis, PZ: Proliferating zone, MZ: Maturation zone, NZ: Necrotic zone.

The blocking of canonical Wnt signalling activity in stem and progenitor cells is an important pre-requisite to sebocyte cell specification and SG formation [104]. In mice expressing a dominant-negative Lef1 (ΔNLef1) (Wnt signalling inhibition) under the control of keratin 14 promoter (Basal layer & ORS promoter), SGs develop at the expense of HFs [105]. In contrast, expression of TCF3 (Wnt signalling mediator) in mouse epidermis inhibited sebocyte transcriptional regulators and SG formation *in vivo* [106]. Further, Blimp1 was shown to regulate sebocyte proliferation and SG homeostasis by suppressing c-Myc expression. Either conditional knockout of Blimp1 or activation of c-Myc in mice epidermis resulted in enhanced sebocyte proliferation, SG hyperplasia and excess production of sebum [107, 108]. Recently, Feldman et al. in 2019 have shown that isolated Blimp1+ cells from mouse are capable of generating SG organoids that constitute all the features of SG *in vivo* [109].

2.3.3 The hair follicle:

Hair follicle (HF) is a complex mini-organ of the skin, which is formed by neuroectodermal-mesodermal interaction [110]. The HF is divided into two regions; the upper permanent region (constant/ non-cyclic region) of the HF, which does not regenerate during the HF cycle while the lower temporary region (cyclic region) regenerates itself during every HF cycle that vary in the length depending on the stage of the HF cycle [12, 68]. The permanent region of the HF includes the infundibulum, isthmus and bulge regions. The infundibular region comprises of the portion of the epidermal invagination up to the sebaceous duct opening. Isthmus is the area between the sebaceous duct opening and the bulge. The bulge region (consists of multipotent HFSCs) is the area of the follicle marked by the insertion of arrector pili muscle (Figure 2.5A).

The different segments of the HF permanent region have their own resident SCs that are involved in tissues homeostasis [111]. The infundibulum region of the HF consists of Lrig1+

SCs. The upper region of the isthmus called as junctional zone, consists of Lrig1+ SCs, which contribute to the sebaceous gland and interfollicular epidermal homeostasis [100]. The isthmus, which forms the lower portion of the upper pilosebaceous unit, contains multiple partly overlapping populations of cells expressing Lgr6, Plet1/Mts24, and Lrig1 [78, 99]. The bulge region of the HF consists of multipotent HFSCs marked by CD34, α6-Integrin, Lgr5, Sox-9 and K15 [112-114]. Finally, the cyclic region of the HF extends from the bulge region to the base of the follicle. This segment includes the hair bulb, which contains the follicular matrix surrounding dermal papilla (DP). The matrix keratinocytes in the hair bulb, proliferate to form the hair shaft (HS) of growing hair [115-117].

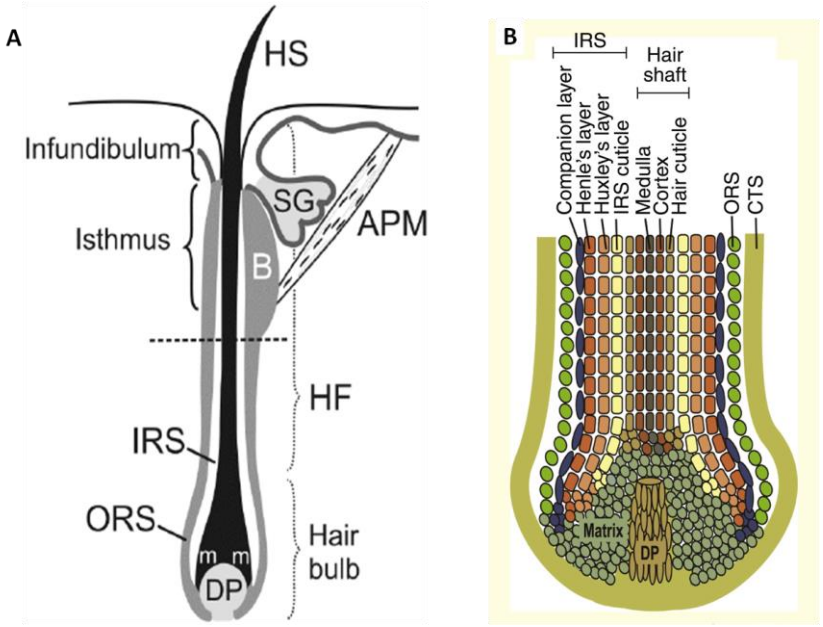

Figure 2.5: A. Hair follicle anatomy B. Different layers of Hair follicle

A. (Adapted from Rishikaysh P et al. 2014, Int J Mol Sci.)[118]

B. (Adapted from Schneider M et al. 2009, Curr Biol.)[119]

A. Different regions of the hair follicle are represented. Hair shaft (HS), dermal papilla (DP), sebaceous gland (SG), Bulge (B), arrector pili muscle (APM), matrix (m), the dashed line seperates the upper permanent and lower cycling regions of hair follice (HF).

B. Schematic drawing illustrating the concentric layers within different layers of HF. outer root sheath (ORS), inner root sheath (IRS), connective tissue sheath (CTS).

The HS consists of an inner core known as the medulla, which is surrounded by the cortex (middle layer) and outer cuticular layer. The hair shaft is encased by inner root sheet (IRS), which consists of cuticle (inner), huxley (middle) and henley's (outer) layers. Finally, the HS and the IRS are enclosed by outer root sheath (ORS) which is continuous with the basal layer of the epidermis (Figure 2.5 B) [119-122].

2.3.3.1 Hair follicle morphogenesis:

HF morphogenesis in mice starts at embryonic stage E14.5. The development of HFs involves a sequential series of epithelial-mesenchymal cell interactions through molecular cues [110]. The different phases of morphogenesis are categorised into: a) induction, b) organogenesis and c) cyto-differentiation. In the induction phase, Wnt β-Catenin signal arising from mesenchymal cells directs the overlying epithelial cells to form hair placode [123, 124]. During the organogenesis phase, a complex interchange of signals between the epithelial and mesenchymal cells occurs. The epithelial cells now direct the dermal cells to undergo proliferation and to change their orientation to form a dermal condensate which later forms the dermal papilla (DP). Fibroblast growth factor (Fgf) and sonic hedgehog (Shh) signalling was shown to play a prominent role during organogenesis [125, 126]. Dermal Shh signalling up regulates the expression of Noggin that counteracts Bmp mediated Wnt signalling inhibition thereby promoting the HF growth [126]. Further, loss of SHH expression during HF morphogenesis results in arrest of HF growth at the placode stage and the underlying dermal cells fail to mature and condensate to form DP suggesting the role of SHH in the epithelial-mesenchymal crosstalk, cell proliferation and DP functions [127, 128]. Additionally, transforming growth factor-β2 (TGF-β2) through activation of transcription factor Snail regulates the epithelial cell proliferation, junctional remodelling and bud

formation, which helps in proper progression of hair morphogenesis [129]. The hair placode upon receiving these growth signals from the DP, grow downwards into the dermis by first forming a hair peg and then a hair bulb eventually enveloping the dermal papilla. The matrix of the growing HF contains lineage-restricted precursor cells located around the DP [130].

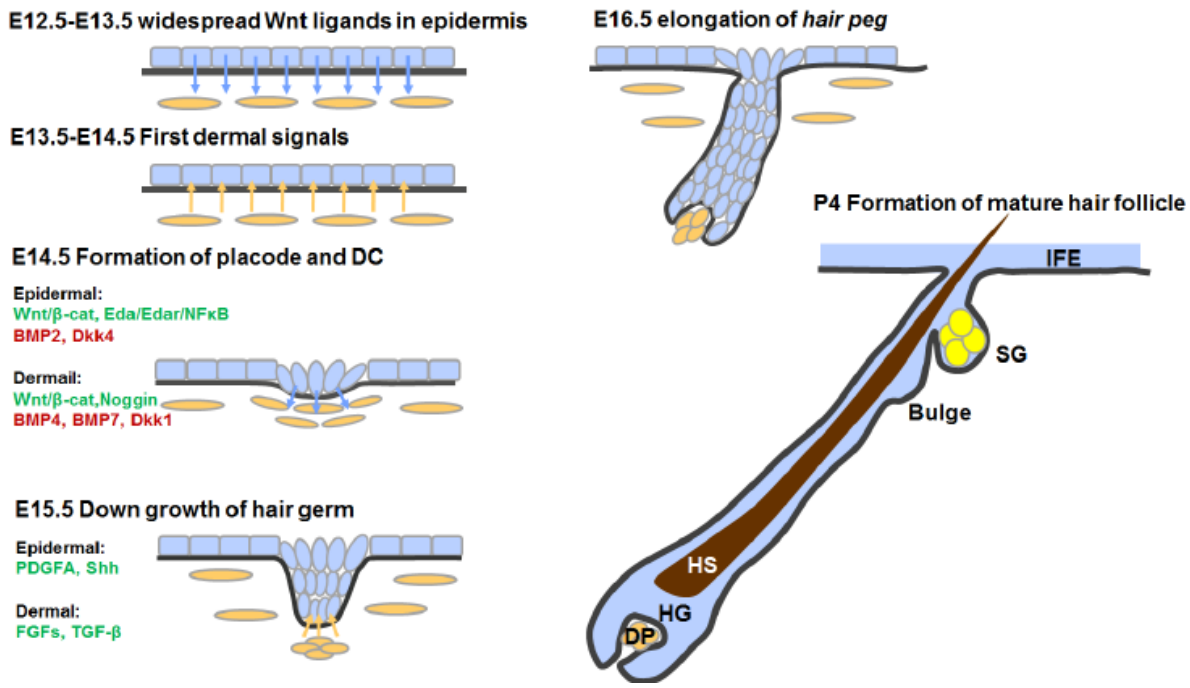

Figure 2.6: Stages of hair follicle morphogenesis

(Adapted from Liu S et al, 2013, Int J Mol Sci.) [64]

The process of the hair follicle morphogenesis starts from the embryonic day E12.5 and continue till first postnatal week. Different stages of the hair follicle morphogenesis are represented along with the signalling molecules involved. (IFE- inter follicular epidermis, SG- sebaceous gland, DP- dermal papilla, E- Embryonic day, P- Postnatal day, Bu- bulge, HS- Hair shaft, HG-hair germ)

In cyto-differentiation stage, Reciprocal signalling between the epidermal progenitor cells in the matrix and DP cells leads to the activation of the differentiation program, which eventually leads to the formation of the six layers of fully grown HF (IRS & HS), creating concentric rings of differentiated cell types [110, 119]. Bone morphogenic proteins (Bmp's)

and Bone morphogenic protein receptor 1A (Bmpr1a) play important roles in HF differentiation [120]. Bmpr1a is crucial for the differentiation of progenitor cells of the IRS and HS. Bmp4 binds Bmpr1a that activates Gata3 thereby promoting the differentiation of IRS progenitor cells [120]. Further, transcription factor Dlx3 upregulates Hoxc13 and Gata3 transcription factors, which regulate HS and IRS differentiation [131]. Additionally, Sox-2 regulates the expression Bmp6, which in turn is involved in regulating hair shaft progenitor cell differentiation and migration [132]. The morphogenesis completes with the formation of the completely differentiated IRS layers and the formation of the complete hair shaft that emerges from the follicle [133].

2.3.3.2 Hair follicle stem cells (HFSCs):

The stem cell niche is the "specialized tissue compartment that hosts the SCs and every other component necessary for their proper function, including neighbouring cell populations, molecular signals and other extracellular components"[8]. In case of HF, HFSCs are located in the bulge region of the follicle below the sebaceous gland within the permanent region of the follicle. The bulge region of the HF as the HFSCs compartment was first reported in 1990 by Cotsarelis and colleagues. Pulse chase experiments was performed by subcutaneously injecting tritiated thymidine ([^{3}H]TdR) into new born mice (PD2-PD7) that labelled almost 100% of nuclei in mouse epidermis, hair follicles, and sebaceous glands as well as fibroblasts and endothelial cells. Further, these mice were chased for a period of 4 weeks to identify the slow cycling label retaining cells (LRCs). The results showed that the rest of the epidermal compartments (IFE, SG, infundibulum & isthmus) lost their [^{3}H]TdR label. However, the label was retained in the bulge region of HF suggesting the presence of slow cycling SCs within this region [134]. Later, Taylor et al. in 2000, performed the bromo-deoxyuridine (BrdU) pulse chase experiments confirming the presence of slow cycling LRCs in the bulge region of the HF[135]. Importantly, Tumbar et al., in 2004 adapted a new system to label the

LRCs i.e. they have crossed transgenic mice that express green florescent protein (GFP) tagged Histone-2B (H2B-GFP) regulated by tetracycline responsive regulatory element (TRE-mCMV-H2B-GFP) along with mice expressing Keratin-5 (K5) promoter driven tet-repressor VP16 transgene. After doxycycline treatment only the cells in the bulge region were able to retain the GFP Signal. Further, these H2B-GFP positive cells were identified to express high levels of a cell surface marker, CD34 [112, 136]. Importantly, molecular characterization of these LRCs within the bulge by different study groups, have identified various HFSCs markers such as Keratin 15 (K15) [137, 138], Sox-9 (SRY box9) [139], Tcf3 (T-cell factor3), Lhx2 (LIM/homeobox protein2) [104, 106, 140], NFATc1 (Nuclear factor of activated T-cells, cytoplasmic1) [141] and Axin-2 [142] and Lgr5 (Figure 2.7).

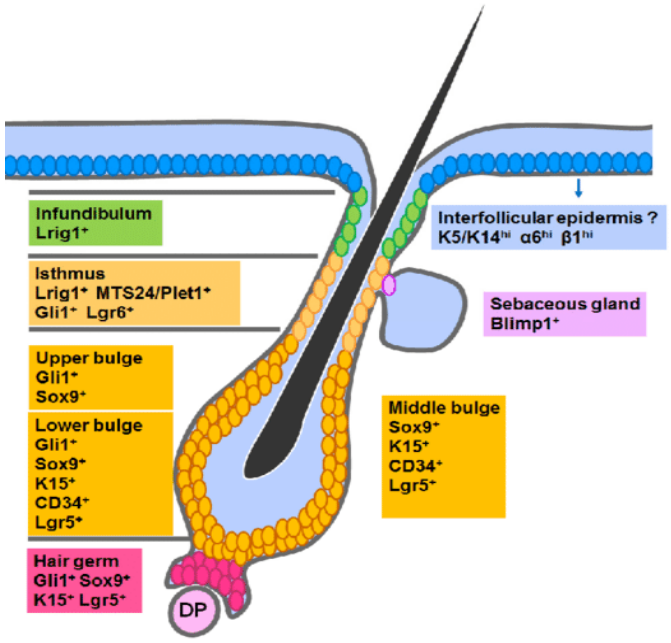

Figure 2.7: Different regions of hair follicle and their respective stem cells

(Adapted from Liu s. et al, 2013, Int J Mol Sci.)[64]

The image represents epidermal stem cell populations present within different hair follicle compartments. DP-dermal papilla, Hi-high, + positive

Importantly, Oshima et al. in 2001, reported the first study that discusses the stemness characteristics and multipotency of the HFSCs. They dissected the Rosa26 Lac-Z labelled bulge region and transplanted it into the unlabelled HF of the immune-deficient mice. These labelled bulge cells in the unlabelled HF were able to differentiate into cells of all the epithelial lineages that form the HF (ORS, IRS and hair shaft), SG and IFE [143]. Further, Morris et al. in 2004 used the lineage tracing approach by using Krt15 (keratin 15) specific promoter to drive the expression of the LacZ in the bulge region. The result showed that the bulge cells are capable of generating cells of all epidermal lineages consisting of HFs, SGs and IFE [135, 144]. More interestingly, Blanpain et al., in 2004, have shown that HFSCs can be FACS sorted and grown in *in vitro* conditions, which generate holoclones. Moreover, when the cells from holoclones are grafted into nude mice they gave rise to not only HFs and SGs but also epidermis, demonstrating that keratinocytes derived from individual bulge cells possesses the classical defining features of bona fide SCs [114]. However, the study from the Ito et al., in 2005, showed that the HFSCs does not contribute to the normal epidermal homeostasis but rather migrate and contribute to the wound re-epithelialization by generating transit (TA) amplifying cells [145, 146].

Jaks et al. in 2008, showed that the actively cycling cells of lower bulge expressed Lgr5 marker. These Lgr5 expressing lower bulge cells are multipotent in nature i.e. they are capable of giving rise to new HFs and maintain all epidermal cell lineages (bulge, hair germ, isthmus and SG) of the HF over long periods of time [147]. Further, Lim et al., in 2016, using lineage tracing experiments have shown that, autocrine Wnt signalling is active in the outer bulge cells throughout the hair cycle quiescence and growth, which helps in maintaining their stem cell potency. Further, ablation of Wnt signalling in the HFSCs using Axin2–CreERT2 (bulge specific promoter) causes them to lose their stem cell potency and undergo premature differentiation [142].

2.3.3.3 Hair follicle regeneration and hair cycling:

After HF morphogenesis, post-natal HFs have a distinct ability to undergo spontaneous cycles of regeneration throughout the lifetime of the organism, which is commonly referred to as “hair cycle”. The hair cycle consists of three discrete phases namely anagen (growth phase), catagen (regression phase) and telogen (resting phase) (Figure 2.8) [11, 12]. Further, a fourth phase has been recognised known as exogen phase, where shedding of the club hair occurs [148]. In mice the hair cycle lasts for about 28 days and given the life time of mice is about 2 years, there occurs around 15-20 hair cycles on an average in a life time of mice. During the initial HF formation, i.e. HF morphogenesis, the downward growth of the follicle matrix cells is complete by post-natal day 8 (PD8) and the matrix cells proliferate and differentiate into the six layers of the IRS and HS during the next 6-7 days. At PD15, the proliferation of matrix cells ceases and the HF enters into a regression phase (catagen), where matrix cells and hair bulb undergo extensive apoptosis for the next 3-4 days. The DP is drawn upward and comes to rest just below the bulge [11]. The HF enters the first telogen at PD19 that lasts for two to four days depending on the genetic background of mice [12].

The first anagen of the adult hair cycle starts at around PD21 that can be divided into six different sub-phases (anagen I to VI) [150]. During anagen I, the HF is similar to telogen phase follicle but cells at the bottom of the HF i.e., hair germ starts proliferating. In anagen II, the DP is enlarged with more than half of DP is covered by proliferating keratinocytes of the growing hair matrix. The developing hair bulb and the DP are located at the border between the dermis and the subcutis. The anagen III is further subdivided into 3 phases; anagen IIIa, anagen IIIb and anagen IIIC. In anagen IIIa, the proliferating matrix cells forms the hair bulb. The matrix cells start differentiating and form a cone of keratinized cells (IRS cone) above the DP. During this stage, Melanin granules start to appear in the matrix cells and the hair bulb still resides at the border of dermis and sub-cutis.

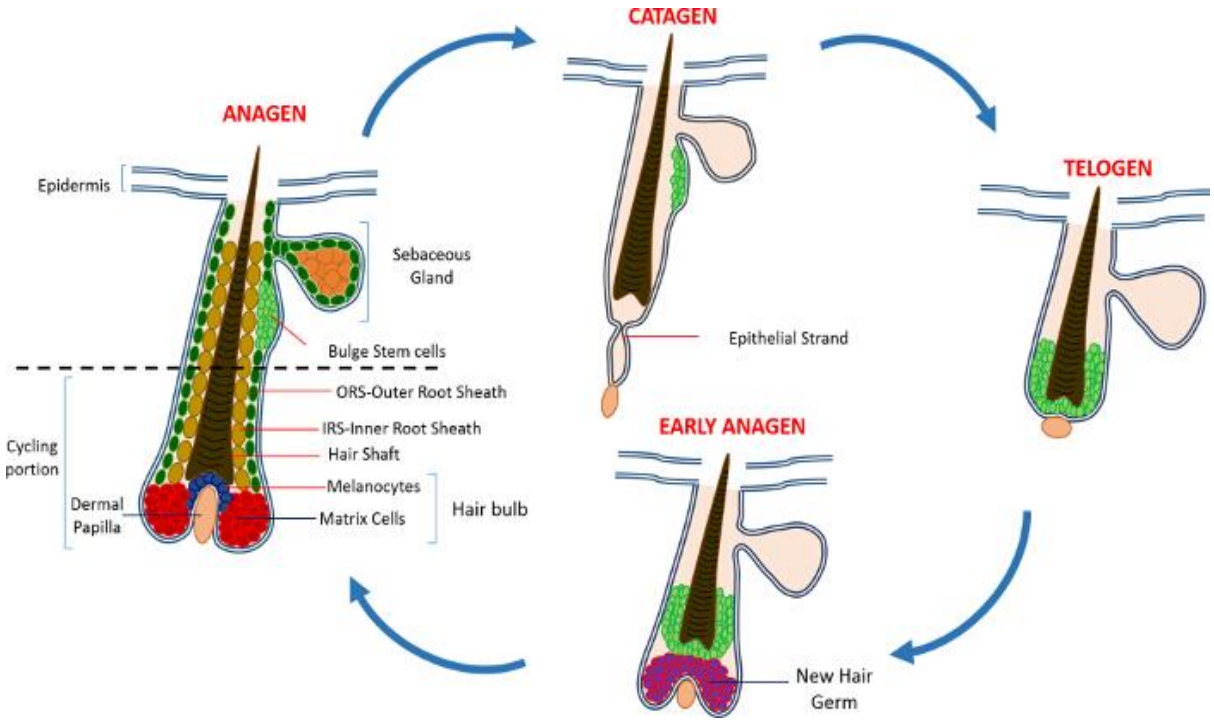

Figure 2.8: The hair follicle cycle

(Adapted from Soteriou D. et al, 2016, J Vis Exp.) [149]

Hair follicle progresses through different phases of the hair cycle such as Anagen, Catagen and Telogen. The lower region of the follicle undergoes morphological changes while the upper region remains constant.

In anagen IIIb, the hair bulb enlarges and the matrix cell start differentiating into all the lineages of hair shaft and IRS. The length of the hair shaft reaches up to middle of the HF that is enclosed by IRS. The lower region of the HF and DP are in the middle of sub-cutis at this stage. During the anagen stage IIIc, the hair bulb grows to its maximum size/volume while the DP becomes thinner. The matrix cell differentiation continuous and the hair shaft grows up to the length of the follicle where SG is attached to the follicle, and is still enclosed by the IRS. At this stage, the HF bulb and DP are deep in the subcutis and above the panniculus cornosus (PC). During the stage IV, the DP further narrows down and the tip of the HS and IRS reach the hair canal. In the anagen V, the IRS growth development stops at the insertion

of SG in the HF. The tip of the HS enters the hair canal by the end of this stage. During the final stage of the anagen i.e. anagen VI, the HS tip emerges through the epidermis and the HF is fully developed [11]. The anagen phase is completed at around PD35 in the mouse back skin.

After a period of continuous active hair growth (anagen), proliferative potential of the matrix cells cease that no longer contributes to the growing HF (the differentiation of hair shaft and IRS ceases). This leads to the HF entry into the catagen phase or degenerative phase [151]. However, the exact mechanism that triggers the transition from anagen-to-catagen is not well understood. Different factors such as exhaustion of matrix cells proliferative potential, inhibitory signals from DP and other sources are speculated to fuel this transition [152-154]. During catagen, the follicular cells within the matrix and hair bulb undergo rapid apoptosis leading to regression of the hair bulb. The regressing matrix cells forms a narrow epithelial strand that retracts upwards. The DP becomes highly condensed (compact ball shape) that moves upward trailing at the tip of epithelial strand [151, 155]. As the epithelial strand gradually disappears through apoptosis, it pulls the DP towards the bulge region present in the permanent region of the HF. The cells from the ORS that survive the regression phase home back to the niche forming, at least in part, the new hair germ [156]. At the end of the catagen, the ORS cells forms a new bulge which retain the newly synthesized club hair shaft, while the old bulge maintains the previously formed hair shaft. Once the old club hair shed off the older bulge gradually disappears. The shedding of the older club hair is now recognised as a new phase of hair cycle called as the exogen phase. The time required for the progression of the HF in the anagen and catagen phases is similar for all the hair cycles; however, the telogen phase gets extended that become longer in the subsequent hair cycles [148, 157-159].

The last phase of the murine hair cycle is a resting phase known as the telogen phase. During this phase, the activity of the HFSCs ceases, the growth of the hair shaft is terminated and dermal papilla is in close contact with the bulge. Importantly, signalling molecules such as Bmp (Bmp4, Bmp6), Tgf-β and Fgf (Fgf-8) ligands as well as Wnt inhibitors, secreted by the dermal papilla or from the inner bulge act collectively to maintain quiescence of HFSCs in the niche during the telogen phase [160, 161]. Further, recent study has identified two stages of the telogen phase. The initial phase where the induction for the new anagen onset is inhibited is known as refractory telogen; whereas, the later stage when HFSCs responds to the activating signals from the HFSCs niche is known as competent telogen [160, 162].

2.3.3.4 Proliferation dynamics of the HFSCs:

Tissue homeostasis is governed by the adult/tissue SCs, which undergo proliferation and give rise to TA cells or committed progenitors (CP) that further divide and differentiate into multiple lineages of cells of the tissue [9]. SCs divide during the tissue regeneration throughout the life of an individual; hence, there is a possibility of accumulation of mutations within these cells, which can lead to cancer [163]. Multiple hypotheses have been put forward in the past few decades as to how SCs prevent accumulation of mutations. One of the earliest hypothesis put forward by Cairns et al., in 1975 is the asymmetric DNA segregation called as "immortal strand hypothesis" in which the template DNA strand is retained within the SCs pass on the newly synthesized copy to the short-lived non-stem cell daughter [164]. This hypothesis was proven to be true in muscle SCs and neural SCs using two different DNA labels (bromo-deoxyuridine [BrdU], chloro-deoxyuridine [CldU], and iodo-deoxyuridine [IdU]) during two subsequent rounds of replication [165, 166]. On the contrary, different studies showed that many adult tissue SCs divide symmetrically but minimize the introduction of the replication errors by maintaining the quiescent state within the niche [167-

172]. . Skin is one of the highly regenerative tissues, which has an epidermal turnover rate of 7days on an average [173]. It was reported that bulge LRCs has high proliferative potential *in vitro.* However, it is not clearly understood as to how these HFSCs maintain their label *in vivo* i.e. how the quiescent HFSCs pool is maintained. Whether, all the HFSCs divide with same frequency upon activation? Waghmare et al., in 2008 used a novel strategy to count the SCs division in unperturbed mouse skin tissue. They used pTRE-H2BGFP: K5tTa double transgenic mice (Tet-Off) system to visualize the sequential HFSC division mediated serial dilution of H2BGFP (Figure 2.9). This study demonstrated that the SCs within the HFSC niche divide infrequently to preserve the SC genomic integrity (~3 times on average/ hair cycle). Further, by performing BrdU pulse chase experiments in mice they have shown that the chromosomes segregated symmetrically between bulge cell daughters at each division. Collectively, this study explains that the HFSCs undergo random segregation of chromosomes thereby suggesting that all the HFSCs do not participate equally during normal homeostasis thereby maintaining genome integrity in the reserved SC pool [174-176].

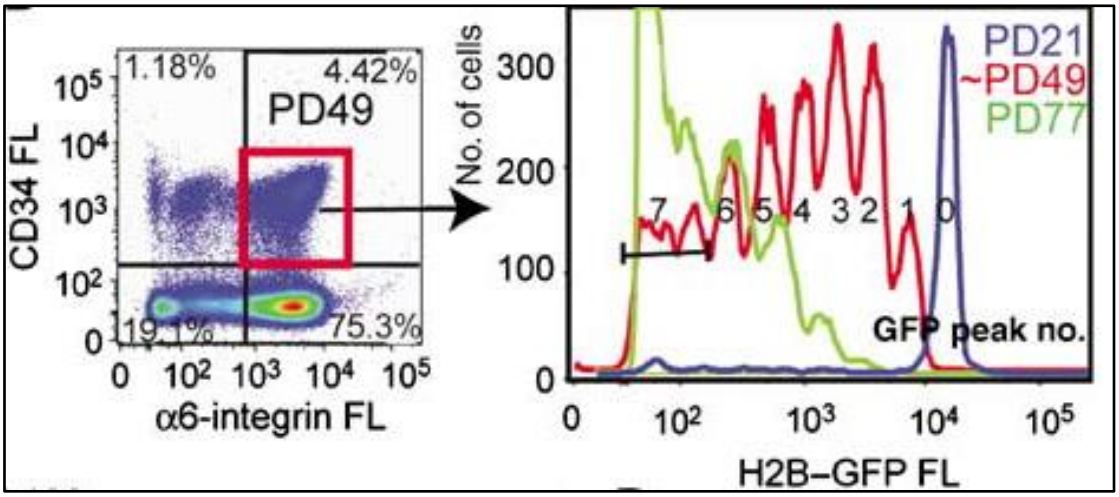

Figure 2.9: Serial dilution of H2BGFP signal with each stem cell division

(Adapted from Waghmare et al., 2008, EMBO) [174]

The double transgenic mice (H2BGFP: K5tTa) were chased using doxycyclin for different time points and the HFSCs were separated by using stem cell markers - CD34 and α6-

integrin (on left), which were later separated into different peaks based on GFP intensity (on right). PD21 (no chase, blue), PD49 (4-weeks chase, red) and PD77 (8-weeks chase, green).

2.4 Signalling pathways in HFSCs Regulation:

Mammalian skin protects the living organisms against different environmental insults such as UV irradiation, microbes and toxic chemicals etc. SCs play a vital role in skin homeostasis which is crucial for the survival of the organism. Amassing evidence from the past few decades have shown that multiple signalling pathways play a prominent role in the epidermal development, HF formation, HFSCs regulation and skin homeostasis [177-180]. These signalling pathways include Wnt, Shh, Bmp, Tgf-β and Notch etc. which are described in detail here under.

2.4.1 Wnt/β-catenin signalling and HFSCs:

Wnt signalling is an evolutionary conserved pathway, which is mediated through secreted hydrophobic glycoproteins called as Wnt ligands (Wnts) and their respective frizzled receptors (Fzd) and co-receptors such as low-density-lipoprotein-related protein5/6 (LRP5/6) [181, 182]. Wnt signalling plays an important role in cell proliferation, cell migration, cell polarity, cell fate determination and in SCs self-renewal and maintenance during embryogenesis as well as in adult tissue homeostasis [183, 184]. Wnt signalling is broadly classified into the canonical and the non-canonical pathways. In canonical pathway, binding of the Wnt ligands to the extracellular FZD receptor leads to the destabilization of destruction complex (Axin, GSK-3β, APC & CKII), which phosphorylates and targets β-catenin to ubiqitin mediated proteasomal degradation. This stabilises the β-catenin which accumulates in the cytoplasm. Further it translocates into the nucleus where it regulates the expression of various Wnt target genes (Figure 2.10). The non-canonical pathways include the planar cell

polarity pathway (PCP pathway) and the Wnt Ca^{2+} pathway. The PCP pathway plays a crucial role in polarizing epithelial cells within the plane of a tissue and control directed cell migration events through regulation of the actin cytoskeleton [185]. PCP pathway activates either Rho associated kinase (ROCK) or Rac1/JNK leading to actin polymerization and cytoskeleton remodelling [186]. The Wnt Ca^{2+} pathway is involved in maintaining the intracellular Ca^{2+} levels and also regulates the Canonical Wnt pathway. Further, Wnt/Ca^{2+} pathway is important in the development of dorso-ventral polarity during the embryonic development by regulating canonical Wnt β-catenin signalling [187].

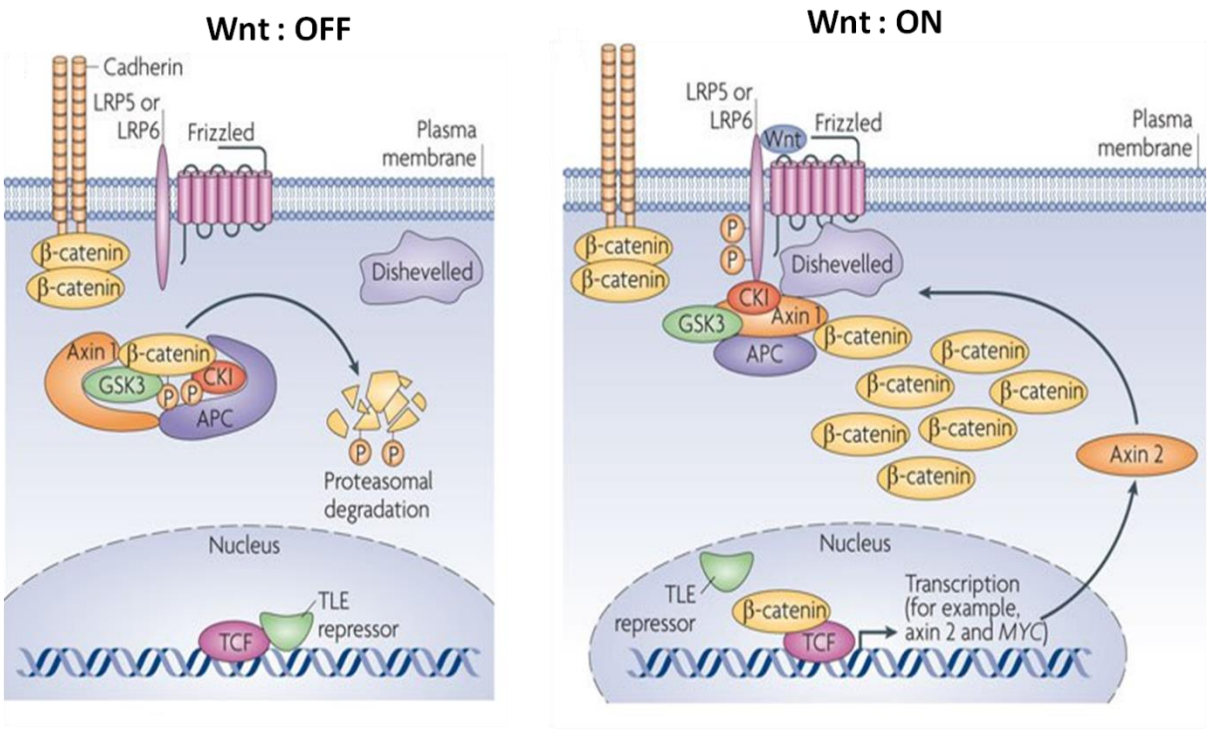

Figure 2.10: Wnt signalling pathway

(Adapted from McNeill H.et al. 2010, Nat Rev Mol Cell Biol.)[188]

Absence of Wnt ligand results in destruction of β-catenin through destruction complex mediated phosphorylation and proteasomal degradation. Binding of the Wnt ligands to the receptor stabilizes β-catenin in the cytoplasm that further translocates into the nucleus and initiates expression of the Wnt target genes.

Wnt signalling is involved in epidermal stratification, HF morphogenesis, hair cycling and HFSCs regulation. In the induction phase, Wnt β-Catenin signal arising from mesenchymal cells directs the epithelial cells to form hair placode [123, 124]. Loss of β-catenin or over expression of Wnt antagonist (Dkk1) blocked HF placode formation [123, 124]. Conversely, β-catenin over expression under K14-promoter results in *de-novo* HF morphogenesis during anagen [189]. Further, based on their expression during morphogenesis, Wnts are classified as primary Wnts (Wnts 3, 4 and 6) and secondary Wnts (Wnts 2, 7b, 10a and 10b). Primary Wnts are essential for HF initiation while secondary Wnts are involved in HF development [123, 190]. Further, during the hair cycling, it was shown that β-catenin activation in the bulge using K19Cre-ER (Bulge specific promoter) is sufficient to induce hair growth independently of mesenchymal dermal papilla-niche signals normally required for hair regeneration [191]. Loss of β-catenin expression in the bulge region during the anagen induction results in the HFs to remain in telogen phase without progressing into anagen [192]. Importantly, Wnt signalling inhibition either by deletion of β-catenin or over expression of DKK1 (a Wnt inhibitor) after anagen induction, results in HFs to rapidly cease proliferation and enter into premature catagen [192]. In contrast, to the earlier notion that Wnt signalling is active only at telogen-to-anagen transition and during anagen progression, Lim et al., in 2016, have shown that autocrine Wnt signalling is active in the HFSCs throughout the hair cycle even in telogen phase, which is involved in maintaining the stemness properties of HFSCs. Moreover, ablating Wnt signalling in the bulge cells causes them to lose their stem cell potency and undergo premature differentiation [142]. Taken together, all these studies indicate that the differential activity of the Wnt signalling is required for the regulation of almost all aspects of the HFSCs behaviour. Different components of the Wnt signalling regulating various processes during HF morphogenesis and hair cycle have been extensively

studied since last three decades. Major phenotypic observations of the genetically mutated mouse models are summarized in the below table.

Signals	Mutation type	Hair follicle phenotype	Reference
1. Wnt signalling componants			
Wnt3	*K14-Wnt3*	Reduced hair follicle length, premature catagen onset	Millar et al., 1999 [173]
Wnt7a	*K14-Wnt7a*	Increased hair follicle neogenesis upon wounding	Ito et al., 2007 [157]
Wnt5a	*Adenovirus-mediated Wnt5a expression*	Inhibits the telogen-to-anagen transition	Xing et al., 2013 [174, 175]
Wnt10b	*Adenovirus-Mediated Wnt10b Overexpression*	Induces Hair Follicle Regeneration	Yu-Hong et al., 2013 [176]
Dvl2	*K14-Dvl2*	Reduced hair follicle length, premature catagen onset	Millar et al., 1999 [173]
Dkk1	*K14-Dkk1*	Lack of placode formation	Andl et al., 2002 [103]
	K5rtTA; *TRE-Dkk1*	Lack of hair follicle neogenesis upon wounding	Ito et al., 2007 [157]
APC	*K14-Cre*; $APC^{fl/fl}$	Aberrant hair follicle growth, short, curly whiskers	Kuraguchi et al., 2006 [177]
Lef1	*Lef1 −/−*	Lack of body hair and whisker follicles	van Genderen et al., 1994 [178]
	K14-Lef1	Clustered hair follicles, irregularly angled shafts	Zhou et al., 1995 [179]
	K14-ΔNLef1	Suppressed hair follicle differentiation, enhanced sebocyte differentiation	Merrill et al., 2001 [84]
	K14-ΔNLef1	Progressive hair loss and cyst and tumor formation	Niemann et al., 2002 [85]

Signals	Mutation type	Hair follicle phenotype	Reference
β-Catenin	*K14-ΔNβ-catenin (constitutively active)*	De novo hair follicle induction	Gat et al., 1998 [169]
	K14-Cre; β-catenin$^{fl/fl}$	Lack of placode formation, loss of hair in the first hair cycle	Huelsken et al., 2001 [104]
	K5-S33Yβ-cateninER	Anagen induction and enhanced hair follicle proliferation	Van Mater et al., 2003 [180]
	K14-ΔNβ-cateninER	Anagen induction and de novo hair follicle formation	Lo Celso et al., 2004 [181]
	K14-ΔNβ-catenin (hemizygous)	Precocious bulge stem cell activation	Lowry et al., 2005 [182]
	K14-CreER^{tm}; β-catenin$^{fl/fl}$	Loss of bulge stem cell quiescence and maintenance	Lowry et al., 2005 [182]
	K14-CreER^{tm}; β-catenin$^{fl/fl}$	Lack of hair follicle neogenesis upon wounding	Ito et al., 2007 [157]
	K14-Cre; Ctnnb1$^{(ex3)fl/+}$ (dominant active)	Premature hair follicle placode development, predominant differentiation toward hair shaft, defects in hair follicle development	Zhang et al., 2008 [183]
	Cor-Cre (DP specific); Ctnnb1$^{fl/fl}$	Reduced hair follicle length and thinning	Enshell-Seijffers et al., 2010 [184]
	K15-ΔNβ-cateninER	Increased bulge proliferation and expansion	Baker et al., 2010 [185]
	ΔK5ΔNβ-cateninER	Ectopic hair follicle induction In sebaceous gland	Baker et al., 2010 [185]
	Axin2–CreERT2/β-cat$^{Δex2-6-fl/+}$	Loss of HFSC maintenance	Lim et al., 2016 [122]
	K19CreER;β-catenin flox$^{(Ex3)/+}$	Activation of HFSC and anagen induction even in absence of DP signals	Deschene et al., 2014 [171]
Tcf3/4	*K14-ΔNTcf3*	Suppressed epidermal differentiation	Merrill et al., 2001 [84]
	K14rtTA; TRE-mycTcf3	Lack of epidermal differentiation and sebaceous gland	Nguyen et al., 2006 [86, 186]
	K15CrePGR;TRE-mycTcf3	Over expression of TCF3 results in inhibition of telogen to anagen transition	Lien et al., 2014

Table 2.1 Role of Wnt signaling components in epidermal homeostasis

(Modified from Lee et al., 2012, Semin Cell Dev Biol)[193]

2.4.2 Bone morphogenic protein (BMP) signalling:

Bone morphogenic proteins belong to a subfamily within the TGF-β family [194]. Bmp signalling is mediated through the Bmp ligands and the type 1 (Bmpr1a and Bmpr1b) and type II (Bmpr-II) serine-threonine kinase receptors [195, 196]. Bmp ligands bind to heterotetrameric complex of type II and type I receptors, and repulsive guidance molecule (RGM) family proteins that serve as co-receptors [197, 198]. The type II receptor kinase phosphorylates the GS (glycine and serine-rich domain) domain of type I receptor, which is crucial in signal transduction. The activated Bmp receptor phosphorylates receptor-regulated Smads (R-Smad 1/5/8) that further binds to the common-partner Smad-4 (Co-Smad4) and then translocates into the nucleus, where they regulate target gene expression (Figure 2.11) [195, 199-201]. The secreted Bmp antagonists such as Chordin, Noggin, and Follistatin are the main regulatory molecules that prevent binding of the Bmp ligands to the Bmp receptor thereby regulating Bmp signalling activity [110, 202].

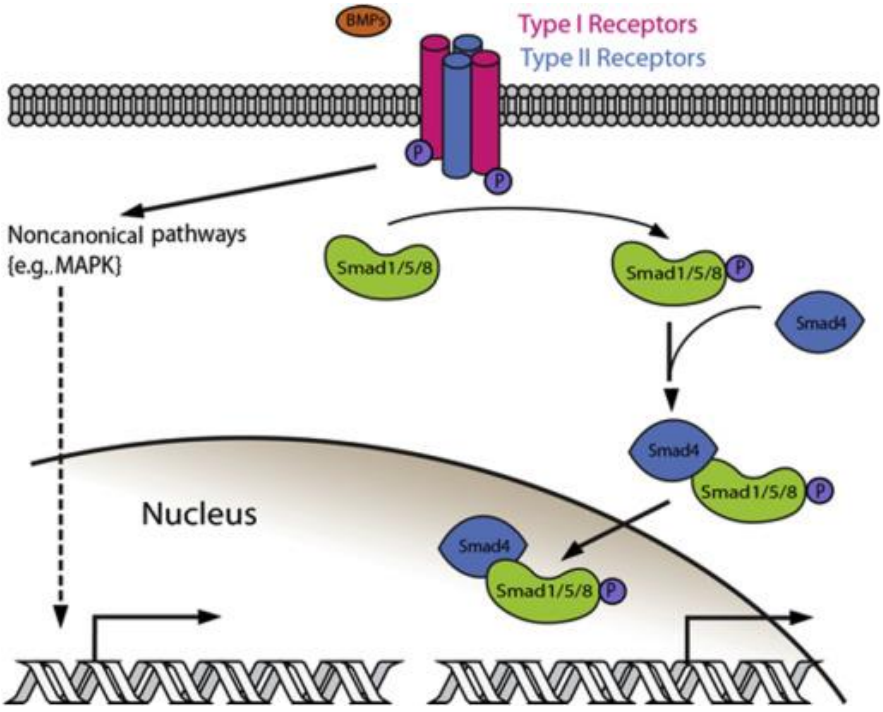

Figure 2.11: Overview of BMP signalling pathway

(Adapted from Cecchi S. et al. 2016, J Orthop Translat.)[203]

The pictorial representation of Bmp signalling pathway shows the binding of Bmp ligands to the type I and type II Bmp receptors, which further activates Smad1/5/8 transcription factors. The activated Smad1/5/8 then binds to Smad4 and translocates into the nucleus and regulates the expression.

In the mice skin, Wnt and Bmp signalling work antagonistically where, Wnt signalling provides activating signals and promotes proliferation of the HFSCs, while Bmp signalling provides the inhibitory signals which maintains the HFSCs in quiescence [160, 204, 205]. During the HF morphogenesis, inhibition of the Bmp by Wnt signalling is required for placode formation. Further, Bmp inhibition by dermal noggin results in HF downward growth and hair bud development through Shh activation [206, 207]. Bmpr1a is indispensible for progenitor cell differentiation within IRS and HS. Bmp4 binds Bmpr1a and activates Gata3 thereby promoting the differentiation of IRS progenitor cells [120]. Additionally, Sox-2 regulates the expression Bmp6, which in turn is involved in regulating hair shaft progenitor cell differentiation and migration [132]. Conditional loss of Bmpr1a results in impaired IRS and hair shaft differentiation in HFs [120, 208, 209]. Overexpression of the noggin under MSX2 promoter in the matrix cells inhibits matrix cell differentiation that is essential for the HS formation [210]. Further, inhibition of Bmp signalling in HFSCs is essential for telogen-to-anagen transition during hair regeneration by activating quiescent HFSCs [211].

2.4.3 Notch signalling:

Notch signalling is an evolutionarily conserved pathway involved in the regulation of cell proliferation, cell fate determination, differentiation and cell death [212, 213]. The Notch signalling is mediated through Notch receptors (Notch1-4) and ligands such as Jagged (Jagged 1&2 and Delta (Delta1-4) [214, 215]. The Notch pathway mediates juxtacrine

cellular signalling, wherein both the signal sending and receiving cells are affected. Notch receptors are single-pass transmembrane proteins composed of functional notch extracellular domain (NECD), transmembrane (TM), and notch intracellular (NICD) domains. Ligand binding to the receptor promotes two proteolytic cleavage events in the Notch receptor. The first cleavage (S2 cleavage) is catalysed by ADAM-family metalloproteases, whereas the second cleavage (S3 cleavage) is mediated by γ-secretase. The second cleavage releases the NICD, which then translocates into nucleus and interacts with the DNA-binding protein CSL and its co-activator Mastermind (Mam) to promote transcription of the target genes (Figure 2.12) [216-218].

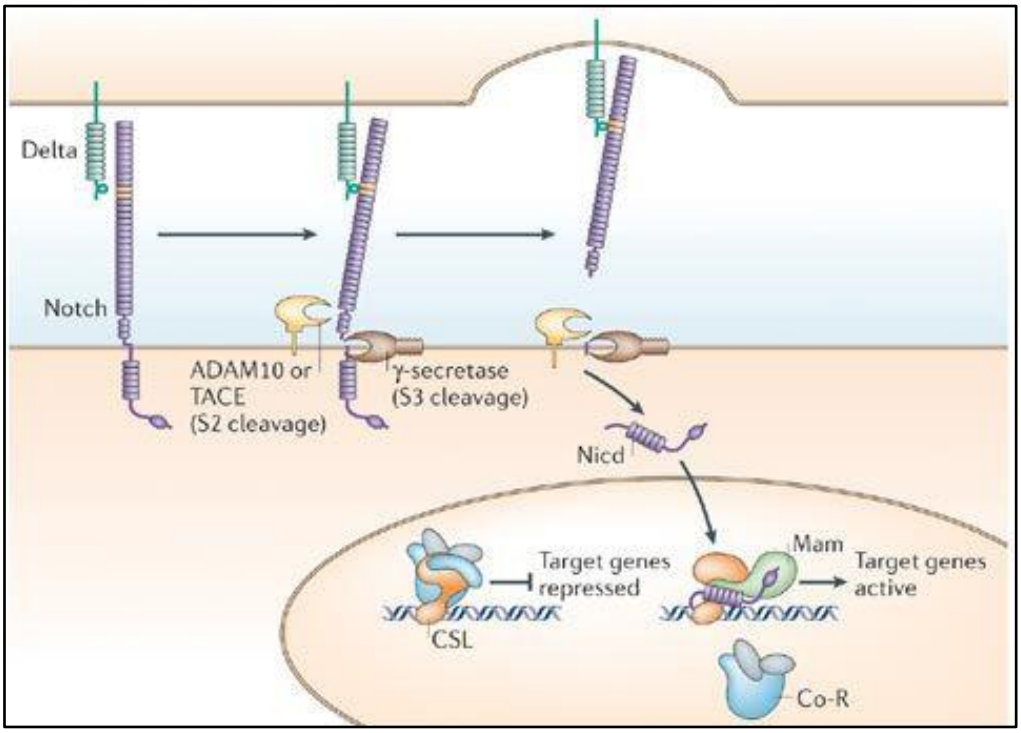

Figure 2.12: Notch signalling pathway

(Adapted from Bray et al., 2006, Nat Rev Mol Cell Biol.) [219]

Notch signalling is activated by the binding of Notch ligands to the extracellular domain of Notch receptor that leads to release of NICD into the cytoplasm through proteolytic cleavage

by adam10 and γ-secretase. The NICD further translocate into the nucleus and regulates the expression of the Notch target genes.

Notch signalling is involved in HF development, differentiation and IFE homeostasis. The expression of Notch receptors (Notch1-4) is well reported in the IFE, HF matrix etc. [220, 221]. Notch signalling is required for the epidermal differentiation that acts as a commitment switch at the basal/suprabasal juncture and induces spinous fate and down-regulates the basal fate [90]. The transcription factors Msx1 and Foxn1 regulate the expression of Notch1 in the HF matrix cells. Loss of Notch1 within matrix cells results in impaired differentiation of medulla and IRS [222]. Notch1 deficiency in the epidermis results in a pleiotropic phenotype, with hair loss, IFE hyperproliferation, and cyst formation [223]. The Notch/RBP-J signalling in the HFSCs inhibits the epidermal cell fate that promotes the HFSCs to differentiate into HF cells [224]. Further, Notch signalling pathway blocks HFSCs from migrating into IFE and undertaking IFE cell fate. Conditional ablation of Notch signalling in murine HFSCs using K15CrePR (Bulge specific promoter) results in HFSC fate change to IFE fate and formation of epidermal cysts [225]. Additionally, deletion of the jagged1 in the basal layer cells and γ-Secretase in the matrix cells demonstrated cyst formation, inhibition of the hair growth cycle and failure to maintain IRS cell respectively [226, 227].

2.4.4 Sonic Hegdehog Signalling:

Sonic Hegdehog (Shh) pathway is an evolutionarily conserved pathway, which plays an important role during embryonic development and in adult tissue maintenance, renewal and regeneration. In mammals, the Shh signalling is mainly governed by three different secretory ligands: Sonic hedgehog (Shh), Indian hedgehog (Ihh) and Desert hedgehog (Dhh) [228]. In the absence of Shh ligand, the activity of the 7-transmembrane protein Smoothened (Smo) is inhibited by the 12-transmembrane protein Patched (Ptch1). The binding of Shh ligand

inhibits the suppression of Smo by Ptch1 [229, 230]. The activated Smo triggers the downstream signalling cascade by activating the zinc-finger transcription factors called Gli proteins (Gli1, Gli2 and Gli3) (Figure 2.13). The Gli proteins translocate into the nucleus thereby activating the transcription of target genes. The Gli1 acts as a full-length transcriptional activator, while Gli2 and Gli3 act as either a negative or positive regulators [231, 232].

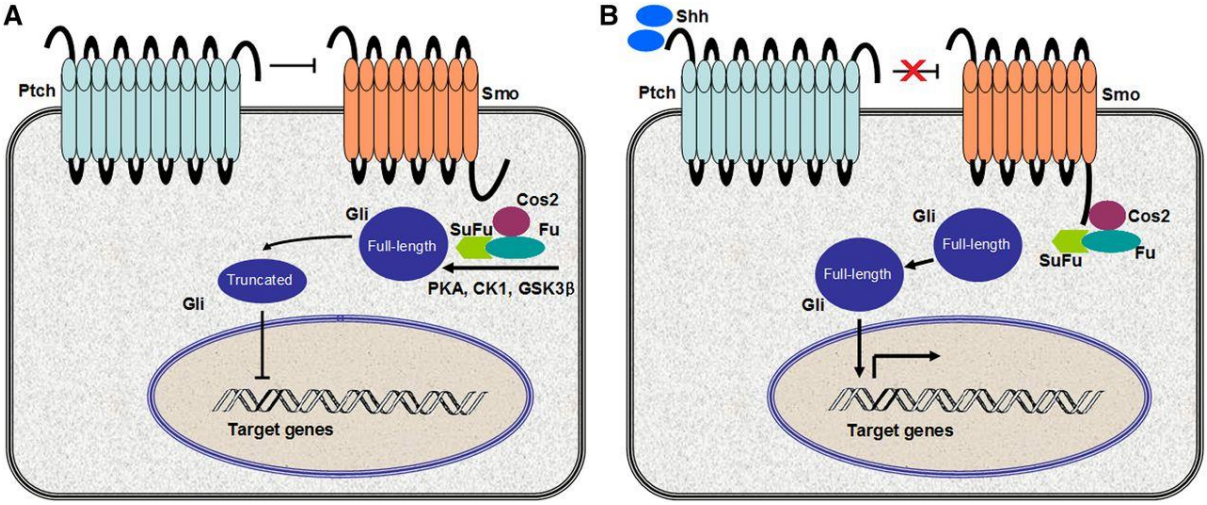

Figure 2.13: Hedgehog signalling pathway

(Adapted from Hu L.et al. 2015, Mol Pharmacol.)[233]

(A) *In the absence of Hh ligand, Ptch inhibits Smo, and the Cos2-Fu-SuFu complex binds to the full-length Gli, which is phosphorylated by glycogen synthase kinase 3β (GSK3β), protein kinase A (PKA), and casein kinase 1 (CK1). Phosphorylated Gli is cleaved to an N-terminal form and then translocates the nucleus to suppress transcription.* ***(B)*** *In the presence of Hh ligand, Ptch activity is suppressed, and thereby Smo interacts and inhibits Cos2-Fu-SuFu complex, and the full length Gli is able to enter the nucleus and induce transcription of target genes.*

During HF morphogenesis, dermal Shh signalling upregulates the expression of Noggin (inhibitor of Bmp signalling), which helps in counteracting Bmp mediated Wnt-β-catenin

signalling inhibition thereby promoting the HF growth [126]. Further, loss of Shh expression during HF morphogenesis resulted in arrest of HF growth at the placode stage and loss in condensation of DP suggesting the role of Shh in the epithelial-mesenchymal crosstalk, cell proliferation and DP functions [127, 128]. Overexpression of Shh under the K14 promoter in the epidermis resulted in the enhanced hair follicle neogenesis in the healed area after wound re-epithelialization [234]. Additionally, overexpression of the Shh under the K14 promoter in skin resulted in massive down-growth of the HFs and basal cell tumor formation [235]. Further, deletion of Gli2 during the HF morphogenesis results in the HF arrest during development with reduced cell proliferation [236]. Importantly, Bronell et al. in 2011 showed that Gli1 marks a unique set of SCs within the telogen HF bulge that are capable of undergoing self-renewal, HF regeneration and contribute to different lineages within the follicle [14].

2.4.5 TGF β signalling:

Transforming growth factor β (Tgf-β) and its associated growth factors play essential roles in embryogenesis and adult tissue homeostasis by regulating cell proliferation, differentiation, death, and migration. Tgf-β signalling is mediated through the type-1 and type-II receptor tyrosine kinases. Upon binding of the ligand to the hetero-tetrameric receptor complex (consists of two type-1 and two type-II receptors), the type-II receptor kinase phosphorylate and activate the cytoplasmic domains of the type-I receptor kinase [237, 238]. Subsequently, the type I receptor kinases phosphorylate the receptor-regulated Smads (R-Smads) 2 and 3. The activated R-Smads forms a complex with the common Smad-4 (C0-Smad-4) and translocate into the nucleus where they regulate the transcription of the target genes (Figure 2.14) [239, 240].

During the embryonic development, Tgf-β2-null mice skin displayed block in follicle bud progression and reduction of hair follicles number to ~ 50 percent [129]. During, telogen-to-anagen transition, DP secreted Tgf-β2 activates Smad2/3 with in HFSCs which in turn increases the expression of Tmeff1 in HFSCs. The increased levels of Tmeff1 lower the Bmp signalling thresholds thereby activating HFSCs [241]. In contrast, Tgf-β1 induces catagen via the inhibition of keratinocyte proliferation and induction of apoptosis wherein Tgf-β1 deletion resulted in delayed catagen entrance [154].

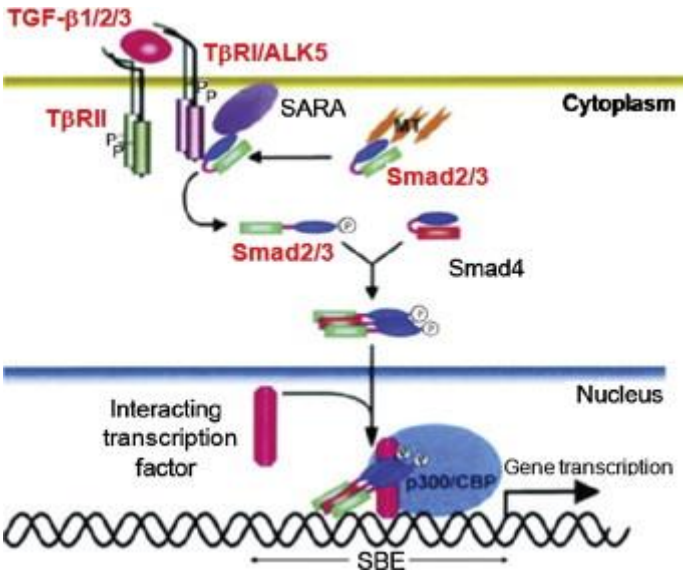

Figure 2.14: TGF-β signalling pathway

(Adapted from Jiang WG et al. 2015, Semin Cancer Biol.) [242]

The pictorial representation of Tgf-β signalling pathway shows the binding of Tgf-β ligands to the type I and type II Tgf-β receptors, which further activates Smad2/3 transcription factors. The activated Smad2/3 then binds to Smad4 and translocates into the nucleus and regulates the expression of the Tgf-β target genes.

Further, ablation of Tgf-β signalling during anagen (PD24-PD30) leads to increased apoptosis in the secondary hair germ and bulb matrix cells with poor IRS and hair shaft differentiation. Importantly, inhibition of Tgf-β signalling in HFSCs and isthmus SCs showed opposing responses i.e. HFSCs proliferation was reduced upon Tgf-β signalling inhibition. However, isthmus SCs proliferation was increased upon Tgf-β signalling inhibition suggesting a differential response of these two SC populations to Tgf-β signalling. Additionally, Tgf-β signalling loss in HFSCs results decrease in their SC characteristics [243].

2.5 Wound healing process:

Wound healing is a natural physiological reaction to tissue injury. Wound healing is a highly complex and dynamic process requiring the collaborative efforts and complex interactions of cytokines, growth factors, mesenchymal cells, epithelial cells and immune cells [244]. In humans, the wound healing is a continuum of processes that is classified into four overlapping phases: homeostasis, inflammation, proliferation, and remodelling (Figure 2.15) [245]. Initial wound healing in mouse primarily occurs via contraction promoted by panniculus carnosus [246, 247]. However, skin healing is similar in humans and mice when considering the distinct and overlapping phases of highly complex cellular and molecular events: homeostasis, inflammation, proliferation, and remodelling [246]. Homeostasis is the first phase that starts immediately after wounding where vascular constriction and blood clotting occurs by platelets, which is activated by the extravascular collagen [248]. Further, platelets releases pro-inflammatory cytokines and secretory growth factors such as Pdgf, Fgf, Egf and Tgf-β which attract inflammatory cells to the wound site and initiate inflammatory response [248]. The inflammation phase is characterized by the sequential infiltration of neutrophils, macrophages, and lymphocytes to the site of injury through chemotaxis. The main function of the neutrophils is to clear the invading microbes and that of macrophages is

to clear apoptotic cells (including neutrophils) and release cytokines that promote the inflammatory response by recruiting and activating additional leukocytes [249, 250]. Further, dendritic epidermal T-cells (DETC) are activated by stressed, damaged, or transformed keratinocytes. The activated DETCs produce fibroblast growth factor 7 (Fgf-7), keratinocyte growth factors (Kgf) and insulin-like growth factor-1 (Igf-1) to support keratinocyte proliferation and cell survival. In this context, mice lacking DETCs showed decrease in the proliferation of keratinocytes and delay in wound closure [251, 252].

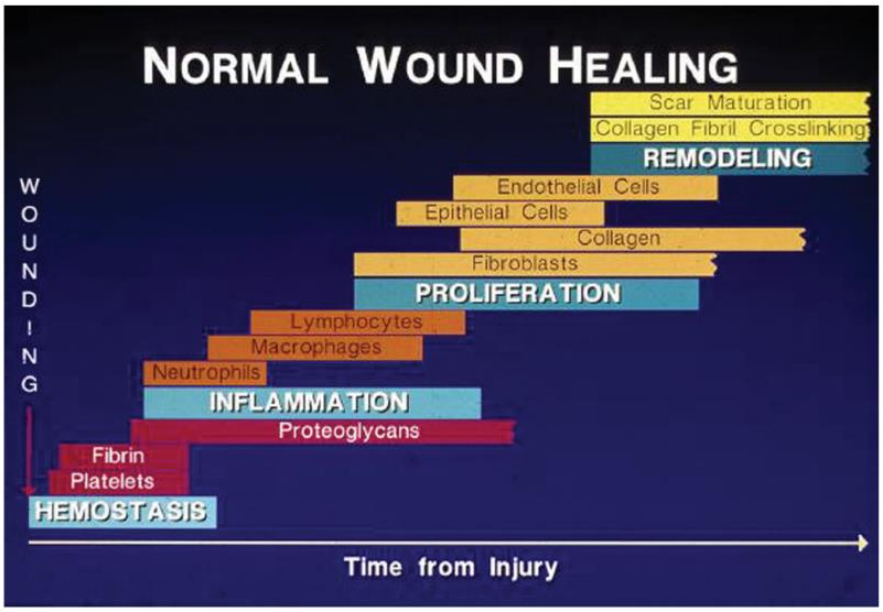

Figure 2.15: Phases of normal wound healing

(Adapted from Schultz GS. et al. 2011, Principles of Wound Healing) [253]

Representation of sequential cellular events that occurs during wound re-epithelialization process from the time of injury.

The third phase is the proliferative phase, which starts after two days of the injury and extends up to 2 to 3 weeks. The proliferative phase is characterised by re-epithelialization of skin by epithelial cell proliferation and migration. Concurrently, angiogenesis, extra-cellular matrix (ECM) formation and granular tissue formation occurs by the endothelial cells and

dermal fibroblasts respectively. The final phase is the remodelling phase where remodelling of ECM to the normal tissue architecture and regression of capillaries to attain the normal capillary density occurs, which would last up to a year or more [254-257].

2.5.1 HFSCs in the wound healing process:

HFSCs are multipotent and give rise to different epidermal cell lineages comprising of HF, SG and IFE [135, 144]. In addition to normal tissues homeostasis, these SCs are involved in acute epithelial wound repair. Recent studies using novel technologies revealed that within 24 hours of wounding, the HFSCs get activated and migrate out of the SCs niche to participate in the wound re-epithelialisation process [135, 136]. For instance, Levy et al. in 2008, using ShhGFPcre;R26R mice showed that HFSCs migration towards the wound can be observed as early as one day after wounding. [258]. In addition, Ito et al, in 2008, performing lineage analysis of HFSCs using the K15 promoter-driven LacZ expression system, showed that the HFSCs and their progeny migrate and participate in the wound healing process as the repaired epithelium showed LacZ positive cells. Nevertheless, bulge-derived progeny cells (transit amplifying cells) in the repaired epithelium are gradually replaced by the IFE derived progeny cells [145]. Moreover, Heidari F et al. in 2017, have shown that wounds treated with HFSCs exhibited accelerated wound closure with more re-epithelialization, angiogenesis and dermal structural regeneration as compared to control group in rats [259]. Chovatiya et al. in 2017, using K14-aPLA$_2$-IIA over-expressing mice have shown that loss of HFSC pool resulted in delay in initial wound healing response [260]. In contrast to the HFSC where the HFSC progeny are gradually replaced after wound re-epithelialization, the Lgr6+ SCs in the isthmus was reported to permanently contribute to wound healing, including hair neogenesis [78]. Importantly, Gli1$^+$ SCs present in the upper bulge region (i.e. in Shh perineural stem cell niche) are capable of wound re-epithelialization after injury. Further, these Gli1$^+$ SCs also have a distinctive ability to change their lineage and to become epidermal SCs after

wound re- epithelialisation. (Figure 2.16) [14]. Langton et al. in 2008, using Edaradd$^{cr/cr}$ mouse with no HF formation (i.e. no HFSCs) have shown that there is a delay in the re-epithelialization demonstrating that HFSCs play a role in wound healing process [261].

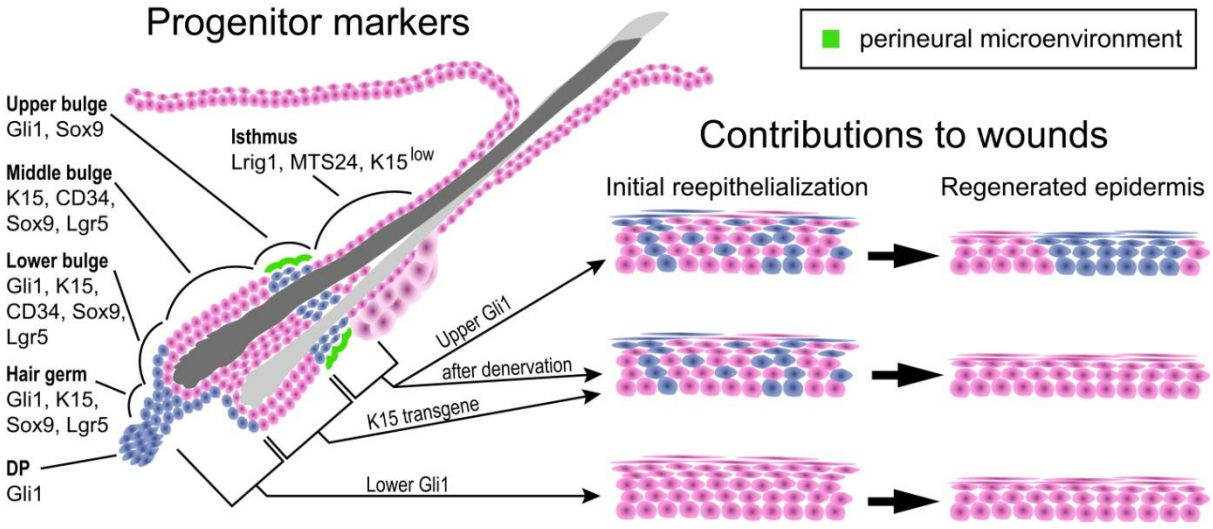

Figure 2.16: HFSCs in wound healing

(Adapted from Brownell I. et al. 2011, cell stem cell) [14]

Diagrammatic representation of HFSCs contribution in wound re-epithelialization process. Gli1 (+) upper bilge cells are capable of re-epithelialization and have a distinctive ability to become epidermal stem cells after wounding. However, the progeny of stem cells from middle and lower bulge in the wound are gradually replaced by cells from IFE stem cells.

2.5.2 IFE stem cells in the wound healing process:

HFSCs are shown to contribute in re-epithelialization of skin after wounding. At the same time, genetic mouse mutants such as Edaradd$^{cr/cr}$, with complete absence of HFSCs, showed incisional wound healing with a delay in the re-epithelialisation, demonstrating that IFE SCs are also capable of wound re-epithelialization (Figure 2.17) [261]. Further, Mascre et al., in 2012, have labelled two distinct cell populations in the IFE using K14-Cre-ER (long term SCs) and Inv-Cre-ER (short term SCs) and have shown their respective contributions in the

wound healing. A large number of K14-Cre-ER (Basal layer and ORS promoter) labelled stem cell population have migrated from the periphery to the centre of the wound establishing their major contribution to the wound re-epithelialisation, while only a few Inv-Cre-ER cells participated in wound healing [76]. In addition, Sada et al. in 2016, have shown that two distinct IFE SCs populations (Dlx1 and Slc1a3 expressing SCs) are present in the IFE that are inter convertible and capable of wound re-epithelialization upon injury [77]. Importantly, Ito et al. in 2007, showed that apart from wound re-epithelialization the basal cells of the genetically normal adult mice have the ability to program follicular neogenesis after wound healing process, which is dependent on the Wnt signalling [177]. Together, these studies showed that the IFE SCs are functionally sufficient for re-epithelialization following wounding that are capable to generate new HFs after re-epithelialization.

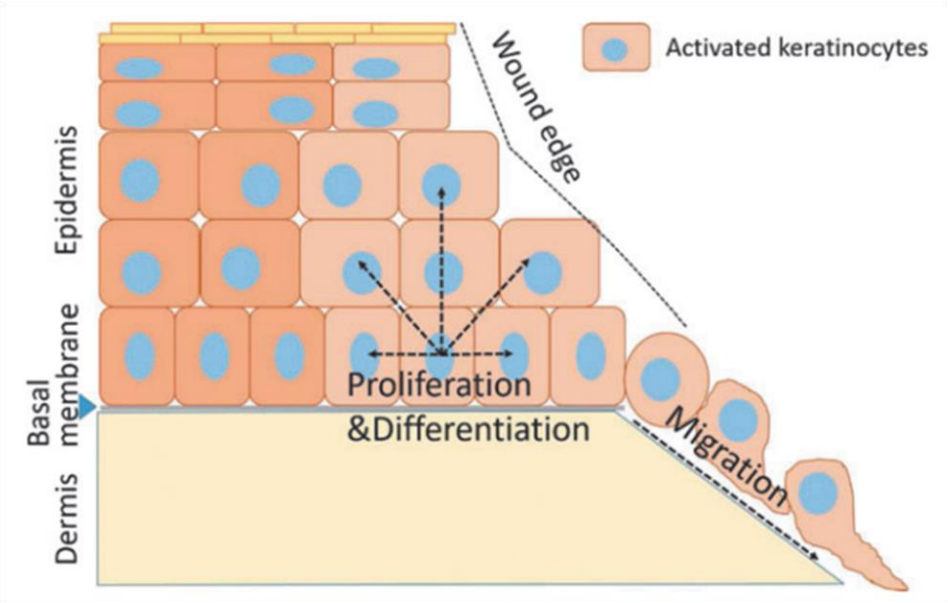

Figure 2.17: Epidermal stem cells in wound healing

(Adapted from Li Y. et al. 2017, Adv Wound Care)[262]

The keratinocytes at the leading edge i.e. near the corners of the wound migrate towards the centre of the wound, while the basal keratinocytes behind the front line start to proliferate and differentiate, restoring the barrier function of the epithelium

2.6 Skin Carcinogenesis:

Skin cancers are of two types; the malignant melanomas arising from the melanocytes and non-melanoma skin cancer (NMSC) arising from basal keratinocytes or HFSCs [263]. Skin cancer is one of the most common malignancies; with NMSC being the 5th most commonly occurring cancer affecting humans worldwide according to globocan cancer statistics [264]. The NMSC includes Basal cell carcinoma (BCC) & Squamous cell carcinoma (SCC) and BCCs accounts for the 80% of the NMSC [265]. Skin cancer is a multi-factorial disease as both genetic and environmental factors contribute to the development of disease. It can occur either sporadically due to environmental factors or in people who are predisposed to develop cancer due to genetic factors or in some cases both. The genetic factors for NMSC include conditions such as basal cell nevus syndrome, xeroderma pigmentosum, epidermolysis bullosa, or oculocutaneous albinism [266]. The environmental factors for the skin cancer development include UV-A & B, arsenic in drinking water, infection with human papilloma viruses type 6 & 11 and climate changes etc. [267-269]. The UV radiation causes DNA damage (cyclobutane pyrimidine dimers), double stranded breaks, oxidative stress and importantly mutations in p53gene all of which have important role skin cancer development [270]. Both BCC and SCC are shown to be directly proportional to amount of UV radiation received and inversely proportional to skin pigmentation [271]. Arsenic tends to accumulate in skin and induces oxidative stress, chromosomal abnormalities and p53 dysfunction that can lead to development of BCC and SCC [272]. There are several mouse models that have been extensively used in studying to molecular mechanisms that regulate the skin cancer induced by UV and chemical carcinogens. The immunocompetent SKH-1 mice (hair less mice) is one of the best model to study UV induced skin carcinogenesis as is lacks hair coat, which might otherwise interfere with UV treatment [273]. Further, FU et al. in 2013, using SKH-1 mice that overexpresses pro-protein convertases furin and PACE4 have shown ~70% increase in

SCC compared to control SKH-1 when exposed to UV radiation [274]. Further, chemical carcinogenesis studies in mouse skin has been confirmed as a valid tool (Gold standard model) to study human NMSC because it replicates the human cancers both at progression of benign lesions to SCCs in a stepwise manner including the signalling alterations (due to activating mutations in H-Ras gene) were similar to those produced by UVR exposure in humans [275-278].

The cellular origin of BCC and SCC is a well studied area and multiple reports have shown that both HFSCs and IFE SCs can give rise to BCC and SCC. HFSCs and IFE stem cells. Over expression of Hh signalling in HFSCs leads to development of nodular BCCs and in IFE leads to development of superficial BCCs [279]. Additionally, Peterson et al., in 2015, have showed that multiple HFSCs populations form BCCs upon Hh signalling activation (*Ptch1* deletion) using Gli-Cre^{ERT2} (Markers SCs in lower and upper bulge) and Lrig1-Cre^{ERT2} (marks SCs in Isthmus region) [280]. Importantly, Lapouge et al., in 2011, using K19CREER/KRas$^{LSL-G12D}$ mice and InvCREER/KRas$^{LSL-G12D}$ have shown that SCCs can develop both from HFSCs and IFE stem cells respectively and these tumors irrespective of the cell of origin express CD34 indicating that expression of HF markers by tumor cells does not necessarily reflect their cellular origin [281]. Further, White et al, in 2011, using K15crePR KRas $^{LSL-G12D}$ mice have shown HFSCs as the cell of origin for SCC, whereas developmentally restricted TA cells are unable to generate even benign tumors within the same genetic context [282]. Adriana et al, in 2018, showed that a small percentage of slow cycling Lgr5+ve cells survive and are responsible for BCC relapse after treatment discontinuation[283]. Together, these studies have shown that both BCC and SCC can develop either from HFSCs or IFE stem cells.

2.6.1 Two stage skin carcinogenesis model:

Two stage skin carcinogenesis in mice is a well established *in vivo* models to study the sequential and stepwise development of tumors [284]. In particular, this model has assisted in identifying the underlying cellular and molecular mechanisms that are associated with the different stages of skin cancer development. In this model, tumor development occurs via three distinct stages: initiation, promotion, and progression (Figure 2.18), which are discussed thoroughly in the following section. In this model, the mice are initially treated topically with mutagen/initiating agent such as DMBA, which induces an irreversible and specific mutation in the oncogenic *H-ras* gene (codon 61 with glutamine to leucine) [285]. This application is followed by multiple regular applications of non-mutagenic tumor promoter, such as TPA that enhances proliferation of epidermal cells, which leads to clonal expansion of mutated cells [286, 287]. Certain parameters should be considered when utilizing the two-stage protocol such as; **(1)** Mouse strain susceptibility to the mutagen and promoter agent. This is because certain strains are more susceptible than others eg: FVB strain is more susceptible than C57BL/6, **(2)** Appropriate concentrations of mutagen and promoting agent as very high or low doses may affect the papilloma formation and subsequent SCC progression, **(3)** Genetically altered mice (such as knockouts and transgenic mice) may exhibit altered susceptibility to mutagen and promoting agent [288].

The advantages of the two-stage skin carcinogenesis model include:

1. Tumor development can be conveniently monitored visually throughout the life span of the mouse.
2. As the tumor response is highly reproducible, the efficacy of chemo-preventive agents or the effect of dietary manipulation can be assessed.

The role of various genes and cell-signalling pathways in tumor initiation & progression can be explored in this model through the use of either transgenic or knockout mice of specific gene of interest.

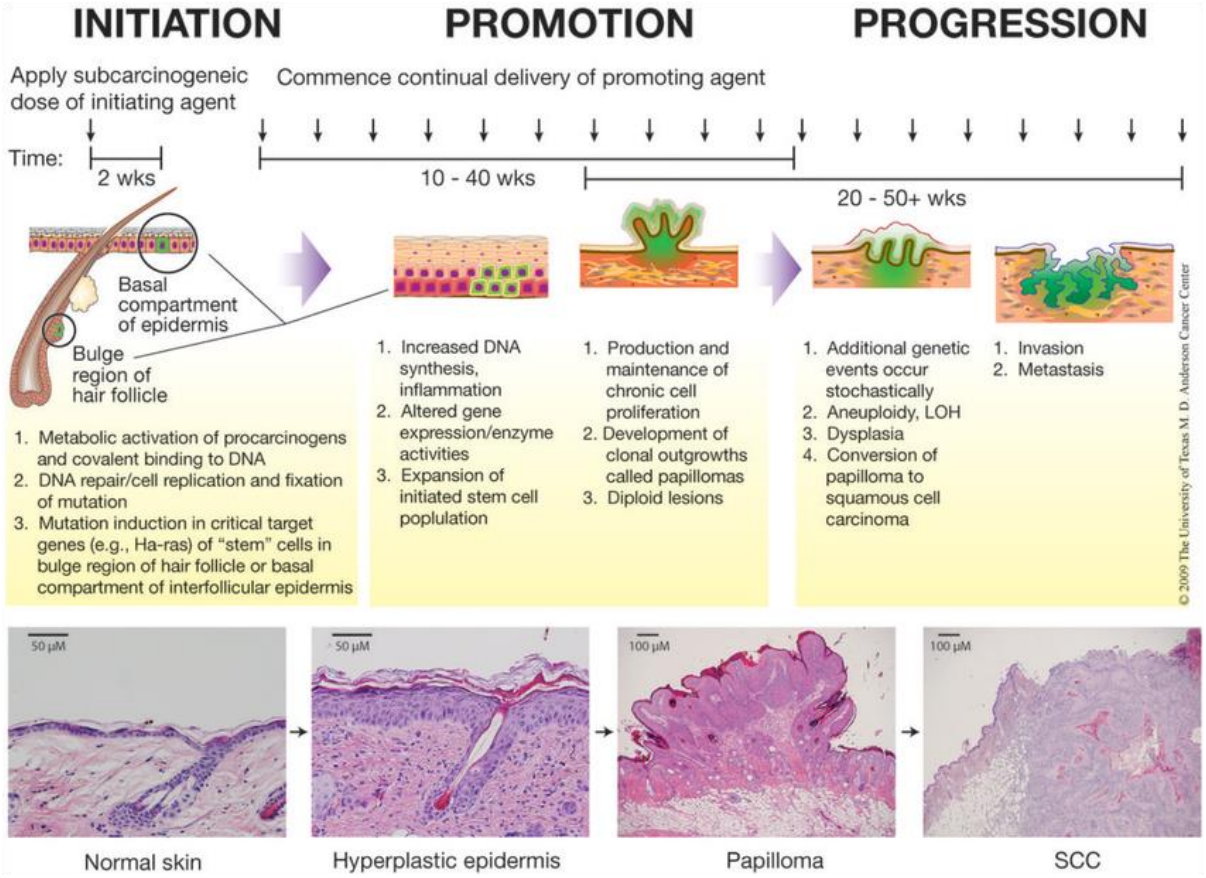

Figure 2.18: Two stage skin carcinogenesis model

(Adapted from Abel et al. 2009, Nat protocol)[284]

Pictorial representation of two stage skin carcinogenesis model in mice. The carcinogenesis process is divided into three stages: Initiation, Promotion and Progression. The molecular, cellular and phenotypic changes that occur during different stages are represented.

2.6.2 Initiation:

Initiation is the first step in the two-stage chemical induced carcinogenesis. During initiation, the mice are topically treated with a carcinogen (initiating agent) such as polycyclic aromatic hydrocarbon - DMBA during the telogen phase of the hair follicle cycle. Application of DMBA results in mutations of key regulatory genes in epidermal keratinocytes as DMBA interacts with DNA forming N^6-dAdo DNA adducts [275]. The hall mark mutation is the A to T transversion in the H-Ras proto-oncogene at codon 61(CAA to CTA: Glutamine to leucine), which results in constitutively active Ras protein [276]. The H-*Ras* mutations in the epidermis of the mouse model can be observed one week after the application of DMBA [289]. Different initiating agents such as benzo[a]pyrene , N-Methyl-N-Nitrosourea, N-methyl-N-nitrosoguanidine (MNNG) etc. can be used as a initiating agents [284]. The initiation event is an irreversible event and tumors will be only developed unless promoted by repeated application of tumor promoting agent.

2.6.3 Promotion:

During promotion, the mutated cells clonally expand to form pre-malignant papillomas after repeated application of tumor promoting agents such as TPA (a phorbol ester).The promoting agent leads to epidermal hyperplasia, where the initiated cells that have acquired a growth advantage proliferate more as compared to surrounding non-initiated cells thereby giving rise to tumors [290, 291]. The hydrophobic acyl chain in phorbol esters is critical for their tumor-promoting ability, Additionally, phorbol esters are reported to increase mRNA expression and protein synthesis [275]. TPA is an analog of diacylglycerol (DAG) that binds to protein kinase C (PKC), leading to activation of PKC downstream targets thereby increasing the proliferative potential of cells [292]. Further, tumor promotion is altered by several factors such as age, sex, diet and hormone balance [293]. Different promoting agent such as

telocidin, benzoyl peroxide, chrysarobin and UV radiation can be used as promoting agents. Different promoting agents stimulate the cell proliferation through different modes such as: a) activating cell signalling molecules (Pkc, Akt, and Stat3 etc), b) increasing the production of growth factors and their receptors (Tgf, Egf, Egfr and Vegf etc), c) enhancing oxidative stress and d) tissue inflammation (cytokines, interleukins etc). The, short-term markers of tumor promotion include increased epidermal thickness, proliferation of basal keratinocytes, increased DNA synthesis and inflammatory cell infiltration [275, 294]. Papilloma formation begins after approximately 6-12 weeks of promotion (treatment with TPA) depending upon the mice strain and genetic variation it harbours [284].

2.6.4 Progression:

During the progression the benign papillomas formed during the promotion stage gets converted to SCC after approximately 20 weeks of promotion. This conversion occurs randomly and is independent of tumor promoting agent. During progression, the tumors acquire additional genetic mutations, loss of heterozygosity (LOH), epithelial to mesenchymal transition (EMT) and chromosomal abnormalities (aneuploidy) that drive benign papillomas to SCCs [275, 295, 296]. The resulting SCC may be both invasive and metastatic. The frequency of malignant conversion is dependent on the genetic background of mice and the concentrations of initiator and promoter doses used, which influence the tumor burden. For instance, as few as 1–10% of papillomas progress to SCC in BALB/c mice, whereas up to 50% of papillomas in FVB mice gets convert into SCC [297-300]. Importantly, the percentage of SCC that undergo metastases to organs such as lung or lymph nodes, and the frequency with which metastasis occurs depends upon genetic background of mice [301].

2.7 Cancer stem cells (CSCs):

CSCs represent a small subset of cells within the tumor which have indefinite self-renewal potential. They give rise to all the cell types within a tumour and are resistant to traditional cancer therapies [36]. The existence of CSCs is a highly debated topic in the past few decades' right from their initial discovery in 1977 by Bonnet and Dick [39]. There exist two different schools of thoughts of tumor growth and heterogeneity i.e. the CSC model and stochastic model (Figure 2.19).

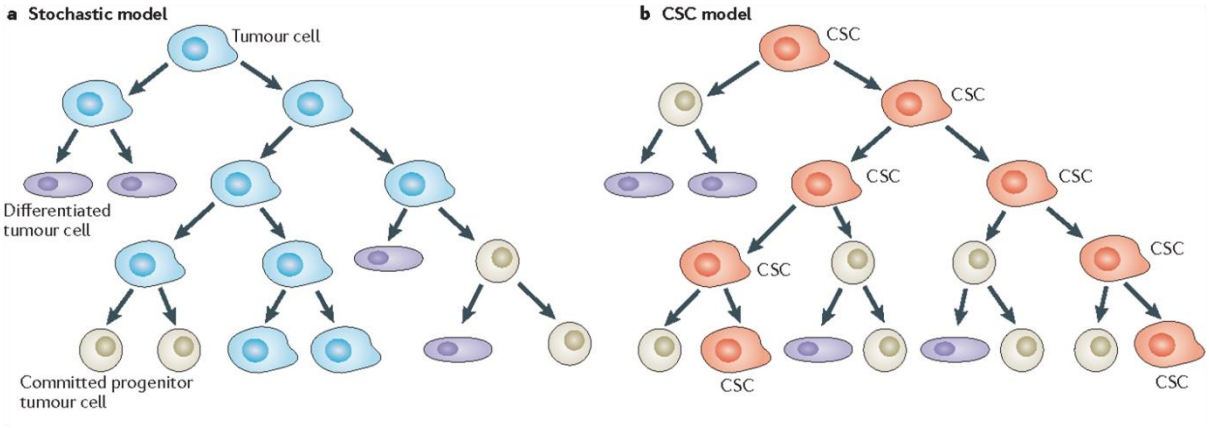

Figure 2.19: Models of tumor growth A. Stochastic model B.CSC model

(Adapted from Beck B. et al. 2013, Nat Reviews Cancer)[302]

A. *In the stochastic model of tumour growth, all tumour cells are equipotent and stochastically self-renew or differentiate, leading to tumour heterogeneity.* ***B.*** *In the CSC model of tumour growth, only a subset of tumour cells has the ability for long-term self-renewal and these cells give rise to progenitors with limited proliferative potential that eventually terminally differentiate.*

In the CSC model, only a sub-population of tumour cells called as CSCs has the capacity to undergo self-renewal and to give rise to CP or TA cells. These CP/TA cells have limited proliferative potential that give rise to the differentiated cells within the tumor. Owing to the

similarity to that of normal SCs, the tumors are hierarchically organized with CSCs at the top of the pyramid giving rise to both the CSCs and CP cells upon proliferation. However, in case of stochastic model of tumour growth, all tumour cells are equipotent and stochastically self-renew or differentiate, leading to tumour heterogeneity [302].

The existence of CSCs in leukaemia was first reported by Bonnet and Dick in 1997, where they have shown that leukemic cells that express HSCs markers ($CD34^{+}CD38^{-}$/Lin-) undergo self-renewal and are more efficient at propagating the leukaemia in immune-deficient mice. These cells are termed as leukemic stem cells (LSCs) that were able to differentiate *in vivo* into leukemic blasts, indicating that there is a hierarchy in AML [39]. Further, in solid tumors, Al Hajj et al. in 2003, showed that, there exists a subgroup of cells expressing $CD44^{+}CD24^{-/low}/Lin^{-}$ markers, which acts as tumor initiating cells, capable of giving rise to tumors even with 100 cells when transplanted into immune-deficient mice. These cells give rise to both $CD44^{+}CD24^{-/low}/Lin^{-}$ cells in addition to other differentiated cells within the tumors and are termed as breast CSCs (BCSCs) [40]. Subsequently, CSCs were identified and prospectively isolated from multiple solid tumors, including brain cancers [41, 42], melanoma [43], colon [44], pancreatic [45], and head and neck cancers [46] etc.

Further, strong evidence for the existence of the CSCs came from three independent studies utilising Lineage-tracing studies coupled with clonal analysis in murine models. Drissens et al. in 2012, performed clonal analysis studies in mice squamous skin tumours using K14Cre-ER/Rosa-YFP mice. They have marked individual cells in the basal layer of skin by adjusting the concentration of tamoxifen required to activate the CRE recombinase. They showed that only the marked basal SCs have the capacity to persist long term and give rise to tumors upon tumor induction. On the other hand the marked basal progenitor cells were lost eventually through terminal differentiation that did not give rise to tumors [49]. Further, Schepers et al., in 2012, using $Lgr5^{EGFP\text{-}Ires\text{-}CreERT2}/Apc^{fl/fl}$ mice where Cre-recombinase is expressed under

intestinal stem cell marker Lgr5, have shown the existence of cellular hierarchy in intestinal adenomas. The Lgr5-GFP^{hi} cells in the adenoma are enriched with stem cell markers (e.g., Olfm4, Ascl2) that are located adjacent to adenoma paneath cells (existence of adenoma stem cell niche) and most importantly are capable of giving rise to all differentiated tumor cell lineages.

Parada and colleagues in 2012 used lineage ablation method to prove the existence of CSCs in glioblastoma multiforme (GBM). They have expressed suicide gene herpes simplex virus tyrosine kinase (Hsv-tk) under the Nestin promoter, which is expressed only in GBM CSCs. Lineage ablation of Nestin^{+} slow-cycling CSCs by ganciclovir administration delayed tumor progression and improved the survival rates of mice with GBM, thereby demonstrating the importance of Nestin^{+} CSCs [50].

CSCs play an important function in tumor maintenance and progression. Further, CSCs are the main reason for the therapy (chemo/radio therapy) resistance and contribute to tumor relapse. These cells can be either intrinsically resistant to therapy, and thus persist after treatment and cause a relapse, or extrinsically instructed by the tumor microenvironment to become resistant under the selective pressure of therapy. Therapy resistance in CSCs are acquired through different modes such as expression of higher levels of ROS scavengers (protected against ROS-induced DNA damage) [303], expressing drug efflux ABC transporters (leading to efflux of drug) [304] and enhancing EMT transcription factors (low levels of ROS generation) [305], activation of aldehyde dehydrogenase (ALDH) and altering developmental pathways. All these mechanisms are regulated by specific signalling pathways and therefore, understanding the molecular mechanism involved in the CSC regulation would help to develop better treatment strategies for the benefit of the patient.

2.8 Signalling pathways regulating CSCs:

The developmental signalling pathways that govern normal stem cell homeostasis are tightly regulated. However, these pathways are abnormally activated or repressed in multiple human cancers. Such aberrations contribute to the self-renewal, proliferative, survival, and differentiation properties of CSCs. Myraid reports from the past two decades has provided substantial evidence that signalling pathways such as Wnt, Notch and Hedgehog has a significant role in the maintenance and regulation of CSCs. The developmental signalling pathways in CSCs maintenance and self-renewal are discussed here under.

2.8.1 Wnt signalling in CSCs:

Wnt signalling is an evolutionary conserved pathway, which has a significant role in cell proliferation, cell migration, cell polarity, cell fate determination, stem cell self-renewal and maintenance during embryogenesis as well as in adult tissue homeostasis [183, 184]. Aberrations in Wnt signalling pathway has been reported in multiple cancers such as breast cancer [306-308], hepato-cellular carcinoma (HCC) [309, 310], glioblastoma [311, 312], HNSCC [313, 314] and skin cancer [315, 316] etc. Further, multiple studies over the past decade have also reported Wnt signalling in the regulation and maintenance of CSCs that fuel the tumor growth in different cancers. For instance, ΔNp63 (Isoform of Trp63 transcription factor) enhances CSCs like phenotype by enhancing the expression frizzled-7 (Fzd7), which in turn enhances Wnt signalling in breast cancer [317]. Conversely, activated microRNA-1(miR-1) down regulated breast CSC stemness, proliferation, and migration by inhibiting the Wnt/β-catenin signalling through regulation of Fzd7 and Tankyrase-2 (TNKS2) [318]. Further, miR-203 enhances the expression of Dkk1 (Wnt inhibitor) thereby reducing the Wnt signalling, which results in decreased stemness and EMT in the breast cancer [319]. In the case of glioblastoma multiforme, stem cells (GBM- SCs), overexpression of PLAGL2

upregulates canonical Wnt signalling that enhances their self-renewal and inhibits differentiation [320]. Rheinbay et al., in 2013, have shown that human achaete-scute homolog (ASCL1) activates Wnt signalling in GBM-SCs by repressing the negative regulator Dkk1 [321].

In HNSCC CSCs, Wnt β-catenin signalling is involved in self-renewal capacity, stemness-associated gene expression, chemoresistance, and *in vivo* tumourigenicity. Further, β-catenin knockdown resulted in decreased Oct-4 expression that abrogated their stemness potential [322]. Le et al., in 2019, have shown that Wnt signalling activation increased CSC characteristics like sphere formation and invasiveness in HNSCC [323]. In ovarian cancer, active Wnt/β-catenin signalling either due to over expression of β-catenin or mutations in Ctnnb1, Axin, or Apc promote CSCs self-renewal, metastasis, and chemoresistance in endometrioid and mucinous subtypes [324, 325]. Importantly, the role of Wnt signalling has also been reported in skin CSCs. Malanchi et al., in 2008, showed that ablation of β-catenin resulted in loss of CSCs and complete tumor regression in cutaneous SCC [315, 326]. Recently Bai et al., in 2018, showed that overexpressing miR-142-5p induced CSC-like properties in cutaneous SCC via activating Wnt signalling [327]. Further, deletion of adenomatous polyposis coli (APC) in Lgr5+ intestinal SCs using *Lgr5-creER*^{T2}: *Apc*$^{flox/flox}$ mice resulted in β-catenin accumulation and development of adenomas in small intestine and colon [328]. In Acute myeloid leukemia (AML), loss of Tcf1 and Lef1transcription factors hinders leukemic stem cells (LSCs) self-renewal and inhibits their leukemia initiation and progression properties [329].

2.8.2 Notch Signalling in CSCs:

The Notch signalling is a highly conserved pathway, which is primarily involved in regulating SC maintenance, cell fate decisions, differentiation and proliferation [330], [331].

Notch pathway is involved in CSCs self-renewal in multiple cancers and is thus receiving increased attention as a target to eliminate CSCs. Grudzein et al., in 2010, have shown that inhibition of notch signalling in T47D breast cancer cell line using gamma secretase inhibitor (GSIs) reduced the number of stem-like cells, and completely abolished secondary mammosphere formation [332]. In HNSCC, utilization of Notch1 inhibitor DAPT (GSI-IX) has significantly reduced CSCs population and their self-renewal ability [333].

Further, activation of Notch signalling in ovarian cancer leads to enrichment of ovarian CSCs (OCSCs) leading to cisplatin resistance and poor overall survival [334, 335]. Further targeting Notch-Hes1 signalling pathway through sequential combination of cisplatin and eugenol in ovarian cancer patients resulted in the elimination of resistant CSCs [336]. In pancreatic cancer, Notch signalling is involved in maintaining CSCs and inhibition of notch signalling either through gamma secretase inhibitor or Hes1 shRNA resulted in a decrease in the percentage of CSCs and tumorsphere formation [337]. Additionally, in lung adenocarcinoma SCs, high Notch signalling results in increased sphere formation, resistant to chemotherapy and increased tumorigenicity in serial xenotransplantation assays. Further, the overall survival of lung adenocarcinoma patients with high expression levels of Hes1 is poor as compared to patients with low expression [338]. Notch4 signalling is highly enriched in BCSCs [ESA(+)/CD44(+)/CD24(low)] as compared to non SCs and pharmacological or genetic inhibition of Notch4 results in reduced *in vitro* sphere formation and *in vivo* tumor initiation capabilities [339]. In GBM-SCs, inhibition of notch signalling reduces their proliferation, self-renewal and increases their susceptibility to radio-therapy [340]. Further, notch signalling in prostate CSCs results in their increased *in vivo* tumor initiating capacity and chemo-resistance to docetaxel [341]. Elevated levels of Notch1 are reported in HNSCC and inhibition of Notch1 by DAPT (GSI-IX) significantly reduces CSCs population and self-renewal ability [333]. As Notch signalling is involved in CSC maintenance in different,

gamma secretase inhibitors (GSI) have gained popularity to be used in combination therapy with conventional drugs to eliminate CSCs [333, 337].

2.8.3 Hedgehog (Hh) in CSCs:

Hedgehog (Hh) signalling is an evolutionarily-conserved pathway essential for self-renewal of adult somatic SCs and cell fate determination. Aberrant Hh signalling is associated with the development and progression of various types of cancers and is implicated in multiple aspects of tumourigenesis, including the maintenance of CSCs.

In chronic myeloid leukaemia (CML) Hh pathway activity increases through upregulation of Smo thereby controlling the frequency and maintenance of leukemic stem cells (LSCs); whereas, genetic inactivation of Smo in mouse model of CML decreases the number of LSC [342, 343]. In addition to CML, Hh signalling is also involved in maintenance and regulation of self-renewal in acute lympboblastic leukaemia (ALL) (both B- and T-cell origin) and acute myeloid leukaemia (AML). Moreover, treatment with the Smo inhibitors, cyclopamine or IPI-926, significantly reduces long-term self-renewal potential in ALL LSCs and AML LSCs [344, 345]. Further, Hh signalling was reported to be highly active in glioblastoma multiforme (GBM) derived neurospheres and glioma stem cell cultures (gliomaspheres), as they highly express Gli1, Ptch1, Smo and Shh. Blockade of Hh pathway in GBM neurospheres by cyclopamine reduces Gli1 mRNA expression, inhibits cell growth and promotes differentiation of neurospheres, and downregulation of stemness genes Oct-4, Sox-2, Nanog, Nestin and Bmi-1 [346-348]. In breast cancer, the breast cancer stem cells ($CD44^{+}/CD24^{-/low}/Lin^{-}$ BCSCs) over express polycomb gene Bmi-1 through upregulation of SHH signalling, involved in regulating self-renewal of BCSCs [349]. Furthermore, SHH signalling inhibition in chemoresistant prostate cancer stem cells (PCSCs), by cyclopamine or GANT61 significantly reduced the PCSCs viability, self-renewal capacity, tumorsphere and

colony formation ability [341, 350]. In Lung squamous cell carcinoma (LSCC) Shh signalling is activated cell-autonomously through a protein kinase Ci (PKCi)-Sox-2-Hh acyltransferase signalling axis, to maintain CSC like phenotype [351]. Most importantly, Hh signalling has been reported in the development of skin cancers such as melanoma and BCC. Moreover, Hh-Gli1 signalling was shown to play an important role in controlling self-renewal and tumor initiation of melanoma CSCs (MCSCs). Inhibiting the Hh signalling using either Smo or Gli1 inhibitors significantly decreased MCSCs self-renewal [352]. Further, in CD133+ laryngeal carcinoma stem cells (LCSCs), Hh signalling regulates their self-renewal and is also involved in their resistance to chemo/radio therapy [353]. In case of colon cancer, autocrine non- canonical Shh signalling which is Ptch1dependent and Gli independent is required for the maintenance of colon CSCs in an undifferentiated state and for their survival [354]. Moreover, in pancreatic adenocarcinoma, Hh pathway plays an important role in the regulation of self-renewal and chemoresistance of pancreatic CSCs (PCSCs). Inhibition of Hh signalling using cyclopamine resulted in decreased PCSCs self-renewal and increased susceptibility to gemcitabine [355].

Taken together, compelling evidence from myriad number of studies suggest that inhibition of Wnt, Notch and HH signalling in CSCs results in reduced stemness, CSC differentiation, enhanced apoptosis and decreased chemo/radio resistance, which is supported by reduction in pluripotency markers, clonogenicity and enhanced cell death. Hence, the CSCs can no longer fuel tumors thereby reducing the reoccurrence of tumors. Therefore, the combinatorial targeting of CSCs and tumour bulk with WNT/Notch/Hh inhibitors along with conventional chemotherapeutics is an attractive approach to prevent tumour relapse and maximize patient outcomes.

Chapter 3: Aims and Objectives

3.1 Statement of the problem:

Tissue stem cells (SCs) play a crucial role in tissue homeostasis, repair and regeneration throughout the life of an organism. The SCs achieve this through their unique ability to undergo self-renewal as well as giving rise to progenitor cells which differentiate into specific lineages of the tissue. These properties of the SCs are regulated by different signalling mechanisms and perturbations within these signalling mechanisms lead to cancer development. Cancer is a heterogeneous disease both at cellular and molecular level and consists of a unique population which has similar characteristics as of tissue stem cells called as cancer stem cells (CSCs) that are involved in tumor maintenance and heterogeneity. CSCs are reported to be involved in therapy resistance and tumor relapse. Since, CSCs harness molecular mechanisms that are similar to the ones present in normal SCs for their self-renewal & survival, understanding the molecular mechanisms that drive these properties in both normal SCs and CSCs may provide crucial insights into developing CSC specific therapies.

3.2 Hypothesis:

Signalling pathways such as Wnt, Sonic hedgehog, Notch and others like EGFR etc have been well reported in self-renewal, proliferation, differentiation of stem cells and their deregulation results in various cancers. Sfrp1, a secreted antagonist of Wnt signaling pathway, is known to be involved in hematopoietic, bronchoalveolar and mesenchymal stem cell regulation and its loss was reported in various cancers such as breast, cervical, hepato-cellular carcinoma etc. Though Sfrp1was reported to be highly expressed in HFSCs, its role in epidermal stem cell regulation and cancer is still obscure. Therefore, elucidating the role of Sfrp1in regulating HFSCs and CSCs may provide insights into epidermal tissue homeostasis

and cancer development which might help in developing novel treatment strategies for skin cancer.

3.3 Objectives:

1. To unravel the effect of SFRP1 on epidermal stem cell regulation
2. Investigating the stem cell fate in normal skin homeostasis and in skin cancer development, in SFRP1 knockout mice.

3.4 Experimental Plan:

Objective 1: To unravel the effect of SFRP1 on epidermal stem cell regulation

- ***A.*** *Characterization of Sfrp1 knockout mice skin by histological examination during first hair cycle at various postnatal days*
- ***B.*** *Comparative HFSCs analysis in WT and Sfrp1 knockout mice*
- ***C.*** *Analysis of epidermal proliferation and differentiation*
- ***D.*** *Effect of Sfrp1 loss on wound healing response*
- ***E.*** *Comparative gene expression profile analysis (Microarray profiling) of the HFSCs in WT and Sfrp1 knockout mice*
- ***F.*** *Validation of altered signalling pathways in absence of Sfrp1*

Objective 2: Investigating the stem cell fate in normal skin homeostasis and in skin cancer development, in SFRP1 knockout mice.

- ***A.*** *Skin carcinogenesis study using DMBA/TPA in WT and Sfrp1 knockout mice*
- ***B.*** *Characterization of the WT and Sfrp1 knockout mice papillomas and Squamous cell carcinomas*
- ***C.*** *WT and Sfrp1 knockout mice CSCs analysis and their functional characterization*
- ***D.*** *Tumor propagating cell frequency analysis of WT and Sfrp1 knockout CSCs*
- ***E.*** *Comparative gene expression profile analysis (Microarray profiling) of the WT and*

Sfrp1 knockout mice CSCs

F. *Extrapolation of data obtained from murine model to various human epithelial cancers*

3.5 Work done:

The detailed description of the work carried out under the above mentioned objectives are presented as three different chapters as given below.

Chapter 5: To unravel the effect of SFRP1 on epidermal stem cell regulation

a) Introduction for Objective 1
b) Results of work done under Objective 1
c) Discussion

Chapter 6: Investigating the stem cell fate in normal skin homeostasis and in skin cancer development, in SFRP1 knockout mice.

a) Introduction for Objective 2
b) Results of work done under Objective 2
c) Discussion

Chapter 7: Summary and conclusion of both the objectives

Chapter 4: Materials and Methods

4.1 Mice models used in the study:

The protocols for the animal usage in different experimental studies were approved by the "Institutional Animal Ethics Committee (IAEC)'' at ACTREC. All the animal studies were performed by using the standard procedures. The knockout mice models used in this study are mentioned below.

A. Mice models used in this study:

The Sfrp1 knockout mice were a generous gift from Dr. Akihiko Shimono [356]. The homozygous knockout mice ($Sfrp1^{-/-}$) were crossed with the wild type C57BL/6 mice to obtain heterozygous knockout mice ($Sfrp1^{+/-}$). The $Sfrp1^{+/-}$ heterozygous mice were inter-crossed to obtain mice of all the three genotypes viz. WT ($Sfrp1^{+/+}$), heterozygous ($Sfrp1^{+/-}$) and homozygous knockout ($Sfrp1^{-/-}$) from the same litter and are utilized in the experiments.

4.2 Mice genotyping

The mice were weaned after post-natal day 21 (PD21) and were numbered as per universal mouse numbering system. The tail snips were used for genotyping purpose as the distal tail of young mice lacks bone. The tail samples are collected in the lysis buffer and proceed for DNA extraction as described below.

4.2.1 DNA extraction from tail tissue samples

1) The tail samples are collected using sterilized scissors and forceps into a 1.5 ml centrifuge tube (Eppendorf) containing 500 µl of lysis buffer.
2) 10 µl Proteinase K (Stock 20 mg/ml) was added to per 500 µl of lysis buffer and then incubated at 55-60°C overnight.
3) On the next day 300 µl of 5 M NaCl was added to each tube and the tubes were shook vigorously (15-20 times) and then placed on ice for 10min.

4) The tubes were then centrifuged at low speed (7600 rpm) in a table top cooling centrifuge at 4°C for 10 minutes.
5) The supernatant was collected into a fresh centrifuge tube.
6) To the supernatant 650 µl of isopropanol was added and mixed gently by inverting the tubes and incubated at RT for 15 min.
7) After incubation the tubes were centrifuged at 14000RPM for 10 minutes at RT to pellet out the DNA.
8) The supernatant was then discarded and tubes containing the DNA pellet were air dried.
9) 50 µl of sterile water was added to each tube and incubated in dry-bath at 50°C for 5 minutes to dissolve the DNA completely.
10) The DNA concentration and purity (260/280 ratio) was measured by Nano drop quantification.
11) For 25 µl PCR reaction, 1 to 2 µl of DNA was used.

Reagents	**Final Concentration**	**per 500ml**
1M Tris pH 8.0	10 mM	5 ml
5M NaCl	100 mM	10 ml
0.5M EDTA pH 8.0	10 mM	10 ml
10% SDS	0.5 %	25 ml
dH_20		Make up to 500 ml

Table 4.1 Composition of the tail lysis buffer

4.2.2 Primer sequences for the genotyping of Sfrp1, pTRE-H2BGFP and K5tTA

Gene Name	Primer sequence 5'----->3'
Sfrp1 (SAC-II) -Forward	GATTGGTTAACTGCGCGGCTG
Sfrp1(SAC-II) -Reverse	GACTGGAAGCTCACGTAGTCG
Sfrp1(IRES) -Reverse	GGGCCCTCACATTGCCAAAAG

Table 4.2 Primer sequences for mice genotyping

4.2.3 PCR conditions for Sfrp1 mice genotyping:

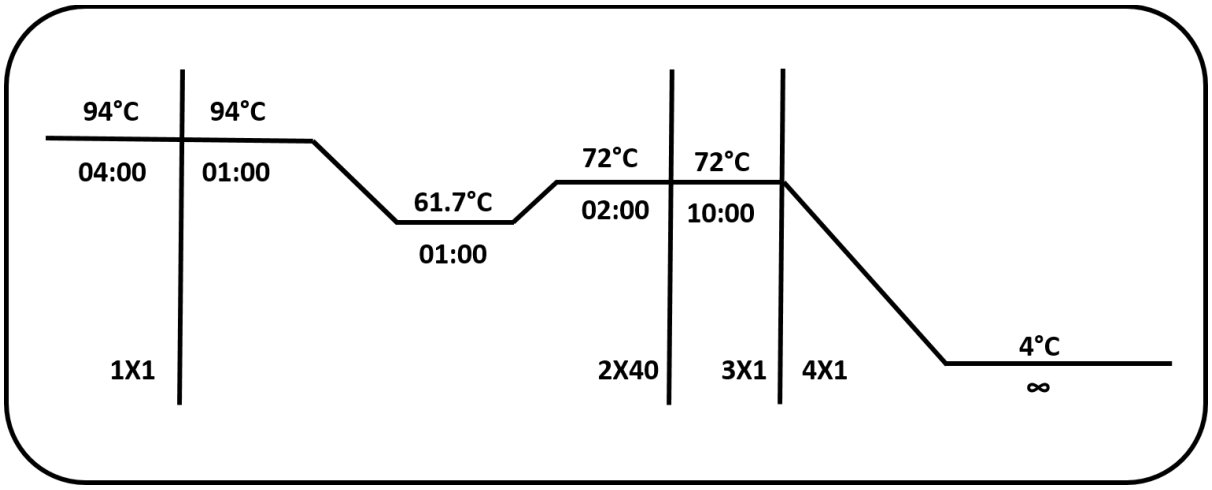

4.3 Tissue processing for histology and paraffin blocks

The mice were eithanised at different PDs throughout the first hair cycle (PD21 to PD49) and the skin tissue samples were collected. To prepare the paraffin embedded blocks the skin is fixed in 4% formalin solution over night at RT followed by treatment with 70% ethanol the next day. Further, these tissues were dehydrated using increasing concentration of ethanol in a sequential manner followed by xylene and then embedded in Paraffin wax. For cryo-

sectioning, the skin tissues were directly embedded in the OCT (Tissue-Teck) compound on the same day of sacrifice and stored at -80°C until use.

4.3.1 Hematoxylin & Eosin staining procedure

a) The paraffin wax embedded tissue sections on the slides were incubated at 60°C for 15-20 minutes to deparaffinise the tissue sections completely.

b) These slides were further transferred into the cleaning agent xylene for 15 minutes.

c) The rehydration of the tissue sections was done by transferring the slides in a sequential manner through couplings containing 100% alcohol, 90% alcohol, 70% alcohol for 10 minutes in each.

d) The slides were then washed in couplings containing water for 10 min.

e) The rehydrated tissue slides were kept in the coupling chamber with Hematoxylin solution for 3-5 minutes depending on the concentration of Hematoxylin.

f) The staining was stopped by transferring the slides into the water and washed for 5 minutes. For long-term storage, the stained sections were dehydrated by transferring the slides in a sequential manner through couplings containing 70% alcohol, 90% alcohol, 100% alcohol for 10 min. in each.

g) The slides were then treated with Xylene: alcohol and Xylene for 10 min.

h) After air drying the slides they were mounted using DPX mountant and coverslips.

i) The morphology of the skin tissues and stages of the hair follicle were analyzed by using the upright microscope.

4.4 Immunohistochemical staining (IHC)

Immunohistochemical staining (IHC) was preferably performed on the paraffin-embedded tissues sections as it involves a harsh method of heat mediated antigen retrieval. The general steps of IHC procedure are given below.

a) The slides with paraffin-embedded skin sections were kept at 60°C for 15 minutes and treated with xylene for 15 minutes for complete deparaffinization.

b) The tissue sections were then treated with the xylene alcohol (1:1 mixture), 100% alcohol, 90% alcohol, 70% alcohol and water for 10min. each in sequential manner to rehydrate the tissue sections.

c) The antigen unmasking was performed by using the 10mM sodium citrate buffer, pH 6.0 or Tris-EDTA buffer, pH 9.0 in the microwave for 10 minutes at Hi-power.

d) Sections were then allowed to cool at RT for 45 minutes and washed with water for five minutes.

e) The endogenous peroxidase activity was blocked by treating the sections with a solution of hydrogen peroxide and methanol (3% H_2O_2 in Methanol) for 10 minutes at RT.

f) The sections were then washed twice with 1X PBS 5min. each followed by blocking with normal horse serum (5%NHS in 1X PBS) for 1 hour at RT.

g) The primary antibody was diluted in the blocking buffer and applied on the tissue sections followed by incubation at 4°C overnight.

h) The following day, the sections were washed thrice with the washing buffer (PBST 0.1% Tween20) for 5 minutes each.

i) For the Avidin-Biotin complex (ABC) formation, Reagent A and Reagent B were premixed for 45 minutes and then the mixture was added on to the tissue sections followed by incubation for 1 hour at RT.

j) The solution was removed, and sections were washed with 1X PBST three times for 5 min. each.

k) The DAB (3, 3'-diaminobenzidine) was prepared in the 1X PBS and slides were incubated in the DAB mixture for 10sec. to 2 minutes depending on the development of the staining.

l) The reaction was stopped by transferring the slides to the coupling containing water.

m) The tissue sections were counterstained with hematoxylin for 1 minute and washed with distilled water for 5 minutes.

n) The dehydration of the tissue sections was done by treating the sections using higher grades of the alcohol (70%, 90% and 100% alcohol) in sequential manner followed by xylene:alcohol and xylene 10min each, and the sections were mounted with Dibutylphthalate Polystyrene Xylene (DPX) mountant.

4.5 Immunofluorescence staining (IFA)

a) The skin tissues were embedded in the OCT (Optimal Cutting Temperature) compound and 5 µm to 10 µm sections were cut on to poly-lysine coated slides using Leica cryostat machine and the slides were stored at -80°C freezer.

b) On the day of staining, the slides from -80°C freezer were air dried completely.

c) The fixation was performed by using either 4% paraformaldehyde in 1X PBS for 20 minutes at RT or in chilled Acetone for 20 minutes at the -20°C.

d) The fixative was removed and sections were bordered by using hydrophobic PAP pen.

e) The sections were washed with 1X PBS for three times five min. each.

f) The free sites of the PFA were blocked by using 20mM Glycine solution for three times five minutes each.

g) The sections were washed with 1X PBS for three times five min. each.

h) The solution of 0.2% Triton X-100 in 1X PBS was used for permeabilization of the tissue for 10 minutes.

i) Sections were washed with 1X PBS and blocked by 2.5% NDS, 2.5% NGS, 1% BSA and 2% gelatin for one hour at RT.

j) Primary antibody was diluted in blocking buffer and was added to the sections. The slides were then incubated overnight at 4°C.

k) Next day, the sections were washed using 1X PBS containing 0.1% Tween-20 for three times five minutes each.

l) The appropriate secondary antibody (Anti rat/Anti Rabbit) conjugated with the fluorochrome was diluted in 1X PBS (1:400) and incubated with sections for one hour at RT.

m) Sections were washed with the 1X PBS containing 0.1% Tween-20 for three times five minutes each and incubated with DAPI (stock 1mg/ml).

n) Excess DAPI was removed by 1X PBS washes and the sections were mounted by using Antifade and sealed with nail polish.

o) The images were acquired using LSM 780 Carl Zeiss Confocal system.

4.6 Antibody details

Different primary and secondary antibodies used in this study are mentioned in the below **Table** with its dilution factor in particular application and its source.

Antigen/Antibody	**Dilution /Application**	**Source**
Fluorescence activated cell sorting (FACS)		
CD34 biotin	15µl/Reaction	eBiosciences
APC Streptavidin	7.5µl/Reaction	BD Pharmingen
α-6 integrin-PE	20µl/Reaction	BD Pharmingen
Epcam APC-Cy7	5µl/Reaction	Biolegend
CD31-FITC	4µl/Reaction	Biolegend
CD45-FITC	4µl/Reaction	Biolegend
CD140a-FITC	2µl/Reaction	eBiosciences
Immunofluorescence Assay (IFA)		
CD34	1:100	BD Pharmingen

α-6 integrin	1:100	BD Pharmingen
Active β-carenin	1:100	Cell Signalling Technologies
BrdU	1:100	Abcam
Ki67	1:100	Abcam
Sox-9	1:300	EMD Millipore
Axin2	1:100	Abcam
p-AKT (Ser-473)	1:100	Cell Signalling Technologies
Keratin5 (K5)	1:100	Abcam
Keratin8 (K8)	1:100	Abcam
Vimentin	1:150	Abcam
Sox-2	1:100	Abcam
Anti-Rat FITC	1:400	Jackson Laboratories
Anti-Rat Alexa 568	1:400	Abcam
Anti-Rabbit FITC	1:400	Jackson Laboratories
Anti-Rabbit Alexa 568	1:400	Abcam
Immuno-Histochemistry (IHC)		
Sfrp1 (Human)	1:100	Abcam
Sox-2 (Human)	1:100	Abcam
Vimentin (Human)	1:300	Abcam
Sox-9 (mouse)	1:100	EMD Millipore
Biotin-labelled anti-Rabbit	1:200	Vector Laboratories
Western Blot		
Active β-carenin	1:1000	Cell Signalling Technologies
β-carenin	1:1000	Cell Signalling Technologies
Axin2	1:1000	Abcam
GSK-3β	1:2000	Cell Signalling Technologies
p- GSK-3β (Ser-9)	1:1000	Cell Signalling Technologies
AKT	1:1000	Cell Signalling Technologies
p-AKT (Ser-473)	1:1000	Cell Signalling Technologies
PI3K-110α	1:1000	Cell Signalling Technologies
Cyclin-D1	1:2000	BD Pharmingen
Runx-1	1:2000	Santa Cruz
P21	1:2000	Abcam
Sox-2	1:1000	Abcam
Sfrp1	1:1000	Abcam
Actin	1:4000	Sigma
Anti-Mouse HRP	1:5000	Santa Cruz Biotechnology
Anti-Rabbit HRP	1:5000	Santa Cruz Biotechnology

Table 4.3 List of the primary and secondary antibodies

4.7 BrdU label retention cell (LRC) assay

BrdU (5-bromo-2'-deoxyuridine) is a nucleoside analog of thymidine which gets integrated into newly synthesized DNA strands within proliferating cells. LRC assay exploits the fact that upon replication the BrdU gets equally distributed among the daughter cells and gets diluted with each cell division; however, the non-proliferating cells retain the label for long period of time and are termed as Label-retaining cells (LRCs). The newborn pups (PD3-PD5) were injected with BrdU at the dose of 50mg/kg bodyweight for every 12 hours for a total of six subcutaneous injections. This particular dose is sufficient to label almost all the cells, as the cells of newborn mice are highly proliferative. The pups injected with BrdU were chased upto PD49 (2^{nd} telogen) and sacrificed to analyze LRCs in the hair follicles. The BrdU in the cells was exposed by treating the tissue sections with 2N HCL for 1 hour at 37°C and detected by the anti-BrdU antibody through immunofluorescence assay [136, 174, 175, 357].

4.8 BrdU cell proliferation assay

To study the proliferation difference *in vivo,* mice at 1^{st} telogen (PD20) were injected intraperitoneally with BrdU (50mg/kg of body weight) accompanied by 0.8mg/ml BrdU in water for three days. Mice were then sacrificed at PD23 and IFA for BrdU was performed using anti BrdU antibody on the mice dorsal skin sections. To study *in vitro* keratinocytes proliferation, the primary keratinocytes were treated with incomplete E-media for 24 hours to synchronise their cell cycle phase. Later, the incomplete media is replaced with complete E-media containing BrdU at a final concentration of 10μM was added and the cells were allowed to grow for 8 to 10hrs. The cells were then fixed with 4% paraformaldehyde and BrdU was exposed by 2N HCl treatment for one hour. The BrdU positive cells were labelled by anti-BrdU antibody and detected by immunofluorescence assay. A total of 1000 cells were counted and plotted as % of BrdU positive cells with respective control.

4.9 Fluorescence Activated Cell Sorting (FACS)

4.9.1 Isolation of total epidermal cells

Day I:

a) The mice were sacrificed in a CO_2 chamber and the hairs were removed by using hair clippers/trimmer.

b) The skin was separated from the corpse with the help of clean scissors and forceps.

c) The subcutaneous fat and capillaries were removed from the dermal side by scrapping with a scalpel blade and the skin was washed in 70% ethanol and then in sterile 1X PBS.

d) The skin was placed (Dermal side down) in the 90 mm plate containing 12 ml of the ice-cold 0.25% Trypsin-EDTA solution and the plates were incubated 4°C refrigerator overnight.

Day II:

a) The FACS tubes were coated with 50% FBS in 1X PBS for half an hour and then washed with ice-cold 1X PBS and kept at 4°C.

b) Fresh 12 ml of the 0.25% ice-cold Trypsin-EDTA solution was added in all the plates containing skin and incubated at 37°C for 30 minutes.

c) The trypsin action was inhibited by addition of the 12 ml of ice-cold E-Media containing 15% chelated FBS.

d) The epidermal side was scraped multiple times using scalpel blade to separate the epidermis from dermis.

e) The epidermal chunks were minced using sterile scissors to release the cell clumps into the solution.

f) The solution was passed through pipette multiple times to make single cell suspension that was further strained using 70 µm and then 40 µm strainers.

g) The filtered solution was centrifuged at 2000 rpm for five min. at 4°C.

h) The cell pellet was washed by using ice-cold 1X PBS and centrifuged again.

i) The cell pellet was then dissolved in 750 µl of 5% chelated FBS in 1X PBS (FACS buffer) and stained with the antibodies as described in the table below.

j) Well established HFSCs markers (CD34 and α6-Ingegrin) were used to sort HFSCs using FACS Aria machine (BD Biosciences).

k) The HFSCs were directly sorted into the E-media for colony forming efficiency or into the RNA lysis buffer for RNA extraction.

4.9.2 Staining procedure for hair follicle stem cells

Tube No.	Tubes details	Step-1	Step-2	Step-3	Step-4	Step-5
1	Only cells	100µl cells	**a)** Mix well by gentle tapping and incubate at 4^0C for 30 minutes. Do not allow cells to form pellet during incubation **b)** Add double volume of ice cold 1X PBS in the tube no 6 and 7. **c)** Centrifuge tubes no 6 and 7 at 1000 rpm for 5 minutes at 4^0C. **d)** Discard the supernatant and add 100 µl FACS buffer in tube no. 6 and 750 µl in tube no 7.	---	**a)** Mix well and incubate the tubes at 4^0C for 30 min. keep tapping in between. **b)** Add double the volume of ice cold 1X PBS in all the tubes after incubation. **c)** Centrifuge the tubes at 1000 rpm for 5 min. at 4^0C.	---
2	PI control	100µl cells		---		Add 100 µl of 2X PI, keep the tube on ice
3	PE Isocontrol	100µl cells		1.3 µl PE Iso-type control antibody		Resuspend pellet in 100 µl of FACS buffer, keep the tubes on ice
4	α6 PE	100µl cells		2.6 µl of α6-PE Antibody		
5	APC control	100µl cells		1 µl Streptavidin-APC Antibody		
6	CD34 +APC	100µl cells + 2 µl of CD34 Antibody		1 µl Streptavidin-APC Antibody		
7	Test	750µl cells + 15 µl of CD34 Antibody		7.5 µl Streptavidin-APC + 20 ul α6 PE Antibody		Re-suspend pellet in 1X PI, keep the tubes on ice

Table 4.4 Staining procedure of the HFSCs for flow cytometry

4.10 Primary keratinocytes culture

A. Solutions Preparation:

a) 5 mg/ml Insulin (minimum M.W. = 6000g, approx. 8.3 x 10^{-4} M)

- Weigh out 250 mg of Insulin (Sigma I-5500)
- Add to 50 ml of 0.1N HCl and dissolve it completely
- Store in 10 ml aliquots in 15 ml tubes at 4^0C in a refrigerator

b) 5 mg/ml Transferrin

- Weigh out 250 mg of Transferrin (Sigma T-2252)
- Add to 50 ml of sterile PBS and store frozen in 10ml aliquots

c) 2 x 10^{-8} M T_3 (3,3',5-Triiodo-L-Thyronine)

- Weigh out 13.6 mg of T_3 (Sigma T-2752)
- Dissolve in 100 ml of 0.02N NaOH = 2 x 10^{-4} M T_3 (Freeze)
- Take 0.1 ml of 2 x 10^{-4} M T_3 and dissolve in 9.9 ml of sterile 1X PBS to prepare 2 x 10^{-6} M T_3
- Take 0.1 ml of 2 x 10^{-6} M T_3 and dissolve in 9.9 ml of sterile 1X PBS to prepare 2 x 10^{-8} M T_3

d) 100x Cocktail

5mg/ml Insulin	20 ml
5mg/ml Transferrin	20 ml
2 x 10^{-8} M T_3 (Tri-iodothyronine)	20 ml
140ml 1xPBS (sterile)	140 ml
TOTAL	**200 ml**

- Sterilize the mixed solution and store in aliquots.

e) Hydrocortisone

- Calbiochem: Cat. # 386698
- Prepare stock solution 4mg/ml in 95% EtOH
- Filter-sterilize and aliquot 1ml each into a sterile 15ml Falcon tube
- Store at -20^{0}C

f) Cholera toxin

- MP Biochemicals Cat. # 150005
- To prepare 10^{-6} M stock solution: Dissolve 1mg vial of CT in 11.9 ml of glass distilled water
- Filter and make aliquot of 1 ml and store at 4^{0}C.

B. Media preparation

Prior to the start of media preparation, the fetal bovine serum was chelated using Chelex X-100 resin (Bio-Rad) after adjusting the pH of the resin to 7.4 using HCL. To 850 ml of milliQ water 10.625g calcium free E-media powder, 3.07g sodium bicarbonate and 0.475 gm of glutamine was added to prepare 1L media and the pH was adjusted to 7.2 using 1N HCl. Then compressed CO_2 was applied to the media for a time period of 2.5 min per 1L of media until the amber color develops. To the 150 ml of chelated FBS, a cocktail of growth factors were added as described previously [358]. Further, the 150ml serum with added growth factors was mixed with 850 ml media and the concentration of Ca^{2+} in the media was adjusted to 0.05 mM. The complete E-media was then filter sterilized and checked for contamination prior to use.

C. Primary keratinocyte cell culture

a) The newborn pups (PD2) were sacrificed by decapitation in the culture hood.

b) The skin was removed by using sterile scissors and forceps and placed with dermal side up on a clean paper.

c) The dermal fat tissue and blood capillaries were gently scraped of using a sterile scalpel blade.

d) The skin was then sterilized by transferring it through a series of baths containing 70% ethanol followed by sterile 1XPBS.

e) The skin was then placed dermal side down in a 35 mm plate containing 1 ml (5units/ml) of dispase solution (Stem cell technologies) and incubated overnight at 4^0C.

f) The next day, 4 ml of freshly prepared 0.1% Trypsin:EDTA (1:1) solution was added to a 60 mm plate and kept ready.

g) Using a fine pair of forceps and a bevelled pair of forceps the epidermis was carefully separated from the dermis.

h) The separated epidermis was then placed in the 60 mm plate containing Trypsin:EDTA solution and minced into small pieces using sterile scissors and incubated at 37^0C for 5-10 min.

i) The Petri dish was gently stirred manually (every 5min) and observed under the microscope to make sure that the cells are coming out of the epidermis.

j) 6 ml of cold complete E-media was added to the 60 mm plates and mixed it with 10 ml pipette 5-6times to properly separate the cells.

k) The cell suspension was strained using 100μm strainer into 50 ml tubes to remove the clumps.

l) The strained solution was then transferred to a 15ml centrifuge-tube and centrifuged at 1000 rpm for five min.

m) Supernatant was decanted and the pellet was carefully washed by re-suspending in sterile 1X PBS.

n) The PBS was removed after centrifugation and the pellet was re-suspended in 1 ml of E-media.

o) The cell suspension was carefully added into 60 mm plate containing conditioned E-media with irradiated J2-3T3 fibroblast (prepared one day before).

p) The cells were allowed to attach and grow without any disturbance.

q) Fresh irradiated J2-3T3 fibroblasts were added whenever required during the media change.

r) Once the keratinocytes cell confluency reached 70 to 80 %, the fibroblast were removed by differential trypsinization and the grown keratinocytes were added into new 60 mm plates already containing attached J2-3T3 fibroblast without any dilution.

s) Feeder (J2-3T3 fibroblasts) independent keratinocytes started growing after 8^{th} passage.

4.11 Colony forming efficiency

a) The keratinocytes cultures of all the three genotypes (WT, Sfrp1+/- andSfrp1-/-) were trypsinised and single cell suspension was prepared.

b) The cell number was counted using haemocytometer.

c) 5000 cells of each genotype were plated into six well plates and the plates were kept in Co2 incubator.

d) The colonies were allowed to grow for a week.

e) Once the colonies are formed the colonies were fixed with 4%PFA.

f) Crystol violet staining was performed to stain the colonies and the images were captured.

4.12 Protein isolation from cultured keratinocytes and mice skin

The primary keratinocytes were cultured up till 80% confluency in 60 mm Petri plates. The cells were washed twice using ice-cold 1X PBS. 100µl of ice-cold RIPA buffer (Sigma) with 1x protease/phosphatase inhibitor cocktail (cell signalling technologies) was added to the plate. The cells were then scraped using cell scraper and lysate was collected in the 1.5 ml centrifuge tube. The tubes were kept on ice for 30 minutes with vortexing for 5 seconds at every 10 minutes interval. The whole cell lysate was centrifuged at maximum speed for 45 minutes at 4^0C. The supernatant was collected in fresh tubes and stored at -80^0C. To isolate protein from the mice epidermis, the skin was kept in phosphate buffer containing 0.5 M ammonium thiocyanate, pH 6.8 for 20 min on ice. The epidermis was scraped in lysis buffer (1% NP-40, 0.5%deoxycholate and 0.2% SDS, 150mM NaCl, 2mM EDTA, 0.8mM EGTA, 10mM Tris-HCl, pH 7.4 with protease phosphatase inhibitor cocktail[359]. The protein lysate was prepared as described above. Protein estimation was performed using Bradford's method [360].

4.12.1 Protein estimation by Bradford's method

a) The protein standards with concentrations ranging from 0.0625mg/ml to 1mg/ml were prepared by using Bovine serum albumin (BSA).

b) The unknown samples were diluted 5X to 10X using the same lysis buffer in which they are present.

c) 5µl of each standard and test samples were added in triplicates to the 96well plate.

d) To each well 200µl of 1x Bradford reagent was added.

e) The samples were mixed well on a rocker and the absorbance was measured at 595 nm using a spectrophotometer.

f) The protein concentration was calculated based on the standard curve.

4.13 Western blot:

Day 1:

a) The SDS-PAGE gel was prepared using Bis-Acrylamide: Acrylamide (1:29), Tris HCL (pH-6.8 & 8.8), 10%SDS, 10%APS and Temed.

b) Equal concentrations of proteins along with protein loading dye were loaded on to the gel after denaturing them at 95°C.

c) Once the protein was resolved it was transferred on to nitrocellulose/PVDF membrane.

d) After protein transfer, the membrane was blocked either with 5%BSA or 5% milk prepared in 0.1% TBST for 1hour at room temperature to prevent the nonspecific binding of the antibody.

e) Primary antibody (prepared in 5% BSA in 0.1% TBST) was added to the membrane with respective dilution and incubated at 4°C O/N.

Day 2:

a) The primary antibody was removed and the membrane was washed with 0.1% TBST thrice for 10min.

b) Secondary antibody (prepared in 1% or 2.5% BSA in 0.1% TBST) was then added to the membrane with respective dilution and incubated at room temperature.

c) The secondary antibody was removed and the membrane was washed with 0.1% TBST thrice for 10min.

d) The expression and activity of the proteins were then quantified using ECL prime kit (GE) in a Chemi-doc.

4.14 RNA extraction and Quantification:

HFSCs ($CD34^+/\alpha6\text{-}Integrin^+$) and CSCs ($Lin^-/Epacm^+/\ \alpha6\text{-}Integrin^+/CD34^+$) were FACS sorted using specific markers into RNA lysis buffer from WT, *Sfrp1*$^{+/-}$ and *Sfrp1*$^{-/-}$ mice and their tumors respectively. Further, the RNA extraction was performed using Absolutely RNA Miniprep Kit-Agilent technologies (Cat. no.: 400800). The quality of the RNA was checked using Agilent RNA 6000 Pico Kit (Cat. no.:5067-1513) as per the instructions provided in the manual on the Agilent 2100 Bioanalyzer. Further, the samples with good RNA quality, i.e. RNA integration number (RIN) value greater than 8 were used for gene expression profile analysis.

4.15 RNA extraction from keratinocytes

a) The keratinocytes were cultured up to 80-85% confluency in a 60mm Petri dish.

b) The media was aspirated and the residual media was removed by washing the cells twice using 1X PBS.

c) To the Petri dish 1ml of TRI Reagent (Sigma) was added and the cells were scrapped using a cell scrapper.

d) The lysate was collected into a 1.5ml centrifuge tube and a freeze-thaw cycle was given for efficient RNA extraction.

e) To the lysate 0.2ml of chloroform was added and mixed well by vortexing and incubated at RT for 5min.

f) The samples were centrifuged at 12000g for 15min. at 4°C.

g) The aqueous upper layer was collected into a fresh tube without disturbing the interphase.

h) To the aqueous phase 0.5ml of isopropanol was added and mixed gently by inverting the tubes several times and incubated at RT for 10min.

i) The samples were centrifuged at 12000g for 10min at 4°C.

j) The supernatant was discarded and the pellet was washed using 75% ethanol and centrifuged at 7500g for 10min.

k) The supernatant was discarded and tubes were air-dried and RNA was dissolved in the nuclease-free water.

l) The amount and quality of RNA were analysed by using the Nano-Drop Spectrophotometer (Thermo Scientific, USA).

4.16 Expression profile of HFSCs:

RNA was extracted from the FACS sorted CSCs by using the absolutely RNA miniprep kit as described in the manufacturer's procedure (Cat: 400800, Agilent technologies). The RNA quality was assessed by Agilent RNA 6000 Pico kit on the Agilent 2100 bioanalyzer. For microarray analysis, 1ng RNA was amplified by using the GeneChip® WT Pico amplification Kit (Affymetrix, USA) as per manufacturer recommendation. Further, 1 μg total RNA was reverse transcribed to cDNA with T7 Oligo d (T) primer (Affymetrix). The cDNA was used for in vitro transcription reactions containing T7 RNA polymerase. Then sense-strand cDNA was synthesized by the reverse transcription of cRNA using 2nd-Cycle Primers followed by RNase H hydrolyzes the cRNA template leaving single-stranded cDNA. The purified, sense-strand cDNA was fragmented by uracil-DNA glycosylase (UDG) and apurinic/apyrimidinic endonuclease 1 (APE 1) at the unnatural dUTP residues that break the DNA strand. The fragmented cDNA was labelled by terminal deoxynucleotidyl transferase (TdT) by using the Affymetrix proprietary DNA Labelling Reagent that is covalently linked to biotin. The fragmented and labelled product was loaded onto GeneChip® MTA 1.0 array (Affymetrix, USA) and was hybridized according to the manufacturer's protocol.

Streptavidin-Phycoerythrin (Molecular Probes) was used as the fluorescent conjugate to detect hybridized target sequences. Raw intensity data from the GeneChip array were analyzed by GeneChip Operating Software (Affymetrix). The raw signal intensity data (.CEL files) obtained from the Affymetrix GeneChip® Command Console (AGCC) software were normalized and summarized using the RMA sketch algorithm implemented in Expression Console to generate normalized intensity data (.CHP files).

4.17 Real time PCR

The RNA isolated was utilized to prepare cDNA as per manufacturer's protocol (Thermo Scientific, USA) by using superscript IV reverse transcriptase. Total 3-4 µg of total RNA was reverse transcribed and diluted to10ng/µl before utilizing the cDNA in qRT-PCR reactions. The qRT-PCR was performed by using KAPA SYBR FAST (KAPA BioSystems Cat. no.: KK4601). The expression level of the genes was normalized to the expression of either GAPDH or β-Actin. The fold change was calculated by $2^{\wedge -\Delta\Delta Ct}$ method.

List of primers utilised in the study:

S.NO	GENE	Forward Primer (5'-3')	Reverse primer (5'-3')
1	Snail	GTCTGCACGACCTGTGGAA	CAGGAGAATGGCTTCTCACC
2	E-Cadherin	CAGCCTTCTTTTCGGAAGACT	GGTAGACAGCTCCCTATGACTG
3	N-Cadherin	ATGTGCCGGATAGCGGGAGC	TACACCGTGCCGTCCTCGTC
4	Zeb1	GCCAGCAGTCATGATGAAAA	TATCACAATACGGGCAGGTG
5	Twist1	AGCTACGCCTTCTCCGTCT	TCCTTCTCTGGAAACAATGACA
6	Twist2	CGCTACAGCAAGAAATCGAGC	GCTGAGCTTGTCAGAGGGG
7	Nr2f1	CCAGGCCAGTATGCACTCAC	CCGGGAAGAACGGGATGTT
8	c-Jun	AGCCTACCAACGTGAGTGCT	AGAACGGTCCGTCACTTCAC

9	c-Fos	GCCCAGTGAGGAATATCTGGA	ATCGCAGATGAAGCTCTGGT
10	Sox-2	CCTGGGCAGCGTGGCGGA	CAGACTGCGGGAAGAAGACG
11	p21	ATCCCGACTCTTGACATTGC	ACCCTAGACCCACAATGCAG
12	Vimentin	CGGCTGCGAGAGAAATTGC	CCACTTTCCGTTCAAGGTCAAG
13	Keratin-8	GGACATCGAGATCACCACCT	TGAAGCCAGGGCTAGTGAGT
14	Wnt3A	AATTTGGAGGAATGGTCTCTCGG	CAGCAGGTCTTCACTTCACAG
15	Wnt7B	ATCGACTTTTCTCGTCGCTTT	CGTGACACTTACATTCCAGCTTC
16	Ctnnb1	CCCAGTCCTTCACGCAAGAG	CATCTAGCGTCTCAGGGAACA
17	Tgfβr3	CATCTGAACCCCATTGCCTCC	CCTCCGAAACCAGGAAGAGTC
18	Sfrp1	GACATCGGCTCGTATCAGAG	GTTGGGCAGCACCATCTTC
19	Sfrp2	GGCCACGAGACCATGAAGG	GAAGAGCGAGCACAGGAACT
20	Sfrp3	CGCCGTTGTGGAAGTGAAG	CAGTAAGTGGAGGACAGAGG
21	Sfrp4	AGAAGGTCCATACAGTGGGAAG	GTTACTGCGACTGGTGCGA
22	Sfrp5	GAGATCAAGATAGACAACGGGGA	TTGCGCTTTAAGGGGCCTG
23	Dkk1	ATATCACACCAAAGGACAAGAAGG	AGGTTTACAGATCTTGGACCAGAA
24	Dkk3	AGCTGCTAAAACGTCCTCTGA	CTGGTCTCATTGTGATAGTTGGG
25	Wif1	GATCCAACTGTCAATGTCCCTT	ACACGGGAAACCAACTTGAAC
26	Gsk-3β	AAGCGATTTAAGAACCGAGAGC	AGAAATACCGCAGTCGGACTAT
27	Axin2	AACCTATGCCCGTTTCCTCTA	GAGTGTAAAGACTTGGTCCACC
28	Lgr5	ACATTCCCAAGGGAGCGTTC	ATGTGGTTGGCATCTAGGCG
29	Sox-2 human	GCCGAGTGGAAACTTTTGTCG	GGCAGCGTGTACTTATCCTTCT
30	Sfrp1 human	ACGTGGGCTACAAGAAGATGG	CAGCGACACGGGTAGATGG

Table 4.5 List of primers utilized

4.18 Chemical induced skin carcinogenesis (DMBA/TPA):

The two-stage chemical induced skin carcinogenesis was used in our study. The mice (WT, $Sfrp1^{+/-}$ and $Sfrp1^{-/-}$) at PD22 were shaved to remove the hairs. The mice were then treated with DMBA (50µg; 195nMol per animal) 3 times at PD23, PD-25 and PD27. This was followed by the administration of TPA (2.5µg; 4nMol per animal) twice weekly until the mice were sacrificed. The mice were timely shaved for the topical application of TPA. The time of tumor initiation, number of tumors per mice and size of the tumors were recorded.

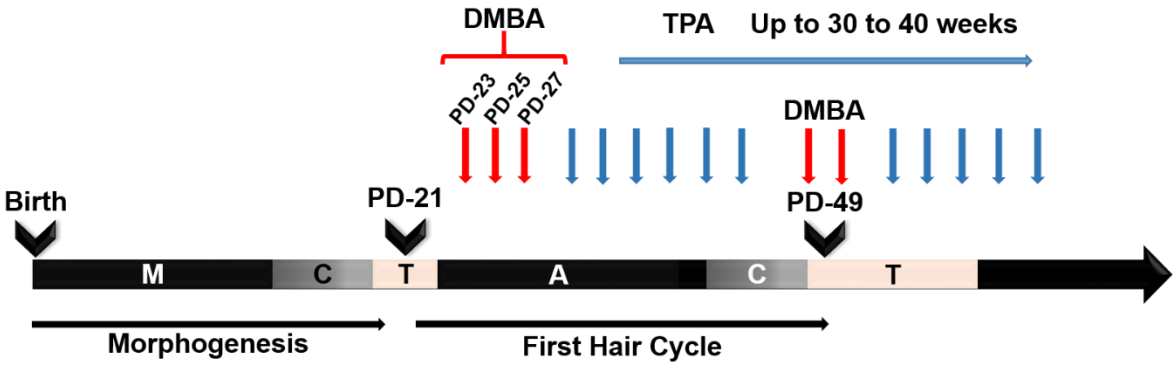

Fig. 4.1: Schematic for DMBA/TPA treatment

Reagent preparation:

DMBA (7, 12-dimethylbenz[a]-anthracene):

- 15mg of DMBA powder was dissolved in 4.68ml of Acetone to prepare the stock solution (3.2µg/µl).
- The stock is diluted 10 fold (1ml of stock in 9ml of acetone) to prepare the working solution of DMBA (0.32µg/µl)
- A volume of 156.25 µl (50µg) was administered to per animal.

TPA (12-O-tetradecanoyl phorbol-13-acetate):

- 1mg/ml stock was prepared by dissolving the TPA in acetone.
- The stock is diluted with acetone to prepare a working solution of TPA (0.0125µg/µl).

- ❖ A volume of 200µl (2.5µg) of working solution was administered per animal.

4.19 Tumor collection and single cell suspension preparation:

a) Mice with tumors were euthanized and then the hairs were removed with hair clippers.

b) The tumors were collected and the excess skin was removed using scalpels.

c) After cleaning the tumors, they were collected in cold 1X HBSS buffer for further processing.

d) In the culture hood, the tumors were washed with 1X HBSS to remove any traces of blood cells etc.

e) The tumor sample was kept in a 60mm Petri dish and then minced with the help of scalpel blade and then digested with 2ml of 0.25% collagenase I in 1X HBSS at 37°C for 1hour.

f) The digestion was inhibited by adding double the volume of 10% FBS in 1XPBS

g) The cell suspension was then passed through the 100µm strainer and the left over tumor chunks were further digested with 2ml of 0.25% trypsin for 10min at 37°C.

h) The trypsin was neutralized by 10% FBS in 1XPBS.

i) The cell suspension was passed through 70µm strainer and then centrifuged at 2000rpm for 5min.

j) The supernatant was discarded and the cell pellet was washed with 1X PBS.

k) 1XPBS was removed after centrifugation at 2000rpm for 5min and the cell pellet was dissolved in 1ml of FACS buffer (5% of FBS in 1X PBS).

4.20 Isolation of Cancer stem cells:

a) The single cell suspension made from the tumors was used for cancer stem cell isolation.

b) The well-established CSCs markers ($Lin^-/Epcam^+/\alpha6\text{-}Integrin^+/CD\text{-}34^+$) [361-363] were utilised for CSCs isolation. The lineage markers utilised includes antibodies for CD45 (leukocyte common antigen that marks immune cells), CD31 (endothelial cells) and CD140a (cancer associated fibroblasts).

c) The primary antibody CD34 biotin (eBiosciences) was added to the tumor cells and incubated on ice for 30min. with intermittent tapping at every 5-10min.

d) After incubation the cells were washed with double the volume of 1xPBS and the centrifuged at 2000rpm for 5min.

e) The supernatant was discarded and the cell pellet was dissolved in FACS buffer.

f) The secondary antibody Streptavidin APC and α6-Integrin conjugated with PE (BD Pharmingen), and all the lineage marker antibodies such as CD31 (Biolegend), CD45 (Biolegend), CD140a (eBiosciences) conjugated with FITC and Epcam-APC-Cy7 (Biolegend) were added to the cells and incubated on ice for 30min. with intermittent tapping at every 5-10min.

g) The cells were then washed with double the volume of 1xPBS and the centrifuged at 2000rpm for 5min.

h) The cell pellet is now dissolved in 1X PI made in FACS buffer.

i) The CSCs were then properly gated based on the controls and sorted using FACS Aria machine (BD Biosciences) into E-Media for *in vivo* tumorigenesis assay and RNA lysis buffer for RNA isolation.

4.21 *In vivo* tumorigenesis assay:

To determine the role of Sfrp1 in CSCs regulation, we have performed *in vivo*-tumorigenic potential assay. CSCs (20,000 cells) from WT and Sfrp1$^{-/-}$ mice skin squamous cell carcinomas were FACS sorted into E-media. The cells were then mixed with matrigel in 3:1 ratio and subcutaneously transplanted into NOD/SCID mice. The tumor development and progression were documented twice every week. The tumor dimensions were measured using a Vernier calliper, and the difference in tumor volume with respect to time between WT and Sfrp1$^{-/-}$ CSCs was plotted by using Graph-Pad Prism6 software.

4.22 Limiting Dilution assay:

Limiting dilution assay was performed to determine the presence of CSCs as well the minimum number of CSCs required for tumor initiation. CSCs as low as 10000, 5000 and 1000 cells were FACS sorted from both WT SCCs and Sfrp1$^{-/-}$ SCCs and transplanted into NOD/SCID mice after mixing them with matrigel. The tumor development and progression was documented twice every week with photographs from time of transplantation to experimental end point. The tumor dimensions were measured using a Vernier calliper, and tumor volume was plotted by using Graph-Pad Prism6 software. The tumor propagating cell (TPC) frequency of WT and of Sfrp1$^{-/-}$ CSCs was calculated as reported earlier [364].

4.23 Cell lines and tumor tissue samples

Primary keratinocyte cell cultures of the all the three genotypes (WT, Sfrp1$^{+/-}$ and Sfrp1$^{-/-}$) were established in the lab and are maintained using E-media at 37°C and 5 % CO2. The A3886 (skin cutaneous SCC cell line, a generous gift from Dr. Colin Jamora's lab, Instem, Bengaluru), MCF-10A (control) and MDA-MB-231 (Triple negative breast cancer) cell lines were cultured by using the Dulbecco Modified Eagle Medium (DMEM) containing 10% foetal bovine serum (FBS) and 1% antibiotics (Invitrogen). The cell lines were passaged by

using 0.25% Trypsin: EDTA solution and maintained at 37°C and 5 % CO2. The OSCC (advanced stage treatment naive samples) and breast tumor (Invasive ductal carcinoma samples) tissues samples used in the study were approved by the Institutional Ethics Committee (IEC) under the project numbers 188 and 164 respectively.

4.24 *In silico* analysis of Sfrp1 and Sox-2 expression in TCGA dataset, their inter-correlation and link with clinical parameters:

To analyze the expression levels of Sfrp1 in normal and tumor samples of HNSCC, TCGA PANCAN normalized raw counts were obtained from UCSC cancer genome browser. These counts were transformed in (log2+1) values and represented between normal and tumor samples. Stage wise data was fetched from clinical data file of cBioPortal. Boxplot representation was performed in R 3.3.3 (http://www.R-project.org/). To see the correlation between Sfrp1 and Sox-2 in tumor samples, Z scores were represented. Z scores for each tumour sample was calculated by subtracting the log2 normalized counts of each tumour sample from average mean log2 normalized count of normal samples and dividing that result by the SD of log2 normalized values of the normal samples. Heat map was also constructed using R 3.3.3 where Z-score >1.5 was considered as up-regulation and <-1.5 was considered as down-regulation. KMsurv package in R 3.3.3 was used to determine the correlation between overall survivals in patients with high and low expression of Sfrp1. The cut off values of Z-scores were used to identify patients with low v/s high expression levels and P values were determined using a chi-squared analysis.

4.25 Statistical analysis

Statistical analysis was performed for tumor incidences, tumor volume, Real-time PCR, proliferation studies and FACS analysis by using unpaired two-tailed student's t-test with Graph Pad Prism 6. The t. test function in R 3.3.3 was used to calculate the p-value for TCGA data. The overall survival plots were plotted using Kaplan-Meier analysis. The p-values for the survival data were determined using chi-squared analysis. Error bar indicates the mean ± SD of the mean values: *=P<0.05, **=P<0.01, ***=P<0.001.

Chapter-5: Objective 1

5.1 Introduction:

Wnt signalling is an evolutionarily conserved pathway among the eukaryotes and is pleiotropic in nature, i.e. Wnt signalling directs various cellular processes such as mitogenic stimulation, cell fate specification, cell migration, cell polarity and differentiation. It is mediated by Wnt ligands and their respective frizzled receptors (Fz and Fzd) and co-receptors such as LRP5 and LRP6 [182, 184, 365, 366]. Wnt ligands are secreted glycolipoproteins, which are of approximately 350-400 amino acids in length that contain an N-terminal signal peptide for their secretion [367]. Frizzled proteins are the principle receptors for the Wnt ligands, which consists of a conserved extracellular cysteine-rich domain (CRD) followed by seven pass transmembrane domain [368]. There are about 19 Wnt ligands and 10 Frizzled receptors in mammals. Signalling through different Wnt ligands and receptors activates either the β-Catenin dependant Wnt canonical pathway or the β-Catenin independent non-canonical pathways (Wnt Ca^{2+} pathway or Wnt planar cell polarity (PCP) pathway).The ligand and receptor combination dictates the activation of canonical & non-canonical pathway downstream [365, 366, 369]. The PCP pathway polarises epithelial cells within the plane of a tissue that control directed cell migration events through regulation of the actin cytoskeleton [185]. PCP pathway activates either Rho associated kinase (ROCK) or Rac1/JNK leading to actin polymerization and cytoskeleton remodelling [186]. Apart from its role in the developmental cell migration, PCP pathway also regulates cancer cell dissemination and migration [370, 371]. The Wnt/Ca^{2+} signalling pathway is vital for dorso-ventral polarity and convergent extension movement during the embryonic development through the regulation of canonical Wnt pathway [187]. Importantly, Wnt Ca^{+2}/CAMKII pathway activation through Wnt5a inhibits cell motility and invasion in thyroid carcinoma [372] and also inhibits tumor growth in late stage basal cell carcinoma (BCC) [373]

Being among one of the developmentally highly conserved pathways, Wnt signalling is tightly regulated at different stages right from the secretion of Wnt ligands to the signal transduction. The multi-pass transmembrane protein Wntless (Wls)/Evenness interrupted (Evi)/Mom-3 plays a crucial role in the release of Wnts [374, 375]. Further, glycosaminoglycan (GAG)-modified proteins such as Dally (division abnormally delayed) and Dally-like (Dly), was shown to facilitate the movement of Wnts and loss of these proteins display defects in Wnt signalling [376, 377]. At the cell surface, Wnt β-catenin signalling is tightly regulated by various secreted antagonists. These antagonists include members of SFRP family (Secreted Frizzled Related Protein) proteins and Wnt Inhibitory factor-1 (WIF-1), which directly binds to the Wnt ligands thereby inhibiting their interaction with the Fzd receptors [378]. Other class of antagonists include members of Dickkopf (DKK) and the SOST families, which antagonize signalling by binding to co-receptors LRP5/6 [379-381]. Further APC down-regulated 1 (APCDD1), a membrane bound glycoprotein inhibit Wnt signalling by binding both the Wnt ligands (Wnt-3a) and LRP [382].

5.1.1 Secreted Frizzled Related Proteins (SFRPs)

SFRPs are a family of soluble glycoproteins, which represents the largest family of Wnt inhibitors. The SFRP family is composed of five secreted glycoproteins, namely, Sfrp1, Sfrp2, Sfrp3, Sfrp4, and Sfrp5 [383, 384]. Based on sequence comparison and phylogenetic analysis, the SFRPs are divided into two sub-groups. Sfrp1, Sfrp2 and Ssrp5 are closely related and cluster together into a subgroup that diverges from the subgroup formed by the related Sfrp3 and Sfrp4. Sfrp1, Sfrp2 and Sfrp5 are encoded by three exons on chromosome 8p12-p11.1, 4q31.3 and 10q24.1 respectively[385], whereas Sfrp3 and Sfrp4 are both encoded by six exons that are located on chromosome 2q31-q33 and 7p14-p13, respectively. The SFRPs are of approximately 300 amino acids (30KD in size) in length and structurally these are modular proteins that fold into two independent domains. SFRPs contain an N-

terminal cysteine-rich domain (CRD), which shares 30% to 50% similarity in sequence homology with the CRD of the Frizzled receptors and a C terminal netrin-related motif (NTR) [386]. Majorly, SFRPs modulate the Wnt signalling pathway by directly binding with Wnt ligands through their CRD domains thereby blocking the interaction between the Wnt ligand and Frizzled receptor [387]. Apart from the CRD domain, SFRPs also interact with Wnt ligands through their netrin like domain [388]. In certain cases, both domains of the SFRP protein are necessary for optimal Wnt inhibition. For instance, a conserved tyrosine residue within the CRD plays a crucial role in this process, together with the last 19 amino acid residues of the NTR, the deletion or replacement of which clearly interfere with SFRP protein function [389]. Moreover, recent reports show that SFRPs can also bind with the Frizzled receptors to form a non-functional complex that prevents Wnt signalling activation [369]. Importantly, the Wnt inhibitory function of SFRPs depends on the following: a) cell type in which they are being expressed, b) concentration of the SFRPs, and c) the binding affinity with which SFRPs interact with Wnt ligands and Fzd receptors.

SFRPs have been reported to have similar functions (redundant functions) as well as opposing functions. During the mouse early embryonic development Sfrp1 *and* Sfrp2 are required for antero-posterior (AP) axis elongation and somitogenesis in the thoracic region. Homozygous mutations in either Sfrp1 *or* Sfrp2 individually did not have any effect; however, mutations in both of them simultaneously resulted in severe shortening of the thoracic region and embryonic lethality at around E16.5, indicating that Sfrp1 *and* Sfrp2 are functionally redundant [356]. Further, in $Sfrp1^{-/-}$/$Sfrp2^{-/-}$ / $Sfrp5^{-/-}$ triple mutant, these defects were further enhanced and showed embryonic lethality at around E12.5 [390]. Conversely, it is also well reported that different SFRPs have opposing effects on the same process. For instance, during the kidney development Sfrp1 blocks kidney-tubule formation and bud branching processes that depend on Wnt4 activity in vivo; however, Sfrp2 blocks Sfrp1 mediated effects and

partially restores tubule differentiation and bud branching [391]. Further, Sfrp1 reduces the apoptosis of dermal fibroblasts [392] whereas Sfrp2 promotes apoptosis that is associated with developmental tissue patterning in chick embryos [393].

5.1.2 Sfrp1, a Wnt inhibitor:

Sfrp1, a secreted Wnt antagonist, is a member of SFRP family that is encoded by Sfrp1 gene located on chromosome 8p11.21. It has a molecular weight of approximately 35kDa comprising of N-terminal cysteine rich domain (CRD) and a C-terminal Netrin domain [387]. Sfrp1 is post translationally modified by N-glycosylation at Asn (172) (approximately 2.8 kDa) [386], and sulphation at tyrosine residues 34 and 36, which are inhibited by treatment with heparin [394]. Sfrp1 inhibits Wnt signalling either by binding to the Wnt ligands or to the FZD receptors [378]. Both the CRD domain and NTR domain of Sfrp1 play crucial role in binding to the Wnt ligands. Sfrp1 has been shown to interact with Wnt-1 and Wnt-2 through its CRD domain and inhibits cytoplasmic accumulation of β-catenin [395]. Interestingly, Sfrp1 was shown to interact with wingless (Wg) even in the absence of CRD domain [396]. Sfrp1 NTR domain mimics the function of the full-length Sfrp1 i.e. it binds to Wnt ligands (Wnt8) and prevents Wnt canonical signalling activation [388].

Sfrp1 has a biphasic effect on Wnt signalling i.e. at low concentrations, Sfrp1 increases Wnt activity; however, at high concentrations of Sfrp1, Wnt activity is decreased [396]. For instance, Sfrp1 was shown to inhibit Wnt-3a induced accumulation of β-catenin in L-cells (mouse fibroblasts), C57MG cells (mouse mammary epithelial cells) and HEK293 cells (human embryonic kidney cells) at higher concentrations but induces Wnt signalling at lower concentrations [397, 398]. Apart from inhibiting Wnt signalling by binding to the frizzled receptors, Sfrp1 has also been shown to interact with frizzled receptors to mediate cellular functions. Sfrp1 potentiates Wnt signalling even at high concentrations in L-cells over

expressing Fzd5 in the presence of Wnt3a [398]. Further the CRD domain of Sfrp1 interacts with Fzd2 receptor of retinal ganglion cells (RGC) to provide Wnt independent axon guidance cues to the growth cones where SFRP1 acts as an active ligand of Fzd mediated signalling [399]. Sfrp1 acts as a tumor suppressor and is frequently inactivated either by epigenetic inactivation (promoter hypermethylation) or by the loss of fragment of chromosome-8 in various cancers such as breast, cervical, colorectal and hepatocellular carcinoma (HCC) etc. [400-403].

5.1.3 Sfrp1 in stem cell regulation:

Sfrp1 is reported in stem cell regulation and maintenance in adult tissue homeostasis. In case of hematopoietic system, Sfrp1, expressed in stromal cells is involved in maintaining hematopoietic stem cells (HSCs) homeostasis through extrinsic regulation of β-catenin. Loss of Sfrp1 affects proliferation and maintenance of HSCs and leads to increased production of hematopoietic progenitors [404]. Further, Sfrp1 also helps in maintaining bronchoalveolar stem cells (BASCs) in a quiescent undifferentiated phase by regulating Wnt signalling; however, Sfrp1 loss in these cells leads to aberrant proliferation [405]. Moreover, *in vivo* over expression of Sfrp1 after lung injury suppressed differentiation and resulted in the accumulation of BASCs. In mesenchymal stem cells (MSC), an increased expression of Sfrp1 enhances MSC function with neo-vessel maturation and stabilization during angiogenesis [406]. During the midbrain dopamine (DA) neuron development, low to medium concentrations of Sfrp1 promoted the dopamine differentiation of progenitors derived from primary ventral midbrain cultures or mouse embryonic stem cells (ESCs). This study suggests the importance of dose dependant regulation of Sfrp1 to enhance the DA differentiation of ESCs [407]. Further, Sfrp1 is critical for maintaining proper mammary gland development. Loss of Sfrp1 results in ductal branching in mammary gland and also significantly increases the number of mammary epithelial cells capable of mammosphere

formation [408]. In skin, multiple studies have reported that Sfrp1 expression is higher in hair follicle stem cells (HFSCs) as compared to non-bulge cells [136, 175, 409]. Taken together, Sfrp1 is involved in the regulation and maintenance of various adult stem cells; however, its role in HFSCs regulation and skin homeostasis is not yet elucidated. Our lab has earlier attempted to understand the role of Sfrp1 in epidermal homeostasis (Pls. refer to our lab's previous doctoral student, Dr. Rahul Sarate thesis, HBNI enrolment number: LIFE09201104006); however, detailed characterization of $Sfrp1^{-/-}$ mouse skin, changes in hair follicle cycling, wound healing and signalling involved in HFSCs regulation in the absence of Sfrp1 were not addressed.

In this study we have performed detailed characterization of HFSCs in the absence of Sfrp1, covering aforementioned points. In addition, we have investigated the molecular mechanism that gets deregulated in the HFSCs in absence of Sfrp1.

5.2 Results:

5.2.1 Sfrp1 loss results in decrease of HFSCs population:

Sfrp1 is highly expressed in the HFSCs as compared to non-stem cells. However its role in HFSCs regulation is not known. Hence, in order to understand the role of Sfrp1 in the HFSCs regulation, WT, $Sfrp1^{+/-}$ and $Sfrp1^{-/-}$ mice were sacrificed at various post-natal days (PD) during the 1^{st} hair cycle. Further, FACS analysis was performed to assess changes in the HFSCs pool using well established HFSC markers such as CD-34 and α6-Integrin (Figure 5.1). Our results showed a decrease in the HFSC population in the $Sfrp1^{+/-}$ and $Sfrp1^{-/-}$ mice during the 1^{st} telogen (PD21). Further, we have also performed FACS at 1^{st} anagen (PD28), which also showed a decrease in the HFSC population in the $Sfrp1^{+/-}$ and $Sfrp1^{-/-}$ mice as compared to WT littermates. However, the decrease was more prominent in $Sfrp1^{+/-}$ mice than in $Sfrp1^{-/-}$ mice as compared to WT littermates. Moreover, stem cell pool analysis at the

end of the first hair cycle i.e. at PD49 (2nd telogen) showed a decrease in stem cell pool only in Sfrp1$^{+/-}$ mice but the Sfrp1$^{-/-}$ mice didn't show any difference in the HFSC pool as compared to WT mice.

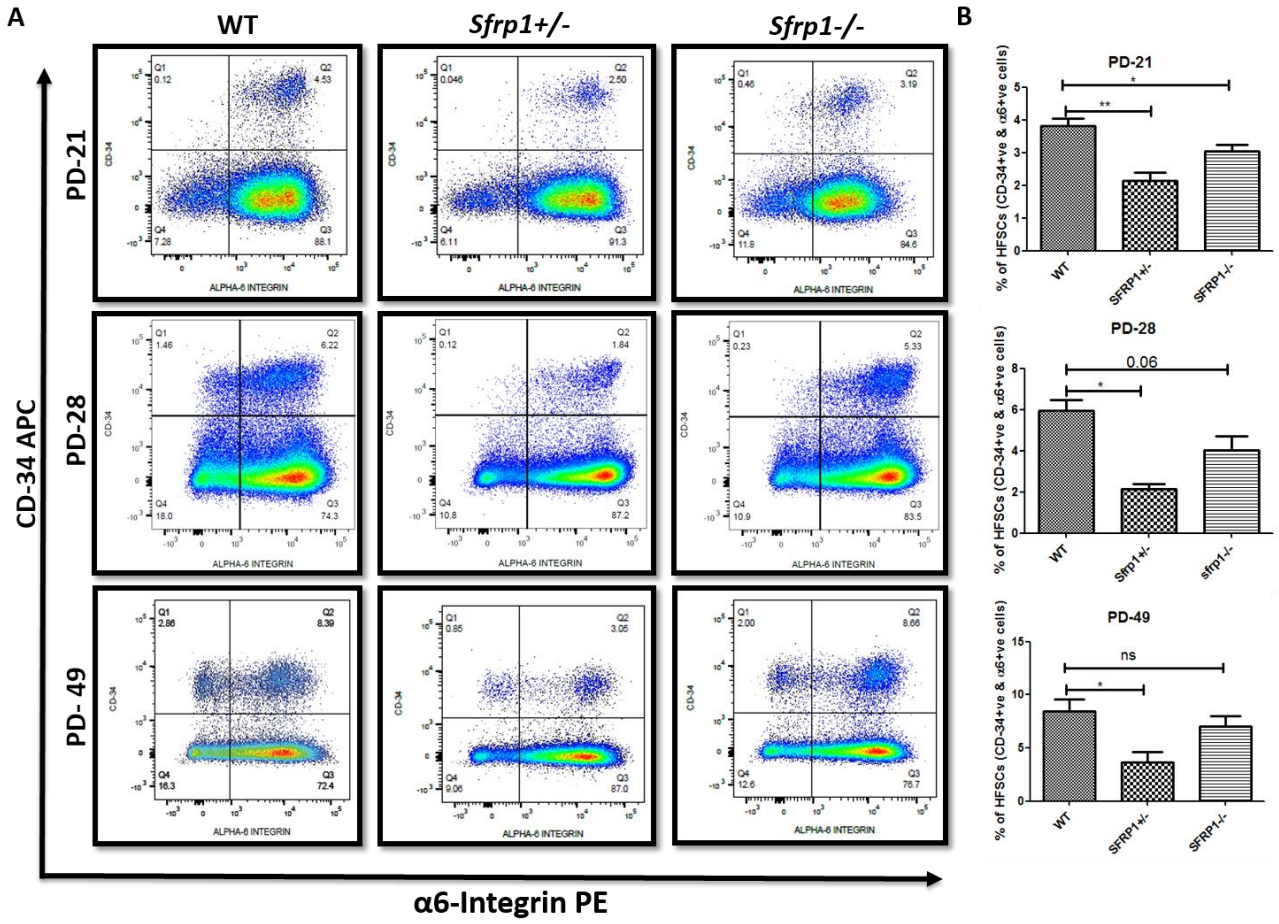

Figure 5.1: Loss of Sfrp1 results in decreased HFSCs pool

A) *FACS analysis of HFSCs population at PD21 (1st Telogen), PD28 (1St Anagen) and PD49 (2nd Telogen) in WT, Sfrp1+/- and Sfrp1-/- mice.* ***B)*** *Graphical Representation of percentage of HFSCs at PD21, PD28 and PD49. (n=5/genotype for PD21 and PD28 and n=10/ genotype for PD49. Data are analyzed by student's t-test and presented as mean ± SEM. ns= non-significant * = P<0.05, ** = P<0.01).*

5.2.2 Loss of Sox-9 positive cells in the absence of Sfrp1

To further validate the decrease in the HFSC pool, we further quantified the number of Sox-9+ (HFSCs marker) cells. In this regard, we have performed immuno-fluorescence assay (IFA) dual staining using anti mouse Sox-9 and CD-34 antibodies on WT, Sfrp1$^{+/-}$ and Sfrp1$^{-/-}$ mice skin sections at PD21 (1st telogen) (Figure 5.2A). Additionally, we have also counted the number of HFSCs expressing Sox-9 in all the three genotypes (Figure 5.2B). Our results showed that, the number of HFSCs cells that express Sox-9 were significantly decreased in both the Sfrp1$^{+/-}$ and Sfrp1$^{-/-}$ mice as compared to the WT mice at PD21. Hence, our results showed that IFA data for Sox-9 was in congruence with FACS data confirming the decrease in the HFSC pool at first telogen.

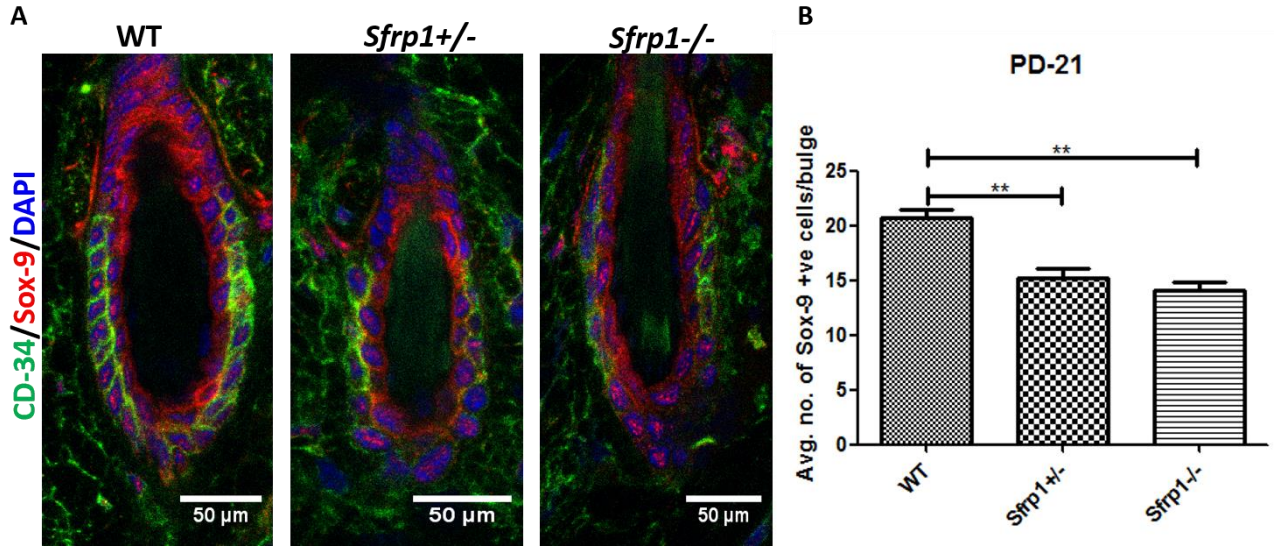

Figure 5.2: Sfrp1 loss results in decrease of Sox-9 positive cells

A) *Immunofluorescence assay (IFA) for CD-34 and Sox-9 at PD21 (1st Telogen) in WT, Sfrp1+/- and Sfrp1-/- mice.* ***B)*** *Graphical Representation of average number of Sox-9 positive cells per bulge in WT, Sfrp1+/- and Sfrp1-/- mice at PD21. (Data are analyzed by student's t-test and presented as mean ± SEM. n=4, scale bar=50µm, ** = P<0.01).*

5.2.3 Sfrp1 loss alters proliferation dynamics of HFSCs

Sfrp1 loss showed initial decrease in the HFSC population in both the $Sfrp1^{+/-}$ and $Sfrp1^{-/-}$ mice as compared to WT littermates. However, at the end of the first hair cycle (PD49), percentage of the HFSCs in WT and $Sfrp1^{-/-}$ mice was found to be almost similar. This warranted understanding the proliferation dynamics of the HFSCs in the absence of Sfrp1. To understand the proliferation dynamics, we have performed BrdU cell proliferation assay in WT, $Sfrp1^{+/-}$ and $Sfrp1^{-/-}$ mice. Briefly, mice at 1^{st} telogen (PD20) were injected intraperitoneally with BrdU (50mg/kg of body weight) followed by 0.8mg/ml BrdU in drinking water for 3 days (Figure 5.3 A). Mice were then sacrificed at PD23 and IFA was performed on the mice skin sections using anti BrdU antibody followed by counting the numbers of BrdU positive cells in the bulge region of hair follicle (Figure 5.3 B & D). Our results showed an increase in the BrdU positive cells in the bulge region of $Sfrp1^{-/-}$ mice as compared to WT thereby indicating higher proliferation in $Sfrp1^{-/-}$ mice HFSCs. However, the proliferation in $Sfrp1^{+/-}$ mice bulge was similar to that of WT mice. The alteration in the proliferation of HFSCs was further confirmed by performing IFA for Ki-67 (proliferation marker) at PD23 during the telogen-to-anagen transition. The results showed an increase in the Ki-67 positive cells in $Sfrp1^{-/-}$ mice bulge as compared to WT mice. The number of Ki-67 positive cells in $Sfrp1^{+/-}$ mice bulge was similar to that of WT mice, thereby confirming the BrdU data on proliferation analysis. Further, we have also counted the number of Ki-67 positive cells in the infundibulum, isthmus and interfolliclar epidermal (IFE) regions of the hair follicles. However, there was no significant change in the number of Ki-67 positive cells in the infundibulum, isthmus and interfolliclar epidermal regions of hair follicle in both the $Sfrp1^{+/-}$ and $Sfrp1^{-/-}$ mice as compared to WT (Figure 5.3 C & E). Further, to observe whether the increased proliferation of HFSCs is either transient or continuous, we have performed IFA for Ki-67 at PD49. The results showed no difference in the proliferation of

Sfrp1$^{+/-}$ and Sfrp1$^{-/-}$ mice HFSCs as compared to WT HFSCs suggesting that the enhanced proliferation is transient in HFSCs. However, there were significantly higher number of proliferative cells in the isthmus, infundibulum and interfollicular epidermal regions of Sfrp1$^{+/-}$ and Sfrp1$^{-/-}$ mice as compared to WT mice (Figure 5.4). Taken together, our data showed a transient increase in the proliferation of Sfrp1$^{-/-}$ mice HFSCs as compared to WT mice.

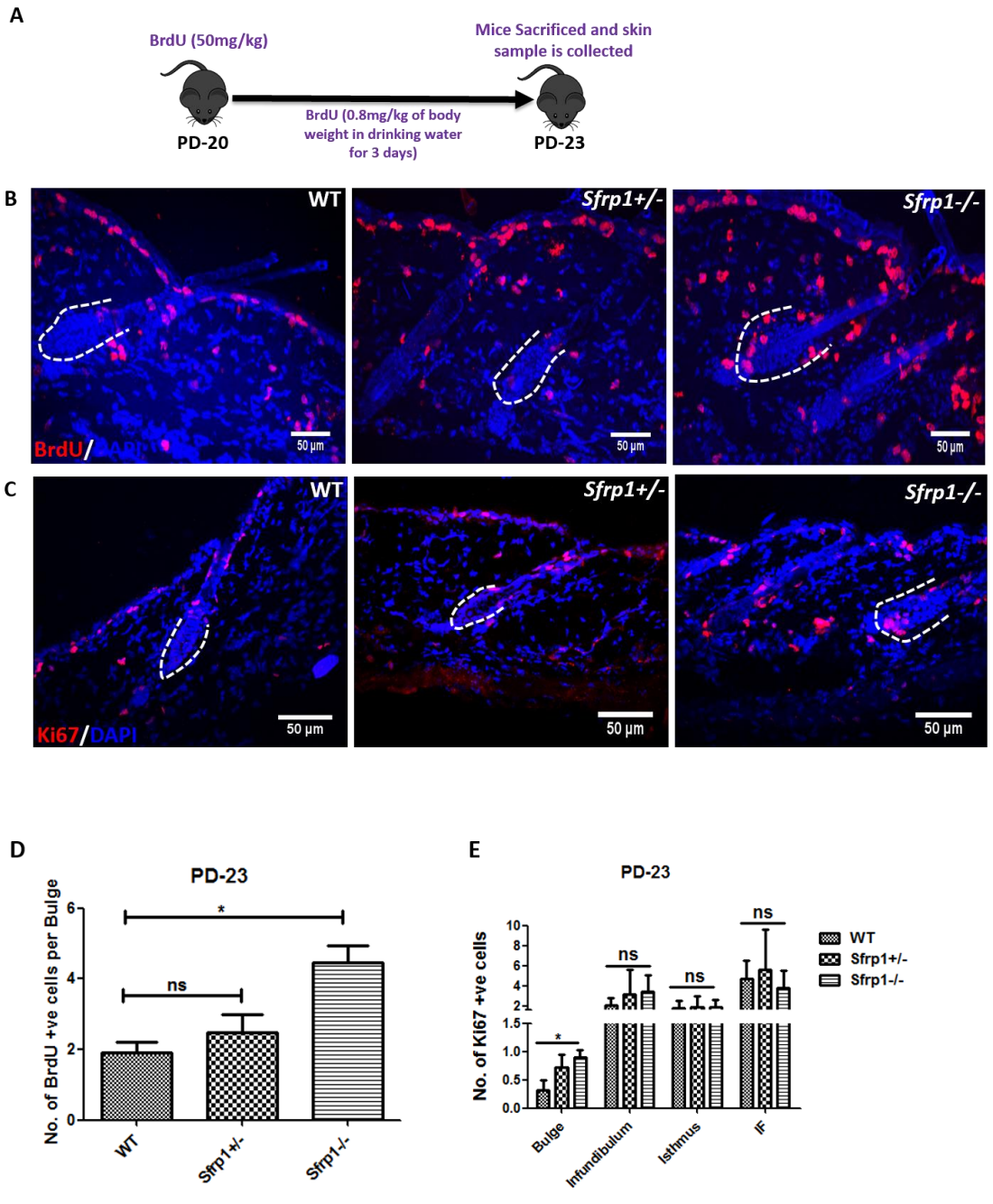

Figure 5.3: Sfrp1 loss alters HFSCs proliferation

A) *Schematic representation of BrdU treatment in mice* ***B)*** *Immunofluorescence assay (IFA) for BrdU on WT, Sfrp1+/- and Sfrp1-/- mice skin sections at PD23.* ***C)*** *Immunofluorescence assay (IFA) for Ki67 on WT, Sfrp1+/- and Sfrp1-/- mice skin sections at PD23.* ***D)*** *Graphical representation of number of BrdU positive cells per bulge.* ***E)*** *Graphical representation of number of Ki67 positive cells in different compartments of hair follicle. (Data are analyzed by student's t-test and presented as mean ± SEM. n=4, scale bar=50µm, * = P<0.05).*

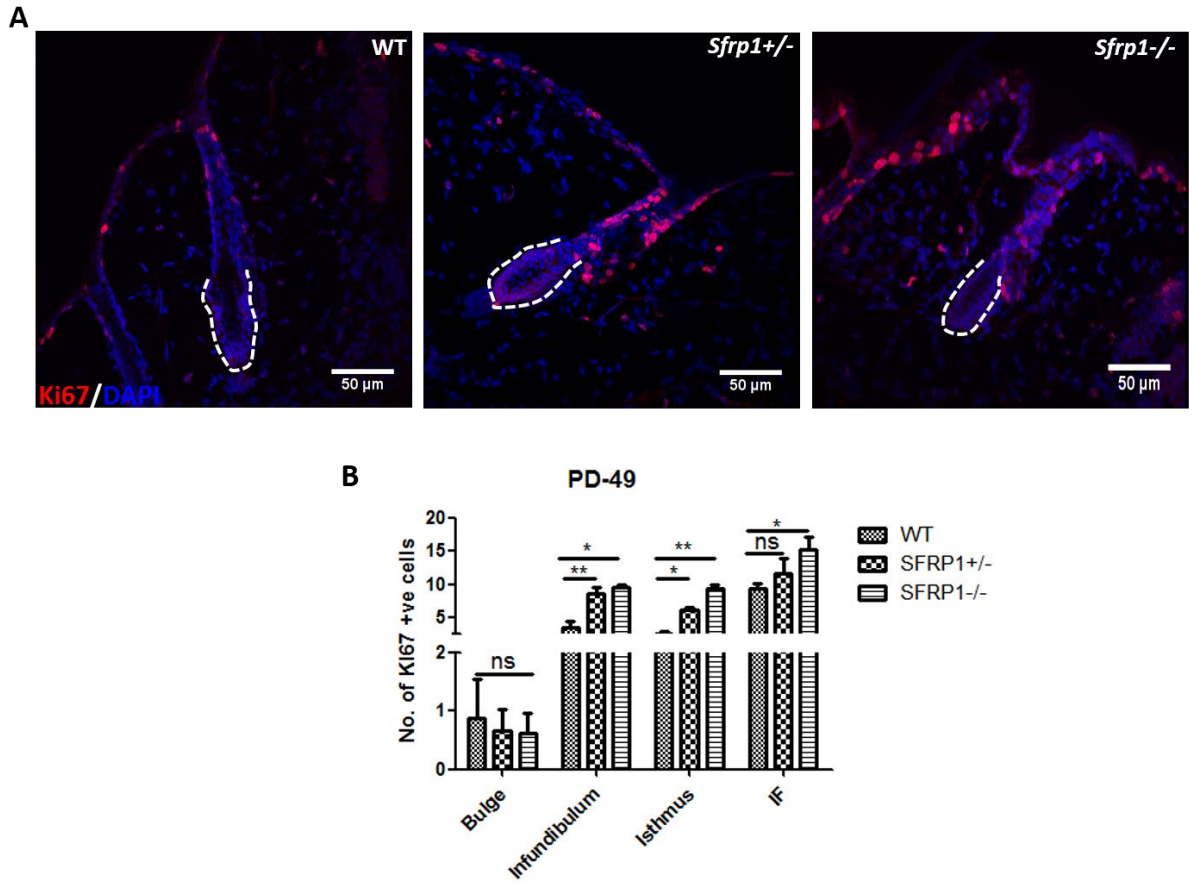

Figure 5.4: Sfrp1 loss results in transient HFSCs proliferation

A) *Immunofluorescence assay (IFA) for Ki67 on WT, Sfrp1+/- and Sfrp1-/- mice skin sections at PD49.* ***B)*** *Graphical representation of number of Ki67 positive cells in different compartments of hair follicle. (Data are analyzed by student's t-test and presented as mean ± SEM. n=4, scale bar=50µm, * = P<0.05, ** = P<0.01).*

5.2.4 Decrease in long term BrdU-LRCs in the absence of Sfrp1

Increase in the proliferation was observed in the Sfrp1$^{-/-}$ mice HFSCs as compared to WT mice during the telogen-to-anagen transition at PD23. Therefore, we checked the number of BrdU label retaining cells (LRCs) within the bulge of Sfrp1$^{+/-}$ and Sfrp1$^{-/-}$ mice as compared to WT litter mates as increase in proliferation should decrease their label retaining capacity. BrdU was injected subcutaneously into pups of all the three genotypes (WT, Sfrp1$^{+/-}$ and Sfrp1$^{-/-}$) at PD3 to PD5 (50mg/kg of body weight) at 12 hours intervals and then the mice were chased up to PD49 (2nd telogen) (Figure 5.5A). Mice were sacrificed and IFA for BrdU was performed on the dorsal skin sections (Figure 5.5B). Further, we counted the number of BrdU positive cells in the bulge region of WT, Sfrp1$^{+/-}$ and Sfrp1$^{-/-}$ mice. A decrease in the number of LRCs was observed in the Sfrp1$^{-/-}$ mice bulge as compared to WT litter-mate, whereas the LRCs in Sfrp1$^{+/-}$ mice were similar to that of WT (Figure 5.5C). Further, we have also checked for the molecular changes involved in the increased HFSC proliferation by investigating the protein levels of Runx1 and P21, which are involved in regulating HFSC quiescence in the dorsal skin, of WT, Sfrp1$^{+/-}$ and Sfrp1$^{-/-}$ mice. Our western blot results have shown that there was a decrease in the levels of Runx1 and P21 in both the Sfrp1$^{+/-}$ and Sfrp1$^{-/-}$ mice as compared to WT mice. Further, the levels of Cyclin-D1 were increased in Sfrp1$^{+/-}$ and Sfrp1$^{-/-}$ mice as compared to WT mice (Figure 5.5D). Hence, our data showed a decrease in the number of LRCs in the Sfrp1$^{-/-}$ mice bulge as compared to WT mice which could be due to decreased levels of quiescence regulating proteins.

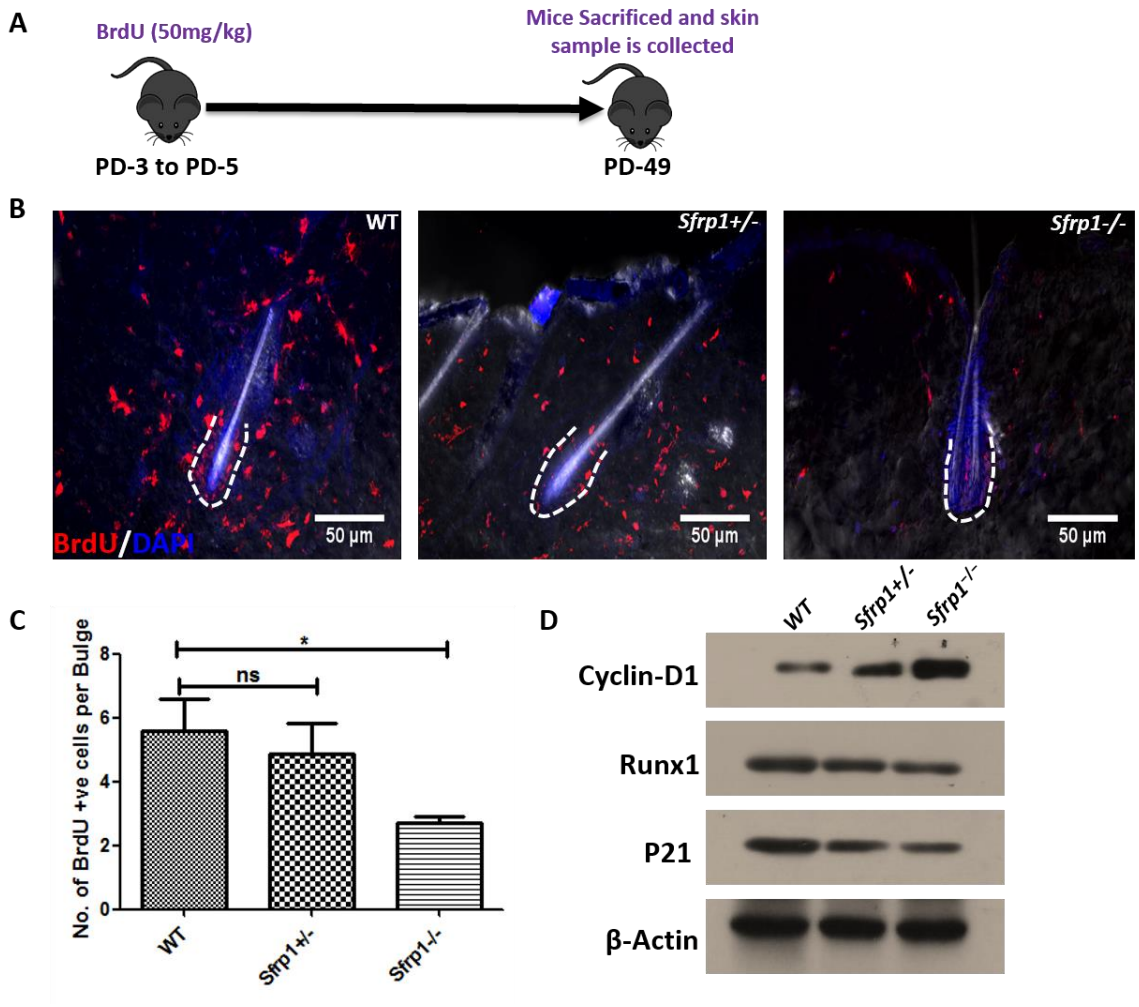

Figure 5.5: Sfrp1 loss results in decrease in LRCs

A) *Schematic representation of BrdU treatment in mice* ***B)*** *Immunofluorescence assay (IFA) for BrdU on WT, Sfrp1+/- and Sfrp1-/- mice skin sections at PD49.* ***C)*** *Graphical representation of number of BrdU positive cells per bulge.* ***D)*** *Western blot for P21, Runx1 and cyclin-D1 (cell cycle regulators). (BrdU=5-Bromo-2'-deoxyuridine, PD-post-natal day. Data are analyzed by student's t-test and presented as mean ± SEM. n=5, scale bar=50µm, ns= non-significant, * = P<0.05).*

5.2.5 Characterization of Sfrp1$^{+/-}$ and Sfrp1$^{-/-}$ mice skin

HFSCs participate in skin tissue homeostasis and hair follicle regeneration. To investigate the role of Sfrp1 in hair follicle regeneration and hair cycling, we examined the hair cycling pattern in dorsal skin of Sfrp1$^{+/-}$ and Sfrp1$^{-/-}$ and WT mice by sacrificing the mice at various postnatal days (PDs) during the first hair cycle. Hematoxylin and Eosin (H&E) staining of the dorsal skin sections was performed at various PDs during first hair cycle (PD21, PD-23, PD25, PD28, PD30, PD32, PD35, PD38, PD40, PD43, PD46 and PD49). The H&E analysis of dorsal skin sections showed a slight difference of two days in the early hair follicle cycling pattern between WT and Sfrp1$^{-/-}$ mice. The WT and Sfrp1$^{-/-}$ mice hair follicles were in telogen at PD21. As the hair follicle cycle progresses the following changes were observed at different PDs. The hair follicles of Sfrp1$^{-/-}$ mice were in anagen-II, whereas the hair follicles of WT mice were in anagen-I at PD23. Further, at PD25 Sfrp1$^{-/-}$ hair follicles were in anagen-IIIA whereas the WT hair follicles were in anagen-II. Moreover, at PD28 Sfrp1$^{-/-}$ hair follicles were in anagen-IIIC whereas the WT hair follicles were in anagen-IIIb. As the hair cycle progressed further, both the WT and Sfrp1$^{-/-}$ mice hair follicles appeared to be in similar phases at around PD32. In addition, the Sfrp1$^{+/-}$ mice showed no difference in the hair follicle cycle pattern as compared to WT mice (Figure 5.6). Additionally, no abnormalities were observed in the epidermal structure and thickness.

A

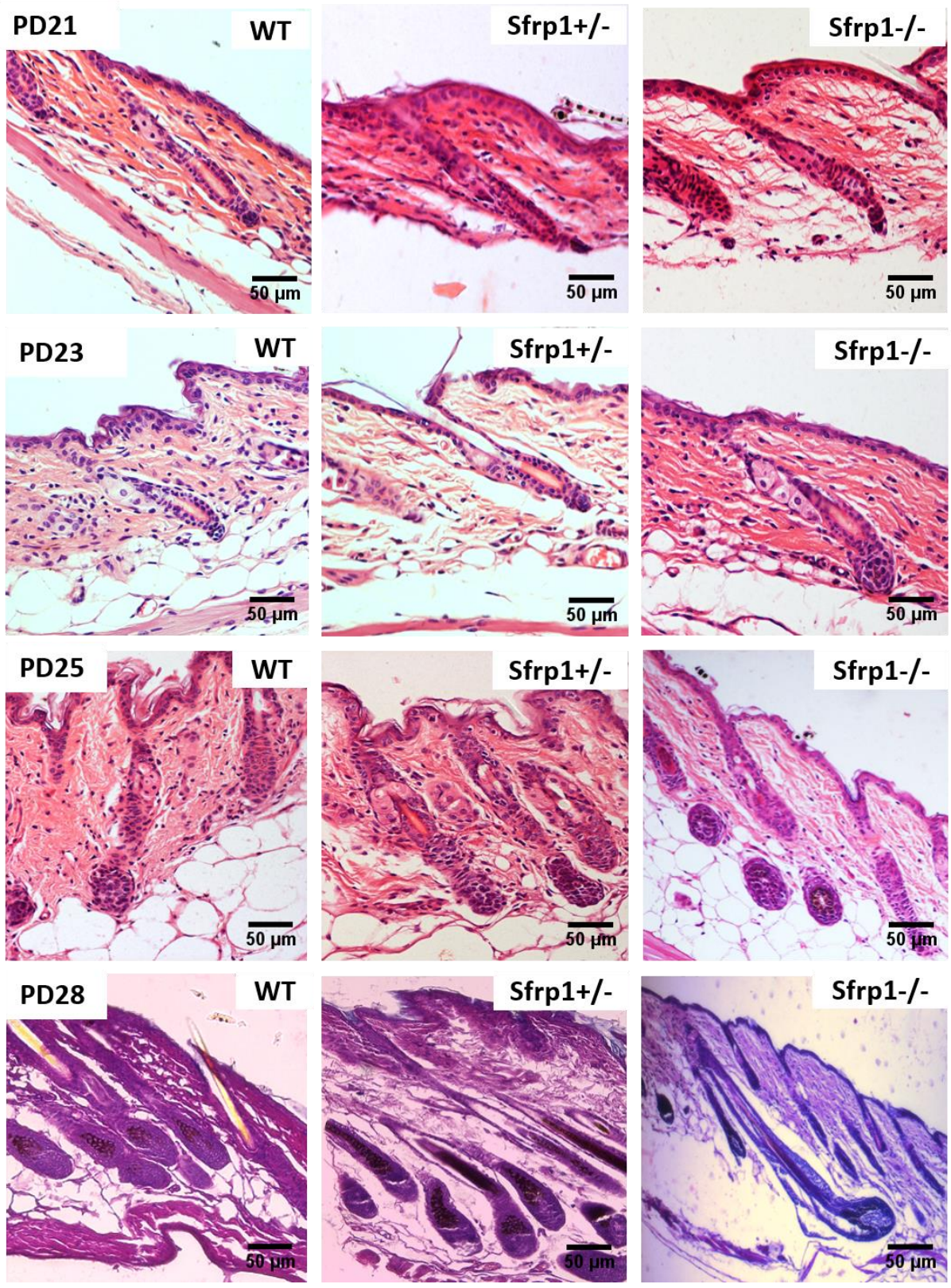
PD21
WT
Sfrp1+/-
Sfrp1-/-
PD23
WT
Sfrp1+/-
Sfrp1-/-
PD25
WT
Sfrp1+/-
Sfrp1-/-
PD28
WT
Sfrp1+/-
Sfrp1-/-
50 µm

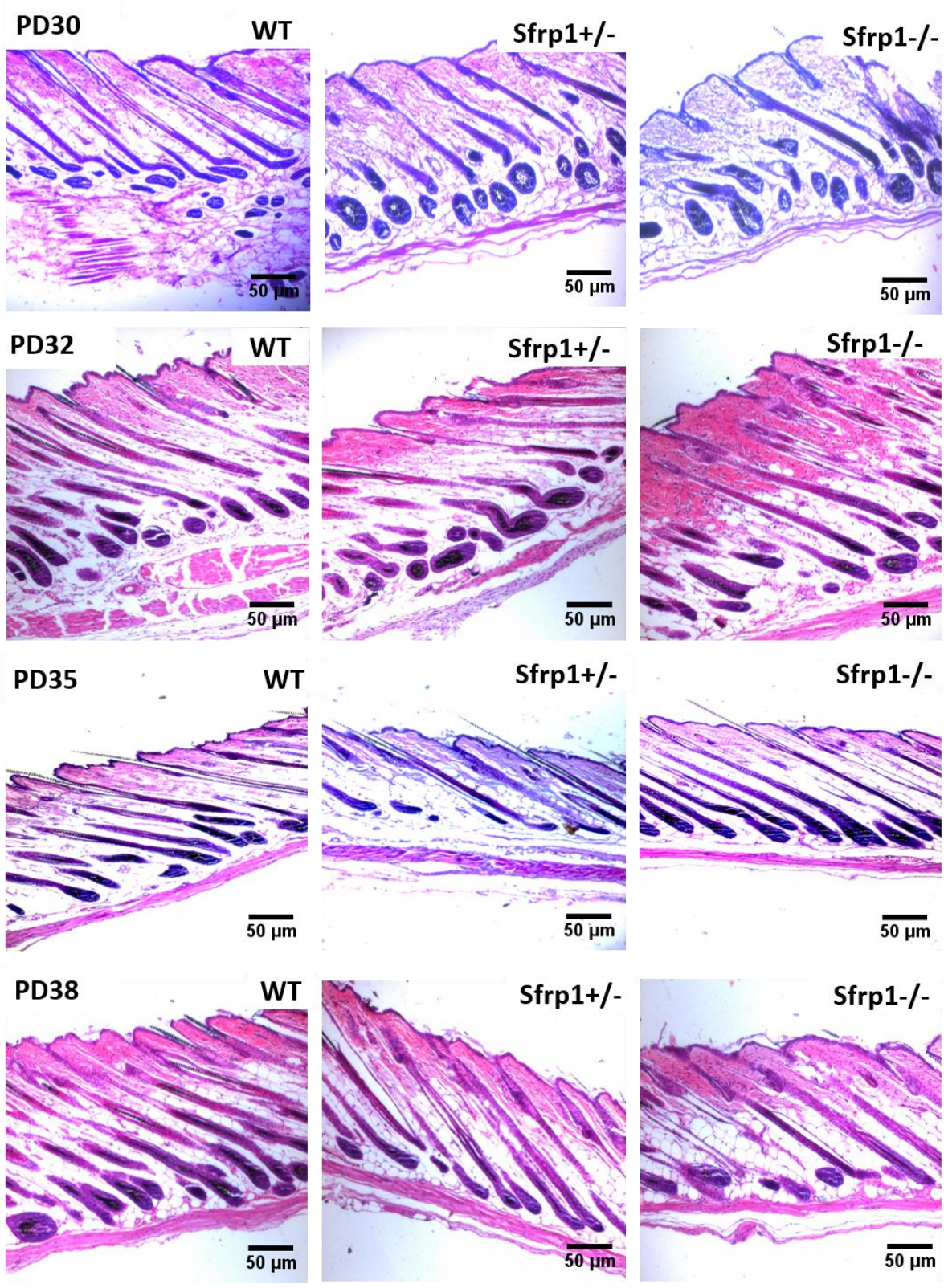
PD30
WT
Sfrp1+/-
Sfrp1-/-
PD32
WT
Sfrp1+/-
Sfrp1-/-
PD35
WT
Sfrp1+/-
Sfrp1-/-
PD38
WT
Sfrp1+/-
Sfrp1-/-
50 μm

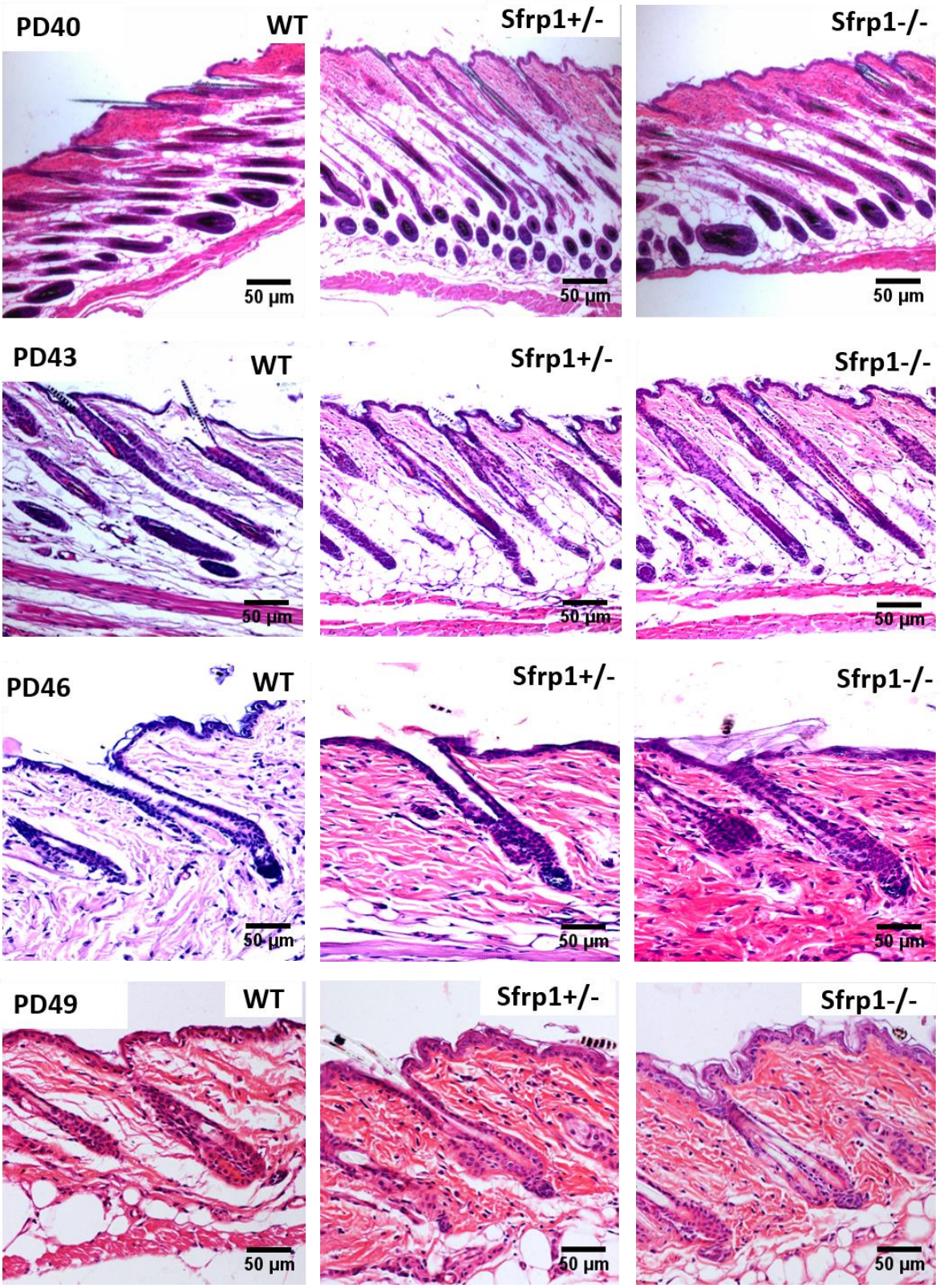
PD40
WT
Sfrp1+/-
Sfrp1-/-
PD43
WT
Sfrp1+/-
Sfrp1-/-
PD46
WT
Sfrp1+/-
Sfrp1-/-
PD49
WT
Sfrp1+/-
Sfrp1-/-
50 µm

B

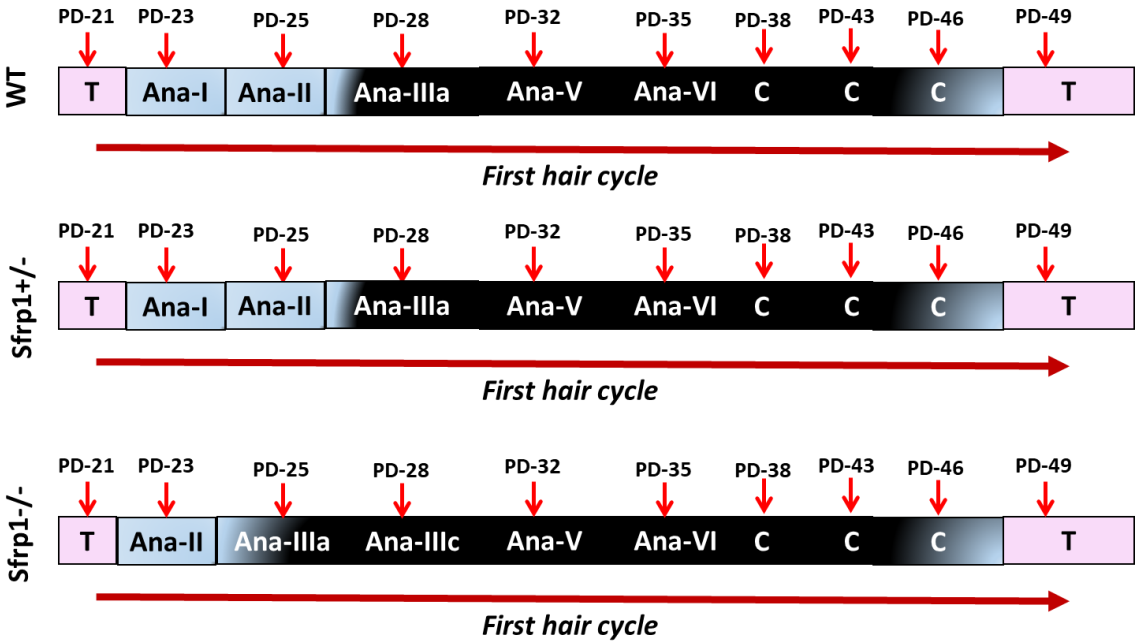

Figure 5.6: Histological analysis of the *WT, Sfrp1$^{+/-}$ and Sfrp1$^{-/-}$* mice dorsal skin

A. *WT, Sfrp1$^{+/-}$ and Sfrp1$^{-/-}$ mice were sacrificed at various postnatal days during the first hair cycle* (PD21, PD-23, PD25, PD28, PD30, PD32, PD35, PD38, PD40, PD43, PD46 and PD49). *The dorsal skin tissue sections were stained by haematoxylin and eosin.* ***B.*** *Schematic representation of hair cycle in WT, Sfrp1$^{+/-}$ and Sfrp1$^{-/-}$ mice. (n=3, scale bar=50µm)*

5.2.6 Sfrp1 loss leads to delay in wound healing

HFSCs were shown to participate in skin tissue homeostasis, hair follicle regeneration and wound repair [410]. We have observed that Sfrp1 loss affects the early stages of hair follicle cycling pattern. However, the role of HFSCs in wound repair in the absence of Sfrp1 is not known. Therefore, in order to check the impact of Sfrp1 loss on wound healing, a punch (5mm) wound was made on the dorsal region of mice from all the three genotypes (WT, Sfrp1$^{+/-}$ and Sfrp1$^{-/-}$) at post-natal day 49. The mice were then followed up to 2 weeks to observe any changes in the wound repair. Our data showed a significant delay in wound repair of Sfrp1$^{+/-}$ mice (3days) and Sfrp1$^{-/-}$ mice (5days) as compared to the WT mice.

Further, the percent of wound area was calculated by taking measurements of the wound every alternative day (Figure 5.7). Taken together, our results showed Sfrp1 loss leads to delay in the wound repair in mice.

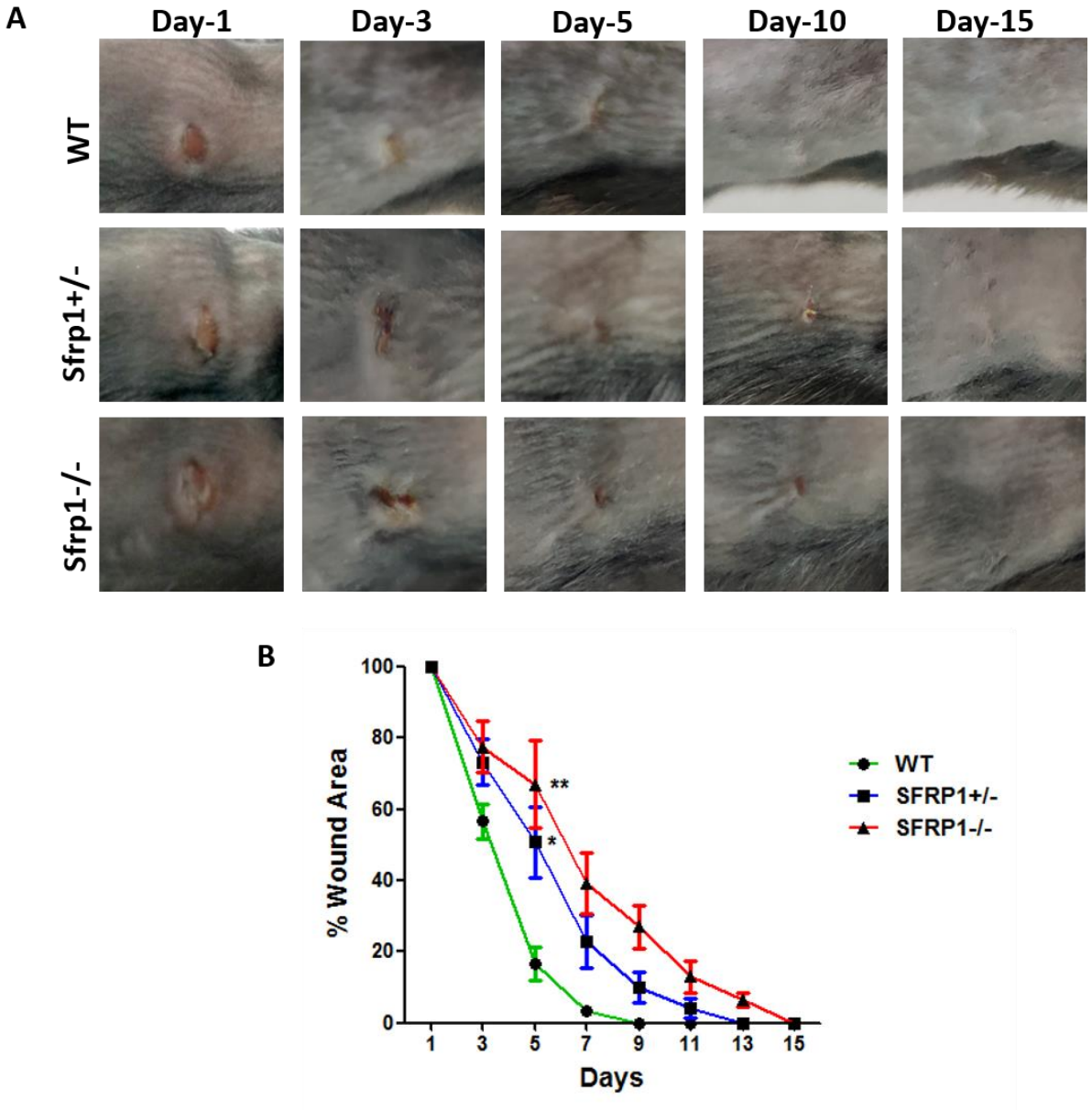

Figure 5.7: Sfrp1 loss results in delay in wound healing

A) *Wound healing in WT, Sfrp1+/- and Sfrp1-/- mice skin on different days after wounding* ***B)*** *Graphical representation of percentage of wound area on different days after wounding (Data are analyzed by student's t-test and presented as mean ± SEM. n=6, * = P<0.05, ** = P<0.01).*

5.2.7 Expression profile of Sfrp1$^{-/-}$ HFSCs

Sfrp1 loss resulted in initial stem cell pool loss, increased proliferation of HFSCs, decreased LRCs and delay in wound healing response. Therefore, it warrants understanding the molecular mechanism involved in regulating the HFSCs in the absence of Sfrp1. HFSCs were FACS sorted using stem cell markers (CD-34 and α6-Integrin) from WT and Sfrp1$^{-/-}$ mice at PD49 followed by RNA isolation. Further, RNA was quantified using bio-analyzer to check its integrity and microarray was performed to understand the complete gene expression profile of HFSCs (Figure 5.8A). Earlier reports have suggested that SFRP family members could show tissue specific redundant functions [390, 411]. Hence, we have checked the redundancy from other SFRP family members in the absence of Sfrp1 in HFSCs. However, the expression profile did not show any change in the mRNA expression of other SFRP family members in the absence of Sfrp1 (Figure 5.8B). Apart from SFRP family, there are other Wnt antagonists that regulate Wnt signalling such as WIF1 (Wnt Inhibitory Factor-1) and Dickkopf (Dkk1 & Dkk3) proteins. Therefore, we have also checked for the changes in the mRNA expression levels of Wif1, Dkk1 and Dkk3. The expression profile did not show any significant change in the expression of these antagonists in the absence of Sfrp1 (Figure 5.7C). The results have been further validated through qRT PCR.

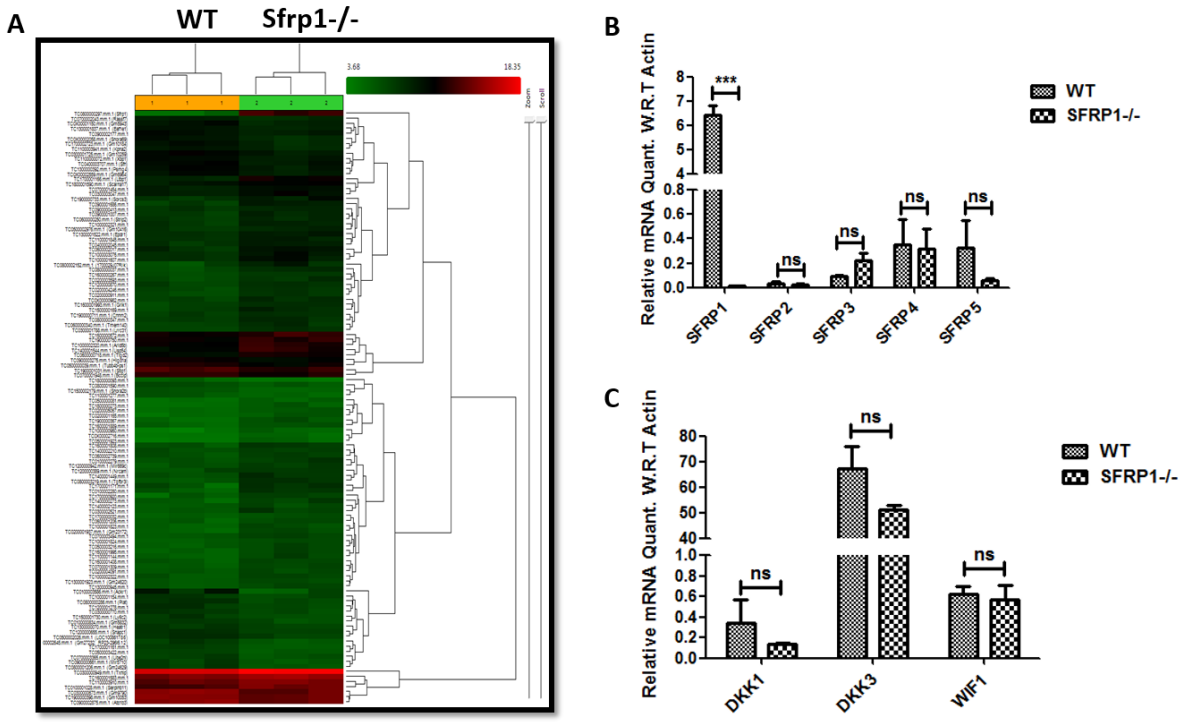

Figure 5.8: Microarray profile of HFSCs at PD49

A) *Heat map of WT and Sfrp1$^{-/-}$ mice HFSCs at PD49* ***B)*** *Graphical representation of mRNA level changes in SFRP family genes in WT and Sfrp1$^{-/-}$ mice HFSCs* ***C)*** *Graphical representation of mRNA level changes in Wnt signalling antagonists (Dkk1, Dkk3 & Wif1) in WT and Sfrp1$^{-/-}$ mice HFSCs. (Data are analyzed by student's t-test and presented as mean ± SEM. n=3mice/genotype, ns=non-significant, *** = P<0.001).*

5.2.8 Sfrp1$^{-/-}$ HFSCs showed decrease in HFSC markers expression

Sfrp1 is a well-known Wnt inhibitor, hence, we further checked for the expression level changes in the Wnt pathway genes. The expression profile showed no significant change in the mRNA expression levels of β-catenin and other Wnt pathway molecules (Gsk-3β, Tcf-1 and Lef-1) (Figure 5.9A). Further, we went onto check the expression of Wnt target genes such as Axin2 and Lgr5, which are also known HFSCs markers [142, 147]. Surprisingly, our results showed a significant decrease in the expression levels of Axin2 and Lgr5 in the Sfrp1$^{-/-}$ HFSCs as compared to WT HFSCs. This decrease in HFSCs markers was further validated

at mRNA level by performing real time PCR. Further, to confirm the changes at protein level, we have performed IFA for Axin2 on PD21 and PD49 dorsal skin sections (Figure 5.9 B-F). The results showed a decrease in the protein levels of Axin2 in the bulge region of Sfrp1$^{+/-}$ and Sfrp1$^{-/-}$ mice as compared to WT littermates.

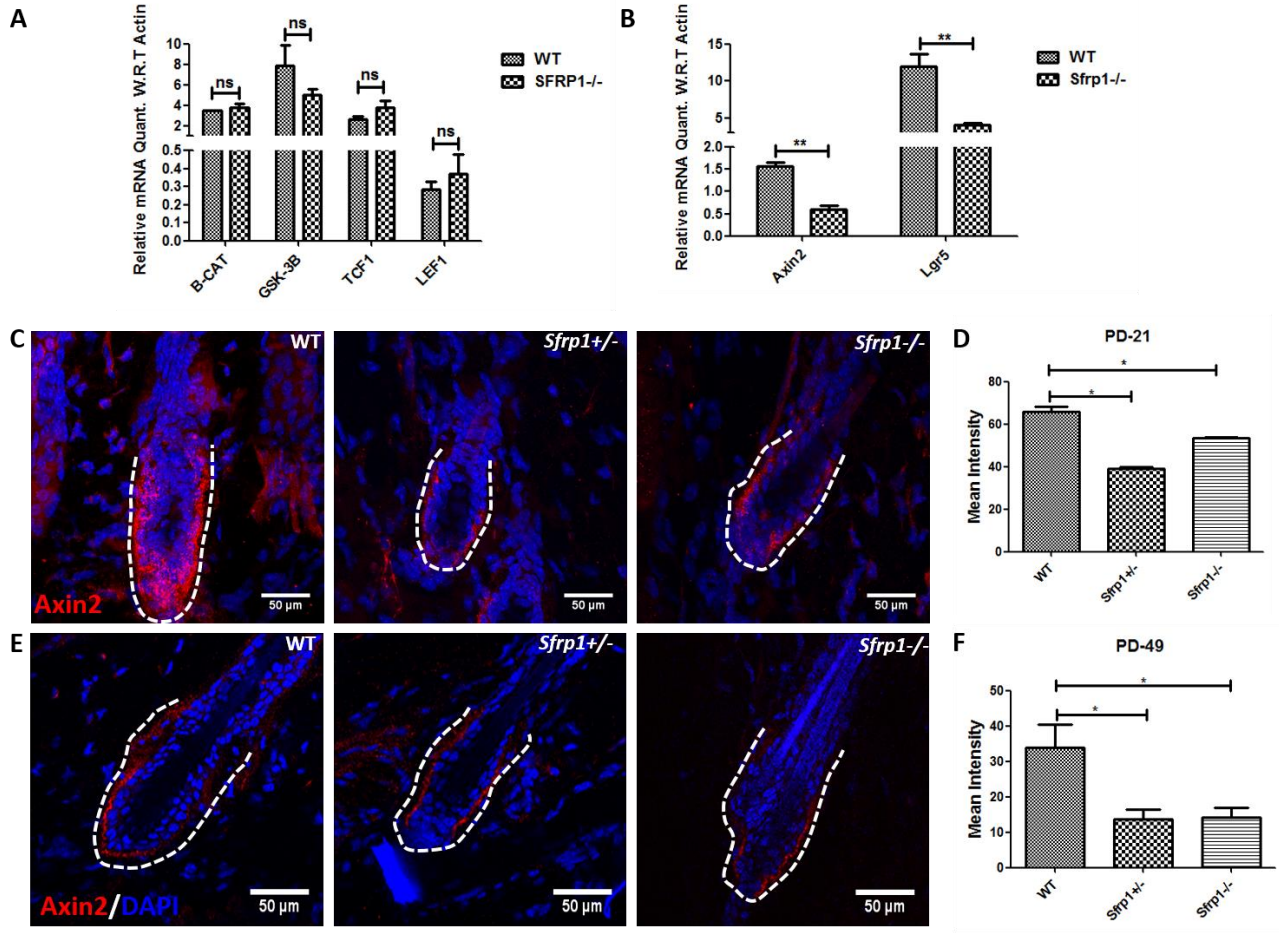

Figure 5.9: Loss in HFSCs markers in the absence of Sfrp1

A) *Graphical representation of mRNA level changes in Wnt pathway genes in WT and Sfrp1$^{-/-}$ mice HFSCs* ***B)*** *Graphical representation of mRNA level changes in Axin2 and Lgr5 genes in WT and Sfrp1$^{-/-}$ mice HFSCs* ***C & E)*** *Immunofluorescence assay (IFA) for Axin2 on WT, Sfrp1+/- and Sfrp1-/- mice skin sections at PD21 & PD49 respectively.* ***D & F)*** *Graphical representation of mean intensity of Axin2 in WT, Sfrp1+/- and Sfrp1-/- mice skin sections at*

*PD21 & PD49 respectively. (Data are analyzed by student's t-test and presented as mean ± SEM. n=3mice/genotype, ns=non-significant, *=P<0.05, **= P<0.01).*

5.2.9 Decrease in Active β-Catenin signalling

Since Sfrp1 is a Wnt inhibitor, Sfrp1 loss ideally should lead to increase in Wnt β-Catenin signalling thereby increasing the expression of Wnt target genes. Conversely, we found a decrease in the mRNA expression and protein levels of Wnt target genes (Axin2 and Lgr5) in both the $Sfrp1^{+/-}$ and $Sfrp1^{-/-}$ mice as compared to WT littermates. Therefore, we further went on to check the activity levels of β-Catenin in WT, $Sfrp1^{+/-}$ and $Sfrp1^{-/-}$ mice. Mice of all the three genotypes were sacrificed at PD49 and protein was isolated from the skin as described in the materials and methods. We further performed western blot analysis using mice skin protein to identify the changes in the activity of β-Catenin within these mice. Our data showed decrease in the active β-Catenin levels in $Sfrp1^{+/-}$ and $Sfrp1^{-/-}$ mice as compared to WT mice. This was further validated by performing IFA for active β-Catenin on the mice skin sections at PD49 (Figure 5.10). Thus, the data showed a decrease in the active β-Catenin thereby resulting in decreased Wnt signalling and its target genes (Lgr5 and Axin2) in $Sfrp1^{+/-}$ and $Sfrp1^{-/-}$ mice as compared to WT mice.

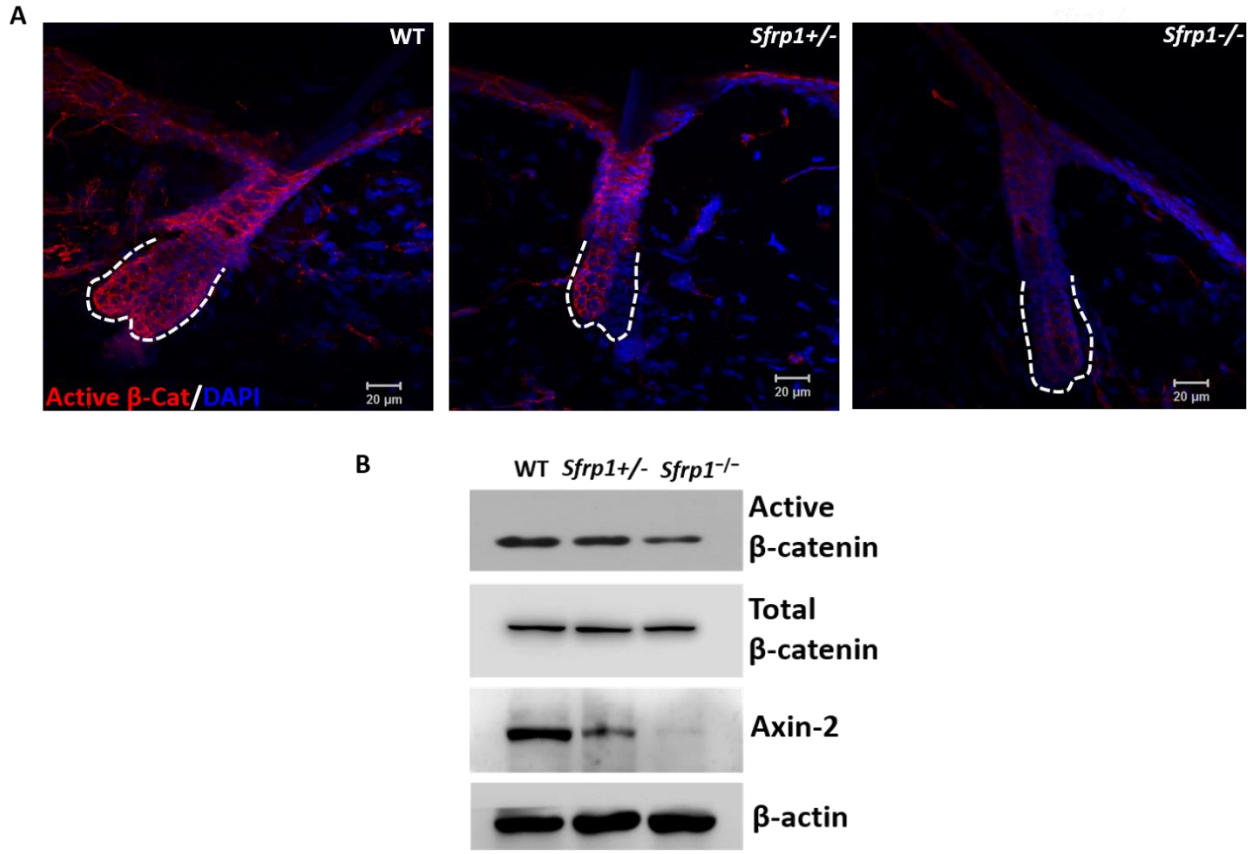

Figure 5.10: Altered Wnt signalling in the absence of Sfrp1

A) *Immunofluorescence assay (IFA) for active β-catenin on WT, Sfrp1$^{+/-}$ & Sfrp1$^{-/-}$ mice skin sections* ***B)*** *Western blot analysis of total and active β-catenin and Axin2 levels in WT, Sfrp1$^{+/-}$ & Sfrp1$^{-/-}$ mice skin. (White dotted line marks bulge region of hair follicle, scale bar=20µm, n=4/genotype)*

5.2.10 Altered WNT/AKT/BMP signalling in Sfrp1$^{-/-}$ mice

Decrease in the active β-Catenin levels was observed in both the Sfrp1$^{+/-}$ and Sfrp1$^{-/-}$ mice skin as compared to WT mice skin. Gsk-3β, a member of destruction complex, was shown to phosphorylate and target β-catenin to proteasomal degradation [366]. Hence, we have checked for the active Gsk-3β levels in the Sfrp1$^{+/-}$ and Sfrp1$^{-/-}$ mice as compared to WT mice. Briefly, mice at PD49 were sacrificed and total protein was isolated from the whole

skin by homogenization as described in materials and methods. Subsequently, western blot was performed to check the levels of active Gsk-3β, P-Gsk-3β (Inactive form) in the WT, $Sfrp1^{+/-}$ and $Sfrp1^{-/-}$ mice protein samples. Our data showed a significant increase in the active Gsk-3β and decrease in P-Gsk-3β levels in $Sfrp1^{+/-}$ and $Sfrp1^{-/-}$ mice in comparision with WT (Figure 5.11 A). P-Akt was reported to assist Wnt signalling by phosphorylating Gsk-3β and inhibiting its function [412] as well as phosphorylating β-Catenin at serine-552 and targeting it to nuclear localization [413]. Therefore, we further checked for the activity of Akt signalling by performing western blotting. We found that the P-Akt (active form) protein levels were lower in $Sfrp1^{+/-}$ and $Sfrp1^{-/-}$ mice in comparision with WT. Moreover, the PI3K levels were also found to be lower in the $Sfrp1^{+/-}$ and $Sfrp1^{-/-}$ mice as compared to WT mice skin (Figure 5.11 B & C).

Further, Bmp signalling inactivates Akt signalling by inhibiting the phosphorylation of Pten. Hence, we have also checked for the changes in the Bmp signalling. The mRNA expression levels of Bmp receptor 1A (Bmpr1a) was increased and Noggin (inhibitor of Bmp signalling) was decreased in HFSCs of $Sfrp1^{+/-}$ and $Sfrp1^{-/-}$ mice as compared to WT HFSCs. Taken together, increase in the Bmp signalling and decrease in the P-Akt levels might be involved in the increase in the active Gsk-3β levels.

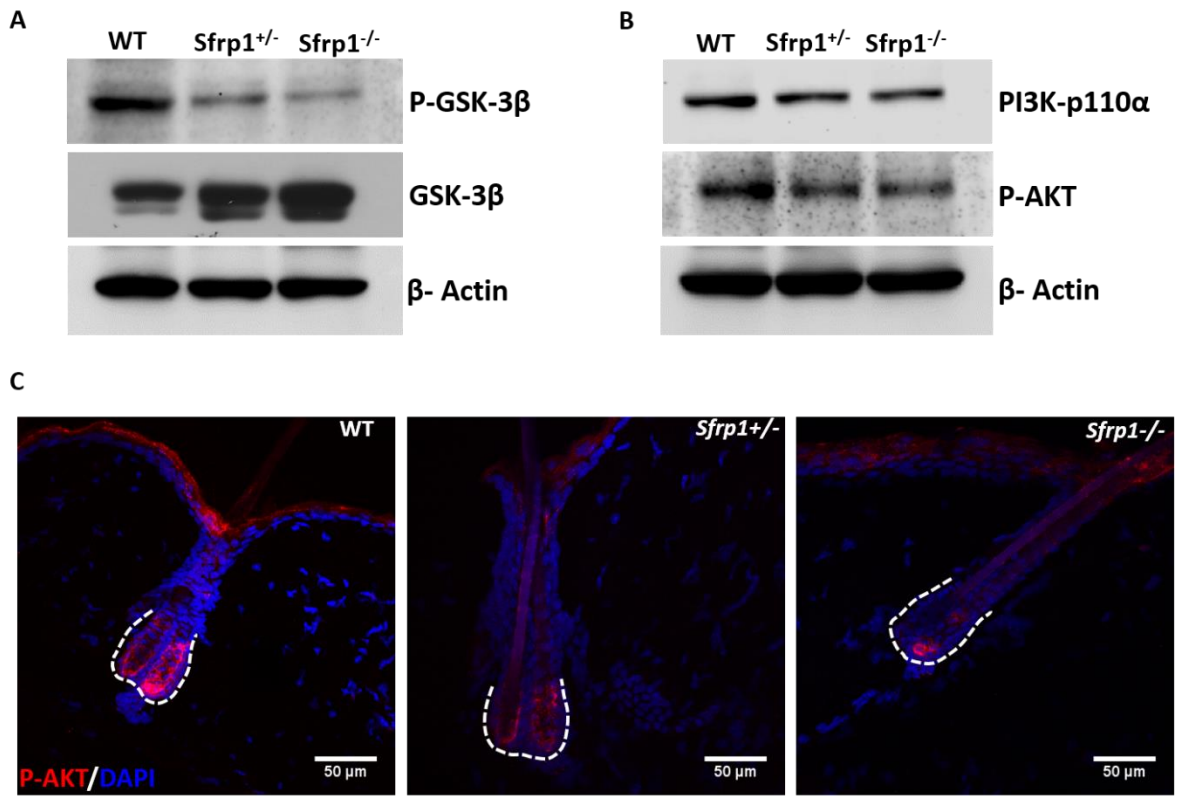

Figure 5.11: Altered AKT signalling in the absence of Sfrp1

A) *Western blot analysis of phospho and non-phospho forms of Gsk-3β levels in WT, Sfrp1+/- and Sfrp1-/- mice skin.* ***B)*** *Western blot analysis of P-AKT and PI3K-110α levels in WT, Sfrp1+/- and Sfrp1-/- mice skin. C) Immunofluorescence assay (IFA) for P-AKT on WT, Sfrp1+/- and Sfrp1-/- mice skin sections (White dotted line marks bulge region of hair follicle, scale bar=50µm, n=4/genotype)*

5.2.11 Establishment of mouse primary keratinocyte cell cultures

Sfrp1 loss affected initial HFSCs pool, their proliferation and the molecular signalling with in HFSCs *in vivo*. Further, in order to evaluate the effect of the Sfrp1 loss *in vitro*, we have established the long-term primary keratinocytes cultures of all the three genotypes (WT, $Sfrp1^{+/-}$ and $Sfrp1^{-/-}$). The epidermal keratinocytes were isolated from new-born mice (PD2) and co-cultured with mitotically inactive (γ-irradiated) feeder cells (J2-3T3/mouse embryonic fibroblast) in E-media (calcium concentration 0.05mM) up till passage eight. After eight

passages, keratinocytes were cultured without feeder cells to develop feeder independent primary keratinoyte cultures. Further, the keratinocytes were confirmed for their genotype both at the expression as well as at protein level. The cultures were primarily checked for redundancy from other Wnt antagonists such as Sfrp2, Sfrp3, Sfrp4 & Sfrp5, Dkk1 & Dkk3 and Wif1 and no redundancy was observed in the absence of Sfrp1 (Figure 5.12)

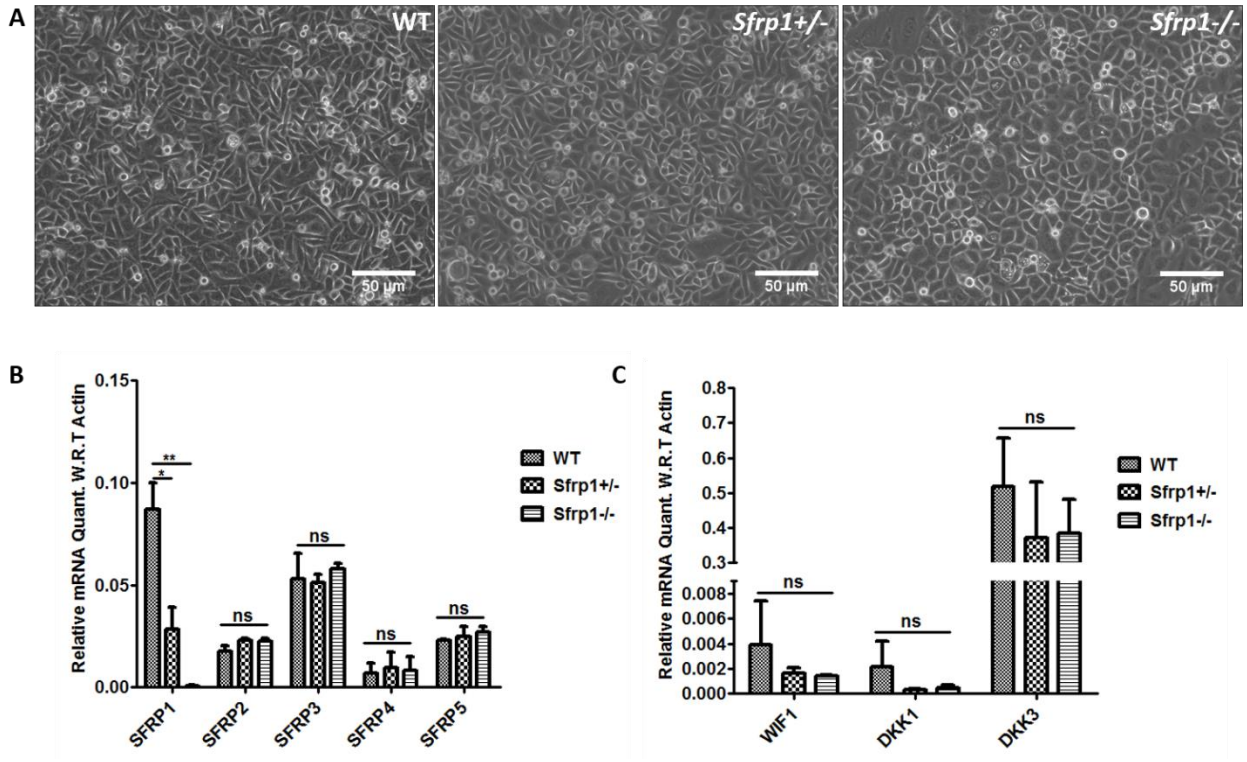

Figure 5.12: Primary epidermal keratinocytes culture

.

A) *Feeder independent keratinocytes cultures of all the three genotypes (WT Sfrp1$^{+/-}$ and Sfrp1$^{-/-}$)* ***at*** *10X magnification* ***B)*** *Graphical representation of mRNA level changes in SFRP family genes in WT, Sfrp1$^{+/-}$ and Sfrp1$^{-/-}$ mice keratinocytess* ***C)*** *Graphical representation of mRNA level changes in Wnt signalling antagonists (Wif1, Dkk1 & Dkk3) in WT, Sfrp1$^{+/-}$ and Sfrp1$^{-/-}$ mice keratinocytes. (Scale bar=50µm, n=5/genotype, ns=non-significant, *=P<0.05, **= P<0.01).*

5.2.12 Altered proliferation in Sfrp1 knockout primary keratinocytes:

To determine the functional effect of Sfrp1 knockout on primary epidermal keratinocytes proliferation, we have performed BrdU incorporation assay. The primary keratinocytes cultures of all the three genotypes (WT, $Sfrp1^{+/-}$ and $Sfrp1^{-/-}$) were serum starved for 24 hours and BrdU (10µM) containing complete E-media was then added and incubated for 8 hours. The cells were then fixed and IFA staining for BrdU was performed to determine the percentage of BrdU positive cells. Our data showed more BrdU positive cells in $Sfrp1^{-/-}$ keratinocytes as compared to WT keratinocytes suggesting higher proliferation in $Sfrp1^{-/-}$ keratinocytes as compared to WT keratinocytes. Conversely, $Sfrp1^{+/-}$ showed less number of BrdU positive cells i.e. decrease in proliferation as compared WT keratinocytes (Figure 5.13).

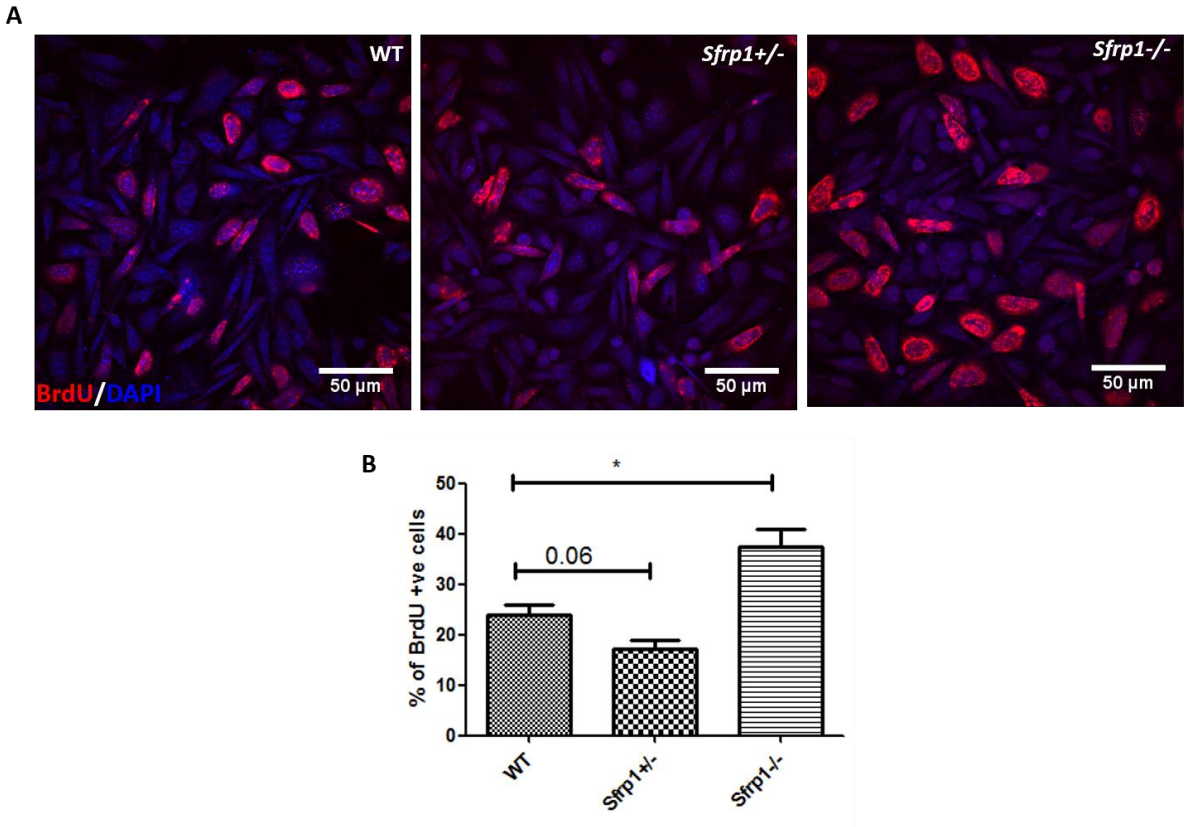

Figure 5.13: Analysis of cell proliferation by BrdU incorporation assay

A) *Immunofluorescence (IFA) for BrdU in mice primary keratinocytes treated with BrdU (10μM) containing complete media after 24 hour serum starvation* ***B)*** *Quantification of BrdU positive cells in WT, Sfrp1$^{+/-}$ and Sfrp1$^{-/-}$ mice keratinocytes. (Data are analyzed by student's t-test and presented as mean ± SEM. scale bar=50μm, n=4/genotype, *=P<0.05).*

5.2.13 Altered colony forming efficiency in Sfrp1 knockout primary keratinocytes:

Sfrp1 loss showed altered proliferation in mouse primary keratinocytes. Therefore, in order to understand the effect of Sfrp1 on functional properties of keratinocytes we have performed colony forming efficiency assay. Briefly, equal number of keratinocytes (5000 cells) of all the three genotypes (WT, Sfrp1+/- and Sfrp1-/-) were plated in 6 well plates and allowed to grow for seven days. The results showed an increase in the colony forming efficiency of Sfrp1-/- compared to WT keratinocytes whereas, Sfrp1+/- showed a decrease in colony forming efficiency as compared to WT (Figure 5.14).

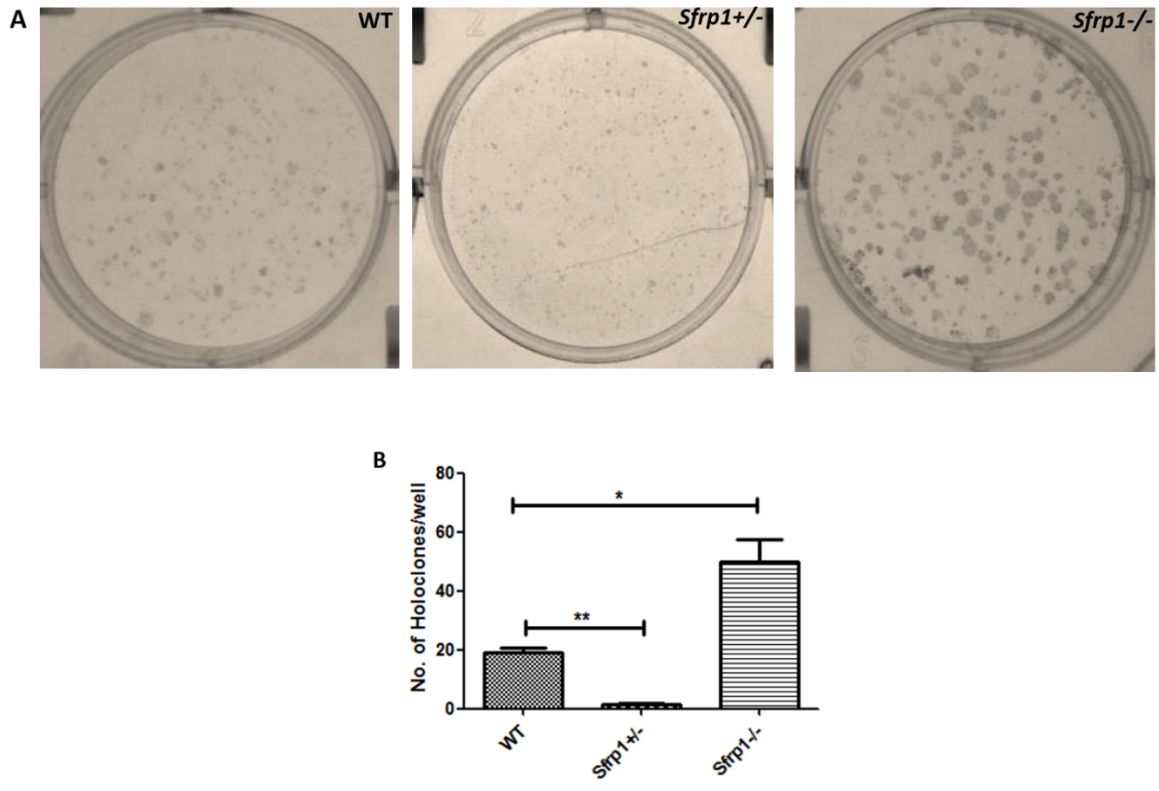

Figure 5.14: Altered colony forming efficiency

A) *Colony forming efficiency of WT, Sfrp1$^{+/-}$ and Sfrp1$^{-/-}$ mice keratinocytes.* ***B)*** *Quantification of number of holoclones (colonies with cell no. >200) per well. (Data are analyzed by student's t-test and presented as mean ± SEM. n=3/genotype).*

5.2.14 Altered Wnt signalling in Sfrp1 knockout keratinocytes

Sfrp1 loss showed altered proliferation and colony forming efficiency in mouse primary keratinocytes. This warrants to understand the underlying molecular mechanisms accountable for these changes. As Sfrp1 is a known Wnt antagonist, we have checked for the changes in the expression and activation levels of Wnt signalling pathway genes (β-catenin, Gsk-3β and Axin2). Western blotting of Wnt pathway and target genes in Sfrp1 knockout keratinocytes showed decrease in active β-catenin levels as well as Axin2 (primary Wnt target gene) protein levels.. Gsk-3β, a component of destruction complex, phosphorylates and targets β-catenin to proteasomal degradation. Hence, we further checked for the active Gsk-3β levels which were found to be higher in the Sfrp1 knockout keratinocytes as compared to WT keratinocytes. Additionally, we have also checked for cell-cycle regulating genes such as P21, Runx1 and cyclin-D1 in mouse primary keratinocytes (Figure 5.15). The results were similar to that of mice skin, where we have observed a decrease in P21and Runx-1 levels and increase in cyclin-D1 levels.

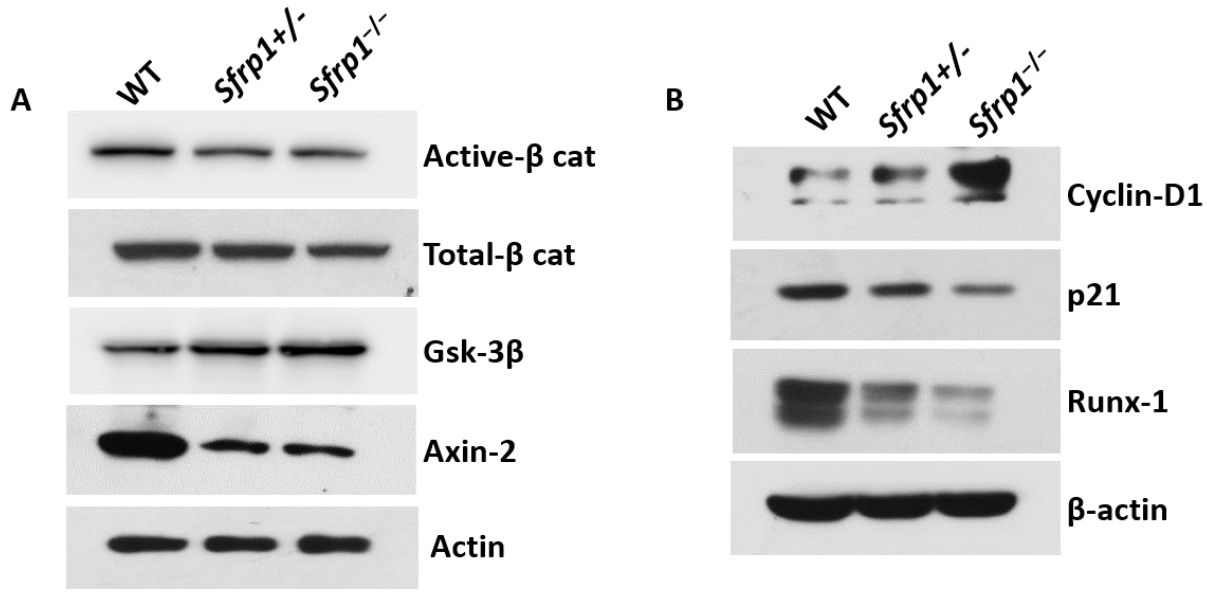

Figure 5.15: Western blot analysis of Wnt signalling and cell cycle regulating genes

A) *Western blot analysis of Wnt signalling pathway genes (β-catenin, Gsk-3β) and Wnt target Axin2 in WT, Sfrp1$^{+/-}$ & Sfrp1$^{-/-}$ mice keratinocytes.* ***B)*** *Western blot analysis of cell cycle regulating genes (P21, Cyclin-D1)and Runx1 in WT, Sfrp1$^{+/-}$ & Sfrp1$^{-/-}$ mice keratinocytes. n=3/genotype.*

5.3 Proposed Model for Sfrp1 in HFSC regulation:

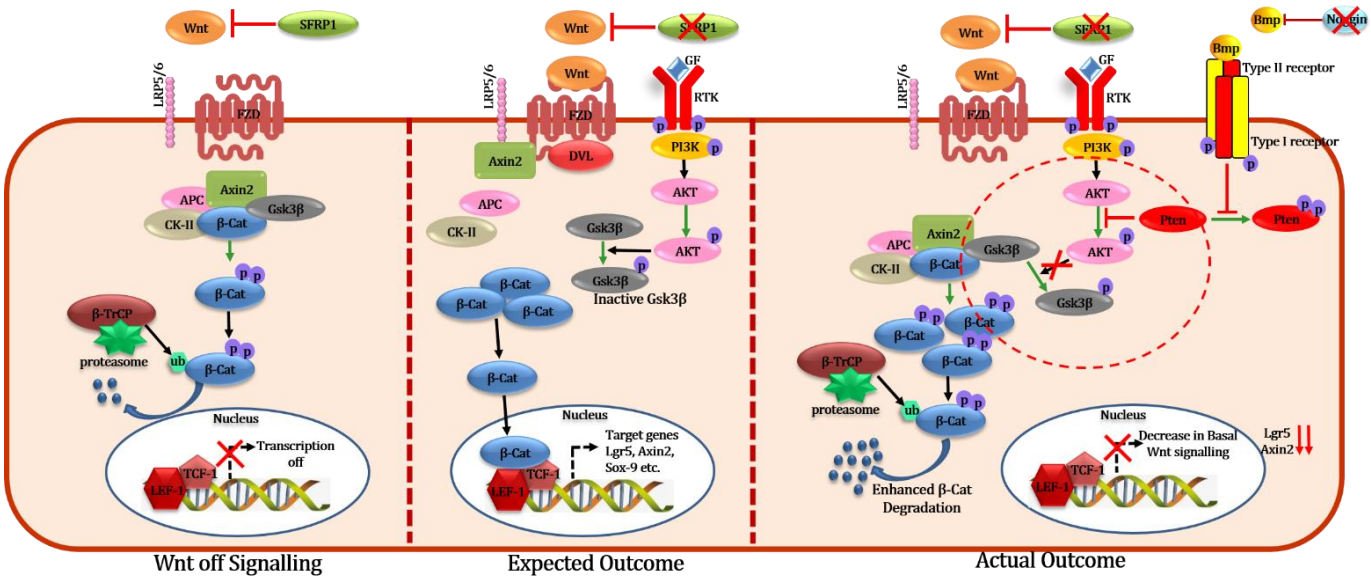

Figure 5.16: Altered BMP/AKT signalling inhibits aberrant activation of Wnt signalling in HFSCs

Diagrammatic representation of altered signalling within HFSCs in the absence of Sfrp1. In the first panel, the presence of Sfrp1 inhibits binding of its Wnt ligand to its receptor thereby resulting in the β-catenin degradation (Wnt off signalling). Middle panel represents the expected outcome in the absence of Sfrp1, where Wnt ligand binds to its receptor resulting in the aberrant expression of Wnt target genes. However, in the case of HFSCs (Last panel), our study reveals a novel hierarchical level of regulation embedded within HFSCs that inhibits aberrant activation of Wnt signalling in the absence of Sfrp1, by regulating Akt activity through the enhanced expression of Bmp signalling agonists (Bmpr1a) and antagonists (Noggin). The activated Bmp signalling inhibits AKT signalling activity resulting in higher active Gsk-3β levels that inhibits aberrant Wnt signalling in the absence of Sfrp1. (GF=growth factor, RTK=Receptor tyrosine kinase, CK=casein kinase, β-cat= β-catenin, APC= adenomatous polyposis coli, FZD=frizzled receptor)

5.4 Discussion:

Wnt signalling pathway is an archaic and evolutionarily conserved pathway that regulates crucial aspects such as stem cell self-renewal, cell fate determination, cell migration, cell polarity, neural patterning and organogenesis during embryonic development and adult tissue homeostasis [365, 414]. Perturbations in the Wnt signalling pathway are reported in multiple human abnormalities [415, 416] and cancers [400, 417, 418]. Hence, Wnt signalling is tightly regulated by various secreted antagonists such as SFRP family proteins, Dickkopf proteins, WIF-1, Sclerostin etc, which prevents the interaction between Wnt ligands and their receptors [378-381]. At the intracellular level, the non-canonical Wnt Ca^{2+} pathway regulates the canonical Wnt signalling by phosphorylating and targeting the β-catenin to proteasomal degradation.

Wnt signalling plays a fundamental role in the epidermal stratification, hair follicle development, HFSC proliferation and differentiation during hair regeneration [191, 192]. Alterations within the Wnt signalling pathway lead to irregularities during hair follicle development as well as hair regeneration. Loss of Wnt signalling in mice skin during development results in the absence of hair follicles in mutant mice [123, 124] and loss of Wnt signalling activity in the bulge region during the anagen induction results in hair follicles to remain in telogen phase without progressing into anagen [192]. Moreover, over expression of DKK1 (a Wnt antagonist) during anagen phase leads to premature entry of hair follicles into catagen phase [192]. Conversely, over-expression of Wnt signalling results in de novo hair follicle morphogenesis during anagen [189]. All of the accumulating evidence suggests the importance of Wnt signalling during hair follicle development, and at different phases of hair follicle cycle progression. Importantly, Sfrp1 a Wnt antagonist is involved in regulating maintenance and functions of different tissue SCs such as BASCs [405], MSCs [406] and ESCs [407]. There are several reports that showed the expression of Sfrp1 is upregulated in

the HFSCs as compared to non–stem cells [136, 175].Given the importance of Sfrp1 in the regulation of different tissue SCs, the role of Sfrp1 in HFSC regulation and maintenance is not yet completely understood.

In the present study, to understand the role of Sfrp1 in HFSCs regulation and in normal tissue homeostasis, we have used Sfrp1 genetic knockout mice [356]. To understand the role of Sfrp1 in regulating HFSCs population, we have performed FACS using HFSCs markers (CD-34 and α6-integrin) at different post-natal days during the first hair cycle (PD21 to PD49). Our results showed that, during the first telogen (PD21) there is a decrease in the HFSCs population in both the $Sfrp1^{+/-}$ and $Sfrp1^{-/-}$ mice as compared to WT mice. In order to further confirm that this decrease in the HFSCs is an actual decrease but not due to any artefact, we further performed IFA on the dorsal skin sections of WT, $Sfrp1^{+/-}$ and $Sfrp1^{-/-}$ mice using a different stem cell marker Sox-9. Sox-9 (HFSCs marker) is not only expressed in the HFSCs but also plays an important role in HFSCs compartment formation and their survival. During morphogenesis i.e. at initial hair follicle formation, Sox-9 is essential for the HFSCs compartment formation and HFSCs marker (CD34) expression [139]. Further, Sox-9 deletion in skin prior to the formation of bulge results in absence of stem cell niche in mice and the mice were nude [139]. Deletion of Sox-9 at PD21 results in defective hair follicle cycling, impaired ORS differentiation, decrease in matrix proliferation and gradual hair loss in mice [139]. Therefore, we have checked for the changes in the number of Sox-9+ cells in the absence of Sfrp1. Our results showed that the number of Sox-9 positive cells in the bulge were also lower in $Sfrp1^{+/-}$ and $Sfrp1^{-/-}$ mice in comparision with WT mice at PD21 backing up or FACS data. Hence, this decreased Sox-9+ cell number might be responsible for low number of HFSCs during the first telogen. This provides evidence that the initial formation of HFSCs is itself lower in $Sfrp1^{+/-}$ and $Sfrp1^{-/-}$ mice.

Further, gradual decrease in the HFSCs population with time was reported with increase in proliferation and differentiation of HFSCs in the bulge region [419]. Therefore, we went ahead to check the HFSCs percentage during the first anagen (PD28), where we found that the HFSCs were lower in $Sfrp1^{+/-}$ and $Sfrp1^{-/-}$ mice in comparision with WT mice. However, at PD49, the percentage of HFSCs in $Sfrp1^{-/-}$ mice were similar to WT mice, whereas HFSCs in $Sfrp1^{+/-}$ mice were lower as compared to WT mice. Importantly, Rampolas et al in 2013, have shown that partial depletion of HFSCs through laser ablation results in the restoration of HFSCs through the proliferation of remaining HFSCs and hair germ cells [420].Therefore, to understand how $Sfrp1^{-/-}$ mice HFSCs percentage was similar to that of WT mice we have performed BrdU cell proliferation assay at PD23 i.e. during the telogen-to-anagen transition. Our results have shown that there was an increase in the HFSCs proliferation in $Sfrp1^{-/-}$ mice in comparison with WT littermates. Moreover, this increase in the HFSCs proliferation was further validated throgh IFA for Ki-67 (proliferation marker) at PD23. The results showed an increase in the Ki-67 positive cells in $Sfrp1^{-/-}$ mice bulge as compared to WT thereby confirming the BrdU data. This increased proliferation could be the reason behind the equal number of HFSCs in WT and $Sfrp1^{-/-}$ mice at PD49. However, the proliferation of the $Sfrp1^{+/-}$ mice HFSCs was similar to that of WT mice in both BrdU and Ki-67experiments explaining the lower number of HFSCs within these mice.

SCs mostly remain quiescent and divide infrequently to prevent accumulation of mutations to maintain their genome integrity [167-171]. Recently, Waghmare et al., have demonstrated that the hair HFSCs within the niche have different quiescence potentials and divide infrequently (~3 times on average/ hair cycle) [174]. As these SCs divide infrequently they retain the label (BrdU/EdU) for a longer period of time compared to cells that proliferate more frequently and are called as label retaining cells (LRCs). Increased proliferation of HFSCs leads to loss in the label retaining capacity of the HFSCs in the bulge region [419]. As

there is an increased proliferation in the Sfrp1$^{-/-}$ mice bulge, we further checked for the LRCs within these mice. The number of LRCs in the Sfrp1$^{-/-}$ mice bulge was lower as compared to WT mice bulge, which further supports the data that there in an increased proliferation Sfrp1$^{-/-}$ mice bulge. However, this increased proliferation is transient and did not lead to loss of HFSCs pool as it is evident from the Ki-67 IFA at PD49, which did not show any change in the number of proliferative HFSCs in Sfrp1$^{-/-}$ bulge as compared to WT bulge. Moreover, this transient increased proliferation might be responsible for the restoration of HFSC pool in Sfrp1$^{-/-}$ mice bulge.

Since there is an increased proliferation and decreased LRCs in Sfrp1$^{-/-}$ mice bulge as compared to WT mice bulge, we further went on to check the molecular changes involved in the increased HFSC proliferation. Runx1 (Runx family transcription factor 1) is expressed only in bulge and hair germ, but not in other skin epithelial structures, such as sebaceous gland and epidermis [421, 422]. Further, Hoi et al, in 2010 have shown that low levels of Runx1 expression in bulge cells enhance their self-renewal [423]. Moreover, Renstrom et al. in 2009 reported decreased expression of the Runx1 in CD34-LSK cells (hematopoietic stem cells) in the absence of Sfrp1 [404]. Further, Runx1 regulates the expression of P21 which is important in maintaining quiescence in HFSC [424]. Therefore, we further checked for the protein levels of Runx1 and P21 in the dorsal skin of WT, Sfrp1$^{+/-}$ and Sfrp1$^{-/-}$ mice. Our western blot results have shown that there was a decrease in the levels of Runx1 and P21 in Sfrp1$^{+/-}$ and Sfrp1$^{-/-}$ mice in comparision with WT mice. Further, the levels of Cyclin-D1 were increased in Sfrp1$^{+/-}$ and Sfrp1$^{-/-}$ mice in comparision with WT. Hence, this decreased P21 levels and increased Cyclin-D1 levels might be responsible for the increased proliferation of the Sfrp1$^{-/-}$ HFSCs as compared to WT HFSCs. Additionally; the low levels of Runx1 might also contribute in the restoration of HFSC population in Sfrp1$^{-/-}$ mice.

In order to understand whether this increased proliferation in Sfrp1$^{-/-}$ mice bulge has led to any changes in the hair cycle progression, we have characterized mice skin at various post-natal days during the first hair cycle. H&E analysis of mice skin sections at different post-natal days during first hair cycle showed a slightly faster hair follicle cycling pattern in Sfrp1$^{-/-}$ mice as compared to WT mice. Further, no visible abnormalities were observed in hair follicle structure, sebaceous gland and epidermal thickness.

We further checked, whether Sfrp1 loss affects wound healing process. Recent studies have revealed that within 24 hours of wounding, the HFSCs get activated and migrate out of the niche and involve in the re-epithelialisation process [135, 136]. Levy et al., in 2007, using ShhGFPcre;R26R mice showed that HFSCs migration towards the wound can be observed as early as a day after wounding and the wound surface is covered in the course of 2weeks [258]. During the initial wound healing process, HFSCs rapidly generate transient amplifying cells that are responsible for acute wound repair [145]. Further, these cells are replaced by the cells generated by the inter-follicular epidermal SCs (IFE-SCs) at a later stage [76]. Importantly, it has been shown that PI3K/AKT/mTOR pathway plays an important role in epithelial cell proliferation, migration and wound healing [425-427]. In our study, we have observed a delay in wound healing process at PD49 (2nd telogen) in Sfrp1$^{+/-}$ and Sfrp1$^{-/-}$ mice as compared to WT mice. This delay in wound healing could be attributed to impaired stem cell potential due to loss of Sfrp1 as its was observed that there is a delay in initial wound closure. Additionally, we have also checked for the changes in the PI3K pathway in mice skin by performing western blot. Our results showed that there is a decrease in the P-Akt levels in Sfrp1$^{+/-}$ and Sfrp1$^{-/-}$ mice in comparision with WT mice. Hence, the decreased Akt signalling in mice skin might be adding up to the delay in wound healing process, as the initial delay in the wound healing caused by HFSCs impaired function is not been overtaken by the IFE derived cells even at later stages of wound healing.

Sfrp1 loss resulted in initial stem cell pool loss, increased proliferation of HFSCs, decreased LRCs and delay in wound healing response. Therefore, it warrants understanding the molecular mechanism involved in regulating the HFSCs in the absence of Sfrp1. Hence, we have performed the gene expression profile of WT and $Sfrp1^{+/-}$ and $Sfrp1^{-/-}$ HFSCs. One of the most important questions was whether there exists any redundancy from other SFRP proteins in the absence of Sfrp1. During the mouse early embryonic development Sfrp1 *and* Sfrp2 are required for antero-posterior (AP) axis elongation and somitogenesis in the thoracic region. Homozygous mutations in either Sfrp1 *or* Sfrp2 individually did not have any effect; however, mutations in both Sfrp1 and Sfrp2 simultaneously resulted in severe shortening of the thoracic region and embryonic lethality at around E16.5, indicating that Sfrp1 and Sfrp2 are functionally redundant [356]. Further, Sfrp1 and Sfrp2 show redundant functions in the embryonic sexual development of the mouse. Loss of either Sfrp1 or Sfrp2 had no effects; however, loss of both Sfrp1 and Sfrp2 resulted in multiple defects in gonad morphology, reproductive tract maturation and gonad positioning [411]. Hence, we first checked for the change in the expression levels of other SFRP family members to check for redundancy. Our results did not show any change in the expression of other SFRP family genes such as Sfrp2, Sfrp3, Sfrp4 and Sfrp5. We further checked the expression level changes in other Wnt antagonists such as Dkk1, Dkk3 and Wif1 which also did not show any changes in their expression in the absence of Sfrp1. This shows that there exists no redundancy among the SFRP genes in mouse HFSCs.

Since, Sfrp1 is a well-known Wnt antagonist, we have first checked for changes in the Wnt signalling pathway in WT and $Sfrp1^{-/-}$ HFSCs. No changes in the expression levels of Wnt pathway genes such as β-catenin, Gsk-3β, Tcf1 and Lef1 was observed. However, we found the expression of Wnt target genes such as Lgr5 and Axin2 expression was decreased in $Sfrp1^{-/-}$ HFSCs as compared to WT HFSCs. Lgr5 marks the actively proliferating and yet

multipotent stem cell population within the bulge [147]. Further, Axin2 was reported to be continuously expressed in adult HFSCs through autocrine Wnt signalling and is involved in their maintenance [142]. Earlier reports from Renstrom et al. in 2009 have shown that the active β-Catenin levels were lower in CD34-LSK cells (HSCs) in the absence of Sfrp1 as compared to control [404]. Therefore, we checked the active β-Catenin levels and found them to be lower in $Sfrp1^{-/-}$ mice skin as compared to WT skin. Gsk-3β, a well-known kinase present in the destruction complex of the Wnt signalling, which phosphorylates and targets β-catenin to proteosomal degradation [428], was highly active in $Sfrp1^{+/-}$ and $Sfrp1^{-/-}$ mice skin in comparision with WT skin. Additionally, the phosphorylated form of the Gsk-3β (Gsk3β-Ser-9) was found to be lower in $Sfrp1^{+/-}$ and $Sfrp1^{-/-}$ mice skin. Thus, the activated Gsk-3β might be the one responsible for the β-catenin degradation in $Sfrp1^{+/-}$ and $Sfrp1^{-/-}$ mice skin.

Akt (protein kinase B) a serine/threonine kinase phosphorylates Gsk-3β at Ser-9 resulting in its inactivation. Given that the activity of Gsk-3β was shown to be inhibited by Akt mediated serine-9 phosphorylation, inactivation of Akt results in Gsk-3β activation associated with serine-9 dephosphorylation [429]. Hence, we have checked for the P-Akt levels (active form of Akt), which were found to be less in $Sfrp1^{+/-}$ and $Sfrp1^{-/-}$ mice skin as compared to WT. Further, the phosphorylation of Akt is regulated by Pten (PI3K phosphatase and tensin homolog) [430], which in turn is regulated by Bmpr1a (bone morphogeneic protein receptor type 1A) of Bmp signalling pathway [412]. Previous reports suggest that Bmp signalling pathway regulates the hair cycle by inhibiting β-catenin activity by activating Pten, which inhibits PI3K/AKT signalling downstream [118, 412]. Hence, we further checked for the changes in Bmp signalling. Our gene expression profile results showed that the expression of Bmpr1a was higher and Noggin, a negative regulator of Bmp signalling pathway was lower in $Sfrp1^{+/-}$ and $Sfrp1^{-/-}$ mice HFSCs as compared to WT. Altogether, in the absence of Sfrp1, the expression of noggin decreases in $Sfrp1^{+/-}$ and $Sfrp1^{-/-}$ mice HFSCs as compared to WT

HFSCs, there by activating Bmpr1a mediated Bmp signalling which then activates Pten downstream. Further, Pten inhibits PI3K/AKT mediated signalling thereby activating Gsk-3β which in turn phosphorylates and inhibits β-catenin, in so doing stopping the aberrant activation of Wnt signalling in the absence of Sfrp1.

In conclusion, our study showed that Sfrp1 might have a prominent role in the initial formation of HFSCs. However, the relation between Sfrp1 and Sox-9 during the HFSC formation in skin must be dissected properly. It was reported that the intra stem cell antagonistic competition between Wnt and Bmp signalling determines stem cell activation or quiescence. Our study reveals a novel hierarchical level of regulation embedded within HFSCs that inhibits aberrant activation of Wnt signalling in the absence of Sfrp1, by regulating Akt activity through the expression of Bmp signalling agonists (Bmpr1a) and antagonists (Noggin). This study unveils a cross talk between the Wnt/Bmp/Akt signalling involved in regulating HFSC activation in the absence of Sfrp1.

Chapter 6: Objective 2

6.1 Introduction:

SFRPs act as tumor suppressor genes as their expression is frequently silenced in multiple cancers [431]. Two major mechanisms have been reported for the loss of expression of SFRPs i.e. either by transcriptional inactivation due to promoter hypermethylation or deletion of chromosomal fragment in which the gene is located [432]. Loss in expression of Sfrp1, Sfrp2 & Sfrp5 was reported in OSCC, due to the promoter hypermethylation [433]. Further, the Sfrp1 gene located in chromosomal region (8p22–p12) is frequently deleted in breast cancer [418]. Importantly, restoring the expression of SFRPs inhibited cancer cell growth *in vitro* and tumor growth within mice [434]. However, recent reports have shown that some of the SFRPs show tumor suppressor or oncogenic functions depending upon the cancer type. For instance, Sfrp2 expression is lost due to promoter hypermethylation in OSCC [433]. On the contrary, Sfrp2 was reported to augment the oncogenic activities of Wnt16b signalling thereby facilitating cancer cell proliferation, migration, invasion and more importantly, drug resistance in breast cancer [435]. Further, Sfrp4 acts as a tumor suppressor in mesothelioma where it inhibits proliferation and migration [436], where as in the case of pancreatic ductal adenocarcinoma and prostate cancer it acts as an oncogene [437, 438]. The contradictory roles of SFRPs in different cancers could be due to the following reasons: a) tissue-specific responses to different stimuli, b) biphasic responses to different concentrations of SFRPs, and c) the binding affinities and specificities of different SFRPs for Wnt ligands and Fzd receptors. Importantly, a detailed study of the specific relationship between SFRPs, Wnt ligands and Fzd receptors within normal and tumors tissues would provide a superior understanding of cancer outcome and development of successful therapeutic targets.

6.1.1 SFRP1 in multiple cancers:

Sfrp1, a natural Wnt antagonist, is down regulated in multiple cancers either due to promoter hypermethylation or deletion of chromosomal fragment in which the gene is located [400, 418, 439]. Loss of Sfrp1 expression due to promoter methylation is a predominant mechanism in renal cell carcinoma and non small cell lung carcinoma (NSCLC) [439, 440]. Epigenetic silencing of Sfrp1 occurs early in hepatocellular carcinoma (HCC) development, which contributes to increased cell growth and proliferation. Conversely, re-expression of Sfrp1 in HCC results in increasing the apoptosis rate in tumor cells and inhibiting tumor vascularisation [441, 442]. In case of breast cancer, aberrant promoter methylation is the predominant mechanism of Sfrp1 gene silencing which is associated with tumor progression and poor prognosis [400, 418]. Further, miRNA-27a negatively targets Sfrp1 and promotes proliferation and migration of breast and gastric cancer cells by activating the Wnt/β-catenin signalling pathway [443, 444]. Glioblastoma multiforme (GBM), a malignant brain cancer showed low levels of Sfrp1 expression with activated Wnt β-Catenin signalling. Further, GBM patients with low levels of Sfrp1 have shown poor overall survival as compared to patients expressing high levels of Sfrp1 [445, 446]. On the other hand, miRNA-328 targets Sfrp1 and activates Wnt signalling thereby enhancing invasive properties of Glioma cells. miRNA-1-3p suppresses the proliferation, invasion and migration of bladder cancer cells by up-regulating Sfrp1 expression**.** In case of prostate cancer, Sfrp1 suppresses proliferation by inhibiting androgen receptor transcription [447]; however, Sfrp1 expression in prostate cancer is lost mostly due to epigenetic inactivation of promoter and in some cases due to post translational modification (PTM) i.e. aberrant gain of the histone mark H3K27me3[448]. Methylation associated silencing and loss of heterozygosity in chromosome 8p in which Sfrp1 is located are the two common mechanisms for the loss of Sfrp1 in ovarian cancer [449]. Apart from solid tumors, Sfrp1 expression was also lost in liquid tumors such as Acute

myeloid leukaemia (AML) [450], chronic lymphocytic leukaemia (CLL) [451] and Acute lymphoblastic leukaemia (ALL) [452] due to DNA methylation. Recent studies have shown that Sfrp1 expression was downregulated and Wnt1 was upregulated in skin cutaneous squamous cell carcinoma [453].

6.1.2 Sfrp1 in cancer stem cell regulation:

Deregulation of Sfrp1 was reported in multiple cancers such as breast cancer, prostate cancer, ovarian cancer, OSCC and glioblastoma etc. [400, 418, 454]. Apart from affecting the cancer cell proliferation, migration and invasion Sfrp1 was also reported to regulate and enhance CSC properties in numerous cancers. For instance, Sfrp1 down regulation in mammary epithelial cells enhances EMT, migration, invasion, resistance to anoikis and enhanced $CD24^{low}/CD44^{high}$ cell surface marker expression which are the properties of CSCs [455]. Further, PHD finger protein 21B (PHF21B) promotes CSC like phenotype in prostate cancer by inhibiting Sfrp1 and activating Wnt β-catenin signalling [454]. Sfrp1 loss promotes CSC phenotype in Glioblastoma cells and treatment with recombinant Sfrp1 decreases Glioblastoma stem cell (GBM-SC) marker expression, inhibits proliferation, induces apoptosis and reduces sphere forming efficiency [446]. Importantly, micro RNAs also play a prominant role in enhancing CSCs phenotype by targeting Sfrp1. miR-1301-3p promotes the expansion of PCSCs by inhibiting Gsk-3β and Sfrp1 thereby activating the Wnt pathway [456]. Moreover, miR-582-3p suppresses multiple negative regulators of the Wnt/β-catenin pathway, namely, Axin2, Dkk3 and Sfrp1that promotes CSC traits of non-small cell lung carcinoma (NSCLC) cells [457]. In ovarian cancer, miR-1207 plays a vital role in promoting the CSC-like phenotype through activated Wnt/β-catenin signalling by directly targeting and suppressing Sfrp1[458]. Taken together, these studies highlight the role of Sfrp1 in multiple cancers as well as in CSCs. However, the role of Sfrp1 in regulating skin tumor initiation and CSCs regulation is not yet elucidated.

Earlier reports from our lab showed that Sfrp1$^{-/-}$ mice were highly susceptible towards chemical induced carcinogenesis (DMBA/TPA treatment). Sfrp1$^{-/-}$ mice showed much earlier papillomas formation i.e. within 10-12 weeks of TPA treatment. Whereas, Sfrp1$^{+/-}$ and WT mice papillomas development occurred after 12-14 weeks and 16-18 weeks post TPA treatment respectively. However, Sfrp1loss did not affect the average number of tumors/mice. Further, *in vivo* tumorigenic potential assay studies have shown that, Sfrp1$^{-/-}$ CSCs have increased tumorigenic potential compared to WT CSCs (Pls. refer to our lab's previous doctoral student, Dr. Rahul Sarate thesis, HBNI enrolment number:LIFE09201104006).

However, the detailed tumor characterization in the absence of Sfrp1 was not been attempted. Additionally, the molecular & functional characterization of Sfrp1$^{-/-}$ CSCs was not performed. In this study, we further went ahead to uncover the functional & molecular mechanism regulating the skin CSCs in the absence of Sfrp1. Importantly, the data acquired from the mouse model system was extended to human epithelial cancers to identify the possible molecular targets that could be targeted in treating cancer. All the below represented data has been published in stem cell reports journal [459].

6.2 Results:

6.2.1 Sfrp1$^{-/-}$ tumors show enhanced mesenchymal phenotype

Sfrp1 loss resulted in early tumor initiation in mice with chemical induced carcinogenesis (DMBA/TPA treatment). To further investigate any changes in the tumor histology we performed hematoxylin and eosin (H&E) staining of the papillomas and squamous cell carcinomas (SCC) of WT, Sfrp1$^{+/-}$ and Sfrp1$^{-/-}$ mice. The results showed that, the Sfrp1$^{-/-}$ SCCs mostly had the mixed phenotype (tumor containing both epithelial cells and mesenchymal cells), while a few Sfrp1$^{-/-}$ SCCs showed mesenchymal phenotype. In contrast, the WT SCCs mostly showed a well differentiated epithelial phenotype and a few number of

WT SCCs showed mixed phenotype (Figure 6.1). Hence, our results suggest that *Sfrp1*$^{-/-}$ mice tumors were primarily of mixed/mesenchymal phenotype as compared to epithelial phenotype of WT tumors.

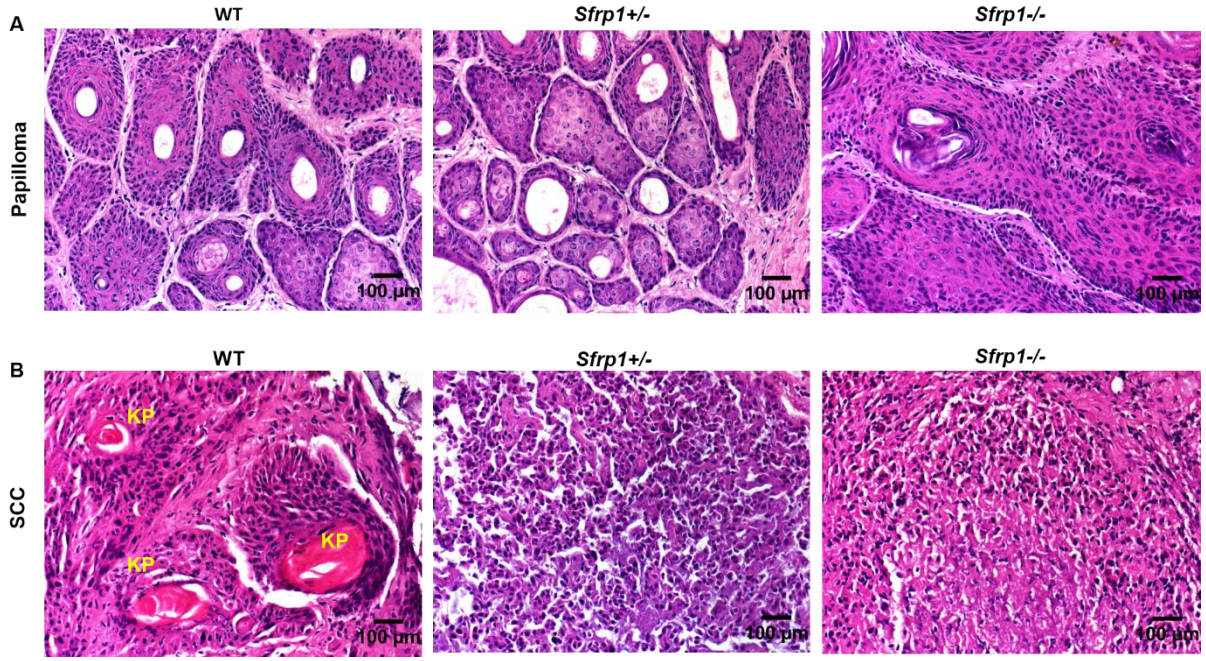

Figure 6.1: Enhanced mesenchymal phenotype in Sfrp1-/- SCC [459]

Haematoxylin and eosin (H&E) stained 5µm thick paraffin embedded sections from ***A)*** *Papilloma and* ***B)*** *SCC of WT, Sfrp1*$^{+/-}$ *and Sfrp1*$^{-/-}$ *mice. (n=6 mice/ genotype, KP= keratin pearl, scale bar: 100µm)*

6.2.2 Serial transplantation assay of Sfrp1$^{-/-}$ CSCs

Sfrp1 loss showed accelerated tumor initiation and enhanced mesenchymal phenotype of the tumors; hence, it is of utmost importance to understand the involvement of the Sfrp1 in tumor initiation and CSCs regulation. Previous reports from our lab have shown that Sfrp1$^{-/-}$ CSCs show enhanced *in vivo* tumorigenic potential as compared to WT CSCs. However, the serial transplantation assay (The gold standard assay) was not performed to confirm if the isolated cells are indeed CSCs. In order to confirm the FACS sorted cells are indeed CSCs, skin SCCs were collected from WT and Sfrp1$^{-/-}$ mice and a single cell suspension was prepared from

them. The percentage of the CSCs was analysed in WT and Sfrp1$^{-/-}$ tumors by FACS using well established CSCs markers (Lin^{-}/ Epcam^{+}/ α6-integrin^{+}/ CD34^{+}). The results showed that there is no change in the percentage of the CSCs in WT and Sfrp1$^{-/-}$ tumors (Figure 6.2A).

Additionaly, to investigate the functional properties of CSCs in the absence of Sfrp1 we have performed *in vivo* tumorigenic potential assay. WT and Sfrp1$^{-/-}$ CSCs (20,000 cells) were FACS sorted and transplanted subcutaneously into NOD/SCID mice to assess the tumorigenic potential of these cells. Our results demonstrated that, Sfrp1$^{-/-}$ CSCs were able to form tumors after 2-3 weeks of transplantation. However, WT CSCs developed tumors only after 5-6 weeks of transplantation (Figure 6.2B-C). *In vivo* serial transplantation assay is the gold standard assay used to confirm the presence of CSCs [460]. Therefore, in order to determine the FACS sorted cells are indeed CSCs, we have performed *in vivo* serial transplantation assay. Hitherto, we have transplanted 20,000 FACS sorted Sfrp1$^{-/-}$ CSCs into NOD/SCID mice (1st serial transplantation) which formed tumors within 3 weeks. Consequently, 20,000 Sfrp1$^{-/-}$ CSCs isolated from tumors arising from the 1st serial transplantation, were injected into NOD/SCID mice (2nd serial transplantation) which formed tumors within 10-14 days after transplantation. Our results showed that CSCs from 2nd serial transplantation were more aggressive as compared to CSCs from 1st serial transplantation. Further, there was an increase in the percentage of the CSCs in the tumors derived from serial transplantation studies as compared to the primary tumors (Figure 6.2D-E). Taken together, the results showed that Sfrp1$^{-/-}$ CSCs showed enhanced tumorigenic potential as compared to WT CSCs. Moreover, the FACS sorted cells are indeed CSCs and the percentage and aggressiveness of the CSCs increased with each serial transplantation in the NOD/SCID mice.

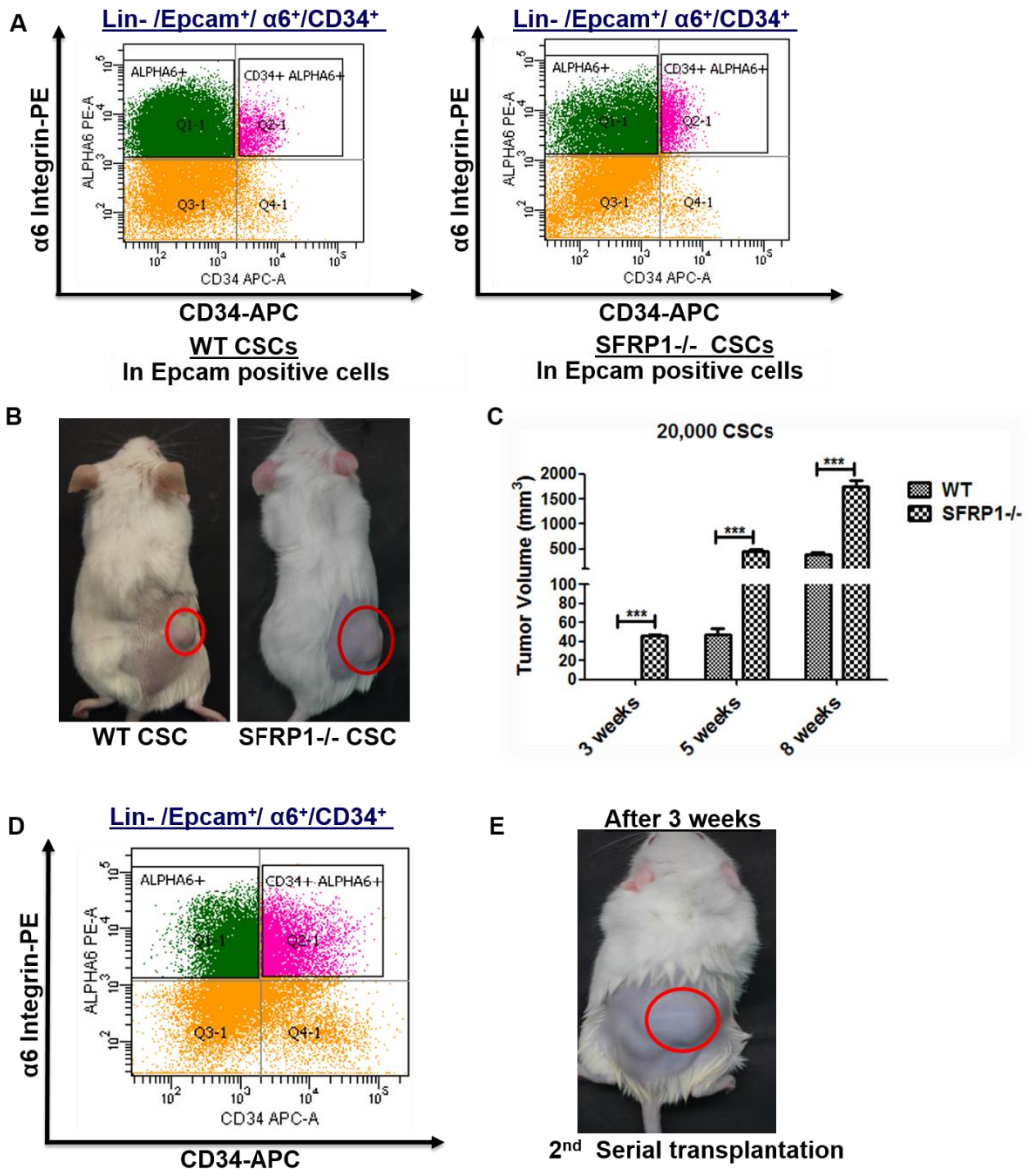

Figure 6.2: Enhanced tumorigenic potential of Sfrp1-/- CSCs [459]

A) *Percentage of CSCs in WT and Sfrp1-/- SCC.* ***B)*** *In vivo tumorigenesis assay using 20,000 FACS sorted CSCs from the WT SCC and Sfrp1$^{-/-}$ SCC injected into NOD/SCID mice. Tumor growth in NOD/SCID mice after 5 weeks of CSC transplantation.* ***C)*** *Graphical representation of tumor volume at 3weeks, 5weeks and 8weeks in NOD/SCID mice after transplanting with 20,000 FACS sorted CSCs from WT SCC and Sfrp1$^{-/-}$ SCC.* ***D)*** *FACS analysis of % of CSCs in tumors after 2nd serial transplantation.* ***E)*** *NOD/SCID mice showing*

*tumor development after 2nd serial transplantation. (*Data are presented as mean ± SEM and were analyzed by student's t-test. n=3 mice/ genotype. ** = p<0.01, ***=P<0.001)

6.2.3 Enhanced tumor propagating cell (TPC) efficiency of Sfrp1$^{-/-}$ CSCs (limiting dilution assay)

CSCs from Sfrp1$^{-/-}$ SCC have shown increased tumorigenicity and aggressiveness when injected into NOD/SCID mice as compared to WT CSCs. Therefore, to further understand whether Sfrp1 loss affects the tumor propagating cell efficiency, we have performed limiting dilution assay. In order to do that, we have transplanted minimal number of cells i.e. 10000, 5000 and 1000 CSCs from both the WT SCCs and Sfrp1$^{-/-}$ SCCs into NOD/SCID mice. The results showed that mice transplanted with 10,000 Sfrp1$^{-/-}$ CSCs developed tumors within 4-5 weeks of transplantation whereas, mice with 10,000 WT CSCs developed tumors after 7-8 weeks (Figure 6.3 A-B). Further, NOD/SCID mice with 5000 Sfrp1$^{-/-}$ CSCs developed tumors after 6-7 weeks of transplantation and no tumors were observed in mice which were transplanted with 5000 WT CSCs (Figure 6.3C). Moreover, no tumors were observed in mice transplanted with 1000 CSCs either from WT SCCs or Sfrp1$^{-/-}$ SCCs (Figure 6.3D). Importantly, we further calculated the tumor propagating cell (TPC) frequency of both WT and Sfrp1-/- CSCs and it was found that 1/8442 (estimate value) of Sfrp1$^{-/-}$ CSCs and 1/34761 (estimate value) of WT CSCs are able to form tumors when transplanted into NOD/SCID mice (Figure 6.3E). Hence, our results suggest that low numbers of Sfrp1$^{-/-}$ CSCs are capable of forming tumors in NOD/SCID mice with enhanced tumor propagating cell efficiency as compared to WT CSCs.

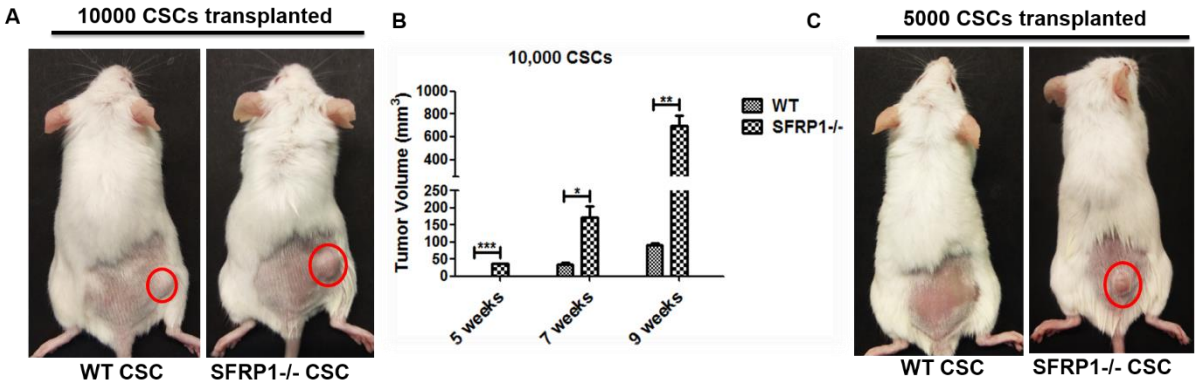

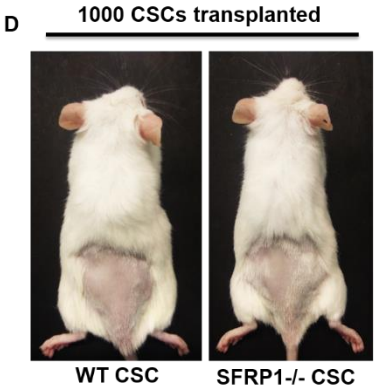

E

No. of CSCs transplanted	WT	SFRP1-/-
10,000	2/5	4/5
5000	0/5	2/5
1000	0/5	0/5
Tumor propagating cell frequency (95% CI)	1/34761 (1/136558 1/8849) (n=5)	1/8442 (1/19022 1/3747) (n=5)
P-value	0.0637	

Figure 6.3: Enhanced Tumor propagating cell frequency in Sfrp1-/- CSCs [459]

A) *In vivo tumorigenesis assay of 10,000 FACS sorted CSCs from WT SCC and Sfrp1$^{-/-}$ SCC injected into NOD/SCID mice. Tumor growth in NOD/SCID mice after 7 weeks of CSC injection.* ***B)*** *Graphical representation of tumor volume at 5weeks, 7weeks and 9weeks in NOD/SCID mice after injecting with 10,000 FACS sorted CSCs from WT SCC and Sfrp1$^{-/-}$ SCC.* ***C & D)*** *In vivo tumorigenesis assay of 5,000 & 1000 FACS sorted CSCs from WT SCC and Sfrp1$^{-/-}$ SCC injected into NOD/SCID mice respectively.* ***E)*** *Summary of TPC frequency estimated by the injection of limiting dilution of CSCs from WT SCC and Sfrp1$^{-/-}$ SCC into NOD/SCID mice. The data are represented in the ratio of injections that formed tumors out of total number of injections. The ratio in red color represent the estimated TPC frequency, while the ratios in blue and brown represent the lower and upper estimates of TPC respectively.*

6.2.4 Progressive Sfrp1 expression level changes with DMBA/TPA treatment:

To determine the changes in the expression levels of Sfrp1 with time during the DMBA/TPA treatment, we have quantified Sfrp1 mRNA levels in WT mice epidermis at various time points such as 5 weeks, 10 weeks, 15weeks and 20 weeks. In order to do that, mice at specified time points were sacrificed and total RNA was isolated from the epidermis followed by cDNA preparation and quantitative real time PCR. The results showed progressive decrease of Sfrp1 with time in mice epidermis with TPA treatment (Figure 6.4A)**.** Further, we went on to check the difference in the mRNA expression levels of Sfrp1 in WT mice normal epidermis (without DMBA/TPA treatment) and chemically induced (DMBA/TPA) WT SCCs. The results showed significant decrease in Sfrp1 expression in WT SCC as compared to WT normal epidermis (Figure 6.4B). Importantly, we have also checked the difference in the Sfrp1 expression levels between WT CSCs and WT non-CSCs population. The WT CSCs (Lin^-/ $Epcam^+$/α6-$integrin^+$/ $CD34^+$) and the non-CSCs (Lin^-/ $Epcam^+$/α6-$integrin^+$/ $CD34^-$) were FACS sorted and the RNA was isolated followed by cDNA preparation and real time PCR. Our results showed that there is a significant decrease in Sfrp1 expression in WT CSCs as compared to WT non-CSC population (Figure 6.4C). Taken together, our results showed progressive decrease in Sfrp1 mRNA levels with TPA treatment and WT CSCs have low Sfrp1 levels as compared to WT non-CSCs.

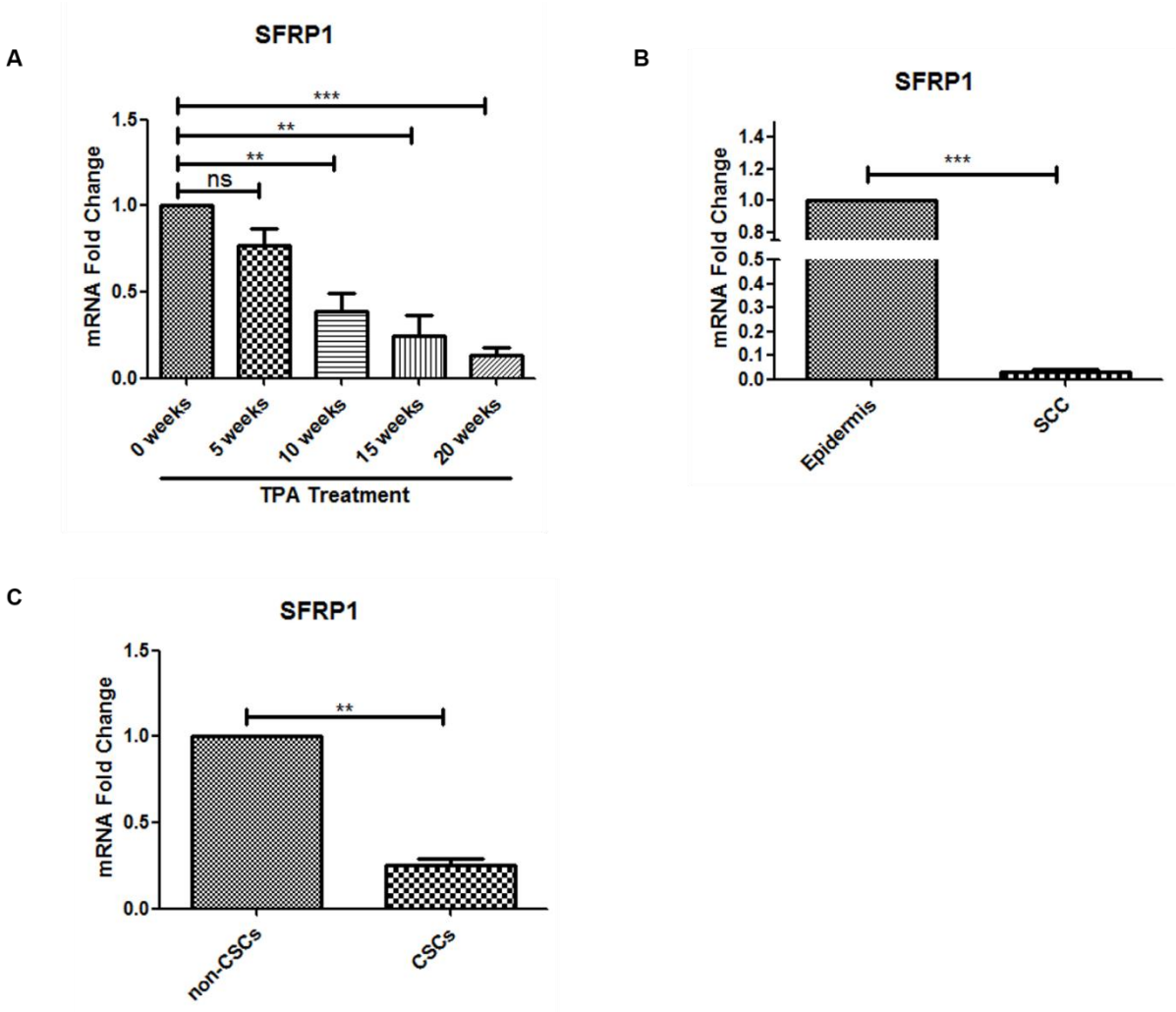

Figure 6.4: Sfrp1 expression level changes at different time points during DMBA/TPA treatment [459]

A) *Graph representing mRNA expression levels of Sfrp1 in WT mice epidermis at 5weeks, 10weeks, 15weeks and 20weeks during DMBA/TPA treatment.* ***B)*** *Graph representing Sfrp1mRNA expression levels in WT epidermis as compared to WT SCC.* ***C)*** *Graph representing Sfrp1 mRNA expression levels in CSCs Vs non-CSCs in WT SCC. (*Data are presented as mean ± SEM and were analyzed by student's t-test. n=3 mice/ genotype. ** = p<0.01, ***=P<0.001)

6.2.5 Altered growth factor signalling and enhanced stemness and EMT in Sfrp1$^{-/-}$ CSCs:

CSCs isolated from the Sfrp1$^{-/-}$ tumors showed higher tumorigenic potential and enhanced TPC frequency as compared to WT CSCs. To investigate the molecular mechanism involved in the enhanced tumorigenic potential of Sfrp1$^{-/-}$ CSCs, we performed expression profiling on both the CSCs of Sfrp1$^{-/-}$ and WT tumors. CSCs from WT and Sfrp1$^{-/-}$ tumors were FACS sorted using skin CSCs markers (Lin^{-}/ Epcam^{+}/α6-integrin^{+}/ CD34^{+}) followed by RNA isolation. Further, RNA was quantified using bio-analyzer to check its integrity and microarray was performed to understand the complete gene expression profile of the CSCs. The gene expression profile data showed that, growth factor receptors (Ghr, Pdgfra, Tgfbr3 and Eps8) and their downstream signalling molecules (Akt3 and Mapk3/Erk1), which are associated with tumor aggressiveness, metastatic potential and proliferation were highly upregulated in the Sfrp1$^{-/-}$ CSCs population as compared to WT CSCs. Further, the genes involved in the cell to ECM (Extracellular matrix) interaction such as Spp1(161.7), Vcam1 (3.89) and Fn1(92.5), which are known to promote tumor invasion and metastasis were highly upregulated in Sfrp1$^{-/-}$ CSCs as compared to WT CSCs (Figure 6.5 A-E). Importantly, EMT (Epithelial to Mesenchymal Transition) markers such as the Twist1 (2.33), Twist2 (2.04), Vimentin (45.85) and Zeb1 (2.07) showed increased expression in the Sfrp1$^{-/-}$CSCs, while E-cadherin (-19.31), epithelial marker was highly downregulated within these cells as compared to WT CSCs. Further, the mesenchymal marker N-Cadherin is highly upregulated in Sfrp1$^{-/-}$CSCs as compared to WT CSCs (Figure 6.5 F-G).

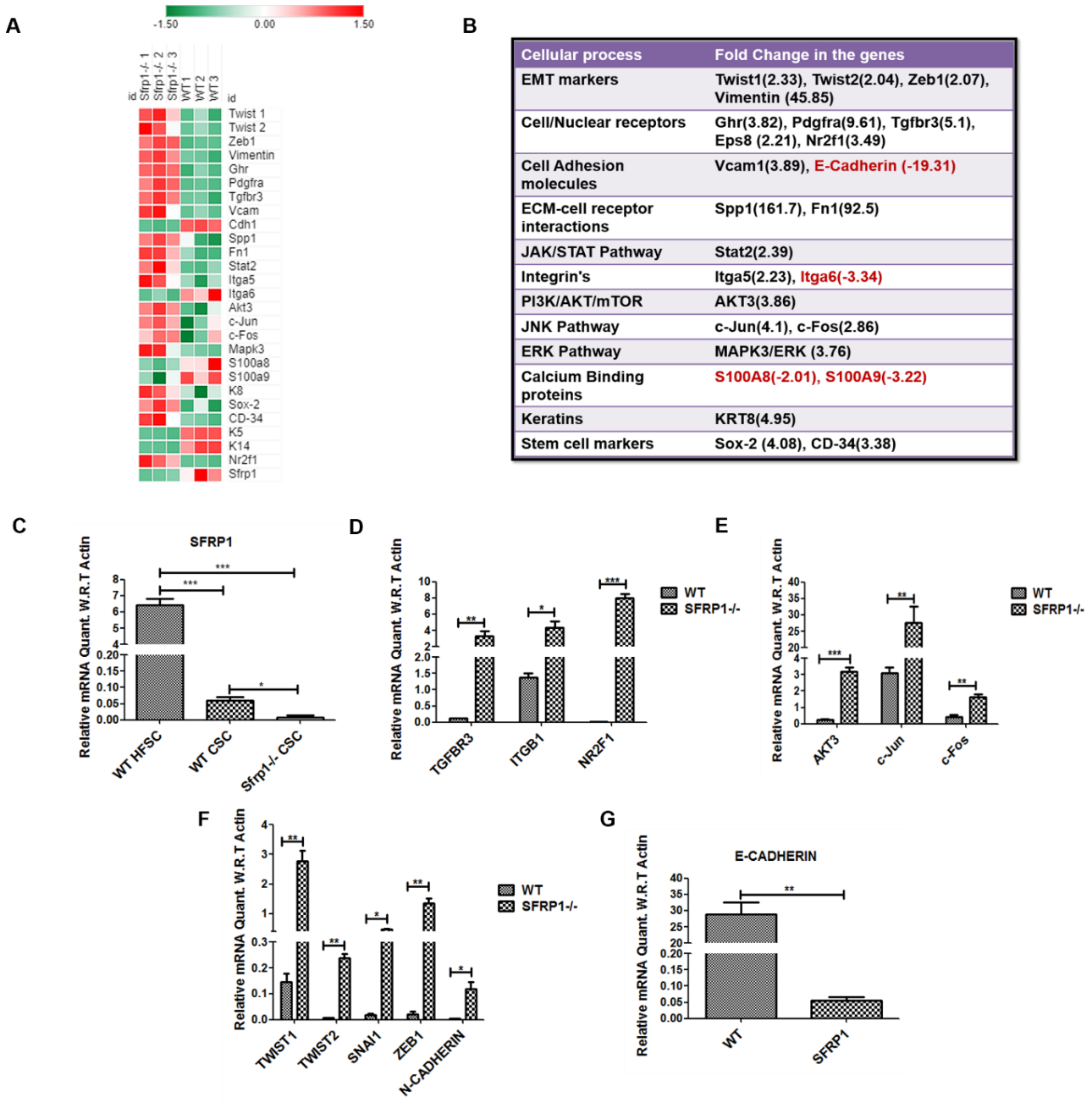

Cellular process	Fold Change in the genes
EMT markers	Twist1(2.33), Twist2(2.04), Zeb1(2.07), Vimentin (45.85)
Cell/Nuclear receptors	Ghr(3.82), Pdgfra(9.61), Tgfbr3(5.1), Eps8 (2.21), Nr2f1(3.49)
Cell Adhesion molecules	Vcam1(3.89), E-Cadherin (-19.31)
ECM-cell receptor interactions	Spp1(161.7), Fn1(92.5)
JAK/STAT Pathway	Stat2(2.39)
Integrin's	Itga5(2.23), Itga6(-3.34)
PI3K/AKT/mTOR	AKT3(3.86)
JNK Pathway	c-Jun(4.1), c-Fos(2.86)
ERK Pathway	MAPK3/ERK (3.76)
Calcium Binding proteins	S100A8(-2.01), S100A9(-3.22)
Keratins	KRT8(4.95)
Stem cell markers	Sox-2 (4.08), CD-34(3.38)

Figure 6.5: Altered signalling in *Sfrp1*$^{-/-}$ CSCs as compared to WT CSCs [459]

A) *Heat map of the significantly deregulated genes between the WT CSCs and Sfrp1*$^{-/-}$ *CSCs.* ***B)*** *table representing expression profile of various deregulated genes in Sfrp1*$^{-/-}$ *CSCs as compared to WT CSCs.* ***C)*** *Graph representing the mRNA expression levels of the Sfrp1 in WT HFSCs, WT CSCs and Sfrp1*$^{-/-}$ *CSCs.* ***D & E)*** *Graph representing the expression levels changes in cell surface receptors and their downstream signalling molecules in WT CSCs*

and Sfrp1$^{-/-}$ CSCs. ***F & G)*** *Graph representing the expression levels changes in EMT genes in WT CSCs and Sfrp1$^{-/-}$ CSCs. (HFSC= Hair follicle stem cells, CSCs= Cancer stem cells, EMT= epithelial to mesenchymal transition,. The mRNA expression levels were normalized to the expression of β-Actin. Data are analyzed by student's t-test and presented as mean ± SEM. *=P<0.05, ** = P<0.01, *** = P<0.001).*

The expression of stem cell marker, Sox2, involved in regulating tumor initiation and CSC regulation, was upregulated by 4 fold in the CSCs of Sfrp1$^{-/-}$ mice. Further, the Keratin 8 (K8) expression, a marker for highly invasive and undifferentiated skin tumor, was also higher by 4-5 fold in Sfrp1$^{-/-}$CSCs. Importantly all the data was validated by performing real time PCR where the results are in congruence with microarray data. Moreover, this data was also validated by performing IFA Vimentin and Sox-2 with in the tumor sections of WT and Sfrp1$^{-/-}$ tumors (Figure 6.6). Overall, the data suggests the loss of Sfrp1 leads to enhanced stemness and EMT signatures within CSCs through altered signalling.

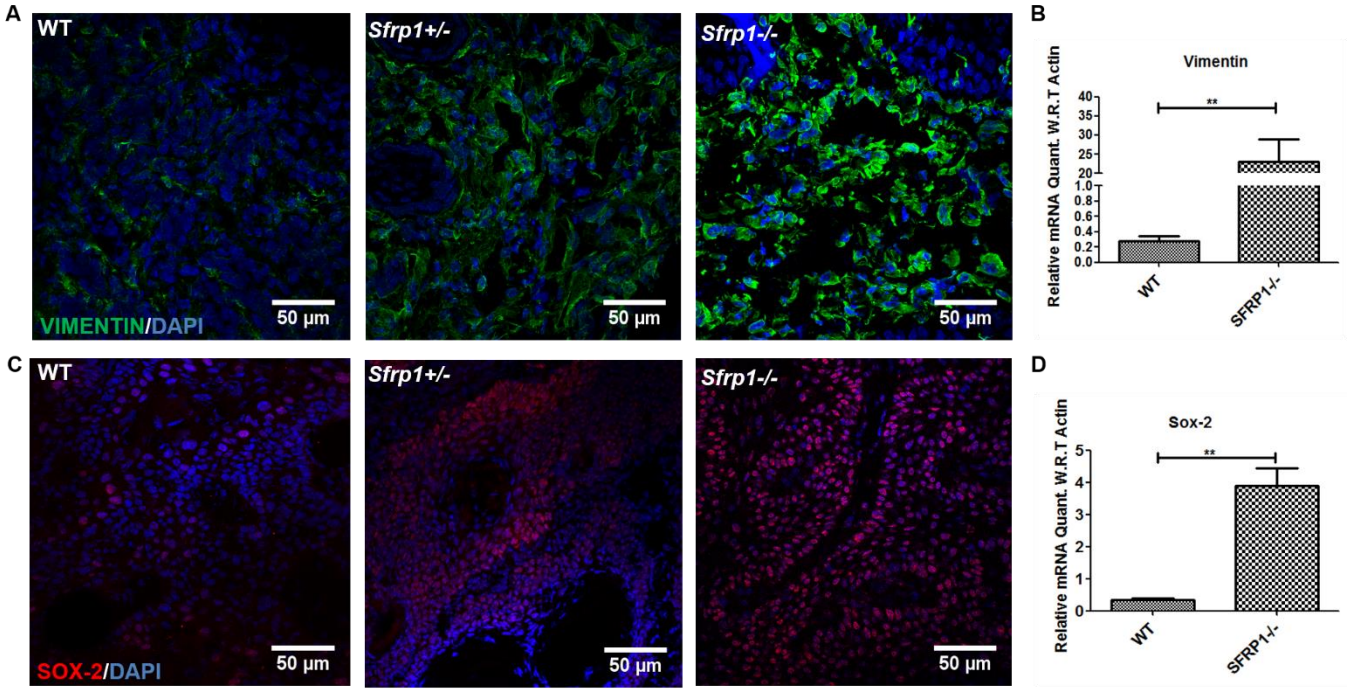

Figure 6.6: Enhanced EMT and stemness in *Sfrp1*$^{-/-}$ SCC [459]

A & C) *Immunofluorescence assay for Vimentin and Sox-2 in WT SCC, Sfrp1$^{+/-}$ SCC and Sfrp1$^{-/-}$ SCC respectively.* ***B & D)*** *Graphical representation of mRNA expression level changes in Vimentin and Sox2 in WT CSCs and Sfrp1$^{-/-}$ CSCs respectively. (Data are analyzed by student's t-test and presented as mean ± SEM. n=3/genotype Scale bar: 50µm, ** = P<0.01).*

6.2.6 Sfrp1 and Sox-2 show inverse correlation in human skin SCC

Sfrp1$^{-/-}$ CSCs showed enhanced tumorigenic potential, enhanced TPC frequency and their expression profiling revealed higher expression of EMT markers and markers associated with invasive and undifferentiated nature of CSCs. Most importantly, absence of Sfrp1 resulted in upregulation of stem cell marker, Sox-2 which is not only associated with tumor initiation but also involved in CSC regulation. Hence, we further went on to check whether loss of Sfrp1 affects stemness even in human skin cancers as Sfrp1 was reported to be lost in human skin cancers due to promoter hypermethylation. We have isolated RNA from A3886 (human cutaneous SCC cell line) and HaCaT (spontaneously transformed human keratinocyte cells) followed by cDNA preparation and real time PCR. The results showed a decrease in the expression of Sfrp1 and increase in the expression of Sox-2 in A3886 as compared to HaCaT (Figure 6.7A). We further confirmed the results at protein level by performing western blotting. Most importantly, we have performed reversion studies to check whether addition of Sfrp1 can decrease the levels of Sox-2 in A3886. We have treated A3886 cells with Sfrp1 containing media for 48 hours and western blotting for Sfrp1and Sox-2 was performed on the isolated protein to check the changes in the Sfrp1and Sox-2 protein levels in comparison with untreated cells. The Sox-2 protein levels were highly decreased in Sfrp1 treated A3886 cells as compared to untreated A3886 cells establishing an inverse correlation between Sfrp1 and Sox-2 within these cells (Figure 6.7B).

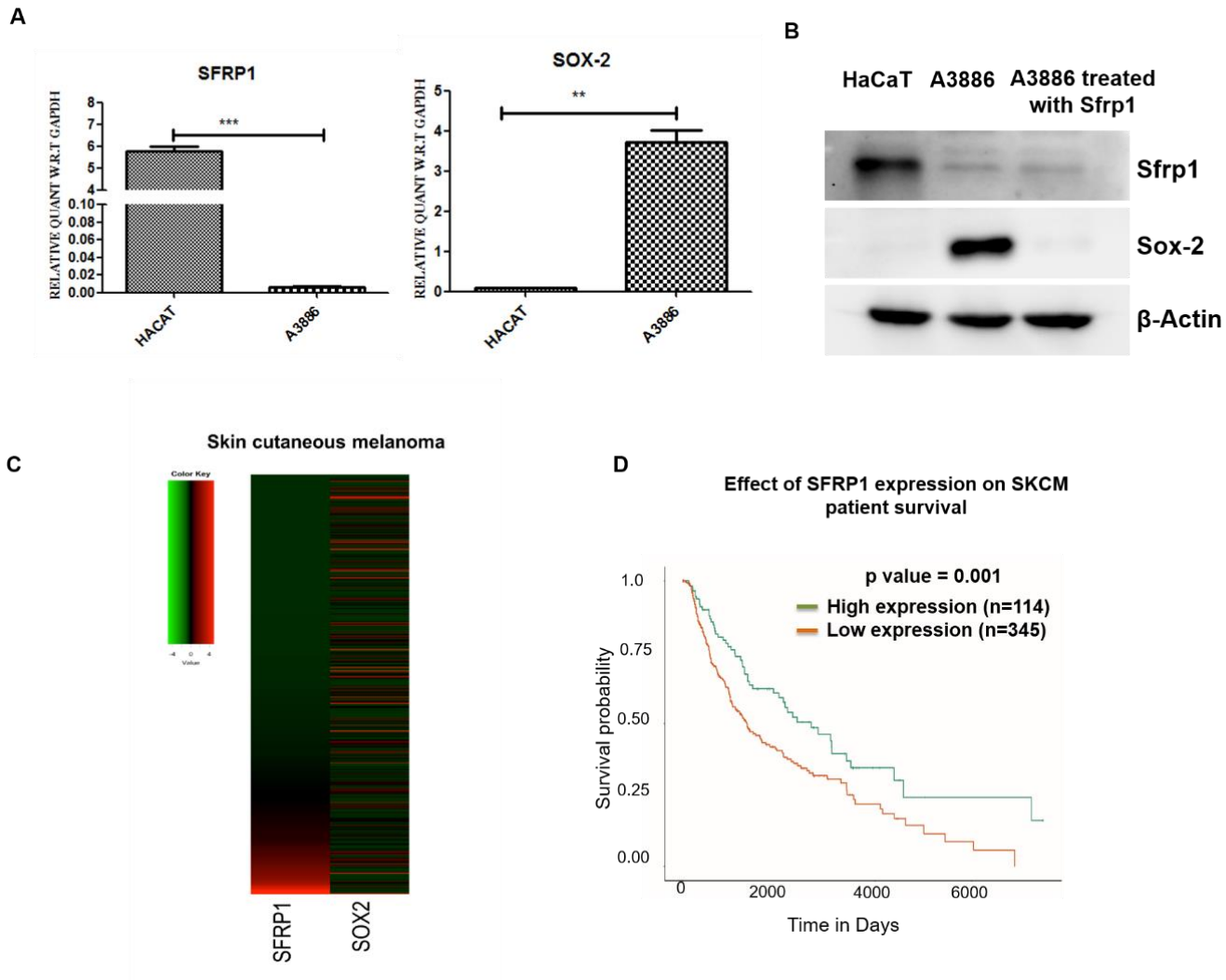

Figure 6.7: Inverse relation of Sfrp1 and Sox-2 in skin Cutaneous SCC [459]

A) *Graphical representation of Sfrp1 and Sox-2 expression levels in A3886 and HaCaT cell lines.* ***B)*** *Western blot for Sfrp1 and Sox-2 in HaCaT, A3886 and A3886 treated with SFRP1 containing media for 48hrs.* ***C)*** *Heat map of Sfrp1 and Sox-2 expression in tumor samples from TCGA data showed inverse correlation among SKCM. Patients were sorted from Sfrp1 low to high expression (Z< -1.5 is down-regulation and Z> 1.5 is up-regulation).* ***D)*** *Survival analysis of TCGA dataset in patients with high and low expression of Sfrp1 (Z< -1.5 is down-regulation and Z> 1.5 is up-regulation) in SKCM (n=114 high and n=345 low). (SKCM: Skin cutaneous melanoma, TCGA: The cancer genome atlas, P values were generated using chi-squared analysis and the survival probability was plotted using Kaplan-Meier analysis)*

Moreover, to further validate this inverse correlation between Sfrp1 and Sox-2 in large cohort of tumor samples, we have performed in silico analysis on the SKCM (skin cutaneous melanoma) samples from TCGA data base. The calculations of Z-scores and generation of heat map was performed as described in the materials and methods section. Though the log odds ratio was found to be 0.05, the trend of Sfrp1 and Sox-2 inverse correlation was clearly observed. Furthermore, we have also checked for the overall survival of the patients with high and low levels of Sfrp1. Kaplan Meier analysis of TCGA data of SKCM patients showed poor overall survival in the patients having low expression of Sfrp1 (n=345) as compared to patients having high expression of Sfrp1 (n=114) with a p-value of 0.001 (Figure 6.7 C-D). Hence, our results suggest that loss of Sfrp1 results in increased stemness (Sox-2) even in human skin cancers and Sfrp1 and Sox-2 show an inverse co-relation with in skin cancer.

6.2.7 Inverse correlation of Sfrp1 and Sox-2 in human OSCC

Sfrp1 and Sox-2 has shown inverse co-relation in both mouse skin SCC and human skin SCC. Importantly, as epidermis share certain similarities with oral epithelium in tissue architecture and in tumor progression, we have further extended our studies to oral cancer to understand if a similar correlation exists between Sfrp1 and Sox-2 even in oral squamous cell carcinoma (OSCC). The advanced stage treatment naive OSCC samples (Indian origin) samples were used in this study to avoid any changes in the expression levels of the Sfrp1 and Sox-2 due to treatment and their adjacent cut margins were used as controls. The OSCC samples and their adjacent cut margins were embedded in paraffin after processing them and 5-7μm sections were cut using microtome. The tumor and adjacent cut margin sections were used to perform immunohistochemistry (IHC) for Sox-2, Sfrp1 and Vimentin markers. The results showed that the protein levels of Sfrp1 were lower and that of Sox-2 were higher in tumor samples as compared to the adjacent cut margins. Further, the expression of Vimentin

(Mesenchymal marker) was higher in tumor samples as compared to the adjacent cut margins. The percentage and intensity of the staining was calculated for Sfrp1, Sox-2 and Vimentin and the results were plotted in the form of H-score (Figure 6.8 A-B). These results were also further validated at the mRNA expression level in tumour samples of OSCC (buccal mucosa) as compared to their normal counter parts (Figure 6.8 C). The results showed a decrease in expression of Sfrp1 and increase in Sox-2 expression in OSCC samples (buccal mucosa).

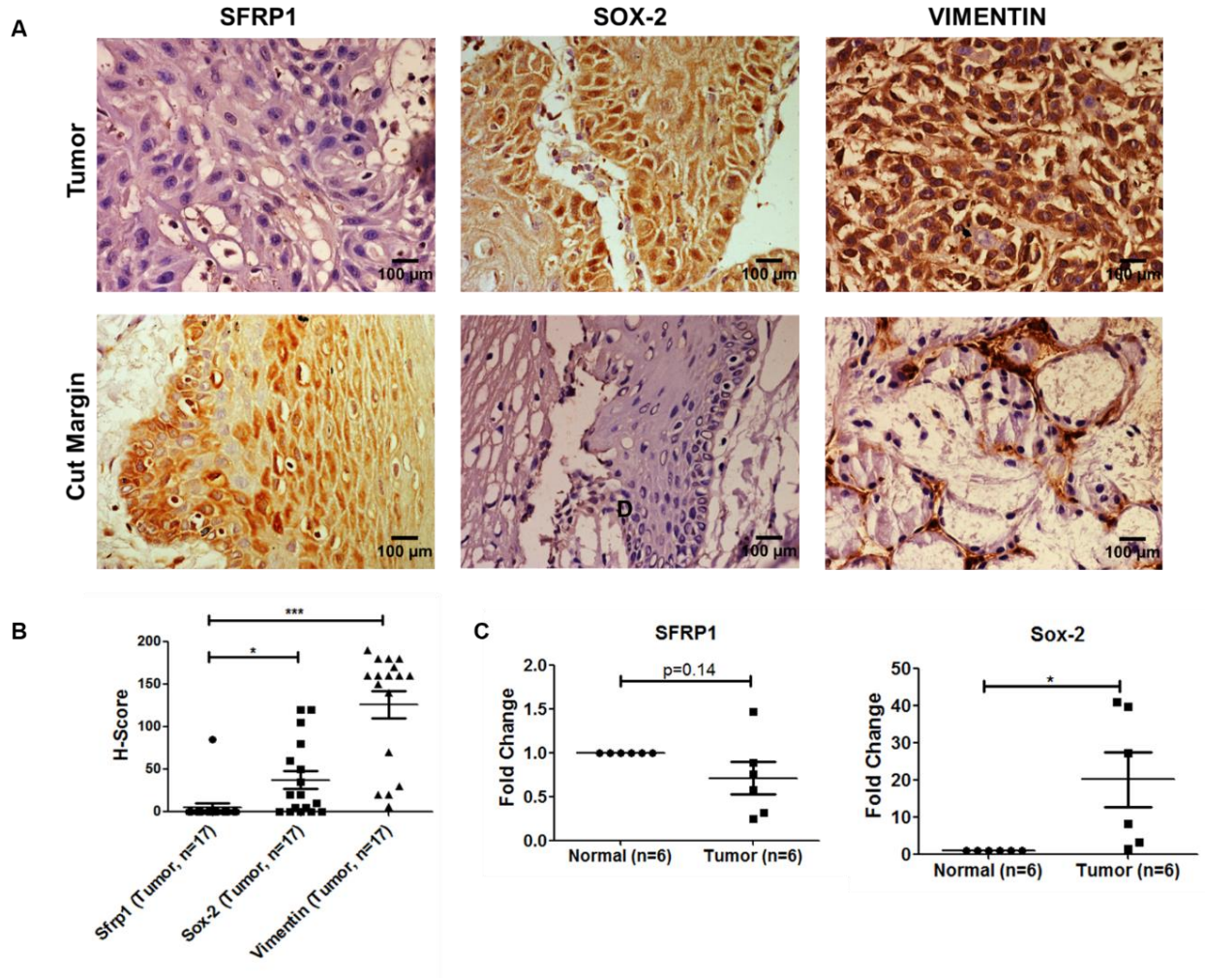

Figure 6.8: Sfrp1 and Sox-2 show inverse correlation in OSCC [459]

A) *IHC for Sfrp1, Sox-2 and Vimentin in HNSCC (Buccal Mucosa) samples along with their adjacent cut margins* ***B)*** *Graph representing H-score for Sfrp1, Sox-2 and Vimentin within*

the tumor samples ***C)*** *Graphical representation of Sfrp1 and Sox-2 expression levels in human HNSCC (buccal mucosa) samples as compared to normal buccal mucosa (n=6). (HNSCC=Head and neck squamous cell carcinoma, EMT=Epithelial to mesenchymal transition, IHC= Immuno-histochemistry. Data are analyzed by student's t-test and presented as mean ± SEM. Scale bar: 100μm, * = P<0.05, ** = p<0.01, *** = p<0.001).*

Further, we have also performed *in silico* analysis on the HNSCC samples from TCGA data base, to validate the inverse relation between Sfrp1 and Sox-2 in large cohort of tumor samples. The expression of Sfrp1 showed a significant decrease in HNSCC tumor samples (n=521), as compared to the normal controls (n=43) (Figure 6.9 A). Further, we went on to check whether this decrease in Sfrp1 is stage dependant. The results showed that the Sfrp1 levels indeed decrease in a stage dependent manner (n=27, 71, 81, 267 in stage-I, stage-II, stage-III and stage-IV respectively) (Figure 6.9B) Further, to determine the inverse relation of Sfrp1 and Sox-2 in HNSCC tumors their expression was first analysed within these tumors. Later the Z-scores were calculated for Sfrp1 and Sox-2 in the tumor samples from normalized log2 transformed counts. Sfrp1 Z-scores were sorted from low to high expression and the expression of Sox-2 was determined in these samples. Further, we calculated the Log odds ratio (-1.9), which suggested a negative correlation between Sfrp1 and Sox-2 in HNSCC (Figure 6.9 C). Further, Kaplan Meier analysis of TCGA data of HNSCC patients showed poor overall survival in the patients having low expression of *Sfrp1* (n=390) as compared to patients having high expression of *Sfrp1* (n=129) with p-values of 0.023 (Figure 6.9 D). Taken together, our results suggest that Sfrp1 and Sox-2 show an inverse co-relation with in HNSCC samples.

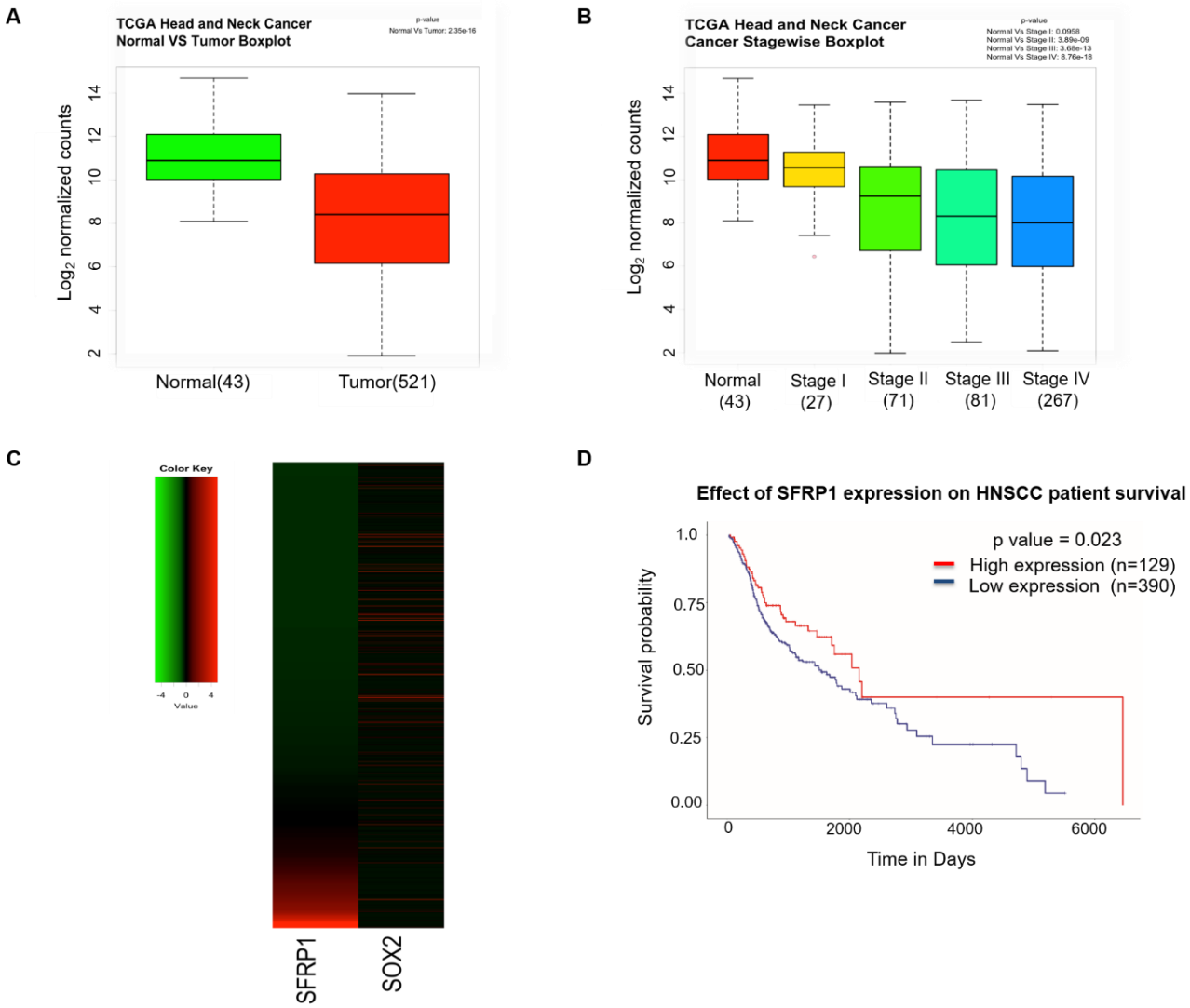

Figure 6.9: Sfrp1 and Sox-2 show inverse correlation in HNSCC (TCGA data) [459]

A) *Sfrp1 mRNA expression in non-tumor (normal) and tumor HNSCC samples from TCGA data* ***B)*** *Sfrp1 mRNA expression in normal, stage-I, stage-II, stage-III and stage-IV tumor samples respectively* ***C)*** *Heat map of Sfrp1 and Sox-2 expression in tumor samples showed inverse correlation. Patients were sorted from Sfrp1 low to high expression (Z< -1.5 is down-regulation and Z> 1.5 is up-regulation)* ***D)*** *Survival analysis of TCGA dataset in patients with high (n=129) and low (n=390) expression of Sfrp1 (Z< -1.5 is down-regulation and Z> 1.5 is up-regulation) in HNSCC patients. (TCGA: The cancer genome atlas, HNSCC: Head*

& neck squamous cell carcinoma, P values were generated using chi-squared analysis and the survival probability was plotted using Kaplan-Meier analysis).

6.2.8 Sfrp1 and Sox-2 show inverse correlation in human breast cancer and pancreatic adenocarcinoma

Epidermis and breast epithelia were reported to share certain similarities in tissue architecture and in tumor progression. Hence, to further validate the inverse correlation between Sfrp1 and Sox-2 in breast cancer, we have checked their expression levels in breast cancer samples (Indian origin) along with their respective controls. Briefly, cDNA was prepared from RNA and quantitative real time PCR was per formed to check the levels of Sfrp1 and Sox-2 within these samples. Our results showed significant decrease in the expression of Sfrp1 and increase in the expression of Sox-2 in breast tumor samples as compared to the controls establishing an inverse correlation between Sfrp1 and Sox-2 even in breast tumor samples (Figure 6.10 A). Further, we have also assessed the levels of Sfrp1 and Sox-2 in breast cancer cell lines such as MDA-MB-231 (triple negative breast cancer cell line) and control MCF-10A. The expression levels of Sfrp1 were highly reduced, whereas Sox-2 was increased in MDA-MB-231 as compared to MCF10A (Figure 6.10 B). Further, at a larger cohort we have also analyzed Sfrp1 and Sox-2 expression in TCGA provisional data in breast invasive carcinoma (n=1105) and have also calculated the Z-scores. Sfrp1 and Sox-2 showed a negative correlation with log odds ratio of -0.737 within breast invasive carcinoma. Additionally, the overall survival was plotted using Kaplan Meier analysis of the TCGA Data of breast invasive carcinoma patients. The data showed poor overall survival in the patients having low expression of Sfrp1 (n=808) as compared to the patients having high expression of Sfrp1 (n=273) with a p-value of 0.011 (Figure 6.11 A-B).

Moreover, we have also checked the expression of Sfrp1 and Sox-2 in other epithelial cancers such as pancreatic adenocarcinoma (PAAD) (n=186). Z-scores were calculated in PAAD, and found to have a negative correlation with log odds ratio of -3. Further, Kaplan Meier analysis of TCGA data of PAAD patients showed poor overall survival in the patients having low expression of Sfrp1 (n=132) as compared to patients having high expression of Sfrp1 (n=45) with a p-value of 0.025 (Figure 6.11 C-D). Altogether, these data demonstrate an inverse correlation between Sfrp1 and Sox-2 expression in breast cancer and pancreatic cancer samples.

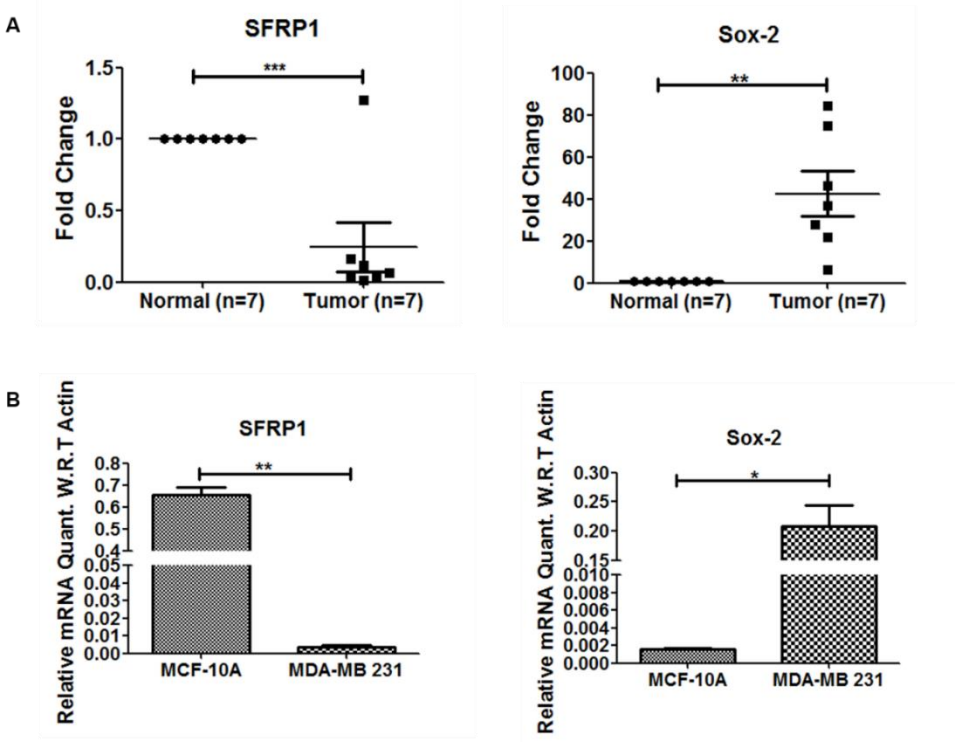

Figure 6.10: Sfrp1 and Sox-2 show inverse correlation in breast cancer [459]

A) *Graphical representation of Sfrp1 and Sox-2 expression levels in breast tumor samples as compared to normal breast tissue.* ***B)*** *Graphical representation of Sfrp1 and Sox-2 expression level in MDA-MB-231 cell line as compared to MCF-10A. (Data are analyzed by student's t-test and presented as mean ± SEM. * = P<0.05, ** = p<0.01, *** = p<0.001).*

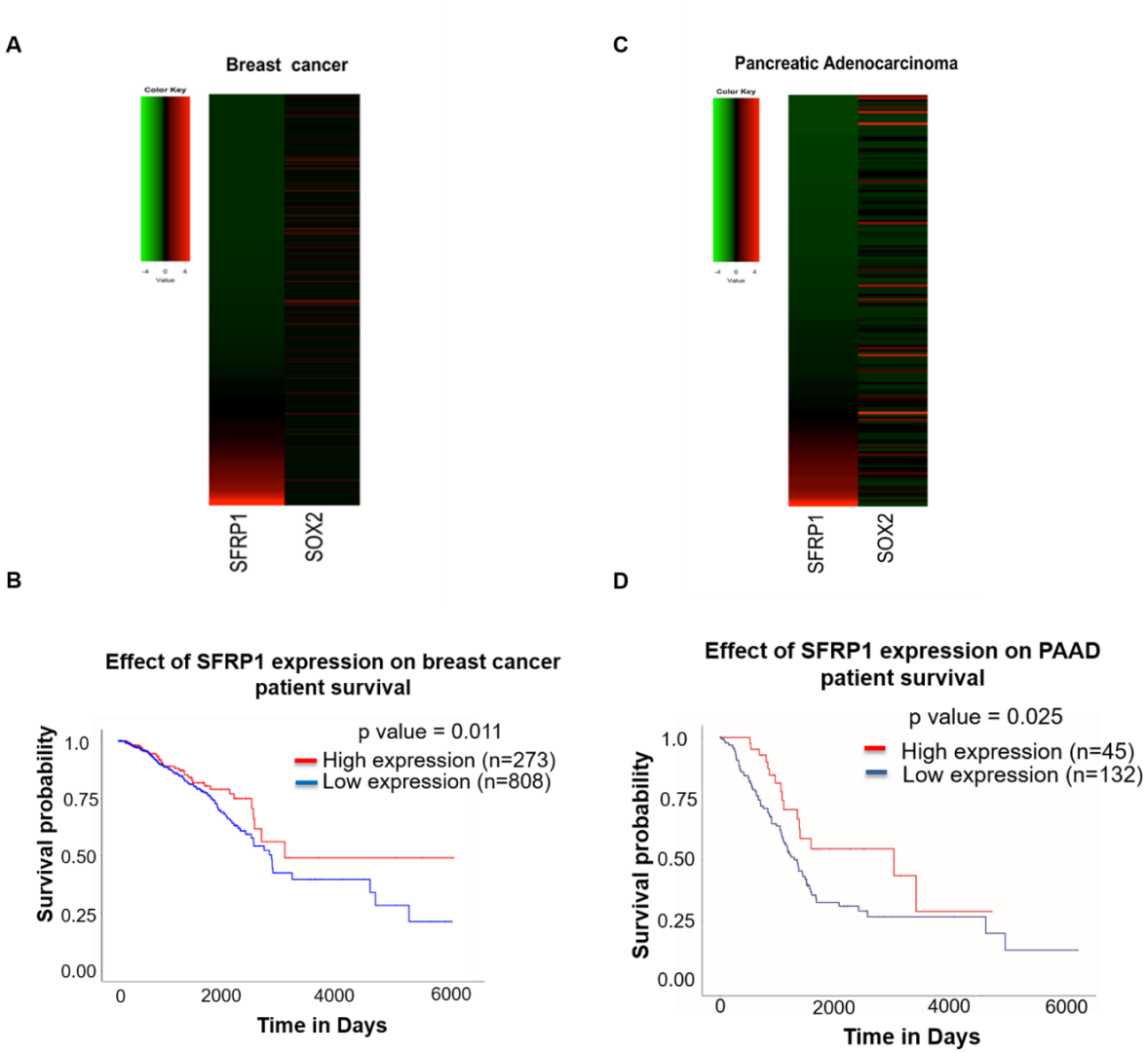

Figure 6.11: Inverse correlation of Sfrp1 and Sox-2 in breast and pancreatic cancers

A & C) *Heat map of Sfrp1 and Sox-2 expression in tumor samples showed inverse correlation among breast and PAAD. Patients were sorted from Sfrp1 low to high expression (Z< -1.5 is down-regulation and Z> 1.5 is up-regulation) in breast and PAAD respectively. Z scores were calculated as described in materials and methods.* ***B & D)*** *Survival analysis of TCGA dataset in patients with high and low expression of Sfrp1 (Z< -1.5 is down-regulation and Z> 1.5 is up-regulation) in breast cancer (n=273 high and n=808 low) and PAAD patients (n=45 high and n=132 low). (PAAD: Pancreatic adenocarcinoma, TCGA: The cancer genome atlas, P values were generated using chi-squared analysis and the survival probability was plotted using Kaplan-Meier analysis.*

6.3 Graphical abstract for Sfrp1 in tumor initiation and CSC regulation

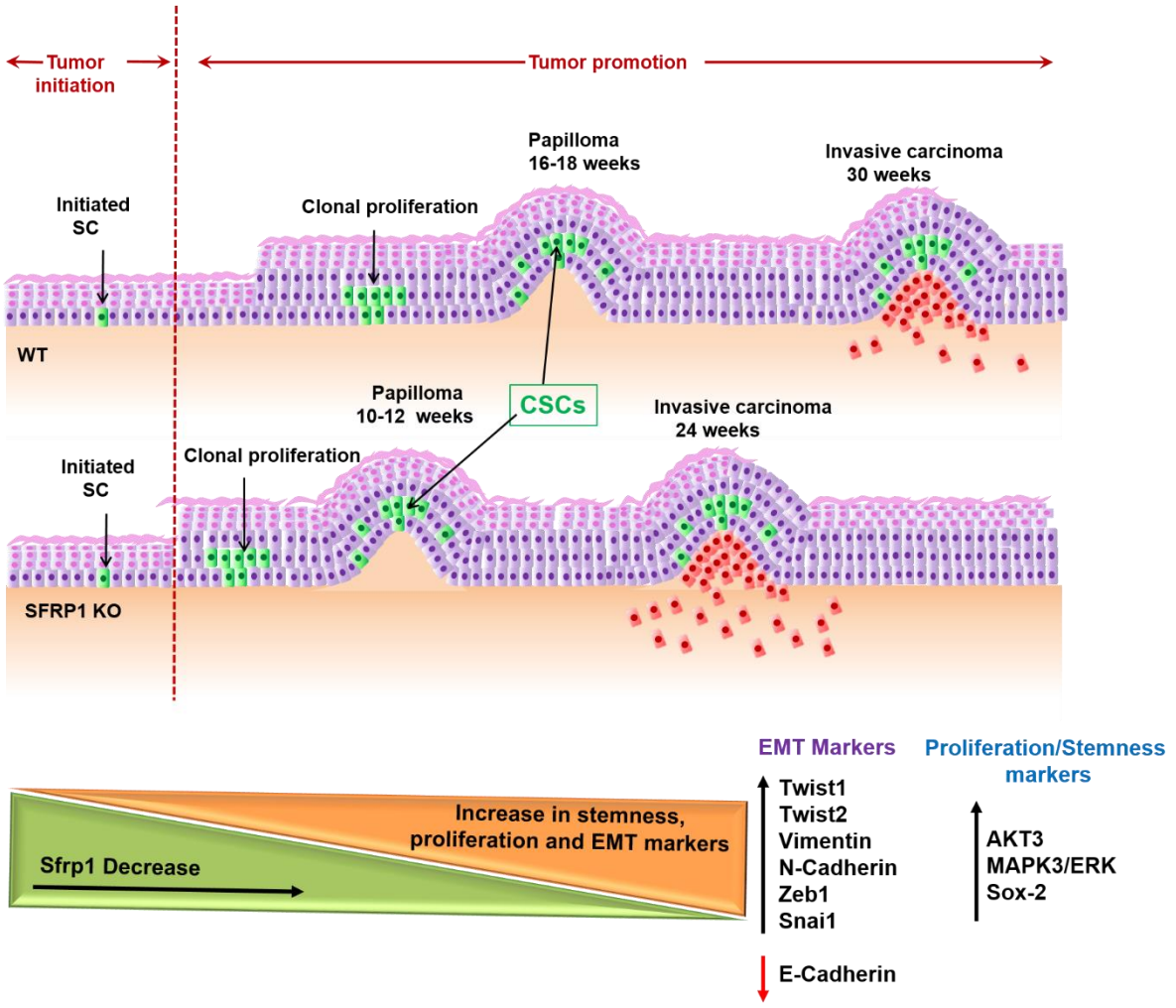

Figure 6.12: Diagrammatic representation of accelerated skin tumor initiation and CSC regulation due to loss of Sfrp1 [435]

Diagrammatic illustration of time points of papilloma and SCC formation in WT and Sfrp1$^{-/-}$ mice skin upon DMBA and TPA treatment. Induced skin carcinogenesis showed early tumor formation in Sfrp1$^{-/-}$ mice (10-12 weeks) as compared to WT mice (16-18 weeks). As Sfrp1 decreases there is an increase in stemness (Sox-2), proliferation and EMT markers in Sfrp1$^{-/-}$ CSCs. (SCC=Squamous cell carcinoma, DMBA=7, 12-Dimethylbenz[a]anthracene, TPA=12-O-tetradecanoyl phorbol-13-acetate, SC= Stem cell, EMT= Epithelial to mesenchymal transition)

6.4 Discussion

Sfrp1, a natural Wnt inhibitor, is lost in multiple human cancers such as breast cancer [400, 461], hepatocellular carcinoma [462], oesophageal squamous cell carcinoma [463], oral squamous cell carcinoma [433], cutaneous squamous cell carcinoma[464] etc. either due to promoter hypermethylation or loss of chromosomal fragment in which Sfrp1gene is located. Apart from these two mechanisms, recent reports have shown that micro RNAs (miRNA) such as miR-1301-3p and miRNA-27a-3p target Sfrp1 thereby promoting expansion and epithelial to mesenchymal transition (EMT) of CSCs [456, 465]. Though SFRP1 was reported to be lost in multiple epithelial cancers its role in skin tumor initiation and CSC regulation is still obscure.

To understand the role of Sfrp1in skin tumor initiation and CSC regulation, here we have used Sfrp1 genetic knockout mice [356]. Sfrp1 knockout in mice does not generate spontaneous tumors even after 1-2 years of age. Hence, two step skin carcinogenesis model (DMBA/TPA) was used to generate tumors as it is an ideal model to study the tumor initiation, promotion and progression [284, 293]. Application of DMBA results in a point mutation in the 61st codon of H-ras gene where CAA is mutated to CTA, resulting in amino acid change from glutamine (Q) to leucine (L) [287, 466]. TPA is a small molecule drug which activates the signal transduction enzyme protein kinase C (PKC), thereby activating proliferation of the cells resulting in clonal expansion of mutated cells. Our study has shown that loss of Sfrp1 led to increased sensitivity to chemical induced carcinogenesis there by resulting in early tumor initiation within these mice. This could be due to the cumulative effect of both Sfrp1loss (a tumor suppressor) and DMBA/TPA induced effect. Hence, it suggests that Sfrp1might be involved in regulating the genes that are essential for tumor initiation.

Though, DMBA/TPA treatment mostly generates papillomas, it has been clearly reported that some of the papillomas progress into invasive SCC [326, 362, 363]. Therefore, we have collected and characterised SCCs from both the WT and Sfrp1$^{-/-}$ mice. The characterization of Sfrp1$^{-/-}$ SCCs predominantly showed SCCs with mixed phenotype (tumor containing both epithelial cells and mesenchymal cells) and a few SCCs with mesenchymal phenotype. However, in the case of WT mice, SCCs mostly showed well differentiated epithelial phenotype, with a few number of SCCs with mixed phenotype. Drissens et al. in 2012, by performing clonal analysis studies of squamous skin tumours have shown that, only the epidermal SCs with mutations give rise to tumors, whereas the progenitor cells with mutations are eventually lost through terminal differentiation [49].The skin comprises of both IFE stem cells and HFSCs. Hence, the tumors could arise from both IFE stem cells as well as HFSCs. Latil et al, in 2017, have shown that, tumors arising from HFSCs mostly show mixed phenotype with a few tumors showing mesenchymal phenotype. Further the tumors arising from IFE stem cells show well differentiated epithelial tumor phenotype [467]. This indicates a possibility that, the tumors of Sfrp1$^{-/-}$ mice may arise primarily from HFSCs as most of the Sfrp1$^{-/-}$ tumors are of mixed phenotype and a few Sfrp1$^{-/-}$ tumors are with mesenchymal phenotype. However, the WT mice tumors may mostly arise from IFE stem cells rather than HFSCs, as most of the tumors showed well differentiated epithelial phenotype. Moreover, high expression of Sfrp1 in WT HFSCs might also prevent tumor formation from HFSCs within these mice. Further, Keratin 8 (K8) expression, an important marker for tumor progression and epithelial to mesenchymal transition of SCC was checked [468]. IFA for K8 have shown that, Sfrp1$^{-/-}$ SCCs have higher K8 expression as compared to WT SCCs. Hence, Sfrp1 might be regulating the expression of K8 involved in the formation of more invasive and undifferentiated skin tumors.

Recent reports have shown that micro RNA, miR-1301-3p is involved in the expansion of CSCs by targeting Sfrp1in prostate cancer [456]. Further, miRNA-27a-3p promotes EMT in OSCC stem cells by targeting Sfrp1 [465]. This clearly shows that Sfrp1 is involved in cancer stem cell regulation of different cancers. Therefore, we have studied the role of Sfrp1 in regulating CSCs within skin SCC. Our results have shown that Sfrp1 loss does not have any effect on the percentage of the cancer stem cells population in mouse skin SCC. Further, we went ahead to check whether Sfrp1 affects the functional properties of the CSCs in skin SCC. In this front, we have performed *in vivo* tumorigenesis study using FACS sorted WT and $Sfrp1^{-/-}$ CSCs, which showed that $Sfrp1^{-/-}$ CSCs have higher tumorigenic potential as compared to WT CSCs. Importantly, in order to determine the FACS sorted cells are indeed CSCs we have performed *in vivo* serial transplantation assay which is a gold standard assay to determine the presence of CSCs [460]. Our results showed that FACS sorted cells are indeed CSCs, and CSCs from the $Sfrp1^{-/-}$ secondary tumors are more aggressive as compared to CSCs from $Sfrp1^{-/-}$ primary tumors and the percentage of the CSCs in the secondary tumors are higher as compared to the primary tumors.

Apart from *in vivo* serial transplantation assay, limiting dilution assay is an important assay to determine the presence of CSCs [364, 469]. Therefore, we have performed limiting dilution assay using cell numbers as low as 10000, 5000 and 1000 CSCs from WT SCCs and $Sfrp1^{-/-}$ SCCs. Our results have shown that both 10,000 and 5000 $Sfrp1^{-/-}$ CSCs are capable of forming tumors. However, only 10,000 WT CSCs were able to form tumors whereas 5000 WT CSCs were unable to form tumors. Both WT and $Sfrp1^{-/-}$ CSCs were unable to form tumors with 1000 cells. The estimated TPC frequency of $Sfrp1^{-/-}$ CSCs was calculated to be in the ratio of 1/8442 whereas the estimated TPC efficiency of WT CSCs was in the ratio of 1/34761. This doubly clarifies that FACS sorted cells are indeed CSCs and $Sfrp1^{-/-}$ CSCs have higher TPC frequency as compared to WT CSCs. Taken together, the data clearly

indicated that Sfrp1 might be involved in regulating the genes that are essential for tumor initiation and aggressiveness of the CSCs.

We performed the gene expression profile of Sfrp1$^{-/-}$ CSCs and WT CSCs to understand the molecular changes that are involved in tumor aggressiveness in the absence of Sfrp1. Growth factor receptors (Ghr, Pdgfra, Fgfr and Tgfbr3) and their downstream signalling molecules (Akt3, Erk1/2 and Stat2/3) play an important role in proliferation, invasion and aggressiveness of different tumors. PDGFRα/β activity enhances expression of self-renewal and EMT markers thereby promoting cancer stem cell phenotype in sarcomas [470]. Recently, PDGFRα was also shown to induce CSC invasion and promotion of distant metastasis in advanced skin SCCs [471]. Further, human growth hormone (hGH) stimulates Erk1/2 pathway resulting in enhanced cell migration and invasion through increased Fibronectin 1(Fn1) and decreased E-cadherin in colorectal carcinoma [472]. Moreover, over expression of Akt3 enhances proliferation of the prostate cancer cells and endows CSC phenotype [473] and its downregulation significantly inhibits growth of spheroid cultures and xenografts in TNBC [474]. Further, Erk pathway plays a prominent role in the survival and maintaining the stem-like phenotype of Rhabdomyosarcoma cells [475]. Activation of Erk1/Erk2 in non-small cell-lung cancer [476] and breast cancer [477] is associated with tumor advancement and aggressiveness.

Our data has also showed an increase in the growth factor receptors in Sfrp1$^{-/-}$ CSCs, such as Ghr, Pdgfra, and Tgfbr3 and their downstream signalling molecules Akt3, Erk and Stat2 which are associated with CSC maintenance, tumor aggressiveness and metastatic potential. Additionally, genes involved in tumor cell migration such as Fn1 [472] and Vcam1 [478] are highly upregulated in Sfrp1$^{-/-}$ CSCs. Further, Akt and Erk signalling pathways are also reported to enhance EMT. Erk1/2 enhance EMT in lung adenocarcinoma by increasing the expression of Zeb1, which in turn down regulates E-cadherin and upregulates Fn1 [479].

Over expression of Akt increases Vimentin (mesenchymal marker) expression and decreases E-Cadherin expression in tongue SCC [480]. Therefore, we have also checked for the expression of EMT markers in skin SCC. The expression of EMT markers such as Twist1, Twist2, Zeb1 and Vimentin were increased and E-cadherin was decreased in Sfrp1$^{-/-}$ CSCs as compared to WT CSCs. Taken together, all these data suggest that altered expression of growth factor receptors and their downstream signalling molecules might be responsible for the higher tumorigenic potential of Sfrp1$^{-/-}$ CSCs.

In addition to growth factor receptors, we have also observed an increase in the expression of the Wnt7b (Non-canonical Wnt Ligand) in the Sfrp1$^{-/-}$ CSCs. Earlier reports have showed that, Sfrp1 binds and inhibits Wnt7b; therefore, knockout of Sfrp1 would enhance Wnt7b mediated non canonical signalling pathway. Moreover, Wnt7b was shown to activate Jnk, which in turn activates c-Jun [481]. Further c-Jun binds to the promoter region of Sox-2 thereby increasing Sox-2 expression, which is involved in tumor initiation, cancer stemness and aggressiveness [362, 473]. Therefore, we have checked the expression level of c-Jun and Sox-2 levels in Sfrp1$^{-/-}$ CSCs, which showed an increase in c-Jun and Sox-2 expression. Hence, this increased Sox-2 levels could be involved in the earlier tumor initiation and aggressiveness observed in Sfrp1$^{-/-}$ CSCs as compared to WT CSCs. Additionally, Akt was shown regulate nuclear translocation of Sox-2 in breast carcinoma thereby enhancing cancer stem cell properties [482] and also regulates the expression of Sox-2 in Glioblastoma stem like cells [483]. Mek/Erk pathway also regulates the expression of Sox-2 required for the self-renewal and maintenance of Glioblastoma SCs [483, 484]. As Sfrp1$^{-/-}$ CSCs show higher expression of Akt, Erk and Wnt7b an in depth study need to be carried out to decipher the molecular signalling pathway through which the expression of Sox-2 is being regulated in skin CSCs. Such a study would provide necessary information required to target the specific

signalling mechanism to inhibit Sox-2 expression thereby reducing the stemness and aggressiveness of skin CSCs.

Importantly, Sfrp1 was shown to be lost due to promoter hypermethylation in human cutaneous SCC [453, 464]. Moreover, Sox-2 which is dispensable for normal epidermal homeostasis was shown to be crucial for the tumor initiating cells (TIC) in cutaneous SCC [485]. However, whether Sfrp1has any role to play in Sox-2 expression in human cutaneous SCC is not known. Hence, we have extrapolated our data obtained from murine skin model i.e. the inverse relation of Sfrp1 and Sox-2 to human skin cancer. The expression levels of Sox-2 both at RNA and protein level were higher and Sfrp1 levels were lower in A3886 cell line as compared to HaCaT. Further, treating the A3886 cells with Sfrp1 containing media led to decrease in the Sox-2 levels establishing an inverse co-relation between Sfrp1 and Sox-2 even in human cutaneous SCC. This inverse correlation was further validated in larger cohort using the data from TCGA database of SKCM.

Interestingly, epithelial tissues such as epidermis, oral epithelium and breast epithelium have been reported to have similarities in tissue architecture and function as well as during tumor progression and metastasis. For instance, all three of them are stratified epithelia expressing characteristic basal layer keratin markers such as K5 and K14. Further, integrins such as α2β1, α3β1and α6β4 are expressed in the basal layer of all the three epithelia [486-488]. Optimum levels of Wnt and notch signalling are required for the maintenance and differentiation of skin, oral and breast epithelia [90, 489-492]. Significantly, Sfrp1 loss due to hypermethylation is reported in skin cutaneous SCC [464], breast cancer [400] and OSCC [433]. Further, Sox-2 promotes proliferation and metastasis in cutaneous SCC [485], OSCC [493] and TNBC [494]. As these epithelial tissues share several common features even in tumor progression and metastasis in addition to the tissue architecture and signalling, we sought to understand whether a similar kind of relation of Sfrp1 and Sox-2 exists even within

these cancers. Our results have shown that, Sfrp1 levels were lower and Sox-2 levels were higher in OSCC samples as compared to the adjacent cut margins establishing an inverse correlation of Sfrp1 and Sox-2 in OSCC samples. In addition we have also found a similar correlation both in breast tumor tissues and in breast cancer cell line (MDA-MB-231). Most importantly, we have verified the observed correlation in large cohort of samples by using TCGA data base, where we found the inverse correlation of Sfrp1 and Sox-2 in multiple epithelial cancers such as HNSCC, breast cancer and PAAD.

Taken together, we have shown that Sfrp1 plays an important role in skin tumor initiation and CSCs regulation. Importantly, the data obtained from the mouse models was extrapolated to human epithelial cancers where an inverse correlation between Sfrp1 and Sox-2 was observed. This study provides a compelling evidence for using murine epithelial models to uncover the molecular signalling in human epithelial cancers. Overall, future studies are warranted in understanding the in-depth molecular mechanism of Sfrp1 that is involved in CSC regulation with respect to tumor aggressiveness, proliferation and EMT regulation, which may pave way in the development of novel strategies in cancer treatment.

Table of Contents

Chapter 3: Aims and Objectives

Chapter 4: Materials and Methods

Chapter 5: Objective-I

Chapter 6: Objective-II

Chapter 7: Summary & Conclusion

7.1 Summary and Conclusion:

Mammalian adult tissues contain resident stem cells (SCs), which play an important role in the maintenance of tissue homeostasis and regeneration following injury, throughout the life of an organism. SCs are uniquely endowed with the ability to both self-renew and differentiate, such that they can replenish the SCs pool while continuing to give rise to differentiated cells that are essential for tissue function. The process of self-renewal and differentiation are carefully controlled as unchecked proliferation of SCs can lead to the development of tumors. Various developmental signalling pathways such as Wnt, Notch and Hedgehog pathways have been reported to govern the cyclic activity and differentiation of stem cells. Deregulation within these signalling cascades disrupts normal tissue homeostasis that leads to cancer development. Further, within the tumors there exists a unique population that has similar characteristics of tissue stem cells, which are involved in tumor maintenance and heterogeneity. These cells are named as cancer stem cells (CSCs) that are responsible for therapy resistance and tumor relapse after treatment. Though deregulated developmental signalling pathways were reported in maintaining CSCs in multiple cancers; however, a complete understanding of CSCs regulation seems be a distant reality.

In the first Part of the study, we have tried to understand the role of Sfrp1 in HFSCs maintenance and regulation. Here we found that Sfrp1 loss affected the initial formation of HFSCs i.e. decreased HFSCs pool was observed in both the $Sfrp1^{+/-}$ and $Sfrp1^{-/-}$ mice as compared to WT mice. However, the increased proliferation in $Sfrp1^{-/-}$ mice HFSCs restored the HFSCs pool by PD49. This increase in the $Sfrp1^{-/-}$HFSCs proliferation could be due to decrease in Runx1 and P21 levels and increase in Cyclin-D1 levels. Further, Sfrp1 knockout mice showed delay in wound re-epithelialization suggesting that Sfrp1 loss affects the HFSCs function. Importantly, decrease in the HFSCs markers such as Lgr5 and Axin2 was observed in $Sfrp1^{-/-}$ HFSCs as there was a decrease in the Wnt/β-catenin signalling. This decrease in

the Wnt/β-catenin signalling could be due to the activated Bmp signalling, which in turn inactivates Akt signalling thereby activating Gsk-3β that phosphorylates and inactivates β-catenin. In conclusion, our work demonstrates a new hierarchical level of regulation embedded within HFSCs that inhibits aberrant activation of Wnt signalling in the absence of Sfrp1, by regulating Akt activity through the expression of Bmp signalling agonists (Bmpr1a) and antagonists (Noggin).

In the second part of the study, we explored the role of Sfrp1 in tumor aggressiveness and CSCs regulation. Previous report from our lab has shown that Sfrp1 loss results in increased sensitivity to chemical induced carcinogenesis. However, the functional properties and molecular mechanism remained unexplored. Here, we have shown that $Sfrp1^{-/-}$ mice tumors were primarily of mixed/mesenchymal phenotype as compared to epithelial phenotype of WT tumors. Importantly, the FACS sorted cells are indeed CSCs by performing the serial transplantation assay (The gold standard assay) and limiting dilution assays. Further, the tumor propagating cell (TPC) frequency was also enhanced in $Sfrp1^{-/-}$ CSCs. This enhanced tumorigenicity and aggressiveness could be due to the increased levels of growth factor receptors in $Sfrp1^{-/-}$ CSCs, such as Ghr, Pdgfra, and Tgfbr3, and their downstream signalling molecules Akt3, Erk and Stat2, which are associated with CSC maintenance, tumor aggressiveness and metastatic potential. The expression of Sox-2 (stemness marker), involved in regulating tumor initiation and CSC regulation, was upregulated in $Sfrp1^{-/-}$ CSCs. Further, we have shown an inverse correlation between Sfrp1 and Sox-2 in mice SCC. Importantly, this inverse correlation between Sfrp1 and Sox-2 was extrapolated to human skin cancer where a similar correlation was observed. In addition, restoration of Sfrp1 levels decreased the expression of Sox-2 in cutaneous skin SCC cell lines thereby establishing their inverse correlation in human skin cancer. As epidermis share certain similarities with oral and breast epithelia in tissue architecture and in tumor progression, we further expanded our studies to

OSCC and breast cancer. Our results (Real time PCR and IHC) have shown that Sfrp1 levels were lower and Sox-2 levels were higher within these cancers. Further, to validate the inverse relation of Sfrp1 and Sox-2 in large cohort of samples we have also performed *in silico* analysis of data from TCGA data base on skin cancer, HNSCC, breast cancer and pancreatic adenocarcinoma (PAAD) samples. The results showed an inverse relation of Sfrp1 and Sox-2 within these cancers even in large cohort of samples with in TCGA data base. Of paramount importance, within the TCGA data, we have found that loss of Sfrp1 results in overall poor survival in skin cancer, HNSCC, breast cancer and PAAD patients. In conclusion, this study provides compelling evidence that Sfrp1 plays pivotal role in skin tumor initiation and CSCs regulation. Importantly, Sfrp1 and Sox-2 expression showed an inverse correlation in mice skin SCC. The murine skin SCC data was further extrapolated and validated in human epithelial cancers such as skin cancer, HNSCC and breast cancer which also showed an inverse correlation of Sfrp1 and Sox-2. In particular, low levels of Sfrp1 showed overall poor survival in skin cancer, HNSCC, breast cancer and PAAD patients suggesting that Sfrp1 could be used as a prognostic marker within these cancers. This study accentuates the importance of using murine epithelial model systems for studying molecular signalling in human epithelial cancers. Overall, future studies are necessary to understand the precise molecular mechanism of Sfrp1 that is involved in CSC regulation with respect to tumor aggressiveness, proliferation and EMT regulation, which may further pave way in the development of treatment strategies in cancer.

Salient findings:

Objective 1:

1. Sfrp1 loss showed an initial decrease in the HFSCs pool in mice skin
2. Loss of Sfrp1 leads to increased HFSCs proliferation at PD23 (telogen-to-anagen transition) and decrease in label retaining cells (LRCs) in $Sfrp1^{-/-}$ mice skin as compared to WT mice at PD49 (2^{nd} telogen). However, no change in proliferation or decrease in LRCs was observed in $Sfrp1^{+/-}$ mice.
3. Decrease in the Runx1 and P21 protein levels while increase in the Cyclin–D1 levels are observed in the Sfrp1 knockout mice as compared to WT
4. Sfrp1 loss leads to delay in wound re-epithelialization as compared to WT
5. Decreased active β-catenin signalling was observed in Sfrp1 knockout mice as compared to WT
6. No redundancy from other SFRP family proteins was observed in the absence of Sfrp1 in mice skin
7. Sfrp1 loss showed a decrease in the expression of HFSCs markers genes such as Lgr5 and Axin2 (targets of Wnt/β-catenin signalling)
8. Increased Bmp signalling and inactivation of PI3K/AKT signalling might be responsible for increase in the active Gsk-3β levels in both the $Sfrp1^{+/-}$ and $Sfrp1^{-/-}$ mice as compared to WT mice skin
9. We propose a model that, in HFSCs the activated Bmp signalling inhibits the activity of the Akt signalling. This in turn increases the active Gsk-3β levels which inhibit the aberrant activation of (β-catenin) Wnt signalling in the absence of Sfrp1.

Objective 2:

1. Enhanced mesenchymal phenotype was observed in Sfrp1$^{-/-}$ SCC as compared to WT SCC
2. CSCs from the Sfrp1$^{-/-}$ induced skin tumors are more aggressive, and possess high tumorigenic potential as compared to WT tumors
3. The tumor propagating cell (TPC) frequency was higher in Sfrp1$^{-/-}$ CSCs as compared to WT CSCs with Sfrp1$^{-/-}$ CSCs as low as 5000 are capable of giving rise to tumors in NOD/SCID mice.
4. Sfrp1 loss results in increased growth factor receptors in Sfrp1$^{-/-}$ CSCs, such as Ghr, Pdgfra, and Tgfbr3, and their downstream signalling molecules such as Akt3, Erk and Stat2, which are associated with CSC maintenance, tumor aggressiveness and metastatic potential
5. Increase in K8 and VIM1(1/2) expression, important markers for tumor progression and epithelial to mesenchymal transition of SCC, in Sfrp1 knockout mice SCC
6. Sfrp1 loss showed an increased Sox-2 expression and EMT markers (Twist1, Twist2, Snai1, Zeb1 and Vimentin) expression within CSCs
7. Sfrp1 and Sox-2 showed inverse correlation in multiple human epithelial cancers and Sfrp1 loss is associated with overall poor survival of the patients.

7.2 Future Perspectives:

Sfrp1 in Hair follicle stem cells regulation:

1) Our study for the first time explored the role of Sfrp1 in HFSCs maintenance and regulation. We have shown that that Sfrp1 loss results in initial decrease in the HFSCs population in both the $Sfrp1^{+/-}$ and $Sfrp1^{-/-}$ mice as compared to WT mice. However, $Sfrp1^{-/-}$ mice showed an increase in the proliferation and recovery of HFSCs during the second telogen but HFSCs with in $Sfrp1^{+/-}$ mice were still low at PD49 as compared to WT. Therefore, it would be interesting to study the molecular changes in the $Sfrp1^{+/-}$ HFSCs and the long term effect of Sfrp1 loss on the functional properties of $Sfrp1^{+/-}$ HFSCs.
2) HFSCs were shown to play an important role in wound re-epithelialization. Further, Akt signalling was shown to play an important role in cell proliferation and migration during wound re-epithelialisation. In our study we have shown that Sfrp1 loss results in delayed wound healing and decreased Akt signalling in $Sfrp1^{-/-}$ mice as compared to WT. Therefore, a detailed study is required to understand whether the delay in the wound re-epithelialisation is only due to loss of HFSCs function or is it a combined effect of both loss of function of HFSCs and decrease in Akt signalling.
3) We propose a model that, in the absence of Sfrp1 the activated Bmp signalling with in HFSCs inhibits the activity of the Akt signalling. Loss of Akt signalling results in increased active Gsk-3β levels which inhibit the aberrant activation of Wnt β-catenin signalling. However, future studies are required to substantiate the proposed molecular mechanism in the absence of Sfrp1, where different inhibitors against the enhanced Bmp signalling and Gsk-3β can be used to perform the reversal studies *in vivo* in the $Sfrp1^{+/-}$ and $Sfrp1^{-/-}$ mice skin.

Sfrp1 in cancer stem cells regulation:

1) The present study highlights the importance of Sfrp1 in skin tumor initiation and CSCs regulation. Sfrp1 loss enhanced CSCs properties such as their aggressiveness, TPC efficiency, altered signalling and most importantly enhanced Sox-2 expression. Sfrp1 loss results in early tumor initiation, therefore, it would be really interesting to study the cellular and molecular level changes that are occurring during tumor initiation.
2) Further, we have shown that the likely origin of the $Sfrp1^{-/-}$ tumors was from HFSCs rather than from the IFE stem cells because $Sfrp1^{-/-}$ tumors are more of mixed and mesenchymal phenotype. Earlier reports from Latil et al. 2017 have shown that tumors arising from HFSCs have mostly mixed and mesenchymal phenotype. However, future studies by performing lineage tracing experiments using HFSCs specific promoter (K15 or Lgr5) is required to confirm this.
3) Importantly, based on gene expression profile of WT and $Sfrp1^{-/-}$ CSCs, we have proposed a putative mechanism through which Sfrp1 might regulate the expression of Sox-2. However, future studies are required to clearly dissect the molecular mechanism that is involved in regulation of Sox-2 expression. Additionally, the deregulation in the growth factor signalling needs to be properly studied to reveal a clear and defined mechanism through which Sfrp1 functions in SCC. This study would help in identifying the signalling molecules to be targeted that may aid in preventing the tumor progression which later can be extrapolated to human cancers for better cancer treatment.

List of Figures

List of Tables

Thesis Highlight

Name of the Student: Mr. Raghava Reddy Sunkara

Name of the CI/OCC: TMC-ACTREC **Enrolment no:** LIFE09201304013

Thesis Title: "Defining the molecular signaling mechanism in epidermal stem cell regulation and cancer"

Discipline: Life Sciences **Sub-Area of Discipline:** Skin stem cell biology

Date of Viva voce: 01-12-2020

Epidermal stem cells (SCs) play an important role in maintenance and repair of the skin throughout the life of the organism. Multi-potent hair follicle stem cells (HFSCs) are essential for hair regeneration during normal homeostasis and also contribute to wound re-epithelialization upon injury. Wnt signaling plays an indispensable role in regulating hair follicle SCs (HFSCs). However, perturbations in the developmental signaling pathways (Wnt & Shh) within epidermal SCs has been reported in the development of basal and squamous cell carcinomas (BCC and SCC). Secreted frizzled related protein 1 (*Sfrp1*), a key Wnt antagonist, is upregulated in the HFSCs as compared to non-stem cells; however, its role in the epidermal SC regulation, tumor initiation and CSC regulation still remains elusive.

Here, using Sfrp1 knockout mice we have shown that Sfrp1 is involved in HFSCs pool regulation at PD21 (1sttelogen). Further, Sfrp1 loss also resulted in decreased HFSC quiescence regulators; Runx1 and P21, enhanced HFSC proliferation, faster hair cycle and delayed wound re-epithelialization. Remarkably, the decreased HFSCs pool was restored by PD49 (2nd telogen) in Sfrp1$^{-/-}$ mice due to increased proliferation of Sfrp1$^{-/-}$ HFSCs as compared to WT. However, this increase in HFSCs proliferation was transient as the aberrant proliferation of HFSCs in the absence of Sfrp1 was normalised due to the down-regulation of Wnt β-Catenin signaling activity through BMP/AKT/GSK3β-mediated signaling present within HFSCs.

Further, we have also showed that Sfrp1 loss results in increased sensitivity to chemical induced carcinogenesis in murine skin. Our work has uncovered early tumor initiation and enhanced tumorigenic potential of Sfrp1 knockout CSCs linked to upregulation of genes involved in proliferation, tumor aggression, EMT, and stemness. Importantly, we have found an inverse correlation of Sfrp1 and Sox2 expression in mouse skin tumors. Further, the data obtained from the murine studies was extended to multiple human epithelial cancers such as skin cutaneous SCC, HNSCC and breast cancers where it was shown that the inverse correlation between Sfrp1 and Sox2 exists even within these cancers. Most importantly, an interesting correlation of Sfrp1 expression within tumors and overall survival of patients was shown which could serve as marker for prognosis.

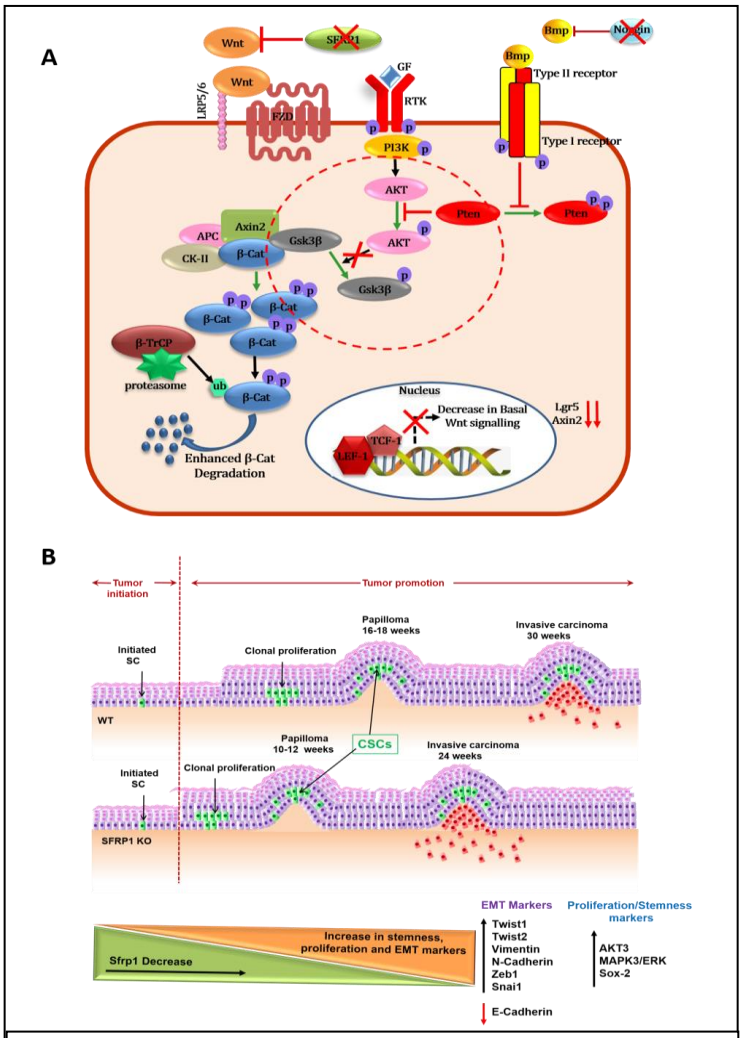

A) BMP/AKT/GSK3β signalling inhibits aberrant activation of Wnt signalling in HFSCs in the absence of Sfrp1 **B)** Diagrammatic representation of accelerated skin tumor initiation and CSC regulation due to loss of Sfrp1